DETERMINISTIC AND STOCHASTIC ANALYSIS OF HCV DYNAMICS WITH HUMORAL IMMUNE RESPONSE

Ph.D. THESIS

by

SONJOY PAN

DEPARTMENT OF MATHEMATICS
INDIAN INSTITUTE OF TECHNOLOGY GUWAHATI
GUWAHATI-781039, INDIA

June, 2020

DETERMINISTIC AND STOCHASTIC ANALYSIS OF HCV DYNAMICS WITH HUMORAL IMMUNE RESPONSE

A Thesis

submitted in partial fulfillment of the requirements

for the award of the degree of

DOCTOR OF PHILOSOPHY

(MATHEMATICS)

by

SONJOY PAN

(Roll Number: 146123007)

to the

DEPARTMENT OF MATHEMATICS

INDIAN INSTITUTE OF TECHNOLOGY GUWAHATI

GUWAHATI-781039, INDIA

June, 2020

Declaration

I hereby declare that the work contained in this thesis entitled **"DETERMINISTIC AND STOCHASTIC ANALYSIS OF HCV DYNAMICS WITH HUMORAL IMMUNE RESPONSE"** was done by me, under the supervision of **Dr. Siddhartha Pratim Chakrabarty**, Professor, Department of Mathematics, Indian Institute of Technology Guwahati for the award of the degree of Doctor of Philosophy and this work has not been submitted elsewhere for a degree.

June, 2020

Sonjoy Pan
Roll No. 146123007
Department of Mathematics
Indian Institute of Technology Guwahati

Certificate

It is certified that the work contained in this thesis entitled **"DETERMINISTIC AND STOCHASTIC ANALYSIS OF HCV DYNAMICS WITH HUMORAL IMMUNE RESPONSE"** has been carried out by **Sonjoy Pan**, a student in Department of Mathematics, Indian Institute of Technology Guwahati, under my supervision for the award of the degree of Doctor of Philosophy and this work has not been submitted elsewhere for a degree.

June, 2020

Dr. Siddhartha Pratim Chakrabarty
Professor
Department of Mathematics
Indian Institute of Technology Guwahati

Dedicated

to

My Beloved

Parents and Elder Brother

Mr. Biswanath Pan (Baba)

Mrs. Uma Pan (Maa)

&

Mr. Rajkumar Pan (Dada)

Acknowledgements

This doctoral thesis would never have been possible without the contributions of numerous people in various stages. I would like to thank them all who motivated and helped me in any way directly or indirectly to carry out this study.

First and foremost, I would like to express my deep and sincere gratitude to my supervisor Professor Siddhartha Pratim Chakrabarty for his generous guidance and advice throughout my research work. I am extremely grateful to him for his continuous support, encouragement and invaluable suggestions in every direction throughout the years. Without his constructive supervision, this thesis would not have been possible. Actually, no words are enough to appreciate his moral support and tremendous help during my Ph.D. study. I must say that I am very fortunate to have him as my Ph.D. supervisor and I could not have imagined having a better advisor and mentor.

I would like to convey my gratitude to my doctoral committee members, Prof. Jiten Chandra Kalita (Chairman), Dr. Arabin Kumar Dey and Dr. Sweta Tiwari for reviewing my research work and giving insightful comments and valuable suggestions for improvement in my research work. I would also like to convey my sincere thanks to Prof. Bhaba Kumar Sarma, Dr. Bhupen Deka and Dr. Sriparna Bandopadhyay for nicely teaching various subjects during my Ph.D. course work. My sincere gratitude and thanks to Prof. Swaroop Nandan Bora (former Head of the Department), Prof. N. Selvaraju (former Head of the Department) and Prof. M.G.P. Prasad (present Head of the Department) for their kind help and support in various official issues in these years. I warmly thank all the staff members of the Department of Mathematics, IIT Guwahati for their assistance in official and technical matters.

I am also grateful to Dr. Sarit Maitra, Department of Mathematics, NIT Durgapur for his worthy guidance during my M.Tech. study. His teaching, inspiration and motivation immensely helped in my doctoral research.

My grateful acknowledgement to the Ministry of Human Resource Development, Government of India, for the financial support for pursuing my Ph.D. I am also thankful to Indian Institute of Technology Guwahati for providing a very nice educational environment and all kinds of support.

I am also indebted to my friends and colleagues of the Department of Mathematics, IIT Guwahati, who have helped me in various situations directly or indirectly. I thank my all peers with whom I have spent a good and memorable time in these years. I especially thank Biswajit and Devanand for their friendly and wonderful company during my research tenure. I take this opportunity to thank my fellows who already completed Ph.D., Dr. Swarup Barik, Dr. Tamal Pramanick, Dr. Ranjan Kumar Das, Dr. Deb Kumar Giri, Dr. Madhusudan Bera and Dr. Koyel Chakravarty for their help and support in various situations, and also Nilay, Abhijit, Dipankar, Ashish and many others for all their encouragement and support during

this period. I am also thankful to my seniors Dr. Kalyan Manna, Dr. Ankur Kanaujiya and Dr. Dinesh Kumar for their inspiration and supporting help several times. My special appreciation towards my close friends Biplab, Amit and Sukumar with whom I have shared some of the best moments of my life and also their inspiration and encouragement give me a lot.

My eternal and deepest gratitude goes to my beloved parents (Mr. Biswanath Pan and Mrs. Uma Pan), my dear elder brother (Mr. Rajkumar Pan), my adorable grandmother (Mrs. Usha Rani Pan) and all other family members for their blessings, love, concern, care, encouragement and moral support throughout my life. Without their infinite love and support, it would never have been possible for me to complete this work.

Finally, I heartily thank everyone who helped and supported me directly or indirectly for the successful completion of this thesis. My sincere apologies if I missed to mentioning someone mistakenly, but I am thankful for their feedback of course.

June, 2020 **Sonjoy Pan**

Abstract

In this thesis, a mathematical model for HCV dynamics incorporating various aspects such as virus-to-cell as well as cell-to-cell transmission and non-cytolytic cure rate with the role of B cells in the activation of the humoral immune response is presented and analyzed. Next, the model is modified by involving delay in the generation of B cells (delay differential equations model). Further, the model is modified by considering the spatial mobility of the virions as well as the immune B cells with general nonlinear incidence functions for both the modes of infection spread (reaction-diffusion model). The feasibility of all these three models is justified by establishing the uniqueness, non-negativity and boundedness of the solutions to the corresponding system. The local as well as global stability of the three equilibria, namely, infection-free equilibrium, immune-free infected equilibrium and immune-activation infected equilibrium for these three models are investigated theoretically as well as numerically in terms of conditions on the basic reproduction number and humoral immune reproduction number. The global stability analysis for these models is examined by constructing suitable Lyapunov functionals. The conditions for the existence of Hopf bifurcation and consequent occurrence of bifurcating periodic orbits around the interior equilibrium for the delay differential equations model is determined by taking time delay as the bifurcation parameter. Numerical simulations are performed to support the theoretical results obtained from these three models. A numerical comparison of the dynamics for HCV models under various consideration is illustrated. The effect of some sensitive parameters such as cell-to-cell transmission rate, cure rate and development rate of B cells are numerically presented and discussed. The numerical findings indicate that the inclusion of cell-to-cell transmission increases the concentration of infected hepatocytes, while the cure rate increases the level of uninfected hepatocytes. The effect of the humoral immune response is crucial in neutralizing the virions and is less impactful on the reduction of infection. The results obtained from the delay model also show that the system becomes unstable from stable and regains stability from instability depending on the development rate of B cells for a fixed delay value. In addition, a numerical comparison of the dynamics resulting from the reaction-diffusion model with bilinear as well as Holling type-II incidence functions for both modes of transmission is studied. Finally, stochastic models for HCV dynamics are constructed and analyzed using the property of linear transformation for multivariate normal distribution, based on both budding and bursting processes with fixed as well as variable burst size for the release of virions from the infected hepatocytes. The branching process approximation technique is used to determine the probability of virus extinction. The stochastic means with standard deviations for the model populations are numerically calculated and are compared with the results from the deterministic model. Moreover, the forward Kolmogorov and moment equations associated to the stochastic models for both budding and bursting processes are derived and numerically illustrated with a particular case.

Contents

Acronyms xviii

Nomenclature xxi

List of Figures xxiii

List of Tables xxvii

1 Introduction 1

1.1 Biological Background . . . 1

1.1.1 Hepatitis C . . . 2

1.1.2 The Immune System . . . 3

1.1.2.1 Natural Killer Cells . . . 3

1.1.2.2 Cellular Immune Response . . . 3

1.1.2.3 Humoral Immune Response . . . 4

1.2 Terminology in Viral Dynamics . . . 4

1.2.1 Budding and Bursting Processes . . . 5

1.2.2 Basic Reproduction Number . . . 5

1.2.3 Incidence Function . . . 6

1.3 Mathematical Preliminaries . . . 6

1.3.1 Properties of Solutions to the System of Differential Equations . . . 6

1.3.1.1 Existence and Uniqueness . . . 7

1.3.1.2 Positivity and Boundedness . . . 7

1.3.1.3 Persistence . . . 8

1.3.2 Stability Theory and Bifurcations . . . 8

1.3.2.1 Local Stability . . . 8

1.3.2.2 Global Stability . . . 9

1.3.2.3 Bifurcations . . . 11

1.3.3 Delay Differential Equations . . . 12

1.3.4 Reaction-Diffusion Equations . . . 13

1.3.5 Stochastic Concepts . . . 14

1.3.5.1 Stochastic Process and Brownian Motion . . . 14

1.3.5.2 Stochastic Differential Equations 15
1.3.5.3 Euler-Maruyama Method 15
1.4 Literature Review 16
1.5 Motivation and Objectives 21
1.6 Thesis Outline 22

2 Modeling and Analysis of HCV Dynamics Incorporating Cell-to-Cell Transmission and Non-cytolytic Cure with Humoral Immune Response 25
2.1 Mathematical Model 26
2.2 Non-negativity and Boundedness of Solution 27
2.3 Existence and Stability of Equilibria 29
2.3.1 Local Stability Analysis 31
2.3.2 Global Stability Analysis 34
2.4 Numerical Simulations and Discussions on the Effect of Parameters 38
2.5 Conclusions 46

3 Dynamics of HCV Model with the Effect of Time Delay in the Generation of B Cells 49
3.1 Mathematical Model 50
3.2 Non-negativity and Boundedness of Solution 51
3.3 Equilibria and Stability 52
3.3.1 Characteristic Equation 53
3.3.2 Local and Global Stabilities of Boundary Equilibria 53
3.3.3 The Interior Equilibrium and Hopf Bifurcation 57
3.4 Estimation of the Maximum Length of Delay to Preserve Stability 61
3.5 Numerical Simulations and Discussions 64
3.6 Conclusions 71

4 Reaction-Diffusion Model for HCV Dynamics Capturing Spatial Mobility of Virions and B Cells 73
4.1 Model Formulation 74
4.2 Properties of Solutions and Equilibria 75
4.2.1 Properties of Solutions 75
4.2.2 Existence of Equilibria 77
4.3 Global Behavior of the System 79
4.4 Numerical Illustrations 85
4.5 Conclusions 90

5 Stochastic Modeling and Branching Process Approximation for Within-Host Dynamics of HCV Infection 93
5.1 Stochastic Model Formulation 94

5.1.1 SDE for Budding Process 94
5.1.2 SDE for Bursting Process 96
5.2 CTMC Model Analysis 98
5.2.1 Branching Process Approximation in Case of Budding 99
5.2.2 Branching Process Approximation in Case of Bursting 100
5.3 Variable Burst Size 102
5.4 Forward Kolmogorov and Moment Equations 104
5.5 Numerical Results and Discussions 109
5.6 Conclusions 119

6 Concluding Remarks and Future Directions **123**
6.1 Concluding Remarks 123
6.2 Future Directions 124

Bibliography **126**

Acronyms

Biological Terms

APC	Antigen presenting cell
BCR	B cell receptor
cccDNA	Covalently closed circular deoxyribonucleic acid
CTL	Cytotoxic T lymphocyte
DAAs	Direct-acting antiviral agents
DC	Dendritic cell
HBV	Hepatitis B virus
HCC	Hepatocellular carcinoma
HCV	Hepatitis C virus
HIV	Human immunodeficiency virus
HTEI	Host-targeting entry inhibitor
HTLV	Human T cell leukemia virus
IFN	Interferon
nAbs	Neutralizing antibodies
NANBH	Non-A, non-B hepatitis
Non-nAbs	Non-Neutralizing antibodies
NK	Natural killer
SVR	Sustained virological response
WHO	World Health Organization

Mathematical Terms

CTMC	Continuous-time Markov chain
DDE	Delay differential equation
EM	Euler-Maruyama
NSFD	Non-standard finite difference
ODE	Ordinary differential equation
PDE	Partial differential equation
SDE	Stochastic differential equation

Nomenclature

Model Variables and Parameters

U or X_1	Concentration of uninfected hepatocytes
I or X_2	Concentration of infected hepatocytes
V or X_3	Concentration of virions
B or X_4	Concentration of B cells
λ	Recruitment rate of uninfected hepatocytes
β_1	Rate of virus-to-cell transmission
β_2	Rate of cell-to-cell transmission
d_1	Death rate of uninfected hepatocytes
d_2	Death rate of infected hepatocytes
d_3	Death rate of virions
d_4	Death rate of B cells
α	Cure rate of infected hepatocytes
k	Production rate of virions
p	Neutralization rate of virion by B cells
c	Development rate of B cells
τ	Time delay
h_1	Virus-to-cell incidence function
h_2	Cell-to-cell incidence function
Δ	Laplacian operator
d_V	Diffusion coefficient of virions
d_B	Diffusion coefficient of B cells

Notation and Symbols

R_0	Basic reproduction number
R_H	Humoral immune reproduction number
$\mathbb{R}^4_{+0}$	Set $\{(x_1, x_2, x_3, x_4) \in \mathbb{R}^4 \vert x_i \geq 0, i = 1, 2, 3, 4\}$
E_0 or (U_0, I_0, V_0, B_0)	Infection-free equilibrium
E_1 or (U_1, I_1, V_1, B_1)	Immune-free infected equilibrium
E^* or (U^*, I^*, V^*, B^*)	Immune-activation infected equilibrium
$E(X)$	Mean of X
$\sigma(X)$	Standard deviation of X
$ic_n,\ n = 1, 2, 3$	Initial conditions

List of Figures

2.1 Schematic representation of the mathematical model (2.1.1). 27

2.2 The trajectories of (a) uninfected hepatocytes, (b) infected hepatocytes, (c) virions, and (d) B cells starting with three different initial conditions $ic_1 := (70, 20, 10, 200)$, $ic_2 := (50, 5, 2, 100)$ and $ic_3 := (150, 10, 20, 400)$, in case of $R_0 < 1$ for the model (2.1.1). 40

2.3 The trajectories of (a) uninfected hepatocytes, (b) infected hepatocytes, (c) virions, and (d) B cells starting with three different initial conditions $ic_1 := (70, 20, 10, 200)$, $ic_2 := (50, 5, 2, 100)$ and $ic_3 := (150, 10, 20, 400)$, in case of $R_H < 1 < R_0$ for the model (2.1.1). 41

2.4 The trajectories of (a) uninfected hepatocytes, (b) infected hepatocytes, (c) virions, and (d) B cells starting with three different initial conditions $ic_1 := (70, 20, 10, 200)$, $ic_2 := (50, 5, 2, 100)$ and $ic_3 := (150, 10, 20, 400)$, in case of $R_H > 1$ for the model (2.1.1). 42

2.5 Comparison of dynamics for various models: (i) BM : basic model, (ii) $BMwAR$: basic model with B cell response (antibody response), (iii) $BMwC2C\&C$: basic model with cell-to-cell transmission and cure rate, (iv) $BMwAR\&C2C\&C$: basic model with B cell response (antibody response), cell-to-cell transmission and cure rate. 43

2.6 Effect of cell-to-cell transmission (β_2) on the dynamical behavior of the model system (2.1.1). 44

2.7 Effect of cure rate (α) on the dynamical behavior of the model system (2.1.1). 45

2.8 Effect of cure rate (α), virus-to-cell transmission rate (β_1) and cell-to-cell transmission rate (β_2) on basic reproduction number (R_0) for the model (2.1.1). 46

3.1 The trajectories of (a) uninfected hepatocytes, (b) infected hepatocytes, (c) virions, and (d) B cells starting with two different initial conditions ic_1 and ic_2, and three immune delays $\tau = 6$, 12, 25, in case of $R_0 < 1$ for the model (3.1.1). Blue lines : $ic_1 := (80, 5, 2, 50)$, red lines : $ic_2 := (120, 20, 10, 100)$, solid lines : $\tau = 6$, dashed lines : $\tau = 12$, dotted lines : $\tau = 25$. 65

3.2 The trajectories of (a) uninfected hepatocytes, (b) infected hepatocytes, (c) virions, and (d) B cells starting with two different initial conditions ic_1 and ic_2, and three immune delays $\tau = 6$, 12, 25, in case of $R_H < 1 < R_0$ for the model (3.1.1). Blue lines : $ic_1 := (80, 5, 2, 50)$, red lines : $ic_2 := (120, 20, 10, 100)$, solid lines : $\tau = 6$, dashed lines : $\tau = 12$, dotted lines : $\tau = 25$. 66

3.3 The time histories and the phase portraits of trajectories shows the local asymptotic stability of E^* for immune delay $\tau = 5 < \tau_0$. 67

3.4 The time histories and the phase portraits of trajectories shows the bifurcating periodic orbits around E^* for immune delay $\tau = 6 \in (\tau_0, \tau_2^{(0)})$. 67

3.5 The time histories and the phase portraits of trajectories shows the local asymptotic stability of E^* for immune delay $\tau = 14 \in (\tau_2^{(0)}, \tau_1^{(1)})$. 68

3.6 The time histories and the phase portraits of trajectories shows the existence of a periodic oscillation around E^* for immune delay $\tau = 25 \in (\tau_1^{(1)}, \tau_2^{(1)})$. . . 68

3.7 The time histories and the phase portraits of trajectories shows the local asymptotic stability of E^* for immune delay $\tau = 35 \in (\tau_2^{(1)}, \tau_1^{(2)})$. 69

3.8 The time histories and the phase portraits of trajectories shows the existence of a periodic bifurcation around E^* for immune delay $\tau = 43 \in (\tau_1^{(2)}, \tau_2^{(2)})$. . . 69

3.9 Effect of the development rate of B cells (c) on the dynamical behavior of the model system (3.1.1). 70

4.1 Dynamics of uninfected hepatocytes (U), infected hepatocytes (I), virions (V) and B cells (B) when $R_0 < 1$ for the case of bilinear transmission function. . 86

4.2 Dynamics of uninfected hepatocytes (U), infected hepatocytes (I), virions (V) and B cells (B) when $R_0 < 1$ for the case of Holling type-II transmission function. 87

4.3 Dynamics of uninfected hepatocytes (U), infected hepatocytes (I), virions (V) and B cells (B) when $R_2 < 1 < R_0$ for the case of bilinear transmission function. 88

4.4 Dynamics of uninfected hepatocytes (U), infected hepatocytes (I), virions (V) and B cells (B) when $R_2 < 1 < R_0$ for the case of Holling type-II transmission function. 89

4.5 Dynamics of uninfected hepatocytes (U), infected hepatocytes (I), virions (V) and B cells (B) when $R_1 > 1$ for the case of bilinear transmission function. . 90

4.6 Dynamics of uninfected hepatocytes (U), infected hepatocytes (I), virions (V) and B cells (B) when $R_1 > 1$ for the case of Holling type-II transmission function. 91

5.1 One sample path and mean of 5000 sample paths with plus or minus standard deviation of (a) uninfected hepatocytes, (b) infected hepatocytes, (c) virions and (d) B cells for the budding SDE model (5.1.1). 111

5.2 One sample path and mean of 5000 sample paths with plus or minus standard deviation of (a) uninfected hepatocytes, (b) infected hepatocytes, (c) virions and (d) B cells for the bursting SDE model with fixed burst size given by (5.1.2).112

5.3 One sample path and mean of 5000 sample paths with plus or minus standard deviation of (a) uninfected hepatocytes, (b) infected hepatocytes, (c) virions and (d) B cells for the bursting SDE model with variable burst size given by (5.3.3). 113

5.4 Probability histograms and approximate normal distributions of (a) uninfected hepatocytes, (b) infected hepatocytes, (c) virions and (d) B cells at $t = 150$ based on 5000 sample paths for the SDE budding model (5.1.1). . . . 114

5.5 Probability histograms and approximate normal distributions of (a) uninfected hepatocytes, (b) infected hepatocytes, (c) virions and (d) B cells at $t = 150$ based on 5000 sample paths for the bursting SDE model with fixed burst size given by (5.1.2). 115

5.6 Probability histograms and approximate normal distributions of (a) uninfected hepatocytes, (b) infected hepatocytes, (c) virions and (d) B cells at $t = 150$ based on 5000 sample paths for the bursting SDE model with variable burst size given by (5.3.3). 116

5.7 (a) One sample path and mean path with plus or minus standard deviation and (b) probability histograms with approximate normal distribution at $t = 150$, based on 5000 sample paths of the variable burst size given by (5.3.1). 117

5.8 Comparison of the deterministic solution given by (2.1.1) for (a) uninfected hepatocytes, (b) infected hepatocytes, (c) virions and (d) B cells, with the stochastic mean of 5000 sample paths obtained from the SDE models in case of budding (5.1.1) and bursting with fixed (5.1.2) and variable (5.3.3) burst size. 119

5.9 Mean path of 5000 sample paths for (a) uninfected hepatocytes, (b) infected hepatocytes, (c) virions and (d) B cells, resulting from using EM method with three different initial conditions $ic_1 := (200, 20, 10, 40)$, $ic_2 := (100, 80, 30, 200)$ and $ic_3 := (300, 100, 50, 100)$ in case of budding model (5.1.1). 120
5.10 Mean path of 5000 sample paths for (a) uninfected hepatocytes, (b) infected hepatocytes, (c) virions and (d) B cells, resulting from using EM method with five different stepsizes $\Delta t = 0.005,\ 0.01,\ 0.02,\ 0.04,\ 0.1$ in case of budding model (5.1.1). 121
5.11 Probability of virus extinction for (a) the CTMC budding model and (b) the CTMC bursting model, with $I(0) = m$ and $V(0) = n$. 121
5.12 Comparison of the moment differential equation at infection-free stage (5.4.1) with the SDE models for budding (5.1.1) and bursting with fixed (5.1.2) and variable (5.3.3) burst size. 122

List of Tables

2.1 Expressions of R_0 and R_H under various conditions on β_2 and α. 31
2.2 The list of parameter values for numerical simulations for the model (2.1.1). 39

3.1 The list of parameter values for numerical simulations for the model (3.1.1) as well as the model (4.1.1). 64

5.1 Possible state change during a small time interval Δt, resulting from budding. 95
5.2 Possible state change during a small time interval Δt, resulting from bursting. 97
5.3 The list of parameter values for numerical simulations for the stochastic models. 110
5.4 Means (μ) and standard deviations (σ) of four model populations (uninfected hepatocytes (X_1), infected hepatocytes (X_2), virions (X_3) and B cells (X_4)) calculated at $t = 150$ based on 5000 independent simulations for the cases of budding, bursting with fixed burst size and bursting with variable burst size. 118
5.5 Means (μ) and standard deviations (σ) of four model populations (uninfected hepatocytes (X_1), infected hepatocytes (X_2), virions (X_3) and B cells (X_4)) calculated at $t = 150$ based on 5000 independent simulations, resulting from using EM method with stepsizes $\Delta t = 0.005, 0.01, 0.02, 0.04, 0.1$ (in budding case). 118

Chapter 1

Introduction

Virus, which is a submicroscopic parasite consisting of genes, nucleic acid and protein, infects the cells of animals, plants or microorganisms, thereby causing virological disease within the host [68]. In absence of the ability to self-reproduce, a virus can replicate itself only inside the living cells of a host organism. Typically, a virus invades a specific target cell of the host, for the abetment of their proliferation. In this thesis, we consider the dynamics of the hepatitis C virus (HCV) that causes liver infection through proliferation inside the human liver by invading the hepatocytes and interacting with the immune cells [34].

The literature on mathematical modeling in the last two decades highlights its prominent role in the study of viral infectivity, immunology and epidemiology [15], paying particular attention to the modeling and analysis of human virological diseases, in order to gain better insights of the quantitative virology and immunology as well as the therapeutic progress [91]. This thesis aims to analyze the within-host dynamics of HCV infection through the mathematical modeling of the interplay between HCV and immune response, and determine the parameter-dependent conditions for the control of chronic infection.

As a prelude to the main thesis work, we begin with a narrative on the biological paradigm of HCV infection and the mathematical tools to be adopted in the course of the thesis.

1.1 Biological Background

In this section, we introduce the epidemiological background to the development and progression of HCV infection. We present some statistical data from HCV progression (from literature) and discuss the immunology associated with this specific virus.

1.1.1 Hepatitis C

In the mid-1970s, a new hepatitis virus was detected in several patients, the structural proteins of which were different from known structure of hepatitis A or hepatitis B virus (then known as non-A, non-B hepatitis (NANBH) virus) [47]. In 1989, Choo et al. [20] discovered that a complementary DNA clone originates from positive-stranded RNA molecule which was present in NANBH infected chimpanzee and also observed that NANBH is a member of Flaviviridae family of viruses, and thereby re-named this agent as HCV. HCV is a positive single-stranded RNA genome encoding polyprotein precursor of amino acids, which binds to the surface of the cells by receptor-mediated endocytosis [100].

HCV causes hepatitis C infection by primarily infecting the hepatocytes (liver cells) and then interacting with the helper T cells ($CD4^+$ T cells). HCV invades the hepatocytes and manipulates them in order to abet the proliferation of the virions, without killing the liver cells [34]. Hepatitis C is mainly transmitted through blood-to-blood contact, such as blood transfusion, unsterilized medical equipment and injecting drug use [27, 93]. As of 2017, an estimated 170 million individuals worldwide (which is approximately 2.3% of the global population and about 4.6 times the number cases of human immunodeficiency virus (HIV)) were persistently infected with HCV [85], which makes it a significant global health concern. HCV infection develops in the host cells through two phases, namely, acute and chronic. In the long-term, HCV infected cases lead to a significant risk of hepatic fibrosis, liver cirrhosis and hepatocellular carcinoma (HCC) [50]. Approximately $55-85\%$ of HCV infected patients progress towards the chronic stage, while the remaining naturally recover within six months of infection due to the immunological response of the body [85]. Further, $15-30\%$ of the chronic cases develop liver cirrhosis and hepatocellular carcinoma (HCC) within 20 years [85]. The most common treatment for HCV patients is the combination antiviral therapy of pegylated interferon (PEG-IFN) and ribavirin [87]. The combination treatment responses could be up to 50% of the cases in the chronic stage [87], as compared to single interferon therapy which is successful in only $11-30\%$ of the cases [81]. The current most effective treatment of HCV infection is the therapy with several combination drugs of direct-acting antiviral agents (DAAs), namely, nonstructural proteins 3/4A protease inhibitors (NS3/4A PIs), nucleoside NS5B polymerase inhibitors, non-nucleoside NS5B polymerase inhibitors and NS5A inhibitors [9, 25]. DAAs directly target the intracellular HCV RNA replication process with the sustained virologic response (SVR) rate being above 90% [9, 25]. However, no vaccine has yet been developed for HCV infection.

1.1.2 The Immune System

The functional process of the human immune system is not completely understood due to its complexity. The immune system responds systematically to defend the body against foreign particles. The first line of defense to protect the body against pathogens is called innate immune response, which comprises of non-specific immune cells, such as macrophages, natural killer cells, leukocytes, lymphocytes, dendritic cells and interferons [36, 95]. The innate immune response activates to immediately destroy the pathogens in the acute phase of infection, and is capable of detecting the virus within the first day of HCV infection [95]. The acute phase of HCV infection is the critical period when the innate immune response plays a crucial role in the control and elimination of the viruses [36]. This phase is asymptomatic and cannot be detected in major cases. The second line of defense refers to the adaptive immune response which consists of the pathogen-specific immune cells. The adaptive immune response starts its functional activities when the innate immune response fails to kill foreign organisms or pathogens. The adaptive immune response can be classified into two categories, cellular and humoral immune responses [36, 58]. The immune system is more activated to release target specific immune cells after about two months of HCV infection and can be more effective in attacking the pathogens.

1.1.2.1 Natural Killer Cells

Natural killer (NK) cells are a type of lymphocyte, which play a crucial role in detecting and neutralizing the virus during the first phase of HCV infection. These cells start their activity as principal innate immune cells, to detect the virus in the early period of HCV infection [95]. NK cells contain special proteins such as perforin and granzymes. This immune response comes into action immediately and produces several proteins (including interferon) which involves reducing the proliferation of virus particle, but is, however, unable to stop the viral production [30]. Interferons regulate NK cells which can identify and eliminate the infected cells. In addition, these cells can help in the secretion of many cytokines like TNF-α and IFN-γ, which enhance the function of the other immune cells such as dendritic cells and macrophage [34].

1.1.2.2 Cellular Immune Response

$CD4^+$ T cells and $CD8^+$ T or Cytotoxic T Lymphocytes (CTLs) cells are the main components of the cellular immune response [36]. These T cells are produced in the thymus and their function is to attack and kill the virus-induced infected cells. $CD4^+$ T cell helps to secrete lymphokine which regulates the activities of $CD8^+$ T cells as well as antigen-specific

B cells. $CD8^+$ T cells are directly involved in the killing and elimination of the infected cells and they also induce the release of antiviral cytokines, which regulates the action of $CD8^+$ T cells [36]. While the specific immune cells attempt to attack and destroy the HCV, the viruses themselves adopt strategies to survive, by changing their behavior and genetic structure [55]. Then the viruses mutate very rapidly so that immune response such as $CD8^+$ T cells experience difficulty in binding to the viruses, as the protein structure on the surface of the virus has already changed [59]. Consequently, the neutralization rate of infected cells gets slower and during this virus-immune interaction, the density of the virus exhibits fluctuations. If the immune system still responds and the virus is not able to escape from the immune cells, then all viruses are expected to be eliminated from the body. This is called the spontaneous clearance of HCV in a non-cytolytic manner and it happens within the first six months of infection [58, 76]. Otherwise, the infection becomes chronic.

1.1.2.3 Humoral Immune Response

The humoral immune response plays a significant role in the elimination of HCV by directly attacking the virus. B cells are the main components of the humoral immune response [58]. They are produced in the bone marrow and generate antibodies which can recognize and bind to the HCV. Antibodies also help other immune cells like $CD8^+$ T cells in identifying and neutralizing the HCV before their replication [55]. Two types of antibodies are mainly involved against HCV, namely, neutralizing antibodies (nAbs) and non-neutralizing antibodies (Non-nAbs). The function of nAbs is to control initial viremia and to protect the body from viral re-infection [58]. In the early phase of HCV infection nAb plays a crucial role in the clearance of HCV and this may cause spontaneous recovery from infection and the regulation of these antibodies are more cross-neutralizing [58]. However, HCV stimulates B cells to produce antibodies using B cell receptor (BCR)-independent process during the chronic stage of infection, that results in the development of lymphoproliferative and autoimmune diseases [58].

1.2 Terminology in Viral Dynamics

In this section, we introduce some basic terminology which is often used in the analysis of viral dynamics models. Note that these terms are described from the mathematical perspective.

1.2.1 Budding and Bursting Processes

Viruses are responsible for any kind of viral infection and specific viruses are involved in a particular infection. A virus generally enters the body thereby infecting the host cells and then they are produced from the infected cells by adopting two different release processes, namely, budding and bursting processes [114, 139].

In the budding process, the viruses are produced and released during the lifespan of infected cells in a continuous manner, that is, the virus "buds" out from the infected cells continuously during its entire life. In this case, the release of viruses does not depend on the death of infected cells. In the bursting process, the burst of an infected cell and the release of viruses happen simultaneously. In this case, the release of virus depends on the lysis of the infected cells, that is, the viruses are released only after any infected cell "bursts". We use N to denote the "burst size" which represents the number of new viruses being produced during the lifespan of an infected cell. The number of viruses will not be changed until an infected cell dies and the death of such a cell results in the release of N viruses. In this case, the production of the virus is dependent on the death of the infected cells.

1.2.2 Basic Reproduction Number

The basic reproduction number or the basic reproductive ratio, typically denoted by R_0, is the expected number of newly infected cases produced by a single infected case during its entire infectious period, in an entirely susceptible population [44]. In viral dynamics, R_0 is the expected number of secondary infected cells produced by an infected cell in its infectious lifespan.

Generally, R_0 acts as a threshold parameter that determines the possibility of the transmission of infection. Many techniques are used in determining R_0 for a viral dynamics model with the next generation method being the most common technique for the determination of R_0. In this method, R_0 is defined as the spectral radius (dominant eigenvalue) of the next generation matrix [44]. First, we have to identify the infected and non-infected compartments appearing in the model. Suppose that the model involves n compartments, of which m are infected. Let us define $Y = y_i,\ i = 1, \ldots, n$, where y_i is the proportion of individuals involved in i-th compartment. Further, let $F_i(Y)$ be the rate of occurrence of new infections in i-th compartment (excluding the transfer from other infected compartments to i-th compartment) and $V_i(Y) = V_i^-(Y) - V_i^+(Y)$, where V_i^- is the departing rate of individuals from i-th compartment and V_i^+ is the entering rate of individuals into i-th compartment. We denote

$$F = \left[\frac{\partial F_i(y_0)}{\partial y_j}\right] \quad \text{and} \quad V = \left[\frac{\partial V_i(y_0)}{\partial y_j}\right],$$

where $i, j = 1, \ldots, m$ and y_0 is the infection-free equilibrium. Then the next generation matrix is given by FV^{-1}. Thus R_0 is determined by the spectral radius of FV^{-1}.

1.2.3 Incidence Function

The incidence function or transmission function involved in the viral dynamics model represents the rate of transmission of infection from one cell to another cell. In the case of HCV, the infection can spread from an infected cell to uninfected cells through virus-to-cell or cell-to-cell mode. In modeling of viral dynamics, several types of incidence function are considered in literature [49, 52, 62, 69, 79, 101, 102, 110, 119, 134]. The incidence functions typically used in modeling of viral dynamics are as follows:

(*i*) The mass action or bilinear incidence function $f(x, y) = xy$.

(*ii*) The standard incidence function $f(x, y) = \dfrac{xy}{x + y}$.

(*iii*) The saturation or Holling type-II incidence function $f(x, y) = \dfrac{xy}{1 + \alpha y}$, $\alpha > 0$.

(*iv*) Beddington-DeAngelis type incidence function $f(x, y) = \dfrac{xy}{1 + ax + by}$, $a, b > 0$.

(*v*) Crowley-Martin type incidence function $f(x, y) = \dfrac{xy}{(1 + ax)(1 + by)}$, $a, b > 0$.

1.3 Mathematical Preliminaries

Some mathematical theories and methods are discussed in this section to study the nonlinear dynamical systems. The concepts are used to analyze the continuous autonomous system of differential equations.

1.3.1 Properties of Solutions to the System of Differential Equations

Let us consider a nonlinear continuous autonomous system of differential equations

$$\frac{dX}{dt} = F(X), \tag{1.3.1}$$

on $t \geq t_0$, where $X = (x_1, \ldots, x_n)^T \in \mathbb{R}^n$, $F : D \to \mathbb{R}^n$, $D \subseteq \mathbb{R}^n$ and $F(X)$ does not depend explicitly on time t, with initial condition

$$X(t_0) = X_0 \geq 0. \tag{1.3.2}$$

1.3.1.1 Existence and Uniqueness

The following theorems establish the existence and uniqueness of solution to the system (1.3.1) with initial condition (1.3.2).

Theorem 1.3.1. *[53]* ***(Local Existence and Uniqueness)***
Suppose that F satisfies the Lipschitz condition, that is,

$$\|F(X) - F(Y)\| \leq L\|X - Y\|,$$

$\forall\ X, Y \in \overline{D} = \{Z \in D \mid \|Z - X_0\| \leq r\},\ \forall\ t \in [t_0, t_1]$. *Then there exists some $\epsilon > 0$ such that the system* (1.3.1) *with initial condition* (1.3.2) *has a unique solution over $[t_0, t_0 + \epsilon]$.*

Theorem 1.3.2. *[53] Suppose that $F(X)$ and $\dfrac{\partial F(X)}{\partial X}$ are continuous on $\overline{D} \subseteq D \subseteq \mathbb{R}^n$. Then F is locally Lipschitz in X on $\overline{D}$, that is, the following relation holds*

$$\|F(X) - F(Y)\| \leq L\|X - Y\|,$$

$\forall\ X, Y \in \overline{D},\ \forall\ t \in [t_0, t_1]$.

Theorem 1.3.3. *[53]* ***(Global Existence and Uniqueness)***
Suppose that F satisfies the Lipschitz condition, that is,

$$\|F(X) - F(Y)\| \leq L\|X - Y\|,$$

$\forall\ X, Y \in D,\ \forall\ t \in [t_0, t_1]$. *Then the system* (1.3.1) *with initial condition* (1.3.2) *has a unique solution over $[t_0, t_1]$, where t_1 is arbitrarily large.*

1.3.1.2 Positivity and Boundedness

The positivity and boundedness properties of solutions to a dynamical or biological system ensure that the system is valid and realistic.

The solution $X(t)$ of the system (1.3.1) with initial condition (1.3.2) is said to satisfy the positivity property if the solution $X(t)$ starting with non-negative initial conditions will remain non-negative for any finite time interval whenever the solution exists.

The solution $X(t)$ of the system (1.3.1) with initial conditions (1.3.2) is said to be bounded if following condition holds for all $t \geq t_0$:

$$\|X(t)\| \leq K, \tag{1.3.3}$$

where $K \equiv K(t_0, X_0) > 0$ depends on initial condition (1.3.2). In addition, if K does not depend on initial condition (1.3.2), then the solution is said to be uniformly bounded. Furthermore, if there exists a $T > 0$ such that the condition (1.3.3) holds for all $t \geq t_0 + T$, then the solution is said to be uniformly ultimately bounded.

1.3.1.3 Persistence

The idea of persistence is an important property of the solutions to the dynamical system. A persistent system biologically implies that all populations exist in the long-term, regardless of initial conditions.

Definition 1.3.4. *[4] The system* (1.3.1) *with initial condition* (1.3.2) *is said to be persistent if the solution* $X(t)$ *satisfies*

$$\liminf_{t\to\infty} x_i(t) > 0, \quad for \quad i = 1, 2, \ldots, n.$$

1.3.2 Stability Theory and Bifurcations

Stability theory provides an idea of whether a small perturbation of initial conditions can disturb the trajectories of dynamical systems. To study the stability theory, first the equilibrium points of the system have to be determined. For local stability, linearization techniques are used to discuss the behavior of the solutions around the equilibrium points. Routh-Hurwitz Criteria can be used to examine the local stability of the equilibrium points, whereas, Lyapunov theory can be applied to investigate global stability. If the equilibrium is not stable, there may exist some bifurcation.

1.3.2.1 Local Stability

An equilibrium point, fixed point, critical point, stationary point, or steady state solution of the system (1.3.1) is a solution of $F(X) = 0$. We define $X = \overline{X}$ to be an equilibrium point of (1.3.1).

Definition 1.3.5. *[103] An equilibrium point* $\overline{X}$ *of the system (1.3.1) is said to be locally stable if for every* $\epsilon > 0$ *there exists a* $\delta > 0$ *such that every solution* $X(t)$ *of the system (1.3.1) with initial condition* (1.3.2) *satisfies*

$$\|X(t) - \overline{X}\| < \epsilon, \quad whenever \quad \|X_0 - \overline{X}\| < \delta, \quad \forall\ t > t_0.$$

If an equilibrium point does not satisfy the condition of local stability, then it is said to be an unstable equilibrium point.

Definition 1.3.6. *[103] An equilibrium point* $\overline{X}$ *of the system (1.3.1) is said to be locally asymptotically stable if it is locally stable and moreover, if there exists some* $r > 0$ *such that*

$$\lim_{t\to\infty} \|X(t) - \overline{X}\| = 0, \quad whenever \quad \|X_0 - \overline{X}\| < r.$$

Theorem 1.3.7. *[4]* ***(Routh-Hurwitz Criteria)***
Consider a polynomial of degree n,

$$P(z) = z^n + c_1 z^{n-1} + \cdots + c_{n-1} z + c_n,$$

where $c_k \in \mathbb{R}$, $k = 1, 2, \ldots, n$. We define the Hurwitz matrices as

$$H_1 = \begin{pmatrix} c_1 \end{pmatrix}, \quad H_2 = \begin{pmatrix} c_1 & 1 \\ c_3 & c_2 \end{pmatrix}, \quad H_3 = \begin{pmatrix} c_1 & 1 & 0 \\ c_3 & c_2 & c_1 \\ c_5 & c_4 & c_3 \end{pmatrix},$$

$$H_n = \begin{pmatrix} c_1 & 1 & 0 & 0 & \cdots & 0 \\ c_3 & c_2 & c_1 & 1 & \cdots & 0 \\ c_5 & c_4 & c_3 & c_2 & \cdots & 0 \\ \vdots & \vdots & \vdots & \vdots & \cdots & \vdots \\ 0 & 0 & 0 & 0 & \cdots & c_n \end{pmatrix},$$

where $c_l = 0$ if $l > n$. Then all the roots of the polynomial $P(z)$ are negative or have negative real part if and only if $det(H_l) > 0$, $l = 1, 2, \ldots, n$.

For the polynomials of degree $n = 2, 3, 4$, the conditions of the Routh-Hurwitz Criteria are as follows:

$$\begin{aligned} n = 2: &\quad c_1 > 0 \text{ and } c_2 > 0. \\ n = 3: &\quad c_1 > 0,\ c_3 > 0 \text{ and } c_1 c_2 > c_3. \\ n = 4: &\quad c_1 > 0,\ c_3 > 0,\ c_4 > 0 \text{ and } c_1 c_2 c_3 > c_3^2 + c_1^2 c_4. \end{aligned}$$

Theorem 1.3.8. *[4] Suppose $J(\overline{X})$ is the Jacobian matrix determined at the equilibrium $\overline{X}$ corresponding to the system* (1.3.1)*. If the characteristic polynomial of $J(\overline{X})$,*

$$z^n + c_1 z^{n-1} + c_2 z^{n-2} + \cdots + c_{n-1} z + c_n,$$

satisfies the Routh-Hurwitz criteria in Theorem 1.3.7, that is, $det(H_l) > 0$, $l = 1, 2, \ldots, n$, then the equilibrium $\overline{X}$ is locally asymptotically stable. Otherwise, if $det(H_l) < 0$ for some $l = 1, 2, \ldots, n$, then the equilibrium $\overline{X}$ is unstable.

1.3.2.2 Global Stability

Global stability means that the trajectory of a dynamical system tends to the attractor of the system, irrespective of initial conditions. Global stability is the strong property of the system. Further, global stability of an equilibrium always implies the local stability of that equilibrium.

Definition 1.3.9. *[4] An equilibrium point $\overline{X}$ of equation (1.3.1) is said to be globally stable if there exists some $\epsilon > 0$ such that*

$$\|X(t) - \overline{X}\| < \epsilon, \ \forall \ t > t_0.$$

Definition 1.3.10. *[4] An equilibrium point $\overline{X}$ of the system (1.3.1) is said to be globally asymptotically stable if it is globally stable and moreover,*

$$\lim_{t\to\infty} \|X(t) - \overline{X}\| = 0.$$

Definition 1.3.11. *[4] Let $S \subseteq \mathbb{R}^n$ be an open set containing the origin and $L : S \to \mathbb{R}$ be a $\mathcal{C}^1$ function. Then L is said to be positive definite on S if the following conditions hold:*

(a) $L(0) = 0$

(b) $L(X) > 0, \ \forall \ X \in S - \{0\}$.

The function L is said to be negative definite on S if $-L$ is positive definite on S.

Let $L : S \to \mathbb{R}$ be a positive definite function in an open neighborhood of origin. Then L is said to be a Lyapunov function for the system (1.3.1) if

$$\frac{dL(X)}{dt} \leq 0, \ \forall \ X \in S - \{0\}.$$

A function $f : \mathbb{R}^n \to \mathbb{R}$ is said to be radially unbounded if

$$f(X) \to \infty \text{ as } \|X\| \to \infty, \ X \in \mathbb{R}^n.$$

Theorem 1.3.12. *[103]* ***(Lyapunov's Stability Theorem)***
Let $\overline{X} = 0$ be an equilibrium of the system (1.3.1) and L be a positive definite $\mathcal{C}^1$ function in a neighborhood S of $\overline{X} = 0$. Then

(a) $\overline{X} = 0$ *is locally stable if* $\dfrac{dL(X)}{dt} \leq 0, \ \forall \ X \in S - \{0\}$.

(b) $\overline{X} = 0$ *is locally asymptotically stable if* $\dfrac{dL(X)}{dt} < 0, \ \forall \ X \in S - \{0\}$.

(c) $\overline{X} = 0$ *is globally stable if it is locally stable with L being radially unbounded.*

(d) $\overline{X} = 0$ *is globally asymptotically stable if it is locally asymptotically stable with L being radially unbounded.*

(e) $\overline{X} = 0$ *is unstable if* $\dfrac{dL(X)}{dt} > 0$ *for some* $X \in S - \{0\}$.

Definition 1.3.13. *[103] A set U is said to be an invariant set for the system (1.3.1) if the solution $X(t) \in U$, $\forall\ t \geq t_0$ whenever $X_0 \in U$.*

Theorem 1.3.14. *[103]* ***(LaSalle's Invariance Principle)***
Let $S \subseteq \mathbb{R}^n$ be a compact invariant set for the system (1.3.1) and $L : S \to \mathbb{R}$ be a $\mathcal{C}^1$ function such that

$$\frac{dL(X)}{dt} \leq 0,\ \forall\ X \in S.$$

We define a set

$$E = \left\{ X \in S \mid \frac{dL(X)}{dt} = 0 \right\}.$$

If M is the largest invariant subset of E, then $X(t)$ approaches M as $t \to \infty$, $\forall\ X_0 \in S$.

1.3.2.3 Bifurcations

A dynamical system undergoes the occurrence of bifurcation when a small change to the parameter values of the system results in a sudden change of its qualitative behavior or topological structure. The bifurcation results in changes in the stability, periodic orbits or other invariant properties. The parameter which changes the qualitative behavior of the system is considered as a bifurcation parameter and the values of the parameter at which the bifurcation occurs are known as bifurcation points. In a local bifurcation, a small change in the parameter values results in a sudden change in the qualitative behavior of the system in the neighborhood of the equilibrium. Some different kinds of local bifurcation are discussed as follows:

Saddle-node bifurcation

Saddle-node or fold bifurcation occurs when two equilibria of the system move towards each other and collide, and then disappear [4]. In this local bifurcation, two equilibria (one is a saddle point and another is a stable node) merge and create an equilibrium only and then it vanishes or vice versa, as the bifurcation parameter passes its critical value.

Transcritical bifurcation

Transcritical bifurcation is a local bifurcation in which two equilibria of the system collide and interchange their stability [4]. In this case, the equilibria switch their stable behavior, one becomes unstable from stable and another becomes stable from unstable, but they never vanish together as the bifurcation parameter varies through its critical value.

Hopf bifurcation

The system undergoes Hopf bifurcation when an equilibrium of the system loses its stability as the bifurcation parameter passes its critical value [4]. In this local bifurcation, a pair of purely imaginary eigenvalues crosses the imaginary axis in the complex plane, resulting in the existence of a limit cycle. The limit cycle may be orbitally stable or unstable and accordingly, the bifurcation is called supercritical or subcritical, respectively.

Pitchfork bifurcation

Pitchfork bifurcation is a local bifurcation in which the system experiences from one equilibrium to three equilibria and vice versa as the bifurcation parameter crosses its threshold value [4]. The bifurcation is called supercritical or subcritical according to the state of the transformed single equilibrium is stable or unstable, respectively.

1.3.3 Delay Differential Equations

In virology, it is generally believed that the biological processes like the creation of infection, production of virus or activation of immune response do not happen instantaneously. Rather, it requires time to start the process and this time gap is known as a delay. A system of differential equations involving delay is called a delay differential equation (DDE) model. A general DDE can be represented as

$$\frac{dX(t)}{dt} = F(X(t), X(t-\tau)) \tag{1.3.4}$$

The rate of change of the variable X at t_0 is dependent on the values of $X(t_0)$ and $X(t_0-\tau)$. Therefore, in order to solve the corresponding initial value problem, we need the information on the entire interval $[t_0-\tau, t_0]$. Thus the initial history or initial function associated with the DDE (1.3.4) is given by the values of $X(t)$ in the interval $[t_0-\tau, t_0]$. The DDE (1.3.4) admits a unique solution for every such initial function.

In order to discuss the stability, we consider a system of first order DDEs

$$\frac{dX(t)}{dt} = CX(t) + DX(t-\tau), \tag{1.3.5}$$

where C and D are two matrices of order $n \times n$, and τ denotes the time delay. The characteristic polynomial corresponding to the system (1.3.5) is

$$\det\left(zI - C - De^{-z\tau}\right) = 0,$$

which gives

$$P(z,\tau) \equiv R(z) + S(z)e^{-z\tau} = 0, \tag{1.3.6}$$

where $R(z)$ and $S(z)$ are polynomials in z. Since, $P(z,\tau)$ is a transcendental equation in z, it has an infinite number of roots. Hence, we can not apply the Routh-Hurwitz criteria to determine the stability of the system (1.3.5). In order to study the local stability, we check the sign of the real parts of the roots of $P(z,\tau)$. If all roots are negative or have negative real parts, then the system is asymptotically stable. If there exists a purely imaginary root and it passes the imaginary axis from left to right, then the system loses its stability. Also, depending on the length of delay, the system can change its stability around the equilibrium and therefore we consider the delay as a bifurcation parameter. If a root of the characteristic polynomial changes from having negative real part to positive real part, on the variation of the length of delay, then the equilibrium loses its stability and consequently there exists a Hopf bifurcation. The conditions for the occurrence of Hopf bifurcation are stated as follows:

Theorem 1.3.15. *[39]* ***(Hopf Bifurcation Theorem)***
Let $(\overline{X},\tau_0)$ be an equilibrium point of the system (1.3.4) *and $J(\overline{X},\tau_0)$ denotes the Jacobian matrix determined at $(\overline{X},\tau_0)$ corresponding to the system* (1.3.4)*. Further, suppose that the following conditions are satisfied:*

(a) $J(\overline{X},\tau_0)$ has a simple pair of nonzero purely imaginary eigenvalues $z(\tau_0)$ and $\overline{z}(\tau_0)$, and there is no other eigenvalue with zero real part.

(b) $\dfrac{d}{d\tau}\left[Rez(\tau)\right]_{\tau=\tau_0} \neq 0.$

Then the system (1.3.4) *undergoes Hopf bifurcation around the equilibrium $(\overline{X},\tau_0)$.*

1.3.4 Reaction-Diffusion Equations

Reaction-diffusion equations are typically used in viral dynamics to capture the diffusive behavior (spatial effect) of virus particles and immune cells in the analysis of pathogen-immune interaction models. A differential equation involving a reaction term and a diffusion term is called a reaction-diffusion equation. It is a semi-linear parabolic partial differential equation. A general reaction-diffusion equation can be represented as

$$\frac{\partial U}{\partial t} = D\Delta U + F(U), \tag{1.3.7}$$

where the state variable $U = U(X,t)$ represents the density of a population at location $X \in \Omega \subset R^n$ (Ω denotes an open set) at time t. The symbol Δ denotes the Laplacian operator. The term $D\Delta U$ describes the "diffusion" with D as diffusion coefficient and $F(U)$ represents the "reaction" term. The reaction term may depend on the first derivative of U and also explicitly on X.

In order to solve a reaction-diffusion problem, we need some initial conditions as well as boundary conditions. The initial conditions refers the initial values of the population in the domain and the boundary conditions are special conditions at the boundary of the domain. The boundary conditions can be considered for a biological system such that the population does not move across the boundary of the domain. Such boundary conditions are called no-flux boundary conditions.

1.3.5 Stochastic Concepts

In recent years, the stochastic process in the modeling of a biological system are increasingly used as technology has started giving a real insight into the intra-cellular process and improvement in computational techniques are enabling the greater usage of stochastic modeling and simulation.

1.3.5.1 Stochastic Process and Brownian Motion

In the stochastic theory, random variable plays a crucial role. Before the study of the stochastic process and Brownian motion, we need to know as to what is a random variable. A random variable or stochastic variable is a variable, the possible values of which depend on the outcomes of a random phenomenon or random experiment. There are two types of random variables, namely, continuous and discrete.

Definition 1.3.16. *[86] A stochastic process or random process is a collection of random variables* $\{X(t) : t \in T\}$ *defined on a common probability space* $(\Omega, \mathcal{F}, P)$*, where* t *usually denotes time and* Ω *represents the sample space. It is said to be a continuous or discrete stochastic process if* T *is a continuous or discrete set.*

Definition 1.3.17. *[86] A stochastic process* $\{W(t) : t \in [0, \infty)\}$ *is said to be a Wiener process or standard Brownian motion, if* $W(t)$ *continuously depends on* t *and satisfies the following conditions:*

(a) *For* $0 \leq t_1 < t_2 < \infty$*, the increment* $W(t_2) - W(t_1)$ *follows normal distribution with mean zero and variance* $(t_2 - t_1)$*, that is,* $\Delta W(t) = W(t_2) - W(t_1) \sim N(0, t_2 - t_1)$.

(b) *For* $0 \leq t_0 < t_1 < t_2 < \infty$*, the increments* $W(t_1) - W(t_0)$ *and* $W(t_2) - W(t_1)$ *are mutually independent.*

(c) *The value of* $W(t)$ *at* $t = 0$ *is almost surely zero, that is, Prob* $\{W(0)=0\}=1$.

1.3.5.2 Stochastic Differential Equations

A differential equation involving a stochastic process is called stochastic differential equation (SDE), the solution of which is also a stochastic process. Generally, SDE contains a random variable such as random white noise (derivative of Brownian motion) or jump process. A general n-dimensional SDE can be expressed as

$$dX(t) = F(t, X(t))dt + G(t, X(t))dW(t) \tag{1.3.8}$$

on $t \geq t_0$, with initial condition $X(t_0) = X_0 \in \mathbb{R}^n$, where $F : \mathbb{R}^n \times [t_0, T] \to \mathbb{R}^n$, $G : \mathbb{R}^n \times [t_0, T] \to \mathbb{R}^{n\times m}$ and $W(t)$ is m-dimensional Brownian motion.

The solution of the equation (1.3.8) is given by

$$X(t) = X_0 + \int_{t_0}^{t} F(s, X(s))ds + \int_{t_0}^{t} G(s, X(s))dW(s).$$

Furthermore, suppose that $F(t, 0) = 0$ and $G(t, 0) = 0$ for all $t \geq t_0$ in the equation (1.3.8). Then the equation (1.3.8) has a solution $X(t) \equiv 0$ corresponding to initial condition $X(t_0)= 0$. This solution is called the equilibrium solution or trivial solution.

1.3.5.3 Euler-Maruyama Method

The Euler-Maruyama (EM) method [6] is a process to approximate the numerical solution of SDEs. It is a generalization of the Euler method for ordinary differential equations to SDEs. Assume that the equation (1.3.8) satisfies the following conditions:

(*a*) $\|F(t, X) - F(t, Y)\| + \|G(t, X) - G(t, Y)\| \leq L_1\|X - Y\|$, for $X, Y \in \mathbb{R}^n$, $t \in [0, T]$ and L_1 is a positive constant (Lipschitz condition) .

(*b*) $\|F(t, X)\|^2 + \|G(t, X)\|^2 \leq L_2(1 + \|X\|^2)$, for $X \in \mathbb{R}^n$, $t \in [0, T]$ and L_2 is a positive constant (Linear growth condition).

(*c*) $\|F(t, X_1) - F(t, X_2)\| + \|G(t, X_1) - G(t, X_2)\| \leq L_3|t_1 - t_2|^{\frac{1}{2}}$, for $X \in \mathbb{R}^n$, $t_1, t_2 \in [0, T]$ and L_3 is a positive constant.

Then the EM method [6] gives an approximation X_i of the exact solution $X(t)$ at the point $t = t_i$, on the interval $[0, T]$, as follows

$$X_{i+1} = X_i + F(t_i, X_i)\Delta t + G(t_i, X_i)\sqrt{\Delta t}\eta_i$$

for $i = 0, 1, \ldots, k - 1$, where $0 = t_0 < t_1 < \ldots < t_{k-1} < t_k = T$, $\Delta t = t_{i+1} - t_i = T/k$, $\eta_i \sim N(0, 1)$ and $X_0 = X(0)$. The error in the EM method is given by

(*a*) $E\big(\|X(t_i) - X_i\|^2 \mid X(t_{i-1}) = X_{i-1}\big) = O((\Delta t)^2)$.

(*b*) $E\big(\|X(t_i) - X_i\|^2 \mid X(0) = X_0\big) = O(\Delta t)$.

1.4 Literature Review

A 2017 dossier of World Health Organization (WHO) [85] reported that approximately 71 million individuals are infected with chronic HCV infection, with an estimated 399 thousand fatalities happening in 2016, mostly from late chronic phase complications such as liver cirrhosis and HCC attributable to HCV infection. Roe and Hall [99] reported that $50-80\%$ of HCV infections progress to the chronic phase, of which $20-30\%$ may develop liver cirrhosis and 5% results in HCC. In a recent study, Aisyah et al. [1] estimated that 19.8% of HCV infected individuals spontaneously cleared the virus from their body within 3 months, 27.9% cleared within 6 months, 36.1% within 12 months and 37.1% achieved the clearance within 24 months.

Mathematical modeling has proven to provide quantitative as well as qualitative analysis and significant insights into the understanding of infection mechanism and control. The basic HCV models were formulated using the ordinary differential equations, usually comprising of three populations, namely, uninfected cells, infected cells and virions, as model variables. One of the earlier models for quantitative analysis of HCV infection, proposed by Neumann et al. [81] based on similar models for HIV and hepatitis B virus (HBV) dynamics, was on the in-vivo dynamics of HCV progression. This model incorporated the role of single antiviral therapy using interferon-α (IFN-α) in the model formulation and demonstrated the effect of IFN-α in the reduction of HCV RNA load. The analysis of the model suggested that IFN is more effective in the blocking of HCV production as compared to its effectiveness in the reduction of viral infection. An improved model developed by Dixit et al. [28], incorporating the combination antiviral therapy of pegylated IFN and ribavirin, examined the effect of combination therapy in HCV infection. The analysis was based on clinical observations, which showed that administration of the combination therapy has a significant therapeutic effect in the reduction of HCV infection as well as in viral load decline, while the monotherapy with ribavirin is not sustainable. Dahari et al. [22] modified the basic model by including the concept of the homeostatic mechanism of the liver in the modeling. This model captured the proliferation of hepatocytes up to a maximum size due to a limitation of the volume of the liver. The model exhibited the biphasic as well as triphasic decline patterns in HCV RNA load, whereas a rapid HCV decay was observed in the first phase. However, in cases of partial response, the relapse in combination therapy resulted in the rebound of viral load to its baseline value. In addition, the model was able to determine a critical measure of the dosage of the combination drug. It was observed that the patients attained eventual clearance of HCV by taking the dosage higher than its critical measure, but they progressed to the chronic stage after getting an initial response in case of lower dosage prescribed. A

further modified model for HCV dynamics [24], comprising of logistic growth terms for both the healthy and infected hepatocytes, detailed the role of ribavirin over the time passed. The analysis of the model suggested that the triphasic viral decline occurs only in case of patients for whom a significantly major proportion of healthy hepatocytes being initially infected. Perelson et al. [90] discussed the pharmacokinetics of antiviral treatment for HCV infection and observed the decay pattern of HCV RNA. The model considered the efficacy of combination drug as a function of drug concentration, which was able to estimate the decay rates of viruses and infected cells. The complexity of HCV kinetics including the sustained virological response (SVR) and clinical observations for the long-term result was analyzed in [104], by estimating the parameters with the prediction of viral extinction threshold. The phenomenon of bistability in HCV model under certain physiological conditions was observed in [26]. The understanding of the behavior of HCV, particularly the mechanism of virus-host interplay during the period of infection becoming chronic is somewhat limited. A mathematical study for this was presented in [23], which provided the quantitative analysis capturing various aspects such as the kinetics of HCV RNA and alanine aminotransferase (ALT) serum. The results showed that the production of virions in the early stage could be inhibited by endogenous type I interferon. Reluga et al. [96] analyzed the dynamics of post-therapeutic progression of HCV RNA through mathematical modeling, that realistically encapsulated the large set of clinical observations.

The investigation of the role of the immune response in the modeling of viral dynamics is essential as the entry of pathogens into body results in stimulation of the immune system. Nowak and Bangham [83] discussed the relationship between the immune response and viral particles, such as viral load and diversity, by including the effect of CTLs to a basic viral dynamics model. The effect of the immune response was predicted by fitting the data from the patients infected with human immunodeficiency virus type 1 (HIV-1) and human T cell leukemia virus type 1 (HTLV-1). Wodarz [126] developed a virus-immune interaction model to study the evolution of the virus and disease progression. The model examined the role of CTL and antibody responses in HCV infection during its acute and chronic phases. The action of CTL was considered to reduce the HCV infection, while the antibody was involved to neutralize the HCV RNA. The study established the correlation between the CTL and antibody in the context of chronic HCV infection. It was observed that the slow activation of CTL is unable to clear the virus, which leads to the pathological condition. Otherwise, the infection would be asymptotic in case of strong response from CTL. The stability of the model in [126] was investigated under the condition on basic reproduction number (with and without the inclusion of therapeutic efficacy) in [73, 137]. Neumann et al. [82] investigated the role of antibody in blocking the HBV and hepatitis B surface antigen

(HBsAg). Further, Wodarz [127] extensively reviewed the significance of lytic and non-lytic immune response to virus infection. The role of the lytic immune response was assumed to reduce the virus-infected cells, while the non-lytic immune cells were involved in blocking the proliferation of viruses without affecting the infected cells. The study elaborately explained the complex interplay between these two immune responses and predicted the states whether the infection would be an asymptotic or a pathological condition in case of HCV patients. Li et al. [64] proposed a complex model to illustrate the role of antigen-presenting cells (APCs) such as dendritic cells (DCs) with the effect of CTL response. The model assumed that CTL is expanded through the cross-presentation of activated DC and reduced by a direct presentation of infected cells. The results indicated that the activation of the immune response could be dependent on the initial level of DC and CTL. However, the understanding of the mechanism of cellular and humoral responses is limited by the means of its effectiveness in acutely infected HCV patients [107].

Further, the non-cytolytic "cure" process in which the infected cells get cured and convert to healthy ones was observed in case of HCV infection [23, 96]. The "cure" rate of infected cells to the mathematical modeling of viral dynamics was introduced in [21, 60, 111]. A generalized viral dynamics model with nonlinear incidence function, which accommodated the "cure" rate, was analyzed in [43]. The inclusion of "cure" rate to the viral model was motivated by the possibility of a "cure" for infected hepatocytes in case of HBV patients, due to noncytolytic process resulting in loss of covalently closed circular DNA (cccDNA) from their nucleus [38]. The authors mentioned that such a "cure" is unlikely to happen in some cases such as HIV infection. The happening of such a non-cytolytic "cure" does have its advantages, that the process of viral infection gets slowed down, which results in better prognosis for patients.

Timpe et al. [107] recently observed that HCV infection can spread not only by virus-to-cell (cell-free) mode, but also through cell-to-cell mode of transmission. Rather, the cell-to-cell spread is more proliferous, owing to many factors involved in cell-free transmission, like delay in the life cycle of virus and action of immune responses against the virions [107]. Xiao et al. [130] examined the effect of cell-to-cell transmission for DAA-resistant HCV and showed that the cell-to-cell transmission is the main factor in spread of DAA-resistant HCV and thus it prevents the virus from eradication. It was also observed that host-targeting entry inhibitor (HTEI) has an essential impact in reducing the cell-to-cell transmission rate. The modeling and quantitative analysis of cell-to-cell transmission in case of other viral diseases like HIV infection were studied in [57, 63]. With the consideration of logistic growth for target cells, the cell-to-cell transmission for viral spreading was taken into account in [57, 63]. Lai and Zou [57] demonstrated the effect of cell-to-cell mode of infection in HIV patients by

comparing the basic reproduction number for the models incorporating or excluding cell-to-cell transmission. Hattaf and Yousfi [42], proposed and analyzed a fairly generalized model incorporating both virus-to-cell and cell-to-cell modes of viral transmission with general incidence function.

The optimal treatment policy was determined for HCV model with combination therapy of IFN and ribavirin in [16, 17]. Estimating the parameters using Latin hypercube sampling technique, Pachpute and Chakrabarty [87, 88] optimized the therapeutic efficacy of combined therapy in HCV infection by mathematical modeling incorporating the proliferation terms for both uninfected and infected hepatocytes. Mojaver and Kheiri [77] optimized the treatment policy of a combined antiviral therapy by the means of mathematical modeling taking cell-to-cell transmission into account for HCV infection.

Moreover, from the biological perspective, the incorporation of intracellular and immune delay in the virus-immune interaction model is more realistic when it comes to analyzing the dynamics. The intracellular delay refers to the time needed for the cells to be infected or for the reproduction of viruses, and the immune delay means the time needed for antigenic stimulation for the development of immune cells, especially B cells or T cells in case of antibody response or CTL response, respectively. The intracellular delay was introduced in an HCV model addressing the role of CTL and antibody response in [141]. Wu et al. [128] reviewed an HBV model by differentiating the infected cells into two categories, latently and actively infected cells, under the delay in the humoral immune response. The existence of a Hopf bifurcation in a general viral dynamics model comprising the delay in humoral immune was observed by Wang et al. [122]. The effect of the various intracellular delays on the dynamics of other viral infections (like HBV, HIV infection), incorporating both virus-to-cell and cell-to-cell transmissions, was studied in [48, 117, 136]. The delay in the latent period of infected cells inducing stability switches, bubbles and chaos in case of the HCV model are illustrated in [140]. The delay dynamics for a fairly generalized viral model incorporating several factors such as viral and cellular transmissions, as well as three delays associated with both transmission modes and the cell-mediated immune response, was extensively studied in [19]. The results showed that the delays could lead to stability switches and occurrence of bifurcating periodic solution, depending upon the intrinsic rate of logistic growth and infection transmission rate as well.

Viral dynamics modeling which considered the spatial mobility into account, consists of partial differential equations, incorporating the motion of viruses (following Fickian diffusion) [116]. Also, it is noted in [120, 132] that the host cells or hepatocytes do not exhibit diffusive behavior. Wang and Wang [120] considered a simple HBV model comprising of uninfected cells, infected cells and virions, and analyzed the dynamics with spatial mobility of virions

under one-dimensional spatial domain, and this work was extended by Brauner et al. [13] by assuming the spatial domain being two-dimensional, specifically square with a periodic boundary condition. Later, Wang et al. [116] argued that the realistic spatial domain for a biological system should be bounded, but it is not a square. These models were studied under a general bounded domain having a smooth boundary, with a zero-flux boundary condition. Further, a diffusive model consisting of virions and immune cells [11, 12], was discussed to observe the interplay between the virus and immune system by assuming the diffusion of both populations. Recently, Wang and Ma [124] studied a nonlocal reaction-diffusion model containing the delay in transmission of HCV infection under an unbounded spatial domain, which captures the effect of high-mobility group box 1 (HMGB1) in blocking of HCV. A diffusive HBV model which considered the spatial diffusion of both HBV and HBV DNA-containing capsids was studied using a non-standard finite difference (NSFD) scheme in [71]. The global dynamics of a diffusive virus model includes cell-to-cell transmission with spatial heterogeneity was studied in [118]. Yang et al. [135] proposed a diffusive virus dynamics model by considering both modes of infection spread and examined the global stability of the equilibria after discretizing the model by using NSFD scheme. Xu and Ma [132] investigated the local and global stability for a spatial diffusion HBV model containing an intracellular delay in Holling type-II transmission rate. Wang and Ma [123] analyzed a nonlocal delayed diffusive model attributed to HIV dynamics with Beddington-DeAngelis type infection transmission function.

There is a keen interest in stochastic modeling for virus dynamics as deterministic models are somewhat limited when it comes to providing sufficient insights into the understanding of the kinetics of the virus and the complex immune system. Moreover, there are cases where a stochastic model can better predict the variability and uncertainty of dynamics, and also provide idea about the disease extinction in finite time [5, 6, 7]. Due to random fluctuations in the environmental parameters, like humidity and temperature fluctuations, several epidemic models of infectious disease, were proposed and analyzed based on the stochastic approaches in [5, 56, 61, 98]. In order to address randomness in the modeling, different stochastic approaches such as parameter perturbation technique [61, 86] and continuous-time Markov chain (CTMC) approximation [2, 3, 56, 113, 115, 139] are typically implemented. Very little work on stochastic analysis of viral disease, particularly for HCV dynamics are available in literature. The complex mechanism of the virus-immune interaction process, intercellular and intracellular processes such as birth and death of cells, leads to stochastic modeling in virology. Chakrabarty and Murray [18] estimated the likelihood of progression of HCV infection from the initial stage to the development of HCC through a stochastic approach. Imran et al. [51] studied a CTMC model for epidemic-analysis of HCV infection.

1.5 Motivation and Objectives

The existing work in literature typically analyzed the dynamics of HCV infection by taking the only virus-to-cell mode of infection transmission into account and rarely incorporated the "cure" case of infected cells. The importance of the immune system on HCV infection is mainly investigated by including the role of T cells, but the effect of B cells is examined only in a few articles [73, 126, 127, 137] which considered only the virus-to-cell mode and without the case of "cure" for the infected cells. However, in the case of HCV infection, a realistic model should consider the cell-to-cell transmission along with the case of "cure" for the infected cells. In HCV dynamics, the cell-to-cell mode appears in [77], while the "cure" case of infected cells is included in [23, 96] with both being considered in [42]. However, none of these work factor in the impact of the immune system. Although the role of the cellular immune response [19] and the humoral immune response [31] was incorporated with both transmission modes in case of HIV dynamics, the "cure" case of infected cells was not considered. Instead, the delay dynamics of the model was analyzed. Further, a general virus-immune interaction model incorporating the effect of the immune response with the "cure" rate was studied by considering only virus-to-cell mode in [29]. It is observed that none of these HCV models with the cell-to-cell transmission has investigated the role of the immune system.

Hence, we are interested in studying the within-host HCV dynamics incorporating the role of the humoral immune response, where both virus-to-cell and cell-to-cell modes along with the non-cytolytic "cure" process of infected cells is also included. Moreover, from the epidemiological perspective, it should be investigated whether the humoral immune delay can disturb the behavior of the dynamical system. Further, it would also be interesting to observe as to what would happen when the mobility of the virus or immune cell is considered into the dynamics. In addition, sometimes deterministic models are not sufficient in understanding the viral dynamics, due to the random behavior of virus and the complex mechanism of the immune system. Besides, the consideration of a stochastic model could lead to the chance of disease extinction in finite time. Accordingly, we further study the stochastic modeling of within-host HCV dynamics.

The main objectives of this thesis are synopsized as follows:

- To present and analyze a mathematical model for HCV dynamics incorporating both virus-to-cell and cell-to-cell transmissions with the cure rate in infected hepatocytes accompanied by the humoral immune response, through a system of coupled ordinary differential equations (ODEs).

- To observe the effect of delay in the generation of humoral immune cells on the dynamics of HCV infection with both modes of transmission and cure rate, by considering a delay differential equation (DDE) model.
- To study a reaction-diffusion partial differential equation (PDE) model for HCV dynamics with general virus transmission functions, under a suitable spatial domain by assuming that the motion of virions, as well as the immune cells, follow the Fickian diffusion.
- To derive and analyze stochastic differential equation (SDE) models and continuous-time Markov chain (CTMC) models for HCV dynamics, with the consideration of both processes for the release of virions, namely, budding and bursting.

1.6 Thesis Outline

This thesis on the deterministic as well as stochastic modeling and analysis of HCV dynamics is divided into six chapters as follows:

Chapter 1 addresses the biological background and mathematical preliminaries to be adopted in the subsequent part of this thesis. In addition, the literature review on the analysis and outcomes of various HCV modeling, is also presented.

In Chapter 2, we present a mathematical model for HCV dynamics incorporating cell-to-cell transmission and non-cytolytic cure in the environment of the humoral immune response. The uniqueness, non-negativity and boundedness of the solution to the model are justified. The local as well as global stability conditions of the three non-negative equilibria for the model system is determined in terms of the basic reproduction number and the humoral immune reproduction number. The analytical results obtained are numerically verified and discussed. Furthermore, several numerical illustrations are performed to support the theoretical results, as well as to observe the various dynamics such as the effect of some sensitive parameters.

In Chapter 3, we introduce the humoral immune delay for the development of B cells and investigate the effect of this delay on the dynamics of the model. We check the properties of the solution to this delay model. The local and global stability of the boundary equilibria is examined theoretically, as well as numerically, under conditions on the basic reproduction number and the humoral immune reproduction number. The conditions for the existence of Hopf bifurcation around the interior equilibrium are determined. A number of numerical computations are performed to support the analytical results obtained, as well as to describe the various scenarios depending upon the value of time delay.

Chapter 4 describes the dynamics after the incorporation of diffusive motion for virions and immune B cells along with the consideration of general nonlinear incidence functions for virus-to-cell as well as cell-to-cell transmissions. The properties of the solution to this PDE driven model are examined. The conditions for the existence as well as the global stability of the possible non-negative equilibria for the model are determined. Further, the numerical illustration of the analytical findings are presented for the case of bilinear as well as Holling type-II incidence functions in a one-dimensional spatial domain.

In Chapter 5, we formulate SDE and CTMC models for the budding and bursting process, based on the possible state changes in the variables of the deterministic model. The bursting process is discussed with the case of fixed as well as variable burst size. The forward Kolmogorov equations and the moment equations for the SDE model variables are derived in order to know the distribution pattern of the model variables. A number of numerical simulations and discussion on the results obtained from the SDE and CTMC models are presented.

Finally, Chapter 6 summarizes the conclusions of the work carried out in this thesis along with the possible directions of future work.

It is noted that all the numerical simulations presented in this thesis were carried out using MATLAB®.

Chapter 2

Modeling and Analysis of HCV Dynamics Incorporating Cell-to-Cell Transmission and Non-cytolytic Cure with Humoral Immune Response

The basic models for HCV dynamics [22, 24, 26, 28, 81, 90, 104] usually comprises of three populations, namely, uninfected hepatocytes, infected hepatocytes and virions. These models analyzed the progression of HCV infection, considering the virus-to-cell mode of infection spread. Some models [64, 73, 126, 127] studied the nature of several immune cells in chronic HCV infection, but it is not adequately understood due to the complex mechanism of the immune system in the body. Recent studies of hepatological conditions [107, 130] suggested that HCV-infected hepatocytes can infect the associated uninfected or healthy hepatocytes, and consequently the HCV infection can spread in the liver through virus-to-cell transmission as well as cell-to-cell transmission. Further, in the study on HCV infection [23, 96], it was observed that few infected hepatocytes spontaneously clear the HCV particles through a non-cytolytic process in its chronic phase and then they become healthy afresh. This phenomenon is known as "non-cytolytic cure" or "cure" of infected hepatocytes.

In this chapter [1], we present a mathematical model for HCV dynamics in the environment of humoral immune response with some important factors attributed to HCV infection, such as cell-to-cell transmission, along with virus-to-cell transmission and non-cytolytic cure. We establish the uniqueness, non-negativity and boundedness of the solutions to the system in order to justify the feasibility of the proposed model. The local as well as global stability analysis of the possible equilibria for the system is investigated. In order to prove the

[1]The presentation in this chapter is based on the article: "Sonjoy Pan and Siddhartha P. Chakrabarty. Threshold dynamics of HCV model with cell-to-cell transmission and a non-cytolytic cure in the presence of humoral immunity. *Commun. Nonlinear Sci. Numer. Simul.* 61 (2018): 180-197".

global stability, we use the method of Lyapunov functional. Furthermore, several numerical simulations are performed to support our theoretical results, as well as to observe the various dynamics. A numerical comparison of dynamics for various HCV models along with the discussion on the dynamical effect of some sensitive parameters is presented.

2.1 Mathematical Model

It is seen in the literature that a few HCV models [73, 126, 127, 137] have addressed the role of the immune system on the dynamics. The importance of the humoral immune response in HCV infection was reported in [14]. The humoral immunity mainly consists of B lymphocytes or B cells which secrete antibodies which exist in humors or body fluids. Further, the cell-to-cell mode of infection transmission is rarely considered in the existing modeling of HCV dynamics. It is also believed that the non-cytolytic cure process also occurs in case of HCV patients [23, 96]. Accordingly, we present a mathematical model to analyze the HCV dynamics incorporating various aspects such as virus-to-cell as well as cell-to-cell transmission and non-cytolytic cure rate with the role of B cells (antibody response) as the activation of the humoral immunity, which is governed by a coupled of ODEs as follows:

$$\begin{aligned}
\frac{dU(t)}{dt} &= \lambda - \beta_1 U(t)V(t) - \beta_2 U(t)I(t) - d_1 U(t) + \alpha I(t),\\
\frac{dI(t)}{dt} &= \beta_1 U(t)V(t) + \beta_2 U(t)I(t) - d_2 I(t) - \alpha I(t),\\
\frac{dV(t)}{dt} &= kI(t) - d_3 V(t) - pV(t)B(t),\\
\frac{dB(t)}{dt} &= cV(t)B(t) - d_4 B(t).
\end{aligned} \tag{2.1.1}$$

Here $U(t)$, $I(t)$, $V(t)$ and $B(t)$ represent the concentrations of the uninfected hepatocytes, infected hepatocytes, virions and B cells (antibodies) at time t, respectively. It is assumed that the uninfected hepatocytes are generated from the source within human liver at a constant rate λ, with the natural death rate being d_1 per cell. The uninfected hepatocytes are being infected at rates of β_1 per virion per uninfected hepatocyte and β_2 per both hepatocytes, using virus-to-cell and cell-to-cell modes, respectively. The infected hepatocytes are decaying from the natural death at a rate d_2 per cell, and also being cured and converted to uninfected ones at a rate α per infected hepatocyte, resulting from the non-cytolytic process. The virions are produced from the infected hepatocytes at a rate k per infected hepatocyte and are cleared at a rate d_3 per virion. Subsequent to the entry of the virions, the humoral immune response stimulates B cells to produce antibodies at a rate c per virion per cell, which in turn decays at a rate d_4 per cell. The virions get neutralized resulting from

the effect of B cells at a rate p per virion per cell. The schematic representation of the model (2.1.1) is presented in Figure 2.1. From the biological perspective, we consider all the model parameters to be positive. Accordingly, the initial condition for the system (2.1.1) is taken as $(U(0), I(0), V(0), B(0)) \in \mathbb{R}^4_{+0}$, where $\mathbb{R}^4_{+0} = \{(x_1, x_2, x_3, x_4) \in \mathbb{R}^4 \mid x_i \geq 0,\ i = 1, 2, 3, 4\}$.

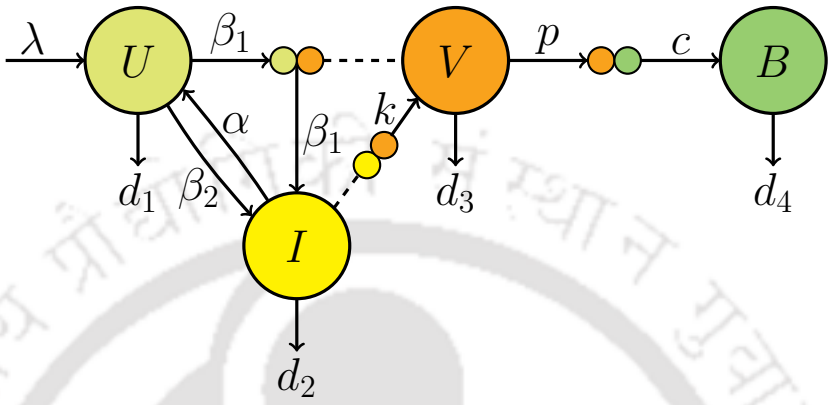

Figure 2.1: Schematic representation of the mathematical model (2.1.1).

2.2 Non-negativity and Boundedness of Solution

In this section, we check the nature of the solution to the system (2.1.1) with initial condition in $\mathbb{R}^4_{+0}$. We establish the uniqueness, non-negativity and boundedness of the solution to the system (2.1.1) in the following theorem:

Theorem 2.2.1. *The system (2.1.1) with the initial condition in $\mathbb{R}^4_{+0}$ possesses unique, non-negative and uniformly ultimately bounded solution. Furthermore, there exists an $\epsilon > 0$ such that $\liminf_{t\to\infty} U(t) \geq \epsilon$.*

Proof. The right-hand side of the system (2.1.1) is continuous and Lipschitz on $[0, a],\ a > 0$. Therefore, the system (2.1.1) with the initial condition $(U(0), I(0), V(0), B(0)) \in \mathbb{R}^4_{+0}$ has a unique solution $(U(t), I(t), V(t), B(t))$.

In order to prove the non-negativity of the solution to the system (2.1.1), we adopt the approach in [10, 125]. From the first three equations of the system (2.1.1), we obtain,

$$\left.\frac{dU}{dt}\right|_{U=0} = \lambda + \alpha I, \quad \left.\frac{dI}{dt}\right|_{I=0} = \beta_1 UV, \quad \left.\frac{dV}{dt}\right|_{V=0} = kI.$$

Suppose that the relation $\left.\frac{dV(t)}{dt}\right|_{V(t)=0} \geq 0$ does not hold for some $t > 0$, that is, there exists a $t_V > 0$ such that

$$t_V = \inf\left\{t \mid V(t) = 0,\ \frac{dV(t)}{dt} < 0,\ t > 0\right\}.$$

Therefore, $\left.\frac{dV(t_V)}{dt}\right|_{V(t_V)=0} = kI(t_V) < 0$. We now define

$$t_I = \inf\left\{t \mid I(t) = 0,\ \frac{dI(t)}{dt} < 0,\ t > 0\right\}.$$

It is clear that $t_I < t_V$. Hence, $\left.\frac{dI(t_I)}{dt}\right|_{I(t_I)=0} = U(t_I)V(t_I) < 0$, which implies that $U(t_I) < 0$, since $V(t_I) > 0$. We further define

$$t_U = \inf\left\{t \mid U(t) = 0,\ \frac{dU(t)}{dt} < 0,\ t > 0\right\}.$$

It follows that $t_U < t_I < t_V$. We observe that $\left.\frac{dU(t_U)}{dt}\right|_{U(t_U)=0} = \lambda + \alpha I(t_U) > 0$, since $I(t_U) > 0$, which is a contradiction to the definition of t_U itself. Therefore, $\left.\frac{dV}{dt}\right|_{V=0} \geq 0$ and hence, $V(t) \geq 0$ for all $t > 0$. Consequently, $I(t) \geq 0$ as well as $U(t) \geq 0$ for all $t > 0$. Finally, from the last equation of the system (2.1.1), we have

$$B(t) = B(0)\exp\left\{\int_0^t [cV(s) - d_4]ds\right\} \geq 0,$$

for all $t \geq 0$. Hence the non-negativity of the solution $(U(t), I(t), V(t), B(t))$ with the initial condition in $\mathbb{R}^4_{+0}$ is guaranteed.

In order to establish the boundedness of the solution to the system (2.1.1), we adopt the approach in [63, 70]. Accordingly, we now define two new variables

$$Y(t) = U(t) + I(t) \quad \text{and} \quad Z(t) = V(t) + \frac{p}{c}B(t).$$

From the first two equations of (2.1.1), we obtain

$$\frac{dY(t)}{dt} = \lambda - d_1U(t) - d_2I(t) \leq \lambda - d_YY(t),$$

where $d_Y = \min\{d_1, d_2\}$. Therefore $\limsup_{t\to\infty} Y(t) \leq \frac{\lambda}{d_Y}$. Further, from the last two equations of (2.1.1), we obtain

$$\frac{dZ(t)}{dt} = kI(t) - d_3V(t) - \frac{d_4p}{c}B(t) \leq kI(t) - d_ZZ(t),$$

where $d_Z = \min\{d_3, d_4\}$. Therefore, $\limsup_{t\to\infty} Z(t) \leq \frac{\lambda k}{d_Yd_Z}$. Hence the solution of system (2.1.1) with non-negative initial condition is uniformly ultimately bounded and belongs to the following closed and bounded positively invariant set

$$\mathcal{D} = \left\{\big(U(t), I(t), V(t), B(t)\big) \in \mathbb{R}^4_+ \mid 0 \leq U(t), I(t) \leq \frac{\lambda}{d_Y};\ 0 \leq V(t) \leq \frac{\lambda k}{d_Yd_Z};\ 0 \leq B(t) \leq \frac{c\lambda k}{pd_Yd_Z}\right\}.$$

Furthermore, from the first equation of the system (2.1.1), we obtain

$$\begin{aligned}\frac{dU(t)}{dt} &\geq \lambda - \beta_1 U(t)V(t) - \beta_2 U(t)I(t) - d_1 U(t)\\ &\geq \lambda - (d_1 + \beta_1 V_u + \beta_2 I_u)\, U(t), \text{ for a large } t,\end{aligned}$$

where $I_u = \frac{\lambda}{d_Y}$ and $V_u = \frac{\lambda k}{d_Y d_Z}$ are the upper bounds of $I(t)$ and $V(t)$, respectively. Therefore,

$$\liminf_{t\to\infty} U(t) \geq \frac{\lambda}{d_1 + \beta_1 V_u + \beta_2 I_u}.$$

This implies that there exists an $\epsilon > 0$ such that $\liminf_{t\to\infty} U(t) \geq \epsilon$. □

2.3 Existence and Stability of Equilibria

The system (2.1.1) admits three equilibria, namely,

1. The infection-free equilibrium, $E_0 = (U_0, I_0, V_0, B_0)$, where

$$U_0 = \frac{\lambda}{d_1} \text{ and } I_0 = V_0 = B_0 = 0.$$

2. The immune-free infected equilibrium, $E_1 = (U_1, I_1, V_1, B_1)$, where

$$U_1 = \frac{d_3(d_2+\alpha)}{\beta_1 k + \beta_2 d_3}, \quad I_1 = \frac{d_1 U_1}{d_2}\left[\frac{\lambda(\beta_1 k + \beta_2 d_3)}{d_1 d_3 (d_2+\alpha)} - 1\right], \quad V_1 = \frac{k}{d_3} I_1 \text{ and } B_1 = 0.$$

3. The immune-activation infected equilibrium, $E^* = (U^*, I^*, V^*, B^*)$, where

$$U^* = \frac{(d_2+\alpha)I^*}{\beta_1 V^* + \beta_2 I^*}, \quad I^* = \frac{-m_2 + \sqrt{m_2^2 + 4m_1 m_3}}{2m_1}, \quad V^* = \frac{d_4}{c} \text{ and } B^* = \frac{d_3}{p}\left(\frac{ck}{d_3 d_4} I^* - 1\right),$$

with

$$m_1 = \beta_2 c d_2, \quad m_2 = \beta_1 d_2 d_4 + c d_1 (d_2+\alpha) - \lambda\beta_2 c \text{ and } m_3 = \lambda\beta_1 d_4.$$

In order to determine the expression of the basic reproduction number, we apply the next generation method [44, 109]. Accordingly, we write the equations associated with infection:

$$\begin{aligned}\frac{dI}{dt} &= \beta_1 UV + \beta_2 UI - d_2 I - \alpha I = \mathcal{F}_1 - \mathcal{V}_1,\\ \frac{dV}{dt} &= kI - d_3 V - pVB = \mathcal{F}_2 - \mathcal{V}_2,\end{aligned}$$

where $\mathcal{F}_1 = \beta_1 UV + \beta_2 UI,\ \mathcal{V}_1 = d_2 I + \alpha I,\ \mathcal{F}_2 = 0,\ \mathcal{V}_2 = d_3 V + pVB - kI$. Hence

$$\mathcal{F} = \begin{pmatrix} \frac{\partial \mathcal{F}_1}{\partial I}\Big|_{E_0} & \frac{\partial \mathcal{F}_1}{\partial V}\Big|_{E_0} \\ \frac{\partial \mathcal{F}_2}{\partial I}\Big|_{E_0} & \frac{\partial \mathcal{F}_2}{\partial V}\Big|_{E_0} \end{pmatrix} = \begin{pmatrix} \frac{\lambda\beta_2}{d_1} & \frac{\lambda\beta_1}{d_1} \\ 0 & 0 \end{pmatrix},$$

$$\mathcal{V} = \begin{pmatrix} \frac{\partial \mathcal{V}_1}{\partial I}\Big|_{E_0} & \frac{\partial \mathcal{V}_1}{\partial V}\Big|_{E_0} \\ \frac{\partial \mathcal{V}_2}{\partial I}\Big|_{E_0} & \frac{\partial \mathcal{V}_2}{\partial V}\Big|_{E_0} \end{pmatrix} = \begin{pmatrix} d_2 + \alpha & 0 \\ -k & d_3 \end{pmatrix}.$$

The basic reproduction number R_0 is given by $R_0 = \rho(\mathcal{F}\mathcal{V}^{-1})$, where $\rho(A)$ is the spectral radius of the matrix A, which in this case is given by

$$R_0 = \frac{\lambda(\beta_1 k + \beta_2 d_3)}{d_1 d_3 (d_2 + \alpha)} = \frac{k\beta_1 U_0}{d_3(d_2+\alpha)} + \frac{\beta_2 U_0}{d_2 + \alpha} = R_{01} + R_{02},$$

where $R_{01} = \dfrac{k\beta_1 U_0}{d_3(d_2+\alpha)}$ and $R_{02} = \dfrac{\beta_2 U_0}{d_2+\alpha}$. Biologically, R_{01} and R_{02} are the basic reproduction number corresponding to the virus-to-cell and cell-to-cell transmissions, respectively [19]. Since U_0 is total number of uninfected hepatocytes in an infection-free environment and k is the production rate of virions per infected hepatocyte which remains infectious for a period of $\frac{1}{d_2+\alpha}$, therefore the average number of virions produced by an infected hepatocyte during its infectious period is $\frac{1}{d_2+\alpha}$. Moreover, each virion infects $\beta_1 U_0$ hepatocytes per unit time and $\frac{1}{d_3}$ is the average lifespan of a virion, therefore quantity R_{01} represents the average number of secondary infected hepatocytes produced by a virion. Similarly, R_{02} represents the average number of secondary infected hepatocytes produced by an infected hepatocyte.

For potential humoral immune response, we have, $cV_1 > d_4$ [126]. Accordingly, we define the humoral immune reproduction number as

$$R_H = \frac{ck\lambda(\beta_1 k + \beta_2 d_3)}{ckd_1 d_3(d_2+\alpha) + d_2 d_3 d_4(\beta_1 k + \beta_2 d_3)},$$

which represents the average number of secondary infected hepatocytes produced in presence of the humoral immune response.

Lemma 2.3.1. *Suppose* $R_1 = \dfrac{ck}{d_3 d_4} I^*$. *Then (i)* $R_1 > 1 \iff R_H > 1$, *(ii)* $R_1 = 1 \iff R_H = 1$ *and (iii)* $R_1 < 1 \iff R_H < 1$.

Proof. (i) We have

$$R_1 > 1 \iff I^* > \frac{d_3 d_4}{ck} \iff \frac{-m_2 + \sqrt{m_2^2 + 4m_1 m_3}}{2m_1} > \frac{d_3 d_4}{ck}.$$

This is equivalent to

$$R_1 > 1 \iff \left(m_2{}^2 + 4m_1 m_3\right) - \left(\frac{2m_1 d_3 d_4}{ck} + m_2\right)^2 > 0.$$

Simplifying the inequality, we can write

$$R_1 > 1 \iff \frac{4\beta_2 d_2 d_4}{k^2}[ckd_1d_3(d_2+\alpha) + d_2d_3d_4(\beta_1 k + \beta_2 d_3)]\,(R_H - 1) > 0.$$

Therefore $R_1 > 1 \iff R_H > 1$. We can prove (ii) and (iii) using a similar argument. □

We notice that $R_H < R_0$. Further, $\frac{ck}{d_3 d_4} I^* > 1$ if $R_H > 1$ (using Lemma (2.3.1)). It is easily seen that the infection-free equilibrium E_0 exists unconditionally, the immune-free infected equilibrium E_1 exits provided $R_0 > 1$ and the immune-activation infected equilibrium E^* exits provided $R_H > 1$.

The expressions for R_0 and R_H under various conditions on β_2 and α, are given in Table 2.1. It is observed that $R_0(0,\alpha) < R_0(0,0) < R_0(\beta_2,0)$, $R_0(0,\alpha) < R_0(\beta_2,\alpha) < R_0(\beta_2,0)$ and $R_H(0,0) > R_H(0,\alpha)$, $R_H(\beta_2,0) > R_H(\beta_2,\alpha)$, $R_H(0,0) < R_H(\beta_2,0)$, $R_H(0,\alpha) < R_H(\beta_2,\alpha)$. Hence the value of R_0 increases with the incorporation of the cell-to-cell transmission and decreases with the consideration of non-cytolytic cure rate in the model.

β_2	α	$R_0(\beta_2,\alpha)$	$R_H(\beta_2,\alpha)$
$\beta_2 = 0$	$\alpha = 0$	$\frac{\lambda\beta_1 k}{d_1 d_2 d_3}$	$\frac{c\lambda\beta_1 k}{d_2 d_3 (cd_1 + \beta_1 d_4)}$
$\beta_2 = 0$	$\alpha > 0$	$\frac{\lambda\beta_1 k}{d_1 d_3 (d_2+\alpha)}$	$\frac{c\lambda\beta_1 k}{cd_1 d_3 (d_2+\alpha) + \beta_1 d_2 d_3 d_4}$
$\beta_2 > 0$	$\alpha = 0$	$\frac{\lambda(\beta_1 k + \beta_2 d_3)}{d_1 d_2 d_3}$	$\frac{ck\lambda(\beta_1 k + \beta_2 d_3)}{ckd_1 d_2 d_3 + d_2 d_3 d_4 (\beta_1 k + \beta_2 d_3)}$
$\beta_2 > 0$	$\alpha > 0$	$\frac{\lambda(\beta_1 k + \beta_2 d_3)}{d_1 d_3 (d_2+\alpha)}$	$\frac{ck\lambda(\beta_1 k + \beta_2 d_3)}{ckd_1 d_3 (d_2+\alpha) + d_2 d_3 d_4 (\beta_1 k + \beta_2 d_3)}$

Table 2.1: Expressions of R_0 and R_H under various conditions on β_2 and α.

2.3.1 Local Stability Analysis

In order to analyze the local stability of the equilibria, we apply the Routh-Hurwitz criteria [2]. Accordingly, we linearize the system (2.1.1), which results in the following Jacobian matrix

$$\begin{bmatrix} -\beta_1 V - \beta_2 I - d_1 & -\beta_2 U + \alpha & -\beta_1 U & 0 \\ \beta_1 V + \beta_2 I & \beta_2 U - d_2 - \alpha & \beta_1 U & 0 \\ 0 & k & -d_3 - pB & -pV \\ 0 & 0 & cB & cV - d_4 \end{bmatrix}.$$

Further, we will need the following arithmetic mean-geometric mean (AM-GM) inequality to establish results for the local stability as well as global stability: If $x_i \geq 0,\ i = 1, 2, \ldots n$, it follows from the AM-GM inequality that

$$\frac{1}{n}\left(\sum_{i=1}^{n} x_i\right) \geq \left(\prod_{i=1}^{n} x_i\right)^{\frac{1}{n}}$$

with equality holding if and only if $x_1 = x_2 = \cdots = x_n$.

Theorem 2.3.2. *The infection-free equilibrium E_0 is locally asymptotically stable when $R_0 < 1$ and unstable when $R_0 > 1$.*

Proof. The characteristic equation of the linearized system corresponding to the model (2.1.1) at E_0 is given by

$$(x + d_1)(x + d_4)(x^2 + A_1x + A_2) = 0,$$

where

$$\begin{aligned} A_1 &= d_2 + d_3 + \alpha - \frac{\lambda\beta_2}{d_1} \\ &= d_3 + (d_2 + \alpha)(1 - R_0 + R_{01}), \\ A_2 &= d_3(d_2 + \alpha) - \frac{\lambda}{d_1}(\beta_1 k + \beta_2 d_3) \\ &= d_3(d_2 + \alpha)(1 - R_0). \end{aligned}$$

Two of the eigenvalues are $x_1 = -d_1$ and $x_2 = -d_4$, both of which are negative, while the other two eigenvalues are given by the solutions to the quadratic equation $x^2 + A_1x + A_2 = 0$. We observe that $A_1 > 0$ and $A_2 > 0$, when $R_0 < 1$. Therefore, by the Routh-Hurwitz criteria, both the roots of the quadratic equation $x^2 + A_1x + A_2 = 0$ are either negative or have negative real parts when $R_0 < 1$. Hence all the eigenvalues of the characteristic equation at E_0 are either negative or have negative real parts when $R_0 < 1$. Also, when $R_0 > 1$, the characteristic equation at E_0 has at least one root with positive real part. Thus the infection-free equilibrium E_0 is locally asymptotically stable when $R_0 < 1$ and unstable when $R_0 > 1$. □

Theorem 2.3.3. *The immune-free infected equilibrium E_1 is locally asymptotically stable when $R_H < 1 < R_0$ and unstable when $R_H > 1$.*

Proof. The characteristic equation of the linearized system corresponding to the model (2.1.1) at E_1 is given by

$$(x + d_4 - cV_1)(x^3 + B_1x^2 + B_2x + B_3) = 0,$$

where

$$\begin{aligned} B_1 &= d_1 + d_2 + d_3 + \alpha + \beta_1 V_1 + \beta_2 I_1 - \beta_2 U_1 \\ &= d_1 + d_3 + (d_2 + \alpha)\frac{R_{01}}{R_0} + \frac{d_1}{d_2}(d_2 + \alpha)(R_0 - 1), \\ B_2 &= (d_2 + d_3)(\beta_1 V_1 + \beta_2 I_1) + d_1(d_2 + d_3 + \alpha - \beta_2 U_1) \\ &= d_1 d_3 + d_1(d_2 + \alpha)\frac{R_{01}}{R_0} + \frac{d_1}{d_2}(d_2 + d_3)(d_2 + \alpha)(R_0 - 1), \\ B_3 &= d_2 d_3(\beta_1 V_1 + \beta_2 I_1) \\ &= d_1 d_3(d_2 + \alpha)(R_0 - 1). \end{aligned}$$

One of the eigenvalues is $cV_1 - d_4 = \dfrac{\lambda ck}{d_2 d_3 R_H}(R_H - 1)$, which is negative when $R_H < 1$. The other three eigenvalues are given are given by the solutions to the cubic equation $x^3 + B_1 x^2 + B_2 x + B_3 = 0$. It is easily seen that $B_1, B_2, B_3 > 0$, whenever $R_0 > 1$. Further

$$\begin{aligned} B_1B_2 - B_3 &= d_1d_3(d_1+d_3) + d_1(d_1+d_3)(d_2+\alpha)\frac{R_{01}}{R_0} + \frac{{d_1}^2}{{d_2}^2}(d_2+d_3)(d_2+\alpha)^2(R_0-1)^2 \\ &\quad + \frac{{d_1}^2}{d_2}(d_2+\alpha)^2\frac{R_{01}}{R_0}(R_0-1) + \frac{d_1}{d_2}(d_1d_2 + 2d_1d_3 + {d_3}^2)(d_2+\alpha)(R_0-1). \end{aligned}$$

Hence, $B_1B_2 - B_3 > 0$ when $R_0 > 1$. Therefore, by the Routh-Hurwitz criteria, all the three roots of the cubic equation $x^3 + B_1x^2 + B_2x + B_3 = 0$ are either negative or have negative real parts when $R_0 < 1$. Hence all the eigenvalues of the characteristic equation at E_1 are either negative or have negative real parts when $R_H < 1 < R_0$. Moreover, when $R_H > 1$, the eigenvalue $cV_1 - d_4$ becomes positive. Thus the immune-free infected equilibrium E_1 is locally asymptotically stable when $R_H < 1 < R_0$ and unstable when $R_H > 1$ □

Theorem 2.3.4. *The immune-activation infected equilibrium E^* is locally asymptotically stable when $R_H > 1$.*

Proof. The characteristic equation of the linearized system corresponding to the model (2.1.1) at E^* is given by

$$x^4 + C_1x^3 + C_2x^2 + C_3x + C_4 = 0,$$

where

$$\begin{aligned} C_1 &= d_1 + \beta_1V^* + \beta_2I^* + \frac{kI^*}{V^*} + \frac{\beta_1U^*V^*}{I^*}, \\ C_2 &= (d_1 + \beta_1V^* + \beta_2I^*)\frac{kI^*}{V^*} + d_2(\beta_1V^* + \beta_2I^*) + cpV^*B^* + \frac{d_1\beta_1U^*V^*}{I^*}, \\ C_3 &= (d_1 + \beta_1V^* + \beta_2I^*)cpV^*B^* + d_2(\beta_1V^* + \beta_2I^*)\frac{kI^*}{V^*} + d_1\left(\frac{\beta_1U^*V^*}{I^*}\right)cpV^*B^*, \\ C_4 &= d_2(\beta_1V^* + \beta_2I^*)cpV^*B^* + d_1\left(\frac{\beta_1U^*V^*}{I^*}\right)cpV^*B^*. \end{aligned}$$

The eigenvalues are given by the solutions to the quartic equation $x^4 + C_1x^3 + C_2x^2 + C_3x + C_4 = 0$. It is easily seen that $C_1, C_2, C_3, C_4 > 0$ whenever U^*, I^*, V^* and B^* are all positive, that is, whenever $R_H > 1$. Further,

$$\begin{aligned} C_1C_2 - C_3 &= (d_1 + \beta_1V^* + \beta_2I^*)\left[(d_1 + \beta_1V^* + \beta_2I^*)\frac{kI^*}{V^*} + \beta_1kU^* + \left(\frac{kI^*}{V^*}\right)^2 + cpV^*B^*\right] \\ &\quad + d_2(\beta_1V^* + \beta_2I^*)\left[d_1 + \beta_1V^* + \beta_2I^* + \frac{kI^*}{V^*} + \frac{\beta_1U^*V^*}{I^*}\right] \\ &\quad + \frac{\beta_1U^*V^*}{I^*}\left[d_1(d_1 + \beta_1V^* + \beta_2I^*) + d_1\left(\frac{kI^*}{V^*}\right) + d_1\left(\frac{\beta_1U^*V^*}{I^*}\right) + cpV^*B^*\right]. \end{aligned}$$

Thus $C_1C_2 - C_3 > 0$ when $R_H > 1$. Moreover,

$$\begin{aligned}
&(C_1C_2 - C_3)C_3 - {C_1}^2C_4 \\
= \;& ckpI^*B^*(d_1 + \beta_1V^* + \beta_2I^*)^2\left[d_1 + \frac{\beta_1V^*U^*}{I^*} + \frac{kI^*}{V^*}\right] \\
&+ \frac{kI^*}{V^*}(d_1 + \beta_1V^* + \beta_2I^*)^2(\beta_1V^* + \beta_2I^*)\left[\frac{d_2kI^*}{V^*} + cpV^*B^*\right] \\
&+ \beta_1kU^*(d_1 + \beta_1V^* + \beta_2I^*)(\beta_1V^* + \beta_2I^*)(d_1d_2 + cpV^*B^*) \\
&+ \frac{d_2kI^*}{V^*}(d_1 + \beta_1V^* + \beta_2I^*)(\beta_1V^* + \beta_2I^*)\left[\beta_1kU^* + \left(\frac{kI^*}{V^*}\right)^2\right] \\
&+ \frac{\beta_1U^*V^*}{I^*}(\beta_1V^* + \beta_2I^*)(d_1d_2 + cpV^*B^*)\left[\beta_1kU^* + \left(\frac{kI^*}{V^*}\right)^2\right] \\
&+ \beta_1d_2ckp(\beta_1V^* + \beta_2I^*)U^*V^*B^*\left[\frac{d_2(\beta_1V^* + \beta_2I^*)}{cpV^*B^*} + \frac{cpV^*B^*}{d_2(\beta_1V^* + \beta_2I^*)} - 2\right] \\
&+ d_2ckp(d_1 + \beta_1V^* + \beta_2I^*)(\beta_1V^* + \beta_2I^*)I^*B^*\left[\frac{d_2(\beta_1V^* + \beta_2I^*)}{cpV^*B^*} + \frac{cpV^*B^*}{d_2(\beta_1V^* + \beta_2I^*)} - 2\right].
\end{aligned}$$

Using the AM-GM inequality, it follows that

$$\frac{d_2(\beta_1V^* + \beta_2I^*)}{cpV^*B^*} + \frac{cpV^*B^*}{d_2(\beta_1V^* + \beta_2I^*)} - 2 \geq 0.$$

Therefore, $(C_1C_2 - C_3)C_3 - {C_1}^2C_4 > 0$ whenever U^*, I^*, V^* and B^* are all positive, that is, whenever $R_H > 1$. By the Routh-Hurwitz criteria, all the four roots of the quartic equation $x^4 + C_1x^3 + C_2x^2 + C_3x + C_4 = 0$ are either negative or have negative real parts when $R_H > 1$. Hence all the eigenvalues of the characteristic equation at E^* are either negative or have negative real parts when $R_H > 1$. Thus the immune-activation infected equilibrium E^* is locally asymptotically stable when $R_H > 1$. □

2.3.2 Global Stability Analysis

To discuss the global behavior of the system (2.1.1), we apply the LaSalle's invariance principle [40] by constructing suitable Lyapunov functional. In order to establish the global stability, we consider the function $g(z) = z - 1 - \ln(z),\ z > 0$. Note that $g(z) \geq 0\ \forall\ z > 0$ and $g(z) = 0$ if and only if $z = 1$.

Theorem 2.3.5. *The infection-free equilibrium E_0 is globally asymptotically stable when $R_0 \leq 1$.*

Proof. We define a Lyapunov functional $L_1(U, I, V, B)$ as

$$L_1(U, I, V, B) = U_0g\left(\frac{U}{U_0}\right) + I + \frac{\beta_1U_0}{d_3}V + \frac{\beta_1pU_0}{cd_3}B + \frac{\alpha}{2(d_1 + d_2)U_0}[(U - U_0) + I]^2.$$

Taking the time derivative of $L_1(U, I, V, B)$ along the solution of (2.1.1), we obtain

$$\begin{aligned}\frac{dL_1}{dt} &= \left(1-\frac{U_0}{U}\right)(\lambda-\beta_1 UV-\beta_2 UI-d_1U+\alpha I)+(\beta_1 UV+\beta_2 UI-d_2I-\alpha I)\\ &+\frac{\beta_1 U_0}{d_3}(kI-d_3V-pVB)+\frac{\beta_1 pU_0}{cd_3}(cVB-d_4B)\\ &+\frac{\alpha}{(d_1+d_2)U_0}[(U-U_0)+I](\lambda-d_1U-d_2I).\end{aligned}$$

Using the relation $\lambda = d_1U_0$, we obtain

$$\begin{aligned}\frac{dL_1}{dt} &= \left(1-\frac{U_0}{U}\right)[-\beta_1 UV-\beta_2 UI-d_1(U-U_0)+\alpha I]+(\beta_1 UV+\beta_2 UI-d_2I-\alpha I)\\ &+\frac{\beta_1 U_0}{d_3}(kI-d_3V-pVB)+\frac{\beta_1 pU_0}{cd_3}(cVB-d_4B)\\ &-\frac{\alpha}{(d_1+d_2)U_0}[(U-U_0)+I][d_1(U-U_0)+d_2I].\end{aligned}$$

We observe that

$$\alpha\left(1-\frac{U_0}{U}\right)I=-\alpha I\frac{(U-U_0)^2}{UU_0}+\frac{\alpha}{U_0}(U-U_0)I.$$

Thus

$$\frac{dL_1}{dt}=-\left(d_1U_0+\alpha I+\frac{\alpha d_1U}{d_1+d_2}\right)\frac{(U-U_0)^2}{UU_0}-\frac{\alpha d_2I^2}{(d_1+d_2)U_0}-\frac{\beta_1 d_4 pU_0B}{cd_3}+(d_2+\alpha)I(R_0-1).$$

Hence $\frac{dL_1}{dt}\leq 0$ when $R_0\leq 1$. Let M_0 be the largest invariant set $\{(U,I,V,B)\mid \frac{dL_1}{dt}=0\}$. We note that $\frac{dL_1}{dt}=0$ if and only if $U=U_0$, $I=0$, $V=0$ and $B=0$. Hence, $M_0=\{E_0\}$. Therefore, it follows from LaSalle's invariance principle that E_0 is globally asymptotically stable when $R_0\leq 1$. □

Theorem 2.3.6. *The immune-free infected equilibrium E_1 is globally asymptotically stable when $R_H\leq 1<R_0\leq 1+\frac{d_2}{\alpha}$.*

Proof. We define a Lyapunov functional $L_2(U, I, V, B)$ as

$$\begin{aligned}L_2(U,I,V,B) &= U_1g\left(\frac{U}{U_1}\right)+I_1g\left(\frac{I}{I_1}\right)+\frac{\beta_1U_1V_1^2}{kI_1}g\left(\frac{V}{V_1}\right)+\frac{\beta_1pU_1V_1}{ckI_1}B\\ &+\frac{\alpha}{2(d_1+d_2)U_1}[(U-U_1)+(I-I_1)]^2.\end{aligned}$$

At the equilibrium E_1, we have

$$\begin{aligned}\lambda-\beta_1U_1V_1-\beta_2U_1I_1-d_1U_1+\alpha I_1&=0,\\ \beta_1U_1V_1+\beta_2U_1I_1-d_2I_1-\alpha I_1&=0,\\ kI_1-d_3V_1-pV_1B_1&=0,\\ cV_1B_1-d_4B_1&=0.\end{aligned}\tag{2.3.1}$$

Taking the time derivative of $L_2(U, I, V, B)$ along the solution of (2.1.1), we obtain

$$\begin{aligned}\frac{dL_2}{dt} &= \left(1-\frac{U_1}{U}\right)(\lambda-\beta_1 UV-\beta_2 UI-d_1U+\alpha I)+\left(1-\frac{I_1}{I}\right)(\beta_1 UV+\beta_2 UI-d_2I-\alpha I)\\ &+\frac{\beta_1 U_1V_1}{kI_1}\left(1-\frac{V_1}{V}\right)(kI-d_3V-pVB)+\frac{\beta_1 pU_1V_1}{ckI_1}(cVB-d_4B)\\ &+\frac{\alpha}{(d_1+d_2)U_1}[(U-U_1)+(I-I_1)](\lambda-d_1U-d_2I).\end{aligned}$$

Using the relation (2.3.1), we obtain

$$\begin{aligned}\frac{dL_2}{dt} &= \left(1-\frac{U_1}{U}\right)[\beta_1U_1V_1+\beta_2U_1I_1-\beta_1UV-\beta_2UI-d_1(U-U_1)+\alpha(I-I_1)]\\ &+\left(1-\frac{I_1}{I}\right)\left(\beta_1UV+\beta_2UI-\frac{\beta_1U_1V_1I}{I_1}-\beta_2U_1I\right)\\ &+\frac{\beta_1U_1V_1}{kI_1}\left(1-\frac{V_1}{V}\right)\left(kI-\frac{kI_1V}{V_1}-pVB\right)+\frac{\beta_1pU_1V_1}{ckI_1}(cVB-d_4B)\\ &-\frac{\alpha}{(d_1+d_2)U_1}[(U-U_1)+(I-I_1)][d_1(U-U_1)+d_2(I-I_1)].\end{aligned}$$

We observe that

$$\alpha\left(1-\frac{U_1}{U}\right)(I-I_1)=-\alpha(I-I_1)\frac{(U-U_1)^2}{UU_1}+\frac{\alpha}{U_1}(U-U_1)(I-I_1).$$

Thus

$$\begin{aligned}\frac{dL_2}{dt} &= -\left[d_1U_1-\alpha I_1+\alpha I+\frac{\alpha d_1U}{d_1+d_2}\right]\frac{(U-U_1)^2}{UU_1}-\frac{\alpha d_2}{(d_1+d_2)U_1}(I-I_1)^2\\ &-\beta_1U_1V_1\left[\frac{U_1}{U}+\frac{IV_1}{I_1V}+\frac{UI_1V}{U_1IV_1}-3\right]-\beta_2U_1I_1\left[\frac{U}{U_1}+\frac{U_1}{U}-2\right]+\frac{\lambda\beta_1kpU_1B}{d_2{d_3}^2R_H}(R_H-1).\end{aligned}$$

Using the AM-GM inequality, it follows that

$$\frac{U}{U_1}+\frac{U_1}{U}-2\geq 0 \text{ and } \frac{U_1}{U}+\frac{IV_1}{I_1V}+\frac{UI_1V}{U_1IV_1}-3\geq 0,$$

We also note that

$$d_1U_1-\alpha I_1=\frac{\lambda}{d_2R_0}(d_2+\alpha-\alpha R_0).$$

Hence $\frac{dL_2}{dt}\leq 0$ when $R_H\leq 1$ and $R_0\leq 1+\frac{d_2}{\alpha}$. Let M_1 be the largest invariant set $\{(U,I,V,B)\mid \frac{dL_2}{dt}=0\}$. We note that $\frac{dL_2}{dt}=0$ if and only if $U=U_1$, $I=I_1$, $V=V_1$ and $B=B_1$. Hence, $M_1=\{E_1\}$. Again, since E_1 exists whenever $R_0>1$, therefore, it follows from LaSalle's invariance principle that E_1 is globally asymptotically stable when $R_H\leq 1<R_0\leq 1+\frac{d_2}{\alpha}$. □

Theorem 2.3.7. *The immune-activation infected equilibrium E^* is locally asymptotically stable when $R_H > 1$ and $d_1U^* - \alpha I^* \geq 0$.*

Proof. We define a Lyapunov functional $L_3(U, I, V, B)$ as

$$\begin{aligned} L_3(U,I,V,B) &= U^* g\left(\frac{U}{U^*}\right) + I^* g\left(\frac{I}{I^*}\right) + \frac{\beta_1 U^* V^{*2}}{kI^*} g\left(\frac{V}{V^*}\right) \\ &+ \frac{\beta_1 p U^* V^* B^*}{ckI^*} g\left(\frac{B}{B^*}\right) + \frac{\alpha}{2(d_1+d_2)U^*}\left[(U-U^*)+(I-I^*)\right]^2. \end{aligned}$$

At the equilibrium E^*, we have

$$\begin{aligned} \lambda - \beta_1 U^* V^* - \beta_2 U^* I^* - d_1 U^* + \alpha I^* &= 0, \\ \beta_1 U^* V^* + \beta_2 U^* I^* - d_2 I^* - \alpha I^* &= 0, \\ kI^* - d_3 V^* - pV^* B^* &= 0, \\ cV^* B^* - d_4 B^* &= 0. \end{aligned} \tag{2.3.2}$$

Taking the time derivative of $L_3(U, I, V, B)$ along the solution of (2.1.1), we obtain

$$\begin{aligned} \frac{dL_3}{dt} &= \left(1-\frac{U^*}{U}\right)(\lambda - \beta_1 UV - \beta_2 UI - d_1 U + \alpha I) \\ &+ \left(1-\frac{I^*}{I}\right)(\beta_1 UV + \beta_2 UI - d_2 I - \alpha I) \\ &+ \frac{\beta_1 U^* V^*}{kI^*}\left(1-\frac{V^*}{V}\right)(kI - d_3 V - pVB) + \frac{\beta_1 p U^* V^*}{ckI^*}\left(1-\frac{B^*}{B}\right)(cVB - d_4 B) \\ &+ \frac{\alpha}{(d_1+d_2)U^*}\left[(U-U^*)+(I-I^*)\right](\lambda - d_1 U - d_2 I). \end{aligned}$$

Using the relation (2.3.2), we obtain

$$\begin{aligned} \frac{dL_3}{dt} &= \left(1-\frac{U^*}{U}\right)\left[\beta_1 U^* V^* + \beta_2 U^* I^* - \beta_1 UV - \beta_2 UI - d_1(U-U^*) + \alpha(I-I^*)\right] \\ &+ \left(1-\frac{I^*}{I}\right)\left(\beta_1 UV + \beta_2 UI - \frac{\beta_1 U^* V^* I}{I^*} - \beta_2 U^* I\right) \\ &+ \frac{\beta_1 U^* V^*}{kI^*}\left(1-\frac{V^*}{V}\right)\left(kI - \frac{kI^* V}{V^*} + pVB^* - pVB\right) \\ &+ \frac{\beta_1 p U^* V^*}{ckI^*}\left(1-\frac{B^*}{B}\right)(cVB - cV^* B) \\ &- \frac{\alpha}{(d_1+d_2)U^*}\left[(U-U^*)+(I-I^*)\right]\left[d_1(U-U^*)+d_2(I-I^*)\right]. \end{aligned}$$

We observe that

$$\alpha\left(1-\frac{U^*}{U}\right)(I-I^*) = -\alpha(I-I^*)\frac{(U-U^*)^2}{UU^*} + \frac{\alpha}{U^*}(U-U^*)(I-I^*).$$

Thus

$$\begin{aligned}\frac{dL_3}{dt} &= -\left[d_1U^* - \alpha I^* + \alpha I + \frac{\alpha d_1 U}{d_1+d_2}\right]\frac{(U-U^*)^2}{UU^*} - \frac{\alpha d_2}{(d_1+d_2)U^*}(I-I^*)^2 \\ &- \beta_1 U^* V^*\left[\frac{U^*}{U} + \frac{IV^*}{I^*V} + \frac{UI^*V}{U^*IV^*} - 3\right] - \beta_2 U^* I^*\left[\frac{U}{U^*} + \frac{U^*}{U} - 2\right].\end{aligned}$$

Using the AM-GM inequality, it follows that

$$\frac{U}{U^*} + \frac{U^*}{U} - 2 \geq 0 \text{ and } \frac{U^*}{U} + \frac{IV^*}{I^*V} + \frac{UI^*V}{U^*IV^*} - 3 \geq 0.$$

Hence $\frac{dL_3}{dt} \leq 0$ when $d_1U^* - \alpha I^* \geq 0$. Let M^* be the largest invariant set $\{(U, I, V, B) \mid \frac{dL_3}{dt} = 0\}$. We note that $\frac{dL_3}{dt} = 0$ if and only if $U = U^*$, $I = I^*$, $V = V^*$ and $B = B^*$. Hence, $M^* = \{E^*\}$. Again, since E^* exists whenever $R_H > 1$, therefore, it follows from LaSalle's invariance principle that E^* is globally asymptotically stable when $R_H > 1$ and $d_1U^* - \alpha I^* \geq 0$. □

Remark 2.3.8. *The conditions that appear in Theorems 2.3.2–2.3.7 are only sufficient, but not necessary. Further, the additional condition required in Theorem 2.3.6, namely* $R_0 \leq 1 + \frac{d_2}{\alpha}$, *is equivalent to* $d_1U_1 - \alpha I_1 \geq 0$, *which implies* $\lambda - \beta_1 U_1 V_1 - \beta_2 U_1 I_1 \geq 0$. *Also, the additional condition required in Theorem 2.3.7, namely* $d_1U^* - \alpha I^* \geq 0$, *which implies* $\lambda - \beta_1 U^* V^* - \beta_2 U^* I^* \geq 0$. *These two additional conditions indicate that the infection rate does not exceed the recruitment rate of uninfected hepatocytes at the equilibrium, which is reasonable from the biological point of view.*

2.4 Numerical Simulations and Discussions on the Effect of Parameters

In this section, we present a number of numerical illustrations for the model (2.1.1) with the parameter values specified in Table 2.2. We numerically analyze the global behavior of the system, as well as present a numerical comparison of the dynamics resulting from the proposed model (2.1.1) and the models appearing previously in the literature. Further, we investigate the effect of the sensitive parameters on the dynamical behavior of the system (2.1.1).

In order to examine the global stability of the equilibria for the model system, we consider three different initial conditions as, $ic_1 := (70, 20, 10, 200)$, $ic_2 := (50, 5, 2, 100)$ and $ic_3 := (150, 10, 20, 400)$, and vary the values of λ and β_2 while retaining the same values for the other parameters to obtain various scenarios for R_0 and R_H. The trajectories of the uninfected hepatocytes (Figures 2.2(a), 2.3(a), 2.4(a)), infected hepatocytes (Figures 2.2(b), 2.3(b),

Parameters	Descriptions	Values [References]	Units
λ	Recruitment rate of uninfected hepatocyte	1, 10 [126, 127]	cells ml^{-1} day^{-1}
β_1	Virus-to-cell transmission rate	0.01 [126, 127]	ml virion^{-1} day^{-1}
β_2	Cell-to-cell transmission rate	0.001, 0.01 (Assumed)	ml cell^{-1} day^{-1}
d_1	Death rate of uninfected hepatocyte	0.01 [22]	day^{-1}
d_2	Death rate of infected hepatocyte	1 [22]	day^{-1}
d_3	Death rate of virion	6 [22]	day^{-1}
d_4	Death rate of B cell	0.3 [97]	day^{-1}
α	Cure rate of infected hepatocyte	0.01 [29]	day^{-1}
k	Production rate of virion	2.9 [22]	virions cell^{-1} day^{-1}
p	Neutralization rate of virion by B cell	0.006 [97]	ml cell^{-1} day^{-1}
c	Development rate of B cell	0.1 [97]	ml virion^{-1} day^{-1}

Table 2.2: The list of parameter values for numerical simulations for the model (2.1.1).

2.4(b)), virions (Figures 2.2(c), 2.3(c), 2.4(c)) and B cells (Figures 2.2(d), 2.3(d), 2.4(d)) starting with initial condition and reaching to the stabilized level for the corresponding equilibrium points are plotted in Figures 2.2–2.4. In order to illustrate the case $R_0 < 1$, we first choose $\lambda = 1$ and $\beta_2 = 0.001$ with the other parameter values taken from Table 2.2, which corresponds to $R_0 = 0.5775 < 1$ and the resulting dynamics is presented in Figure 2.2. It is observed from Figure 2.2(a) that the concentration level of the uninfected hepatocytes increases or decreases progressively with time, depending upon the initial value at lower or higher level, respectively, and ultimately stabilizes at the level of $U = 100$. Further, the trajectories for infected hepatocytes (Figure 2.2(b)), virions (Figure 2.2(c)) and B cells (Figure 2.2(d)) initiating at different levels decline gradually and eventually approach zero level. This simulation proves the global asymptotic stability of the infection-free equilibrium E_0 $(100, 0, 0, 0)$ when $R_0 < 1$, thereby supporting the theoretical result obtained in Theorem 2.3.5. This scenario suggests that the infection does not persist if the infected hepatocytes are not sufficiently produced through the virus-to-cell or cell-to-cell transmission in absence of humoral immune response. Next, in order to elucidate the case $R_H < 1 < R_0$, we choose $\lambda = 1$ and $\beta_2 = 0.01$ with the other parameter values taken from Table 2.2, which results in $R_0 = 1.4686 > 1$ and $R_H = 0.1451 < 1$. Also, $R_0 < 1 + \frac{d_2}{\alpha} (= 101)$ is satisfied (condition for global stability of E_1 appearing in Theorem 2.3.6). The resulting dynamics is shown in Figure 2.3. It is observed from Figure 2.3 that the trajectories of uninfected and infected hepatocytes as well as virions showing oscillatory behavior for a period of time after initiating from different positions, finally stabilizes at their respective levels for the immune-free infected equilibrium, with the concentration of B cells gradually decreasing after initial time or decreasing after a sudden increase (in case of higher initial value), eventually approaching zero. This scenario indicates the globally asymptotic stability of the immune-free infected equilibrium E_1 $(68.0899, 0.3191, 0.1542, 0)$,

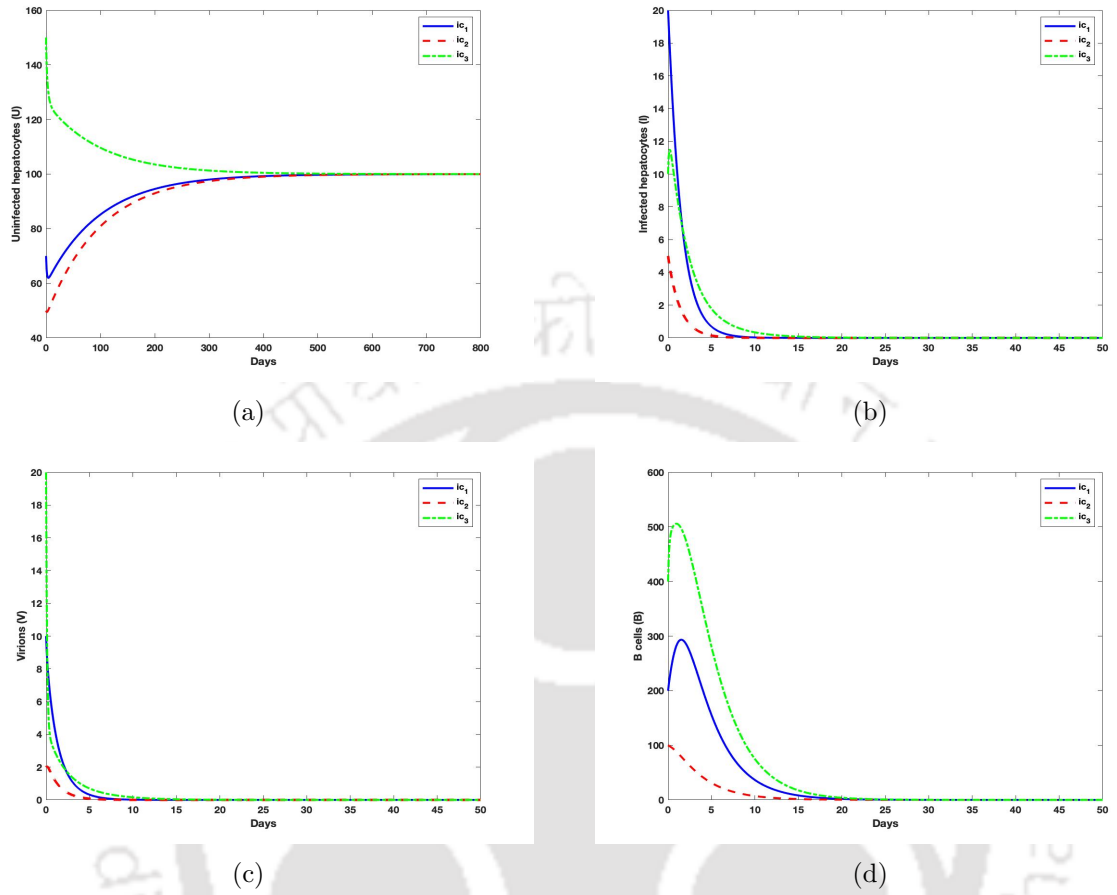

Figure 2.2: The trajectories of (a) uninfected hepatocytes, (b) infected hepatocytes, (c) virions, and (d) B cells starting with three different initial conditions $ic_1 := (70, 20, 10, 200)$, $ic_2 := (50, 5, 2, 100)$ and $ic_3 := (150, 10, 20, 400)$, in case of $R_0 < 1$ for the model (2.1.1).

which is in agreement with the theoretical result in Theorem 2.3.6. This result suggests that the B cells activation cannot be established if sufficient virions are not produced in order to stimulate the humoral immune response, which otherwise would have mounted a response against the virion population. Finally, in order to study the case $R_H > 1$, we choose $\lambda = 10$ and $\beta_2 = 0.01$, which corresponds to $R_H = 1.4518 > 1$ and $d_1U^* - \alpha I^* = 0.67 > 0$ (condition for global stability of E^* appearing in Theorem 2.3.7). In this case, the trajectories followed by the four model populations exhibit oscillatory behavior for sometime before eventually approaching the immune-activation infected equilibrium $E^*(76.2402, 9.2376, 3, 488.2796)$, as presented in Figure 2.4. This reflects that the immune-activation infected equilibrium E^* is globally asymptotically stable as already obtained theoretically in Theorem 2.3.7. This result suggests that the B cells activation will be established provided sufficient amount of virions is produced for continuation of the process of infecting the hepatocytes during the

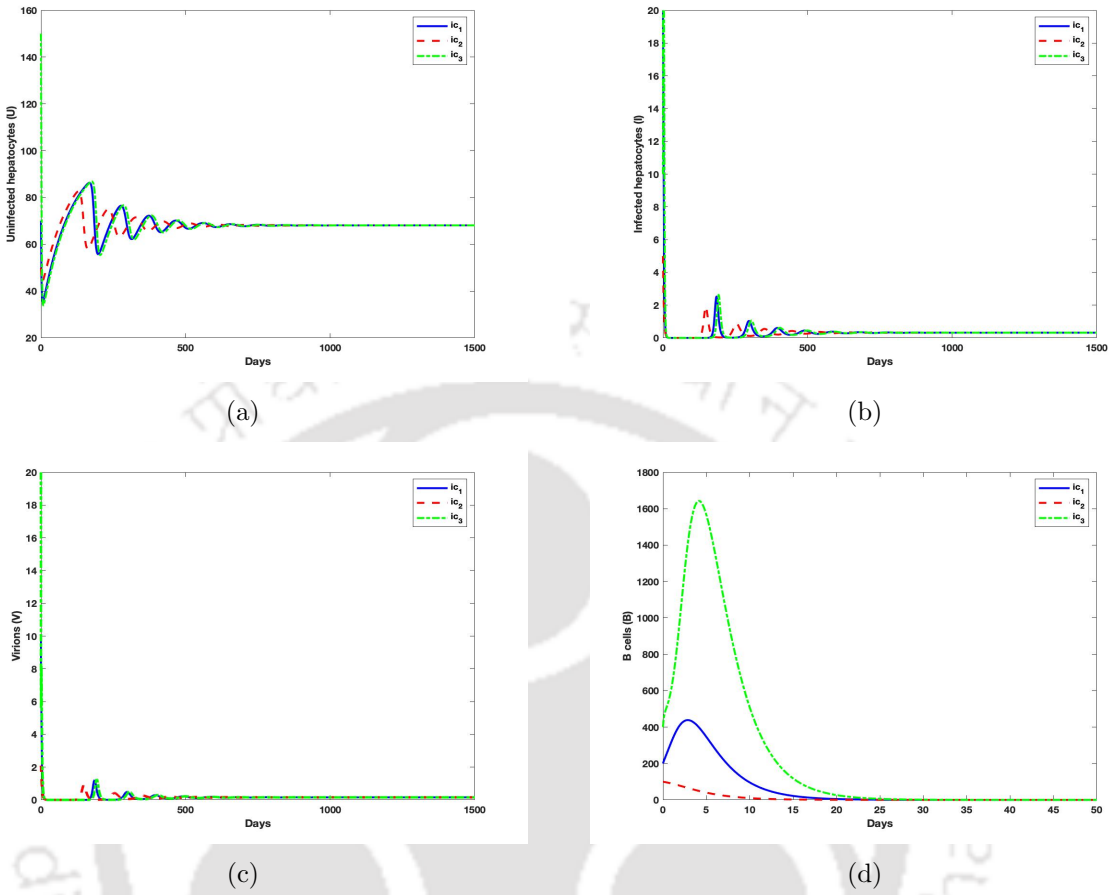

Figure 2.3: The trajectories of (a) uninfected hepatocytes, (b) infected hepatocytes, (c) virions, and (d) B cells starting with three different initial conditions $ic_1 := (70, 20, 10, 200)$, $ic_2 := (50, 5, 2, 100)$ and $ic_3 := (150, 10, 20, 400)$, in case of $R_H < 1 < R_0$ for the model (2.1.1).

chronic phase of the infection.

We now demonstrate a comparison of dynamics for various HCV models with several aspects which are listed below and presented in Figure 2.5.

(i) BM : Basic HCV model where immune response, cell-to-cell transmission and cure of infected hepatocytes are not included, *i.e.,* in this case $\beta_2 = \alpha = p = c = d_4 = 0$.

(ii) $BMwAR$: Basic HCV model with B cell response (antibody response) where cell-to-cell transmission and cure of infected hepatocytes are not included, *i.e.,* in this case $\beta_2 = \alpha = 0$.

(iii) $BMwC2C\&C$: Basic HCV model with cell-to-cell transmission and cure rate without immune response, *i.e.,* in this case $p = c = d_4 = 0$.

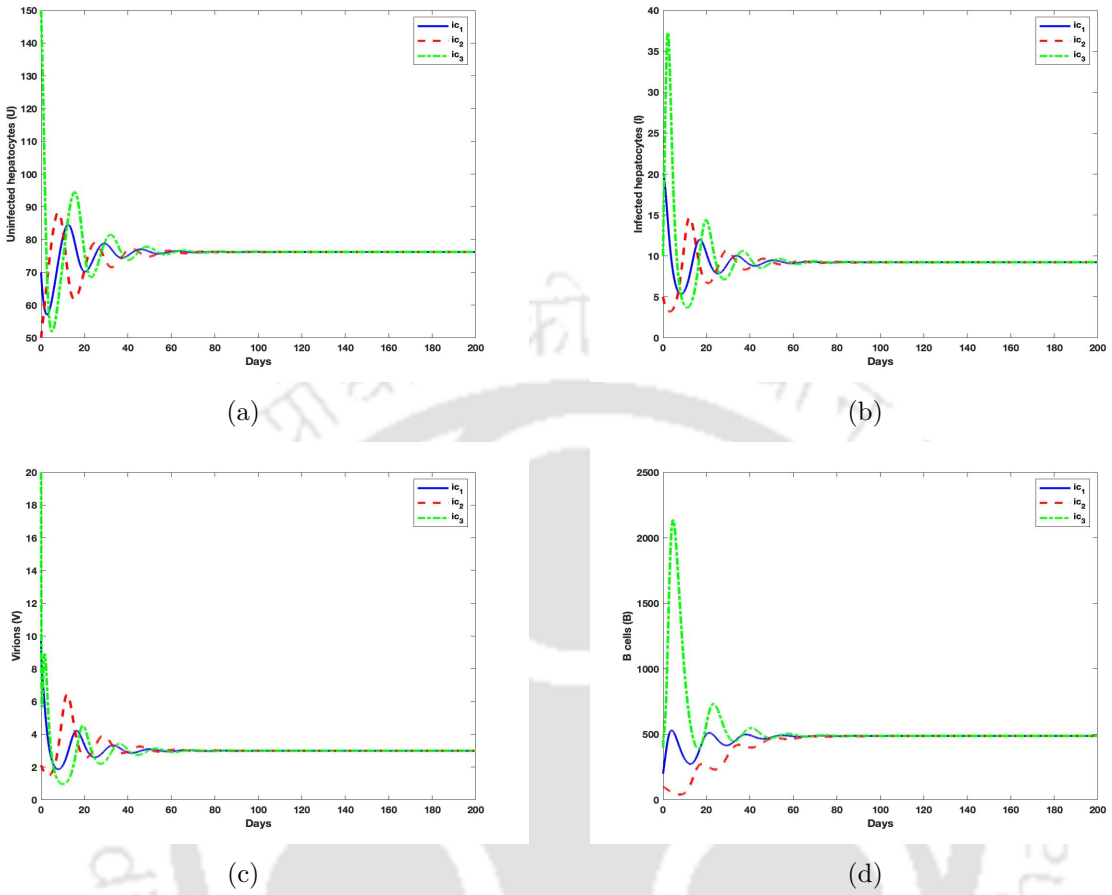

(a) (b)

(c) (d)

Figure 2.4: The trajectories of (a) uninfected hepatocytes, (b) infected hepatocytes, (c) virions, and (d) B cells starting with three different initial conditions $ic_1 := (70, 20, 10, 200)$, $ic_2 := (50, 5, 2, 100)$ and $ic_3 := (150, 10, 20, 400)$, in case of $R_H > 1$ for the model (2.1.1).

(iv) $BMwAR\&C2C\&C$: Basic HCV model with B cell response (antibody response), cell-to-cell transmission and cure rate, *i.e.,* in this case all parameters exist with positive values.

To perform this numerical comparison, the values of the positive parameters are chosen from Table 2.2 with $\lambda = 10$ and $\beta_2 = 0.01$. Here we examine the dynamical changes of the system populations after the inclusion of cell-to-cell transmission, cure rate and B cell response in the model, and these changes for the uninfected hepatocytes, infected hepatocytes, virions and B cells can be seen from Figures 2.5(a)–2.5(d), respectively. We first notice the cases of (i) versus (iii), and (ii) versus (iv), and it is observed that when cell-to-cell transmission with cure rate is allowed in the model (with or without B cell response), the system stabilizes faster. In addition, the uninfected hepatocytes stabilize at lower level, while the stabilized level of

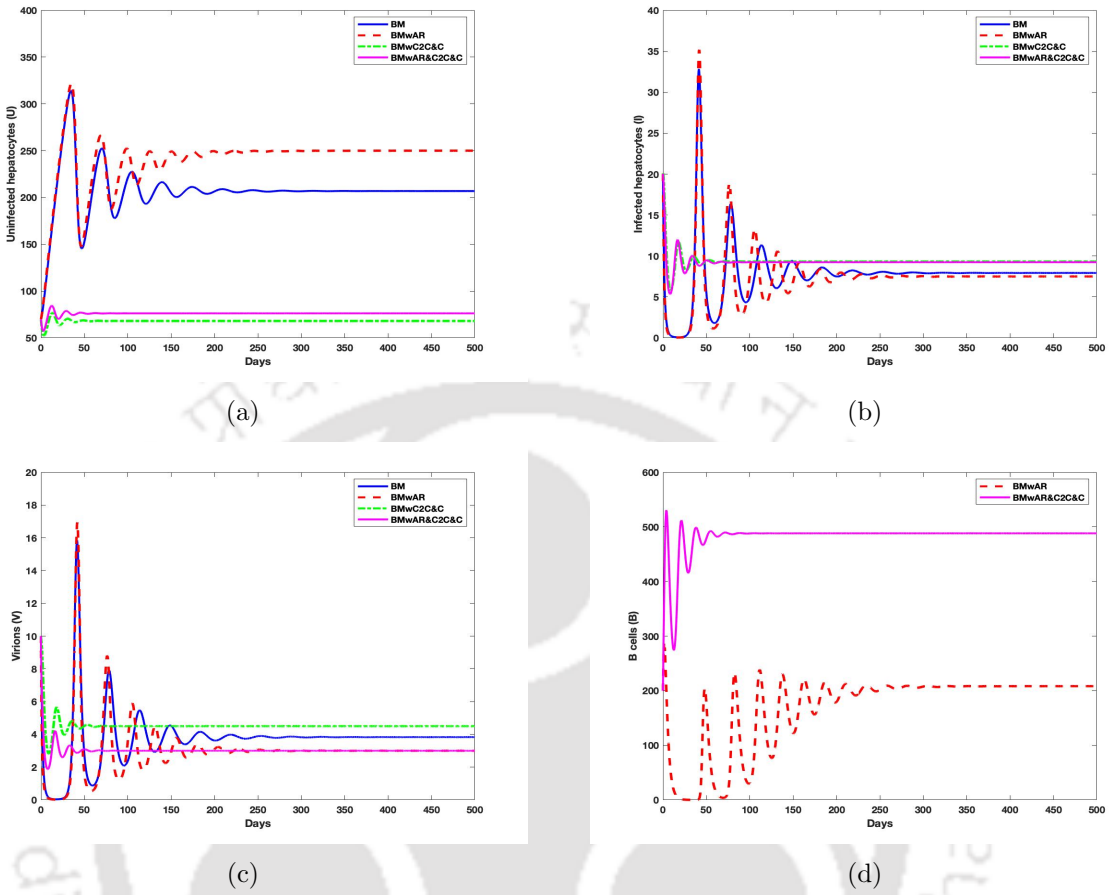

Figure 2.5: Comparison of dynamics for various models: (i) BM : basic model, (ii) $BMwAR$: basic model with B cell response (antibody response), (iii) $BMwC2C\&C$: basic model with cell-to-cell transmission and cure rate, (iv) $BMwAR\&C2C\&C$: basic model with B cell response (antibody response), cell-to-cell transmission and cure rate.

infected hepatocytes goes up. However, the virions increase its stabilized level in absence of B cell response, but remains undisturbed after a period of time when B cell response is considered. Further, we notice the cases of (i) versus (ii), and (iii) versus (iv), and it can be seen that the consideration of B cell response results in the uninfected hepatocytes stabilizing at higher level, accompanied by a reduction in the stabilized level of the virions, with no significant impact on the level of infected hepatocytes. It is also observed from the simulation that the concentration level of B cell increases in conjunction with an increase in infection, in spite of the unchanged virion density at stabilized levels, when cell-to-cell transmission and cure rate are taken into consideration. Therefore, Figure 2.5 suggests that the consideration of cell-to-cell transmission and cure rate in HCV model results in a significant difference in the dynamics of infectivity as well as in the response of B cells.

We illustrate the effects of cell-to-cell transmission rate and non-cytolytic cure rate on

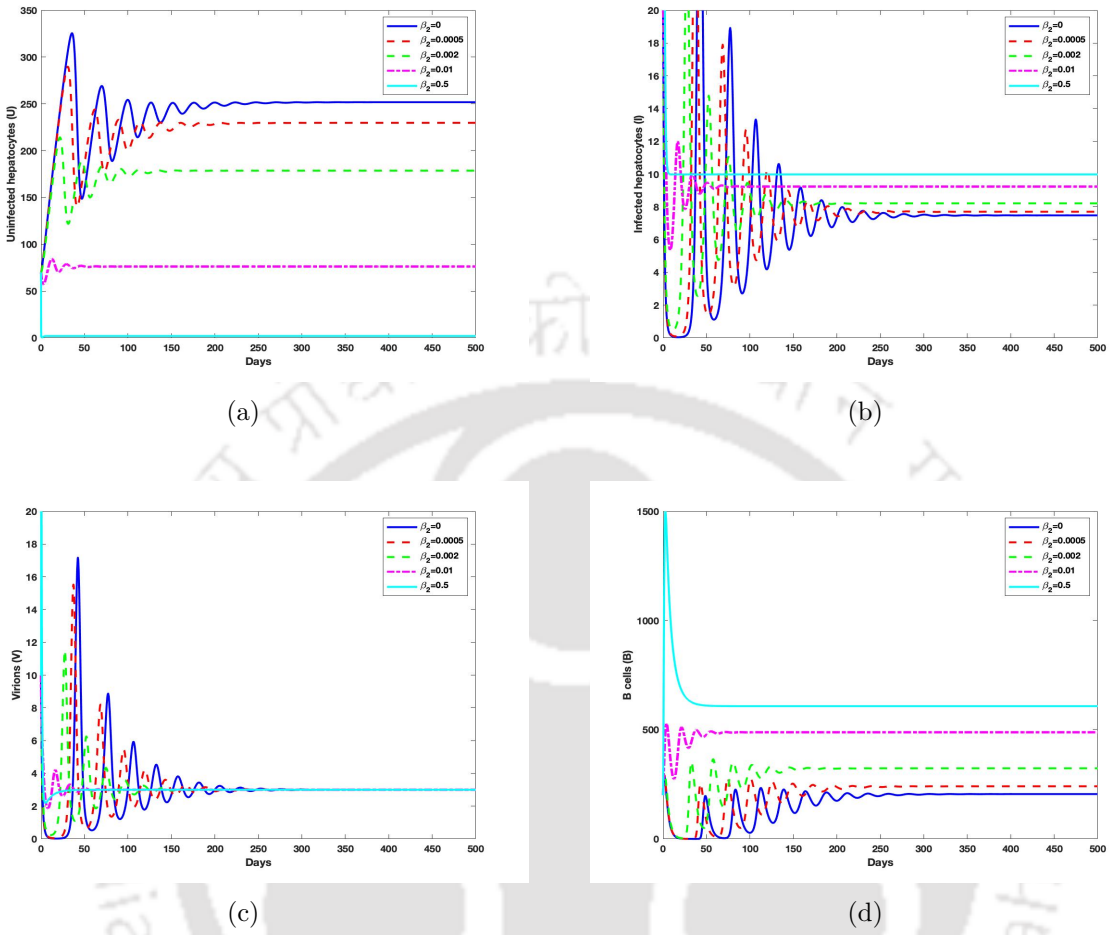

Figure 2.6: Effect of cell-to-cell transmission (β_2) on the dynamical behavior of the model system (2.1.1).

the dynamics of uninfected hepatocytes (Figures 2.6(a) and 2.7(a)), infected hepatocytes (Figures 2.6(b) and 2.7(b)), virions (Figures 2.6(c) and 2.7(c)) and B cells (Figures 2.6(d) and 2.7(d)). In Figure 2.6, we demonstrate the effects of the cell-to-cell transmission rate by simulating the model (2.1.1) for five different values of β_2, namely, $\beta_2 = 0$, 0.0005, 0.002, 0.01, 0.5 and the other model parameter values are chosen from Table 2.2 with $\lambda = 10$ and $\beta_2 = 0.01$. The corresponding values of R_0 are 4.7854, 5.2805, 6.7656, 14.6864, 499.8349 and the values of R_H are 1.2053, 1.2345, 1.3012, 1.4518, 1.6059, respectively. It is noticed that the values of R_0 and R_H are increasing with the increase in β_2. For the case $\beta_2 = 0$, *i.e.,* when there is no cell-to-cell transmission, the trajectory of the uninfected hepatocytes stabilizes at the peak level and the infected cells stabilize at its minimum level, with the lower response of B cells being observed. We observe from the simulation that the system populations stabilize faster with an increase in β_2 and moreover, the level of uninfected

hepatocytes decreases with an increase in the level of the infected hepatocytes as well as the B cells. Consequently, in the case $\beta_2 = 0.5$, it is seen that the concentration of uninfected hepatocytes becomes very less ($U = 2.0079$), while the infected hepatocytes as well as B cells stabilize at a higher level ($I = 9.9799$, $B = 607.8761$). Thus this simulation indicates that changes in β_2 result in the corresponding changes in both the uninfected and infected hepatocytes without effecting the stabilized level of the virions.

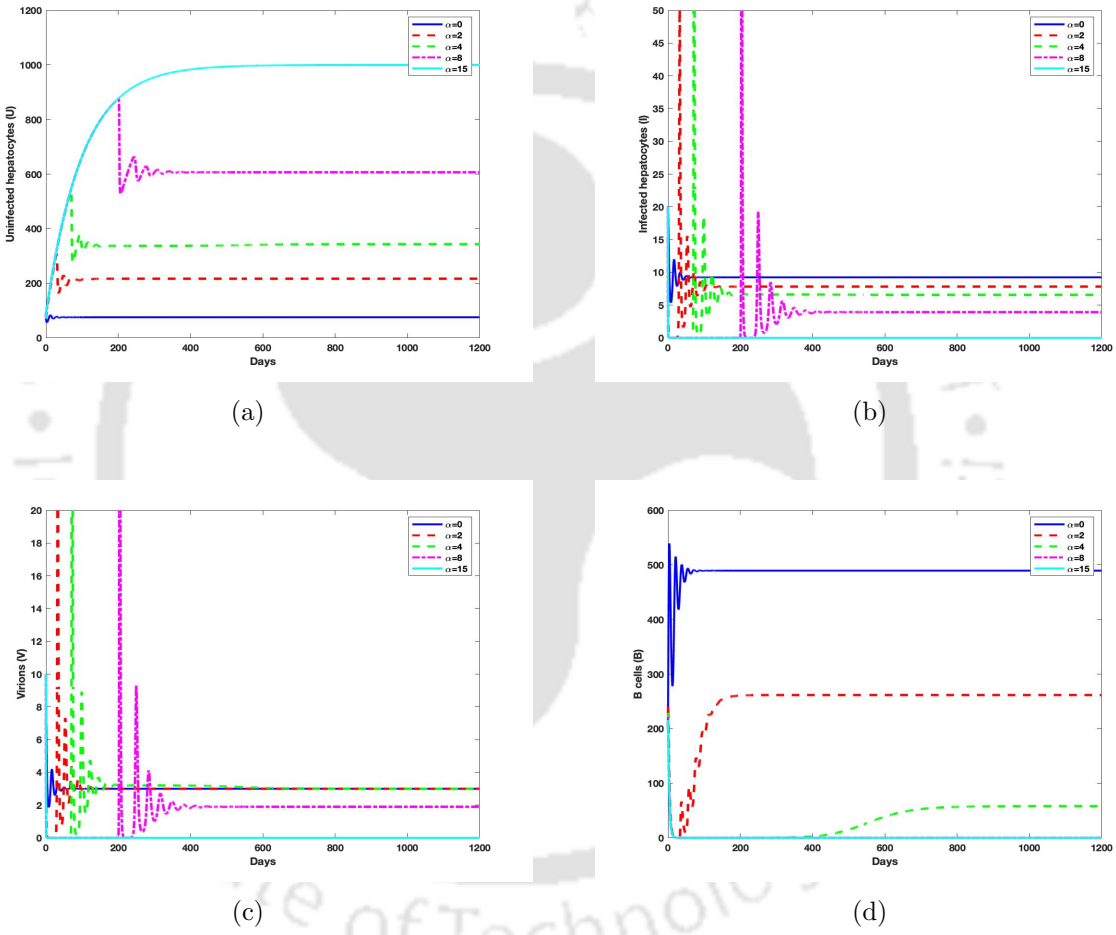

Figure 2.7: Effect of cure rate (α) on the dynamical behavior of the model system (2.1.1).

Further, in Figure 2.7, we present the effect of cure rate of infection on the levels of all the four populations. Accordingly, the simulation was carried out for five different values of α, namely, $\alpha = 0$, 2, 4, 8, 15 and the other parameter values are chosen from Table 2.2 with $\lambda = 10$ and $\beta_2 = 0.01$. For the case $\alpha = 0$, *i.e.,* when the non-cytolytic process is unable to cure the infected hepatocytes, we get $R_0 = 14.8333 > 1$ and $R_H = 1.4533 > 1$. In this case, the level of the uninfected hepatocytes reduces to a minimum while that of the infected hepatocytes as well as B cells reach their maximum stabilized level. The values of R_0

decreases with an increase in α and eventually becomes less than unity for higher values of α. Consequently, the number of uninfected hepatocytes increases while the infected hepatocytes decrease with an improvement of cure rate of infection and B cells response gets lowered. When $\alpha = 8$ ($R_0 = 1.6481 > 1$ and $R_H = 0.8147 < 1$), it is observed that the size of virion population as well as the concentration of infected hepatocytes are both reduced, which was not seen in the earlier cases for lower values of α, namely $\alpha = 0$, 2, 4. However, the B cells do not respond in this case, since the infection is at a lower level. Finally, when $\alpha = 15$ ($R_0 = 0.9270 < 1$ and $R_H = 0.5885 < 1$), the existence of the infection-free equilibrium is observed.

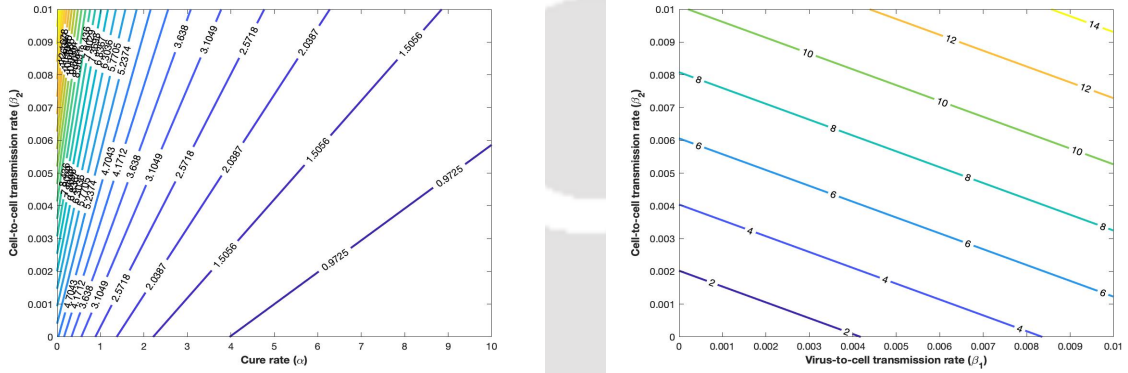

(a) (b)

Figure 2.8: Effect of cure rate (α), virus-to-cell transmission rate (β_1) and cell-to-cell transmission rate (β_2) on basic reproduction number (R_0) for the model (2.1.1).

Finally, in Figure 2.8, we present the effects of the sensitive parameters, namely, α, β_1 and β_2 on R_0, when the other parameter values are fixed as given in Table 2.2 with $\lambda = 10$. From Figure 2.8(a), it can be seen that R_0 is high when α is less and β_2 is high. Moreover, R_0 decreases resulting from a corresponding increase in the cure rate and decrease in cell-to-cell infection rate and eventually becomes less than unity. Figure 2.8(b) suggests that the value of R_0 is directly proportional to the values of β_1 as well as β_2. It is also seen that a small change in the value of β_2 is more sensitive than that of β_1 in making the effect on R_0, with respect to the given set of parameter values.

2.5 Conclusions

We proposed a model for HCV dynamics in the environment of humoral immunity with various factors including cell-to-cell transmission and cure rate, which possesses feasible solution. The existence of three possible equilibria, namely, infection-free equilibrium, immune-free in-

fected equilibrium and immune-activation infected equilibrium along with the results for their local and global stability, were obtained in terms of R_0 and R_H. The results indicate that the humoral immune response does not stimulate B cells to neutralize the virions, unless there are sufficient levels of virions and infection. The infection is eradicated from the host if $R_0 \leq 1$ and persists if $R_0 > 1$. The numerical comparison of the dynamics for various models suggests that incorporation of cell-to-cell transmission and cure rate results in a significant effect on the HCV dynamics. The effects of these two parameters on R_0 are analyzed and we conclude that the cell-to-cell transmission results in rapid infectivity of the host, while the cure rate shares an inverse relation with the infectivity rate. In addition, it is observed that the B cell response is more effective in neutralizing the virions and plays a less important role in reducing the level of infected hepatocytes. The findings suggest that driving the value of R_0 to less than unity (either through an increase of cure rate or decrease in cell-to-cell and/or cell-free transmission) could lead to a partial or complete elimination of infection in the host.

Chapter 3

Dynamics of HCV Model with the Effect of Time Delay in the Generation of B Cells

In virology and epidemiology, there are numerous biological processes which appear as a consequence of some earlier action, such as the generation of infection, production of virus and activation of the immune response since the consequence of virus entry into the body, does not happen instantaneously, but rather, there is time gap (delay) in the initiation of the subsequent processes [46, 66, 80, 89]. The time needed for the cells to be infected or for the replication of the virus is known as an intracellular delay. The immune delay refers to the time required for the trigger and development of the immune response. The consideration of the intracellular delay and the immune delay in the modeling is more realistic when it comes to analyzing the viral dynamics. Note that, delay may lead to instability, resulting in the occurrence of bifurcation, which may give rise to periodic solutions for the biological system [35]. The role of different types of intracellular delay in various viral dynamics models was investigated in [19, 46, 48, 65, 80, 117, 136, 141], while a limited number of models in the literature observed the effect of the immune delay [19, 66, 122, 128]. Further, it was observed in the study of an HIV model incorporating two time delays, that the intracellular delay does not make any effect on the stability in absence of the immune delay, whereas the cellular immune delay alone leads to Hopf bifurcation [89]. Therefore, it is more interesting to study the effect of the immune delay in the viral infection model.

In this chapter [1], we incorporate the humoral immune delay for the development of B cells in the model (2.1.1) presented in Chapter 2 and investigate the effect of this delay

[1]The presentation in this chapter is based on the article: "Sonjoy Pan and Siddhartha P. Chakrabarty. Hopf bifurcation and stability switches induced by humoral immune delay in hepatitis C. To appear in *Indian Journal of Pure and Applied Mathematics*".

in the dynamics of the DDE model. We check the properties of the solution to this DDE model. The stability of the equilibria is examined theoretically, as well as numerically, under the conditions on the basic reproduction number and the humoral immune reproduction number. We examine the existence of Hopf bifurcation around the interior equilibrium with respect to the delay as the bifurcation parameter. The maximum length of the delay to preserve stability is also estimated. We present some numerical simulations to support the theoretical results obtained. Furthermore, the dynamical effect of the development rate of B cells is investigated numerically.

3.1 Mathematical Model

The dynamics of HCV infection with both virus-to-cell and cell-to-cell transmissions as well as the cure rate in the presence of humoral immune response was analyzed in Chapter 2. This model did not consider the case of delay in the generation of B cells. It is noted from the immunological perspective that there is a time delay between the initial viral entry into the liver and the subsequent process of antigenic stimulation to generate B cells [121, 122]. However, it is considered that the process of B cells neutralizing the virions, is immediate [122]. Accordingly, we incorporate the humoral immune delay τ for the development of B cells in the model (2.1.1) and investigate the effect of this delay in the dynamics. Thus the humoral immune response at time t depends on the populations of B cells at time $(t-\tau)$. Therefore, we propose the following DDE model:

$$\begin{aligned}
\frac{dU(t)}{dt} &= \lambda - \beta_1 U(t)V(t) - \beta_2 U(t)I(t) - d_1 U(t) + \alpha I(t),\\
\frac{dI(t)}{dt} &= \beta_1 U(t)V(t) + \beta_2 U(t)I(t) - d_2 I(t) - \alpha I(t),\\
\frac{dV(t)}{dt} &= kI(t) - d_3 V(t) - pV(t)B(t),\\
\frac{dB(t)}{dt} &= cV(t-\tau)B(t-\tau) - d_4 B(t).
\end{aligned} \tag{3.1.1}$$

The initial condition for the system (3.1.1) is taken in the form

$$\begin{aligned}
&U(\theta) = \psi_1(\theta),\ I(\theta) = \psi_2(\theta),\ V(\theta) = \psi_3(\theta),\ B(\theta) = \psi_4(\theta),\\
&\psi_i(\theta) \geq 0,\ \theta \in [-\tau, 0],\ \psi_i(0) > 0,\ i = 1, 2, 3, 4,
\end{aligned} \tag{3.1.2}$$

where $(\psi_1(\theta), \psi_2(\theta), \psi_3(\theta), \psi_4(\theta)) \in \mathbb{C}\left([-\tau, 0],\ \mathbb{R}^4_{+0}\right)$, the Banach space of continuous functions mapping the interval $[-\tau, 0]$ into $\mathbb{R}_{+0}$ with norm $||\psi|| = \sup_{-\tau \leq \theta \leq 0} \{|\psi_i(\theta)|,\ i = 1, 2, 3, 4\}$.

3.2 Non-negativity and Boundedness of Solution

In this section, we prove the uniqueness, non-negativity and boundedness of the solution to the system (3.1.1) with the initial condition (3.1.2).

Theorem 3.2.1. *The system (3.1.1) with the initial condition (3.1.2) has a unique, non-negative and uniformly ultimately bounded solution.*

Proof. The right-hand side of the system (3.1.1) being continuous and Lipschitz on $[0, a],\ a > 0$, it follows from the theory of functional differential equations [40] that the system (3.1.1) with the initial condition (3.1.2) admits a unique solution $\big(U(t), I(t), V(t), B(t)\big)$.

In order to prove the non-negativity of the solution, we represent the system (3.1.1) in vector form as

$$\dot{X}(t) = F(X(t)),$$

where

$$X(t) = \big(x_1(t), x_2(t), x_3(t), x_4(t)\big)^\top = \big(U(t), I(t), V(t), B(t)\big)^\top,$$
$$X(\theta) = \big(U(\theta), I(\theta), V(\theta), B(\theta)\big)^\top \in \mathbb{C}\left([-\tau, 0],\ \mathbb{R}^4_{+0}\right),\ x_i(0) > 0,\ \forall\ i = 1, 2, 3, 4$$

and

$$F(X) = \begin{pmatrix} F_1(X) \\ F_2(X) \\ F_3(X) \\ F_4(X) \end{pmatrix} = \begin{pmatrix} \lambda - \beta_1 UV - \beta_2 UI - d_1 U + \alpha I \\ \beta_1 UV + \beta_2 UI - d_2 I - \alpha I \\ kI - d_3 V - pVB \\ cV(t-\tau)B(t-\tau) - d_4 B \end{pmatrix}.$$

It can be easily shown that

$$F_i(X)\big|_{x_i(t)=0,\ X(\theta)\in\mathbb{R}^4_{+0}} \geq 0,\ \forall\ i = 1, 2, 3, 4.$$

Therefore, by Theorem A.4 in [106] and Lemma 2 in [133], any solution $X(t)$ of the system (3.1.1) with initial condition $X(\theta) \in \mathbb{C}\left([-\tau, 0],\ \mathbb{R}^4_{+0}\right)$ satisfies $X(t) \in \mathbb{R}^4_{+0}$ for all $t > 0$.

In order to establish the boundedness of the solution to the system (3.1.1), we define the variables

$$Y(t) = U(t) + I(t) \quad \text{and} \quad Z(t) = V(t) + \frac{p}{c} B(t + \tau).$$

Adding the first two equations of (3.1.1), we get

$$\frac{dY(t)}{dt} = \lambda - d_1 U(t) - d_2 I(t) \leq \lambda - d_Y Y(t),$$

where $d_Y = \min\{d_1, d_2\}$. Hence, $\limsup_{t\to\infty} Y(t) \leq \dfrac{\lambda}{d_Y}$. Further, the last two equations of (3.1.1) give

$$\frac{dZ(t)}{dt} = kI(t) - d_3 V(t) - \frac{d_4 p}{c} B(t + \tau) \leq kI(t) - d_Z Z(t),$$

where $d_Z = \min\{d_3, d_4\}$. Therefore, $\limsup_{t\to\infty} Z(t) \leq \dfrac{\lambda k}{d_Y d_Z}$. Thus the system (3.1.1) with the initial condition (3.1.2) has a unique, non-negative and uniformly ultimately bounded solution belonging to the following positively invariant set

$$\mathcal{D} = \left\{ \big(U(t), I(t), V(t), B(t)\big) \in \mathbb{R}^4_+ \mid U(t), I(t) \in \left[0, \frac{\lambda}{d_Y}\right];\ V(t) \in \left[0, \frac{\lambda k}{d_Y d_Z}\right];\ B(t) \in \left[0, \frac{c\lambda k}{p d_Y d_Z}\right] \right\}.$$

□

3.3 Equilibria and Stability

From Section 2.3, it follows that the model system (3.1.1) has three equilibria, namely,

1. The infection-free equilibrium, $E_0 = (U_0, I_0, V_0, B_0) = \left(\dfrac{\lambda}{d_1}, 0, 0, 0\right)$.

2. The immune-free infected equilibrium, $E_1 = (U_1, I_1, V_1, B_1)$, where

$$U_1 = \frac{d_3(d_2+\alpha)}{\beta_1 k + \beta_2 d_3}, \quad I_1 = \frac{d_1 U_1}{d_2}\left[\frac{\lambda(\beta_1 k + \beta_2 d_3)}{d_1 d_3 (d_2+\alpha)} - 1\right], \quad V_1 = \frac{k}{d_3} I_1 \ \text{ and } \ B_1 = 0.$$

3. The immune-activation infected equilibrium, $E^* = (U^*, I^*, V^*, B^*)$, where

$$U^* = \frac{(d_2+\alpha)I^*}{\beta_1 V^* + \beta_2 I^*}, \quad I^* = \frac{-m_2 + \sqrt{m_2^2 + 4m_1 m_3}}{2m_1}, \quad V^* = \frac{d_4}{c} \ \text{ and } \ B^* = \frac{d_3}{p}\left(\frac{ck}{d_3 d_4} I^* - 1\right),$$

with

$$m_1 = \beta_2 c d_2, \quad m_2 = \beta_1 d_2 d_4 + c d_1 (d_2+\alpha) - \lambda \beta_2 c \ \text{ and } \ m_3 = \lambda \beta_1 d_4.$$

The basic reproduction number for the system (3.1.1) is given by

$$R_0 = \frac{\lambda(\beta_1 k + \beta_2 d_3)}{d_1 d_3 (d_2+\alpha)},$$

and the humoral immune reproduction number is given by

$$R_H = \frac{ck\lambda(\beta_1 k + \beta_2 d_3)}{ckd_1 d_3 (d_2+\alpha) + d_2 d_3 d_4 (\beta_1 k + \beta_2 d_3)}.$$

It is noted that the infection-free equilibrium (E_0) exists unconditionally, the immune-free infected equilibrium (E_1) exists if $R_0 > 1$ and immune-activation infected equilibrium (E^*) exists if $R_H > 1$. Here E_0 and E_1 are so-called boundary equilibria, and E^* is the interior equilibrium.

3.3.1 Characteristic Equation

In order to determine the local stability of the equilibria, we linearize the system (3.1.1) about the equilibrium and obtain

$$\frac{dS(t)}{dt} = J_1 S(t) + J_2 S(t-\tau), \tag{3.3.1}$$

where

$$S(t) = \big(U(t), I(t), V(t), B(t)\big)^\top,$$

$$J_1 = \begin{pmatrix} -\beta_1 V - \beta_2 I - d_1 & -\beta_2 U + \alpha & -\beta_1 U & 0 \\ \beta_1 V + \beta_2 I & \beta_2 U - d_2 - \alpha & \beta_1 U & 0 \\ 0 & k & -d_3 - pB & -pV \\ 0 & 0 & 0 & -d_4 \end{pmatrix}, \quad J_2 = \begin{pmatrix} 0 & 0 & 0 & 0 \\ 0 & 0 & 0 & 0 \\ 0 & 0 & 0 & 0 \\ 0 & 0 & cB & cV \end{pmatrix}.$$

The local stability is investigated by computing the roots of the characteristic equation

$$det\left(J_1 + J_2 e^{-x\tau} - xJ\right) = 0,$$

where J is the identity matrix of size 4.

3.3.2 Local and Global Stabilities of Boundary Equilibria

Theorem 3.3.1. *The infection-free equilibrium E_0 is locally asymptotically stable for any $\tau \geq 0$ if $R_0 < 1$ and unstable if $R_0 > 1$.*

Proof. The theorem is true for $\tau = 0$ (using Theorem 2.3.2) and since the characteristic equation of the linearized system (3.3.1) at E_0 for $\tau > 0$ is same as that for $\tau = 0$, hence the proof follows. □

Theorem 3.3.2. *The immune-free infected equilibrium E_1 is locally asymptotically stable for any $\tau \geq 0$ if $R_H < 1 < R_0$ and unstable if $R_H > 1$.*

Proof. The characteristic equation of the linearized system (3.3.1) at E_1 is given by

$$\left(x + d_4 - cV_1 e^{-x\tau}\right)\left(x^3 + B_1 x^2 + B_2 x + B_3\right) = 0,$$

where

$$\begin{aligned} B_1 &= d_1 + d_3 + (d_2 + \alpha)\frac{R_{01}}{R_0} + \frac{d_1}{d_2}(d_2 + \alpha)(R_0 - 1), \\ B_2 &= d_1 d_3 + d_1(d_2 + \alpha)\frac{R_{01}}{R_0} + \frac{d_1}{d_2}(d_2 + d_3)(d_2 + \alpha)(R_0 - 1), \\ B_3 &= d_1 d_3 (d_2 + \alpha)(R_0 - 1). \end{aligned}$$

All the three roots of the equation $x^3 + B_1x^2 + B_2x + B_3 = 0$ have negative real parts if $R_0 > 1$ (using Theorem 2.3.3). We now investigate whether any complex root with positive real part exists for the following equation:

$$x + d_4 - cV_1e^{-x\tau} = 0. \tag{3.3.2}$$

Let $x = a + ib$ ($i = \sqrt{-1},\ a \geq 0$) be a root of (3.3.2). Substituting $x = a + ib$ in (3.3.2) and separating the real and imaginary parts, we obtain the following:

$$a + d_4 - cV_1e^{-a\tau}\cos(b\tau) = 0, \tag{3.3.3}$$

$$b + cV_1e^{-a\tau}\sin(b\tau) = 0. \tag{3.3.4}$$

Equations (3.3.3) and (3.3.4) give

$$\begin{aligned} b^2 &= c^2V_1^2e^{-2a\tau} - (a + d_4)^2 \\ &= \left[d_4e^{-a\tau} - d_4 - a - \frac{\lambda cke^{-a\tau}(1 - R_H)}{d_2d_3R_H}\right]\left[d_4 + a + cV_1e^{-a\tau}\right] \\ &< 0, \text{ if } R_H < 1, \end{aligned}$$

which is a contradiction. Therefore every root of (3.3.2) must have negative real part. Hence, E_1 is locally asymptotically stable for any $\tau \geq 0$, if $R_H < 1 < R_0$.

Further, let $F(x) = x + d_4 - cV_1e^{-x\tau}$. Observe that

$$F(0) = d_4 - cV_1 = \frac{\lambda ck}{d_2d_3R_H}(1 - R_H) < 0, \text{ if } R_H > 1 \text{ and } \lim_{x\to+\infty} F(x) = +\infty.$$

Since $F(x)$ is continuous on $(-\infty, \infty)$, therefore by the intermediate value property, it follows that the equation $F(x) = 0$ has at least one positive real root. Hence the characteristic equation at E_1 has at least one positive real root. Thus E_1 is unstable if $R_H > 1$. □

In order to study the global stability of the boundary equilibria, we construct Lyapunov functionals and use the LaSalle's invariance principle [40]. For this purpose, we consider a function $g(z) = z - 1 - \ln(x),\ z > 0$. Obviously, $g(z) \geq 0,\ \forall\ z > 0$ and $g(z) = 0$ if and only if $z = 1$.

Theorem 3.3.3. *The infection-free equilibrium E_0 is globally asymptotically stable for any $\tau \geq 0$ if $R_0 \leq 1$.*

Proof. We define a Lyapunov functional $L_1(U, I, V, B)$ as

$$\begin{aligned} L_1(U, I, V, B) &= U_0g\left(\frac{U}{U_0}\right) + I(t) + \frac{\beta_1U_0}{d_3}V(t) + \frac{\beta_1pU_0}{cd_3}B(t) \\ &\quad + \frac{\alpha}{2(d_1 + d_2)U_0}\left[U(t) - U_0 + I(t)\right]^2 + \frac{\beta_1pU_0}{d_3}\int_{t-\tau}^{t} V(\xi)B(\xi)d\xi. \end{aligned}$$

Differentiating $L_1(U, I, V, B)$ with respect to t along the solution of (3.1.1), we obtain

$$\begin{aligned}\frac{dL_1}{dt} &= \left(1-\frac{U_0}{U}\right)(\lambda-\beta_1 UV-\beta_2 UI-d_1U+\alpha I)+(\beta_1 UV+\beta_2 UI-d_2I-\alpha I)\\ &+\frac{\beta_1 U_0}{d_3}(kI-d_3V-pVB)+\frac{\beta_1 pU_0}{cd_3}\left[cV(t-\tau)B(t-\tau)-d_4B\right]\\ &+\frac{\alpha}{(d_1+d_2)U_0}\left[(U-U_0)+I\right](\lambda-d_1U-d_2I)+\frac{\beta_1 pU_0}{d_3}\left[VB-V(t-\tau)B(t-\tau)\right].\end{aligned}$$

Using the relation $\lambda = d_1U_0$, we obtain

$$\begin{aligned}\frac{dL_1}{dt} &= \left(1-\frac{U_0}{U}\right)\left[-\beta_1 UV-\beta_2 UI-d_1(U-U_0)+\alpha I\right]+(\beta_1 UV+\beta_2 UI-d_2I-\alpha I)\\ &+\frac{\beta_1 U_0}{d_3}(kI-d_3V-pVB)+\frac{\beta_1 pU_0}{cd_3}(cVB-d_4B)\\ &-\frac{\alpha}{(d_1+d_2)U_0}\left[(U-U_0)+I\right]\left[d_1(U-U_0)+d_2I\right].\end{aligned}$$

After simplification,

$$\frac{dL_1}{dt}=-\left(d_1U_0+\alpha I+\frac{\alpha d_1U}{d_1+d_2}\right)\frac{(U-U_0)^2}{UU_0}-\frac{\alpha d_2I^2}{(d_1+d_2)U_0}-\frac{\beta_1 d_4 pU_0B}{cd_3}+(d_2+\alpha)I\,(R_0-1).$$

Therefore $\frac{dL_1}{dt}\le 0$ if $R_0\le 1$. Let M_0 be the largest invariant set in $\left\{(U,I,V,B)\;\middle|\;\frac{dL_1}{dt}=0\right\}$. We observe that $\frac{dL_1}{dt}=0$ if and only if $U=U_0$, $I=0$, $V=0$ and $B=0$. Hence, $M_0=\{E_0\}$. Thus, by the LaSalle's invariance principle, the infection-free equilibrium E_0 is globally asymptotically stable for any $\tau\ge 0$ if $R_0\le 1$. □

Theorem 3.3.4. *The immune-free infected equilibrium E_1 is globally asymptotically stable for any $\tau\ge 0$ if $R_H\le 1<R_0\le 1+\frac{d_2}{\alpha}$.*

Proof. We define a Lyapunov functional $L_2(U, I, V, B)$ as

$$\begin{aligned}L_2(U,I,V,B) &= U_1 g\left(\frac{U}{U_1}\right)+I_1 g\left(\frac{I}{I_1}\right)+\frac{\beta_1 U_1 {V_1}^2}{kI_1}g\left(\frac{V}{V_1}\right)+\frac{\beta_1 pU_1V_1}{ckI_1}B\\ &+\frac{\alpha}{2(d_1+d_2)U_1}\left[(U-U_1)+(I-I_1)\right]^2+\frac{\beta_1 pU_1V_1}{kI_1}\int_{t-\tau}^{t}V(\xi)B(\xi)d\xi.\end{aligned}$$

At the equilibrium E_1, we have

$$\begin{aligned}\lambda-\beta_1U_1V_1-\beta_2U_1I_1-d_1U_1+\alpha I_1 &= 0,\\ \beta_1U_1V_1+\beta_2U_1I_1-d_2I_1-\alpha I_1 &= 0,\\ kI_1-d_3V_1 &= 0.\end{aligned}\tag{3.3.5}$$

Differentiating $L_2(U, I, V, B)$ with respect to t along the solution of (3.1.1), we obtain

$$\begin{aligned}\frac{dL_2}{dt} &= \left(1-\frac{U_1}{U}\right)(\lambda-\beta_1 UV-\beta_2 UI-d_1U+\alpha I)+\left(1-\frac{I_1}{I}\right)(\beta_1 UV+\beta_2 UI-d_2I-\alpha I)\\ &+\frac{\beta_1U_1V_1}{kI_1}\left(1-\frac{V_1}{V}\right)(kI-d_3V-pVB)+\frac{\beta_1pU_1V_1}{ckI_1}\left[cV(t-\tau)B(t-\tau)-d_4B\right]\\ &+\frac{\alpha}{(d_1+d_2)U_1}\left[(U-U_1)+(I-I_1)\right](\lambda-d_1U-d_2I)\\ &+\frac{\beta_1pU_1V_1}{kI_1}\left[VB-V(t-\tau)B(t-\tau)\right].\end{aligned}$$

Using the relation (3.3.5), we obtain

$$\begin{aligned}\frac{dL_2}{dt} &= \left(1-\frac{U_1}{U}\right)\left[\beta_1U_1V_1+\beta_2U_1I_1-\beta_1UV-\beta_2UI-d_1(U-U_1)+\alpha(I-I_1)\right]\\ &+\left(1-\frac{I_1}{I}\right)\left(\beta_1UV+\beta_2UI-\frac{\beta_1U_1V_1I}{I_1}-\beta_2U_1I\right)\\ &+\frac{\beta_1U_1V_1}{kI_1}\left(1-\frac{V_1}{V}\right)\left(kI-\frac{kI_1V}{V_1}-pVB\right)+\frac{\beta_1pU_1V_1}{ckI_1}(cVB-d_4B)\\ &-\frac{\alpha}{(d_1+d_2)U_1}\left[(U-U_1)+(I-I_1)\right]\left[d_1(U-U_1)+d_2(I-I_1)\right].\end{aligned}$$

After simplification,

$$\begin{aligned}\frac{dL_2}{dt} &= -\left[d_1U_1-\alpha I_1+\alpha I+\frac{\alpha d_1U}{d_1+d_2}\right]\frac{(U-U_1)^2}{UU_1}-\frac{\alpha d_2}{(d_1+d_2)U_1}(I-I_1)^2\\ &-\beta_1U_1V_1\left[\frac{U_1}{U}+\frac{IV_1}{I_1V}+\frac{UI_1V}{U_1IV_1}-3\right]-\beta_2U_1I_1\left[\frac{U}{U_1}+\frac{U_1}{U}-2\right]+\frac{\lambda\beta_1kpU_1B}{d_2{d_3}^2R_H}(R_H-1).\end{aligned}$$

Using the AM-GM inequality, it follows that

$$\frac{U}{U_1}+\frac{U_1}{U}-2\geq 0 \text{ and } \frac{U_1}{U}+\frac{IV_1}{I_1V}+\frac{UI_1V}{U_1IV_1}-3\geq 0.$$

Further,

$$d_1U_1-\alpha I_1=\frac{\lambda}{d_2R_0}(d_2+\alpha-\alpha R_0).$$

Therefore $\frac{dL_2}{dt}\leq 0$ if $R_H\leq 1$ and $R_0\leq 1+\frac{d_2}{\alpha}$. Let M_1 be the largest invariant set in $\left\{(U,I,V,B)\mid \frac{dL_2}{dt}=0\right\}$. We observe that $\frac{dL_2}{dt}=0$ if and only if $U=U_1$, $I=I_1$, $V=V_1$ and $B=B_1$. Hence, $M_1=\{E_1\}$. Thus, using the LaSalle's invariance principle and combining the condition for existence of E_1, it follows that the immune-free infected equilibrium E_1 is globally asymptotically stable for any $\tau\geq 0$ if $R_H\leq 1<R_0\leq 1+\frac{d_2}{\alpha}$. □

3.3.3 The Interior Equilibrium and Hopf Bifurcation

The characteristic equation of the linearized system (3.3.1) at E^* is given by

$$x^4 + a_1x^3 + a_2x^2 + a_3x + a_4 - cV^*(x^3 + b_1x^2 + b_2x + b_3)e^{-x\tau} = 0, \tag{3.3.6}$$

where

$$\begin{aligned}
a_1 &= d_1 + d_4 + \beta_1V^* + \beta_2I^* + \frac{kI^*}{V^*} + \frac{\beta_1U^*V^*}{I^*},\\
a_2 &= (d_1 + \beta_1V^* + \beta_2I^*)\left(d_4 + \frac{kI^*}{V^*}\right) + d_2(\beta_1V^* + \beta_2I^*) + (d_1 + d_4)\frac{\beta_1U^*V^*}{I^*} + \frac{d_4kI^*}{V^*},\\
a_3 &= (d_1 + \beta_1V^* + \beta_2I^*)\frac{d_4kI^*}{V^*} + d_2(\beta_1V^* + \beta_2I^*)\left(d_4 + \frac{kI^*}{V^*}\right) + d_1d_4\left(\frac{\beta_1U^*V^*}{I^*}\right),\\
a_4 &= d_2d_4(\beta_1V^* + \beta_2I^*)\frac{kI^*}{V^*},\\
b_1 &= d_1 + d_3 + \beta_1V^* + \beta_2I^* + \frac{\beta_1U^*V^*}{I^*},\\
b_2 &= d_1d_3 + (d_2 + d_3)(\beta_1V^* + \beta_2I^*) + (d_1 - pB^*)\frac{\beta_1U^*V^*}{I^*},\\
b_3 &= d_2d_3(\beta_1V^* + \beta_2I^*) - \left(\frac{\beta_1U^*V^*}{I^*}\right)d_1pB^*.
\end{aligned} \tag{3.3.7}$$

When $\tau = 0$, all the roots of (3.3.6) have negative real parts if $R_H > 1$ (using Theorem 2.3.4), *i.e.,* all the roots lie to the left of the imaginary axis. But, when $\tau > 0$, (3.3.6) becomes transcendental and therefore some of the roots may cross the imaginary axis to the right. We now investigate the existence of purely imaginary roots of (3.3.6). Substituting $x = i\omega$ ($i = \sqrt{-1}$, $\omega > 0$) in (3.3.6) and separating the real and imaginary parts, we obtain the following,

$$\omega^4 - a_2\omega^2 + a_4 = cV^*(-b_1\omega^2 + b_3)\cos(\omega\tau) + cV^*(-\omega^3 + b_2\omega)\sin(\omega\tau), \tag{3.3.8}$$

$$-a_1\omega^3 + a_3\omega = cV^*(-\omega^3 + b_2\omega)\cos(\omega\tau) - cV^*(-b_1\omega^2 + b_3)\sin(\omega\tau). \tag{3.3.9}$$

Squaring and adding the equations (3.3.8) and (3.3.9), we obtain

$$\omega^8 + P_1\omega^6 + P_2\omega^4 + P_3\omega^2 + P_4 = 0, \tag{3.3.10}$$

where

$$\begin{aligned}
P_1 &= a_1^2 - 2a_2 - c^2V^{*2},\\
P_2 &= a_2^2 - 2a_1a_3 + 2a_4 - b_1^2c^2V^{*2} + 2b_2c^2V^{*2},\\
P_3 &= a_3^2 - 2a_2a_4 + 2b_1b_3c^2V^{*2} - b_2^2c^2V^{*2},\\
P_4 &= a_4^2 - b_3^2c^2V^{*2}.
\end{aligned}$$

Let $\gamma = \omega^2$. Then (3.3.10) becomes

$$G(\gamma) \equiv \gamma^4 + P_1\gamma^3 + P_2\gamma^2 + P_3\gamma + P_4 = 0. \tag{3.3.11}$$

Therefore (3.3.6) has a pair of purely imaginary roots $\pm i\omega$ if and only if (3.3.11) has a positive real root ω^2. If (3.3.11) has no positive real root, then (3.3.6) has no purely imaginary root, in which case, the existence of Hopf bifurcation is ruled out and hence E^* is locally asymptotically stable for any $\tau \geq 0$. Now, we suppose that (3.3.11) has m $(1 \leq m \leq 4)$ positive roots, say, γ_n, $n = 1, 2, \ldots, m$. Then (3.3.10) has m positive roots, say, $\omega_n = \sqrt{\gamma_n}$, $n = 1, 2, \ldots, m$.

Solving (3.3.8) and (3.3.9) for $\cos(\omega\tau)$, we obtain

$$\cos(\omega\tau) = \frac{(\omega^4 - a_2\omega^2 + a_4)(-b_1\omega^2 + b_3) + (-a_1\omega^3 + a_3\omega)(-\omega^3 + b_2\omega)}{cV^*[(b_1\omega^2 - b_3)^2 + (\omega^3 - b_2\omega)^2]}. \tag{3.3.12}$$

When $\omega = \omega_n$ $(n = 1, 2, \ldots, m)$, we obtain the following from (3.3.12),

$$\tau = \tau_n^{(j)} = \frac{1}{\omega_n} \arccos\left[\frac{(\omega_n^4 - a_2\omega_n^2 + a_4)(-b_1\omega_n^2 + b_3) + (-a_1\omega_n^3 + a_3\omega_n)(-\omega_n^3 + b_2\omega_n)}{cV^*[(b_1\omega_n^2 - b_3)^2 + (\omega_n^3 - b_2\omega_n)^2]}\right] + \frac{2j\pi}{\omega_n}, \tag{3.3.13}$$

where $n = 1, 2, \ldots, m$ and $j = 0, 1, 2, \ldots$. Hence (3.3.6) has a pair of purely imaginary roots $\pm i\omega_n$ with $\tau = \tau_n^{(j)}$. Further, note that $\{\tau_n^{(j)}\}$ is a monotonically increasing sequence for every $n = 1, 2, \ldots, m$ and $\lim_{j\to\infty} \tau_n^{(j)} = \infty$. Therefore there exists a $n_0 \in \{1, 2, \ldots, m\}$ such that

$$\tau_{n_0}^{(0)} = \min\{\tau_n^{(j)} \mid n = 1, 2, \ldots, m;\ j = 0, 1, 2, \ldots\}.$$

Denote

$$\tau_0 = \tau_{n_0}^{(0)},\ \omega_0 = \omega_{n_0} \text{ and } \gamma_0 = \gamma_{n_0}. \tag{3.3.14}$$

Since E^* is locally asymptotically stable for $\tau = 0$ if $R_H > 1$ (using Theorem 2.3.4). Therefore, by Butler's Lemma [33], E^* remains locally asymptotically stable for $\tau < \tau_0$ if $R_H > 1$. Let $x(\tau) = \xi(\tau) + i\omega(\tau)$ be a root of (3.3.6) near $\tau = \tau_0$ with $\xi(\tau_0) = 0$, $\omega(\tau_0) = \omega_0$. Therefore to prove the transversality condition for the existence of Hopf bifurcation [72] at $\tau = \tau_0$, we establish the following Lemma.

Lemma 3.3.5. *$\left[\frac{dRe(x)}{d\tau}\right]_{\tau=\tau_0}$ and $G'(\omega_0^2)$ have same sign, provided $G'(\omega_0^2) \neq 0$.*

Proof. Differentiating (3.3.6) with respect to τ, we obtain

$$\left[(4x^3 + 3a_1x^2 + 2a_2x + a_3) - cV^*e^{-x\tau}(3x^2 + 2b_1x + b_2) + c\tau V^*e^{-x\tau}(x^3 + b_1x^2 + b_2x + b_3)\right]\frac{dx}{d\tau}$$

$$= -(x^3 + b_1x^2 + b_2x + b_3)cV^*e^{-x\tau}x.$$

This implies

$$\begin{aligned}\left[\frac{dx}{d\tau}\right]^{-1} &= -\frac{4x^3 + 3a_1x^2 + 2a_2x + a_3}{cV^*xe^{-x\tau}(x^3 + b_1x^2 + b_2x + b_3)} + \frac{3x^2 + 2b_1x + b_2}{x(x^3 + b_1x^2 + b_2x + b_3)} - \frac{\tau}{x} \\ &= -\frac{4x^3 + 3a_1x^2 + 2a_2x + a_3}{x(x^4 + a_1x^3 + a_2x^2 + a_3x + a_4)} + \frac{3x^2 + 2b_1x + b_2}{x(x^3 + b_1x^2 + b_2x + b_3)} - \frac{\tau}{x}.\end{aligned}$$

Substituting $x = i\omega_0$, we obtain

$$\left[\frac{dx}{d\tau}\right]^{-1}_{\tau=\tau_0} = -\frac{(-3a_1\omega_0^2 + a_3) + i(-4\omega_0^3 + 2a_2\omega_0)}{\omega_0[a_1\omega_0^3 - a_3\omega_0 + i(\omega_0^4 - a_2\omega_0^2 + a_4)]} + \frac{(-3\omega_0^2 + b_2) + i(2b_1\omega_0)}{\omega_0[\omega_0^3 - b_2\omega_0 + i(-b_1\omega_0^2 + b_3)]} - \frac{\tau}{i\omega_0}.$$

Therefore

$$\begin{aligned}Re\left[\frac{dx}{d\tau}\right]^{-1}_{\tau=\tau_0} &= -\frac{(a_3 - 3a_1\omega_0^2)(a_1\omega_0^2 - a_3) + (2a_2 - 4\omega_0^2)(\omega_0^4 - a_2\omega_0^2 + a_4)}{(a_1\omega_0^3 - a_3\omega_0)^2 + (\omega_0^4 - a_2\omega_0^2 + a_4)^2} \\ &\quad + \frac{(b_2 - 3\omega_0^2)(\omega_0^2 - b_2) + 2b_1(b_3 - b_1\omega_0^2)}{(\omega_0^3 - b_2\omega_0)^2 + (b_3 - b_1\omega_0^2)^2}.\end{aligned}$$

Using (3.3.8) and (3.3.9), we obtain

$$\begin{aligned}Re\left[\frac{dx}{d\tau}\right]^{-1}_{\tau=\tau_0} &= \frac{-(a_3 - 3a_1\omega_0^2)(a_1\omega_0^2 - a_3) - (2a_2 - 4\omega_0^2)(\omega_0^4 - a_2\omega_0^2 + a_4)}{c^2V^{*2}[(b_3 - b_1\omega_0^2)^2 + (\omega_0^3 - b_2\omega_0)^2]} \\ &\quad + \frac{c^2V^{*2}[(b_2 - 3\omega_0^2)(\omega_0^2 - b_2) + 2b_1(b_3 - b_1\omega_0^2)]}{c^2V^{*2}[(b_3 - b_1\omega_0^2)^2 + (\omega_0^3 - b_2\omega_0)^2]}.\end{aligned}$$

This upon simplification becomes

$$Re\left[\frac{dx}{d\tau}\right]^{-1}_{\tau=\tau_0} = \frac{4\omega_0^6 + 3\omega_0^4P_1 + 2\omega_0^2P_2 + P_3}{c^2V^{*2}[(b_3 - b_1\omega_0^2)^2 + (\omega_0^3 - b_2\omega_0)^2]}.$$

Hence

$$Re\left[\frac{dx}{d\tau}\right]^{-1}_{\tau=\tau_0} = \frac{G'(\omega_0^2)}{c^2V^{*2}[(b_3 - b_1\omega_0^2)^2 + (\omega_0^3 - b_2\omega_0)^2]}.$$

Thus

$$\text{sign}\left\{\left[\frac{dRe(x)}{d\tau}\right]_{\tau=\tau_0}\right\} = \text{sign}\left\{Re\left[\frac{dx}{d\tau}\right]^{-1}_{\tau=\tau_0}\right\} = \text{sign}\left\{G'(\omega_0^2)\right\}.$$

□

Thus the result about the existence of Hopf bifurcation is stated in the following theorem:

Theorem 3.3.6. *Suppose $R_H > 1$. Then*

(i) The interior equilibrium E^* is locally asymptotically stable for any $\tau \geq 0$, if (3.3.11) has no positive real root.

(ii) The interior equilibrium E^* is locally asymptotically stable for $\tau \in (0,\ \tau_0)$, if (3.3.11) has at least one positive real root.

(iii) The system (3.1.1) undergoes a Hopf bifurcation from the interior equilibrium E^* as τ crosses the critical value τ_0, if γ_0 is a simple root of (3.3.11), where

$$\tau_0 = \frac{1}{\omega_0}\arccos\left[\frac{(\omega_0^4 - a_2\omega_0^2 + a_4)(-b_1\omega_0^2 + b_3) + (-a_1\omega_0^3 + a_3\omega_0)(-\omega_0^3 + b_2\omega_0)}{cV^*[(b_1\omega_0^2 - b_3)^2 + (\omega_0^3 - b_2\omega_0)^2]}\right].$$

Proof. (i) This case has already been proved in the preceding discussion.

(ii) By the definition of τ_0, (3.3.11) has no positive real roots for $\tau \in (0, \tau_0)$. Hence all the roots of (3.3.6) have negative real parts. Thus E^* is locally asymptotically stable for $\tau \in (0,\ \tau_0)$.

(iii) Suppose γ_0 is a simple root of (3.3.11). Then we have $G'(\omega_0^2) \neq 0$. If $G'(\omega_0^2) < 0$, then (3.3.6) has at least one root with positive real part when τ is slightly less than τ_0, which contradicts conclusion (ii) of Theorem 3.3.6. Therefore, we have $G'(\omega_0^2) > 0$. Hence there exists a Hopf bifurcation for the system (3.1.1) when τ crosses the critical value τ_0.

□

Next, we determine the conditions in terms of the model parameters, for which Hopf bifurcation occurs around the interior equilibrium E^*. Accordingly, we define,

$$\begin{aligned}
&u_1 = \frac{1}{2}P_2 - \frac{3}{16}P_1^2, \quad u_2 = \frac{1}{32}P_1^3 - \frac{1}{8}P_1P_2 + P_3,\\
&D = \left(\frac{u_2}{2}\right)^2 + \left(\frac{u_1}{3}\right)^3, \quad \epsilon = -\frac{1}{2} + \frac{\sqrt{3}}{2}i, \quad i = \sqrt{-1},\\
&v_1 = \left(-\frac{u_2}{2} + \sqrt{D}\right)^{\frac{1}{3}} + \left(-\frac{u_2}{2} - \sqrt{D}\right)^{\frac{1}{3}},\\
&v_2 = \left(-\frac{u_2}{2} + \epsilon\sqrt{D}\right)^{\frac{1}{3}} + \left(-\frac{u_2}{2} - \epsilon^2\sqrt{D}\right)^{\frac{1}{3}},\\
&v_3 = \left(-\frac{u_2}{2} + \epsilon^2\sqrt{D}\right)^{\frac{1}{3}} + \left(-\frac{u_2}{2} - \epsilon\sqrt{D}\right)^{\frac{1}{3}},\\
&y_j = v_j - \frac{3}{4}P_1, \ j = 1, 2, 3.
\end{aligned}$$

Therefore, using Lemma 2.1 and Lemma 2.2 of [67] and Lemma 3.1 of [75], we can restate Theorem 3.3.6 as follows:

Theorem 3.3.7. *Suppose $R_1 > 1$ with τ_0 and ω_0 being already defined in (3.3.14). Then*

(i) The humoral immune activated equilibrium E^* is locally asymptotically stable for any $\tau \geq 0$, if $P_4 \geq 0$ and one of the following conditions is satisfied:

(a) $D > 0$ and $y_1 < 0$.

(b) $D = 0$ and $y_2 < 0$.

(c) $D < 0$ and $y_3 < 0$.

(ii) The humoral immune activated equilibrium E^* is locally asymptotically stable for $\tau \in (0,\ \tau_0)$, if one of the following conditions is satisfied:

(a) $P_4 < 0$.

(b) $P_4 \geq 0,\ D \geq 0,\ y_1 > 0$ and $G(y_1) < 0$.

(c) $P_4 \geq 0,\ D < 0$ and there exists at least one $y \in \{y_1,\ y_2,\ y_3\}$ such that $y > 0$ and $G(y) \leq 0$.

(iii) The system (3.1.1) undergoes a Hopf bifurcation (leading to bifurcating periodic orbits) from the humoral immune activated equilibrium E^* when τ crosses the critical value τ_0 provided $G'(\omega_0^2) > 0$.

3.4 Estimation of the Maximum Length of Delay to Preserve Stability

In the previous section, the existence of bifurcating periodic orbits was investigated. The occurrence of the periodic orbits in a small neighborhood of τ_0 happens either for $\tau < \tau_0$ or $\tau > \tau_0$. In order to analyze the stability of the periodic orbits, we estimate (following the approach in [32]) the maximum length of the delay to preserve the stability of the bifurcating limit cycle.

Let $P(t) = U(t) - U^*,\ Q(t) = I(t) - I^*,\ R(t) = V(t) - V^*,\ S(t) = B(t) - B^*$. Linearizing

(3.1.1) about the interior equilibrium point $E^*(U^*, I^*, V^*, B^*)$, we obtain

$$\begin{aligned}
\frac{dP(t)}{dt} &= (-\beta_1 V^* - \beta_2 I^* - d_1)P(t) + (\alpha - \beta_2 U^*)Q(t) - \beta_1 U^* R(t),\\
\frac{dQ(t)}{dt} &= (\beta_1 V^* + \beta_2 I^*)P(t) + (\beta_2 U^* - d_2 - \alpha)Q(t) + \beta_1 U^* R(t),\\
\frac{dR(t)}{dt} &= kQ(t) - (d_3 + pB^*)R(t) - pV^* S(t),\\
\frac{dS(t)}{dt} &= cB^* R(t-\tau) + cV^* S(t-\tau) - d_4 S(t).
\end{aligned} \tag{3.4.1}$$

Taking Laplace transform of (3.4.1), we obtain

$$\begin{aligned}
(s + \beta_1 V^* + \beta_2 I^* + d_1)\bar{P}(s) &= (\alpha - \beta_2 U^*)\bar{Q}(s) - \beta_1 U^* \bar{R}(s) + P(0),\\
(s + d_2 + \alpha - \beta_2 U^*)\bar{Q}(s) &= (\beta_1 V^* + \beta_2 I^*)\bar{P}(s) + \beta_1 U^* \bar{R}(s) + Q(0),\\
(s + d_3 + pB^*)\bar{R}(s) &= k\bar{Q}(s) - pV^* \bar{S}(s) + R(0),\\
(s + d_4)\bar{S}(s) &= cB^* e^{-s\tau}\bar{R}(s) + cV^* e^{-s\tau}\bar{S}(s) + S(0)\\
&\quad + cB^* e^{-s\tau} K_1(s) + cV^* e^{-s\tau} K_2(s),
\end{aligned} \tag{3.4.2}$$

where

$$K_1(s) = \int_{-\tau}^{0} e^{-st} R(t)dt,\ K_2(s) = \int_{-\tau}^{0} e^{-st} S(t)dt$$

and $\bar{P}(s),\ \bar{Q}(s),\ \bar{R}(s),\ \bar{S}(s)$ are the Laplace transforms of $P(t),\ Q(t),\ R(t),\ S(t)$ respectively. Combining all the equations of (3.4.2) and using (3.3.7), we obtain,

$$\begin{aligned}
&\left[s^4 + a_1 s^3 + a_2 s^2 + a_3 s + a_4 - cV^* e^{-s\tau}(s^3 + b_1 s^2 + b_2 s + b_3)\right]\bar{P}(s)\\
=\ &\left[s^3 + \left(\frac{K^* I^*}{V^*} + \frac{\beta_1 U^* V^*}{I^*} + d_4 - cV^* e^{-s\tau}\right)s^2\right.\\
&+ \left\{\left(\frac{kI^*}{V^*} + \frac{\beta_1 U^* V^*}{I^*}\right)\left(d_4 - cV^* e^{-s\tau}\right) + cpV^* B^* e^{-s\tau}\right\}s + \left.\frac{\beta_1 cpU^* V^{*2} B^*}{I^*} e^{-s\tau}\right] P(0)\\
&+ \left[(\alpha - \beta_2 U^*)s^2 + \left\{(\alpha - \beta_2 U^*)\left(\frac{kI^*}{V^*} + d_4 - cV^* e^{-s\tau}\right) - k\beta_1 U^*\right\}s\right.\\
&\left. - \frac{d_2 d_4 k I^*}{V^*} + \{d_2 kI^* + (\alpha - \beta_2 U^*)pV^* B^*\}ce^{-s\tau}\right] Q(0)\\
&- \left[s^2 + (d_2 + d_4 - cV^* e^{-s\tau})s + d_2(d_4 - cV^* e^{-s\tau})\right]\beta_1 U^* R(0)\\
&+ (s + d_2)\beta_1 pU^* V^* S(0) + cB^* e^{-s\tau} K_1(s) + cV^* e^{-s\tau} K_2(s).
\end{aligned}$$

A necessary and sufficient condition for E^* to be locally asymptotically stable is that all the poles of $\bar{P}(s)$ must have negative real parts [32]. Therefore, by using the Nyquist criterion [84], we obtain the sufficient conditions for local asymptotic stability of E^* as follows

$$ImH(i\eta_0) > 0, \tag{3.4.3}$$

$$ReH(i\eta_0) = 0 \tag{3.4.4}$$

where $H(s) = s^4 + a_1 s^3 + a_2 s^2 + a_3 s + a_4 - cV^* e^{-s\tau}(s^3 + b_1 s^2 + b_2 s + b_3)$, and η_0 is the smallest positive root of $ReH(i\eta_0) = 0$, which satisfies $ImH(i\eta_0) > 0$ as well. Now, (3.4.3) and (3.4.4) give

$$-a_1\eta_0^3 + a_3\eta_0 + cV^*(\eta_0^3 - b_2\eta_0)\cos(\eta_0\tau) - cV^*(b_1\eta_0^2 - b_3)\sin(\eta_0\tau) > 0, \quad (3.4.5)$$

$$\eta_0^4 - a_2\eta_0^2 + a_4 + cV^*(b_1\eta_0^2 - b_3)\cos(\eta_0\tau) + cV^*(\eta_0^3 - b_2\eta_0)\sin(\eta_0\tau) = 0. \quad (3.4.6)$$

Therefore the sufficient condition for stability of E^* is that (3.4.5) and (3.4.6) hold simultaneously. In order to estimate the length of the delay to preserve the stability of E^*, we have to find an upper bound of η_0 (independent of τ). From (3.4.6), we have,

$$\eta_0^4 = a_2\eta_0^2 - a_4 - cV^*(b_1\eta_0^2 - b_3)\cos(\eta_0\tau) - cV^*(\eta_0^3 - b_2\eta_0)\sin(\eta_0\tau). \quad (3.4.7)$$

Using the bounds $|\sin(\eta_0\tau)| \leq 1$ and $|\cos(\eta_0\tau)| \leq 1$, we obtain from (3.4.7),

$$\eta_0^4 - cV^*\eta_0^3 - (a_2 + cV^*|b_1|)\eta_0^2 - cV^*|b_2|\eta_0 - a_4 - cV^*|b_3| \leq 0. \quad (3.4.8)$$

Let η^+ be the smallest positive root of (3.4.8) when the equality holds. Then $\eta_0 \leq \eta^+$. Inequality (3.4.5) can be written as

$$a_2\eta_0^2 < \frac{a_2a_3}{a_1} + \frac{a_2cV^*}{a_1}\left(\eta_0^2 - b_2\right)\cos(\eta_0\tau) - \frac{a_2cV^*}{a_1\eta_0}\left(b_1\eta_0^2 - b_3\right)\sin(\eta_0\tau). \quad (3.4.9)$$

Adding (3.4.6) and (3.4.9), we obtain,

$$cV^*\left[\eta_0^3 + \left(\frac{a_2b_1}{a_1} - b_2\right)\eta_0 - \frac{a_2b_3}{a_1\eta_0}\right]\sin(\eta_0\tau) + cV^*\left[\left(b_1 - \frac{a_2}{a_1}\right)\eta_0^2 + \left(\frac{a_2b_2}{a_1} - b_3\right)\right][1 - \cos(\eta_0\tau)]$$

$$< \frac{a_2a_3}{a_1} - a_4 + cV^*\left(\frac{a_2b_2}{a_1} - b_3\right) + cV^*\left(b_1 - \frac{a_2}{a_1}\right)\eta_0^2 - \eta_0^4.$$

We have $\sin(\eta_0\tau) \leq \eta^+\tau$ and $1 - \cos(\eta_0\tau) = 2\sin^2(\frac{\eta_0\tau}{2}) \leq \frac{\eta^{+2}\tau^2}{2}$. We now suppose that $M_1\tau^2 + M_2\tau < M_3$ holds, where

$$M_1 = \frac{cV^*}{2}\left(\left|b_1 - \frac{a_2}{a_1}\right|\eta^{+4} + \left|\frac{a_2b_2}{a_1} - b_3\right|\eta^{+2}\right),$$

$$M_2 = cV^*\left(\eta^{+4} + \left|\frac{a_2b_1}{a_1} - b_2\right|\eta^{+2} + \frac{a_2b_3}{a_1}\right),$$

$$M_3 = a_4 + \frac{a_2a_3}{a_1} + cV^*\left|\frac{a_2b_2}{a_1} - b_3\right| + cV^*\left|b_1 - \frac{a_2}{a_1}\right|\eta^{+2} + \eta^{+4}.$$

Therefore, (3.4.3) and (3.4.4) are satisfied simultaneously if $M_1\tau^2 + M_2\tau < M_3$ holds. Hence, the Nyquist criterion holds for $0 \leq \tau \leq \tau^+$, where $\tau^+ = \frac{1}{2M_1}\left(-M_2 + \sqrt{M_2^2 + 4M_1M_3}\right)$ is the maximum length of the delay for which the stability of the bifurcating limit cycle is preserved.

Parameters	Descriptions	Values [References]	Units
λ	Recruitment rate of uninfected hepatocyte	1, 10 [126, 127]	cells ml^{-1} day^{-1}
β_1	Virus-to-cell transmission rate	0.01 [126, 127]	ml virion^{-1} day^{-1}
β_2	Cell-to-cell transmission rate	0.001, 0.01 (Assumed)	ml cell^{-1} day^{-1}
d_1	Death rate of uninfected hepatocyte	0.01 [22]	day^{-1}
d_2	Death rate of infected hepatocyte	1 [22]	day^{-1}
d_3	Death rate of virion	6, 1 [22, 126]	day^{-1}
d_4	Death rate of B cell	0.3 [97]	day^{-1}
α	Cure rate of infected hepatocyte	0.01 [29]	day^{-1}
k	Production rate of virion	2.9 [22]	virions cell^{-1} day^{-1}
p	Neutralization rate of virion by B cell	0.1 [78]	ml cell^{-1} day^{-1}
c	Development rate of B cell	0.1 [97]	ml virion^{-1} day^{-1}

Table 3.1: The list of parameter values for numerical simulations for the model (3.1.1) as well as the model (4.1.1).

3.5 Numerical Simulations and Discussions

In this section, we present several numerical illustrations to analyze the effect of time delay in the generation of B cells, in addition to investigating the effect of the development rate of B cells, on the dynamical behavior of the model system (3.1.1). In order to perform the numerical simulation, we chose the parameter values given in Table 3.1. We first demonstrate the global stability of the boundary equilibria of the system (3.1.1) through numerical simulation, by considering two different initial conditions, namely, $ic_1 := (80, 5, 2, 50)$ and $ic_2 := (120, 20, 10, 100)$, each for three different humoral immune delays, namely, $\tau = 6$, 12, 25. The various trajectories of uninfected hepatocytes (Figure 3.1(a), Figure 3.2(a)), infected hepatocytes (Figure 3.1(b), Figure 3.2(b)), virions (Figure 3.1(c), Figure 3.2(c)) and B cells (Figure 3.1(d), Figure 3.2(d)) for two different initial conditions and three different time delays are presented as follows:

- Blue lines : $ic_1 := (80, 5, 2, 50)$,
- Red lines : $ic_2 := (120, 20, 10, 100)$,
- Solid lines : $\tau = 6$,
- Dashed lines : $\tau = 12$,
- Dotted lines : $\tau = 25$.

In order to illustrate the case $R_0 < 1$, we choose $\lambda = 1$, $\beta_2 = 0.001$, $d_3 = 6$ and the other parameter values taken from Table 3.1, which correspond to $R_0 = 0.5775 < 1$. This scenario is presented in Figure 3.1, which shows that the trajectories of the uninfected hepatocytes (Figure 3.1(a)) starting with two different points, increase or decrease gradually, depending upon the initial value at lower or higher level, respectively, and then finally stabilize at the level $T = 100$, whereas the infected hepatocytes (Figure 3.1(b)) as well as virions (Figure

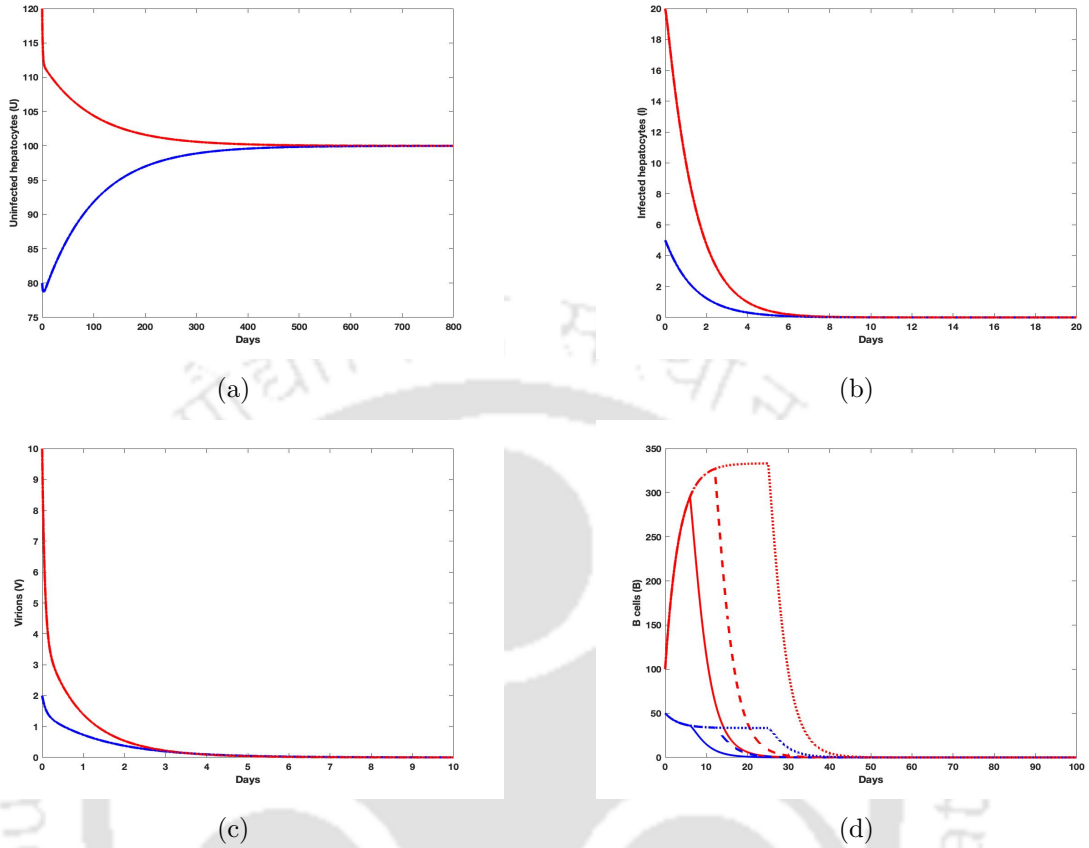

Figure 3.1: The trajectories of (a) uninfected hepatocytes, (b) infected hepatocytes, (c) virions, and (d) B cells starting with two different initial conditions ic_1 and ic_2, and three immune delays $\tau = 6,\ 12,\ 25$, in case of $R_0 < 1$ for the model (3.1.1). Blue lines : $ic_1 := (80, 5, 2, 50)$, red lines : $ic_2 := (120, 20, 10, 100)$, solid lines : $\tau = 6$, dashed lines : $\tau = 12$, dotted lines : $\tau = 25$.

3.1(c)) gradually decrease and eventually converge to zero. The behavior of B cells (Figure 3.1(d)) depends on the initial condition at the beginning, but after a period of time, it also converges to zero. This simulation also indicates that the variation of immune delay does not in any way affect the trajectories of uninfected and infected hepatocytes as well as virion population (solid, dashed and dotted lines merged on same path in Figure 3.1(a), Figure 3.1(b) and Figure 3.1(c)), but the slow convergence of B cells (solid lines of all colors converging to zero earlier than other patterned lines of corresponding colors in Figure 3.1(d)) occurs due to increase in value of the immune delay. This suggests that the infection-free equilibrium E_0 $(100, 0, 0, 0)$ is globally asymptotically stable for any time delay in the generation of B cells, which supports the theoretical result in Theorem 3.3.3. In order to study the case $R_H < 1 < R_0$, we choose $\lambda = 1$, $\beta_2 = 0.01$ and $d_3 = 1$ with the other parameter values being the ones as in Table 3.1, which correspond to $R_0 = 3.8613 < 1 + \frac{d_2}{\alpha} (= 101)$ and

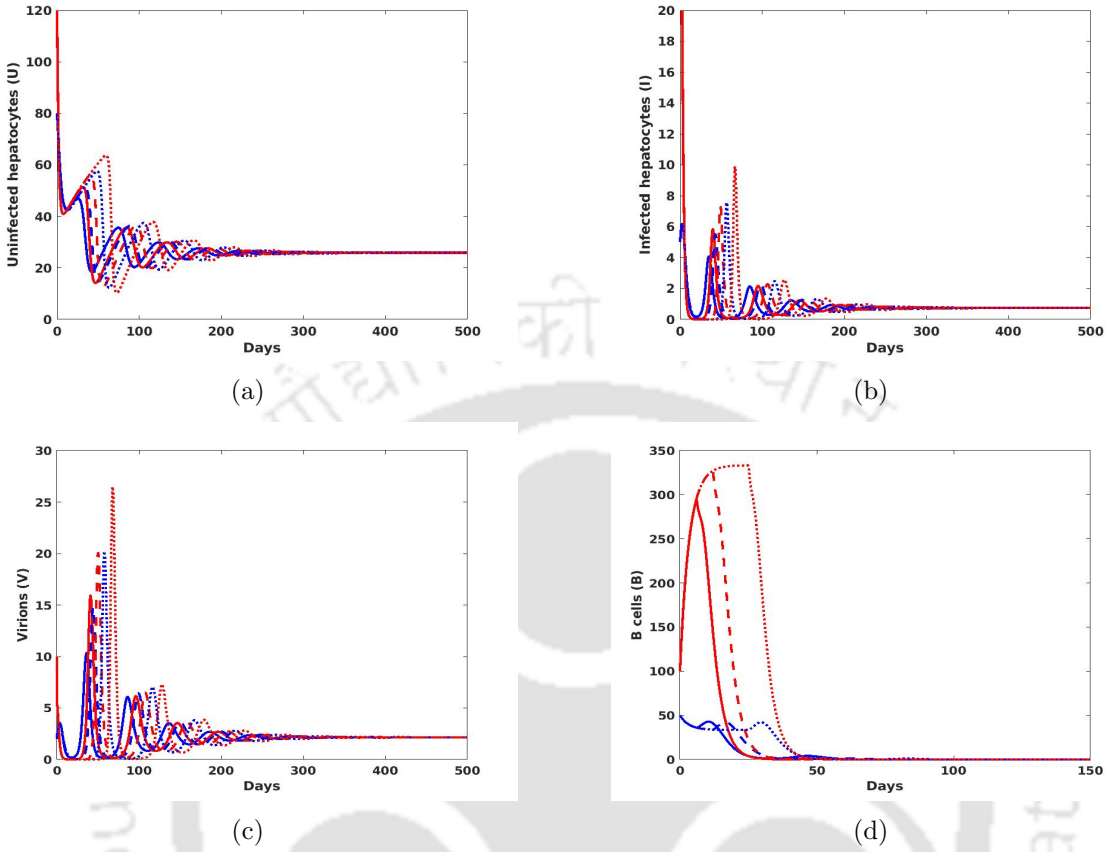

Figure 3.2: The trajectories of (a) uninfected hepatocytes, (b) infected hepatocytes, (c) virions, and (d) B cells starting with two different initial conditions ic_1 and ic_2, and three immune delays $\tau = 6,\ 12,\ 25$, in case of $R_H < 1 < R_0$ for the model (3.1.1). Blue lines : $ic_1 := (80, 5, 2, 50)$, red lines : $ic_2 := (120, 20, 10, 100)$, solid lines : $\tau = 6$, dashed lines : $\tau = 12$, dotted lines : $\tau = 25$.

$R_H = 0.7731$. This scenario is presented in Figure 3.2. This figure shows that the uninfected hepatocytes (Figure 3.2(a)), infected hepatocytes (Figure 3.2(b)) and virions (Figure 3.2(c)) starting with two different positions are oscillating for a period of time and then finally converge to their corresponding stabilized levels ($U = 25.8974$, $I = 0.7410$, $V = 2.1489$). The trajectories of the corresponding populations follow the similar oscillatory behavior in all cases with the larger cycle (slower convergence) being observed due to increase in immune delay. The B cell (Figure 3.2(d)) after starting with different positions changes its behavior depending upon the initial conditions and then suddenly falls down to zero level. It is also observed that B cells take more time to reach the zero stabilized level due to increase in immune delay. This simulation indicates that the process of B cells generation will not be able to continue without a large amount of viral load as well as sufficient infection. This suggests that the immune-free infected equilibrium E_1 $(25.8974, 0.7410, 2.1489, 0)$ is globally

asymptotically stable for any time delay in the generation of B cells, which is obtained theoretically in Theorem 3.3.4.

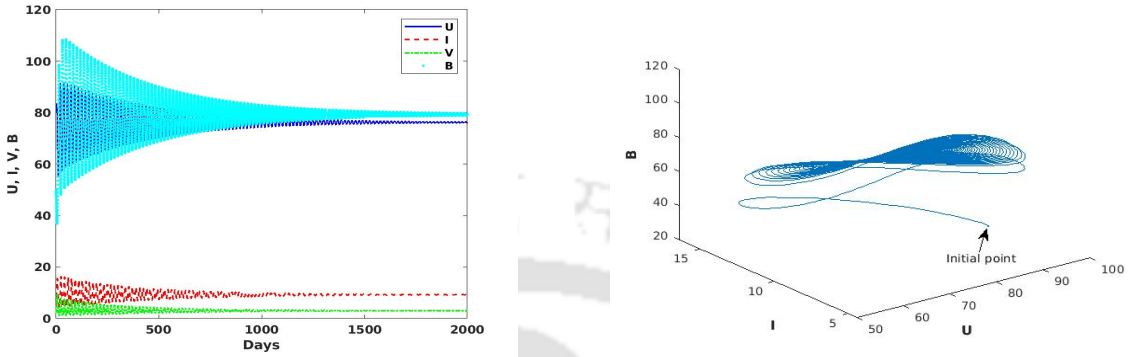

(a) (b)

Figure 3.3: The time histories and the phase portraits of trajectories shows the local asymptotic stability of E^* for immune delay $\tau = 5 < \tau_0$.

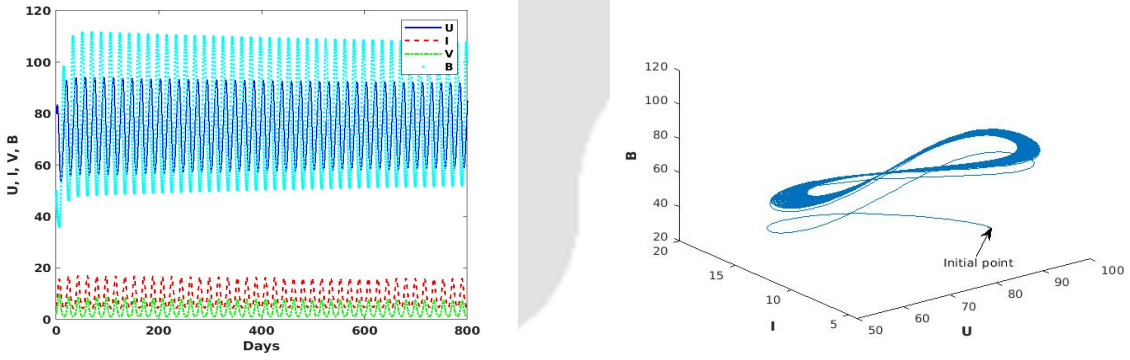

(a) (b)

Figure 3.4: The time histories and the phase portraits of trajectories shows the bifurcating periodic orbits around E^* for immune delay $\tau = 6 \in (\tau_0, \tau_2^{(0)})$.

Furthermore, we perform numerical simulation to show the Hopf bifurcation and stability switches occurring at the interior equilibrium E^* as the immune delay τ increases. For this purpose, we choose the parameter values from Table 3.1 with $\lambda = 10$, $\beta_2 = 0.01$ and $d_3 = 1$. This corresponds to $R_H = 7.7312 > 1$ and $E^* = (76.2402, 9.2375, 3, 79.2967)$. We compute the roots of the equation (3.3.11) and obtain two positive real roots, namely, $\gamma_1 = 0.1235$ and $\gamma_2 = 0.1082$, which satisfy the condition of Theorem 3.3.6. Therefore, using the formula (3.3.13), we calculate $\tau_n^{(j)}$, $n = 1, 2$; $j = 0, 1, 2, \ldots$ as follows

$$\tau_1^{(0)} = 5.7944, \ \tau_2^{(0)} = 7.4298, \ \tau_1^{(1)} = 23.6734,$$

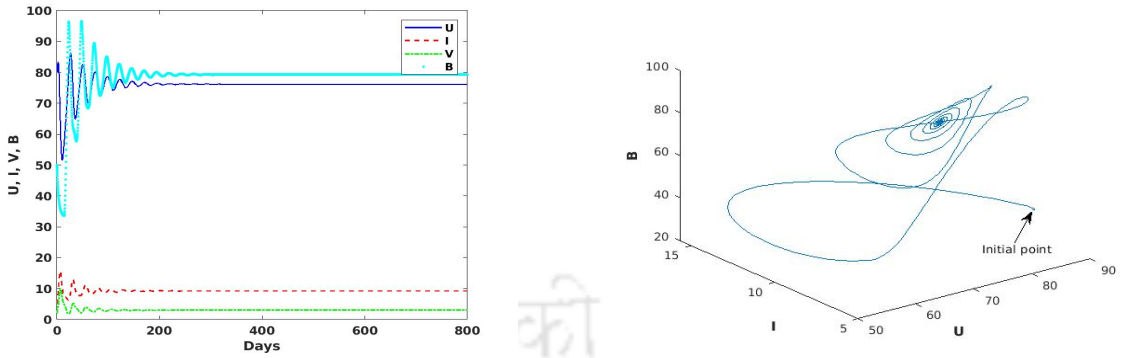

(a) (b)

Figure 3.5: The time histories and the phase portraits of trajectories shows the local asymptotic stability of E^* for immune delay $\tau = 14 \in (\tau_2^{(0)}, \tau_1^{(1)})$.

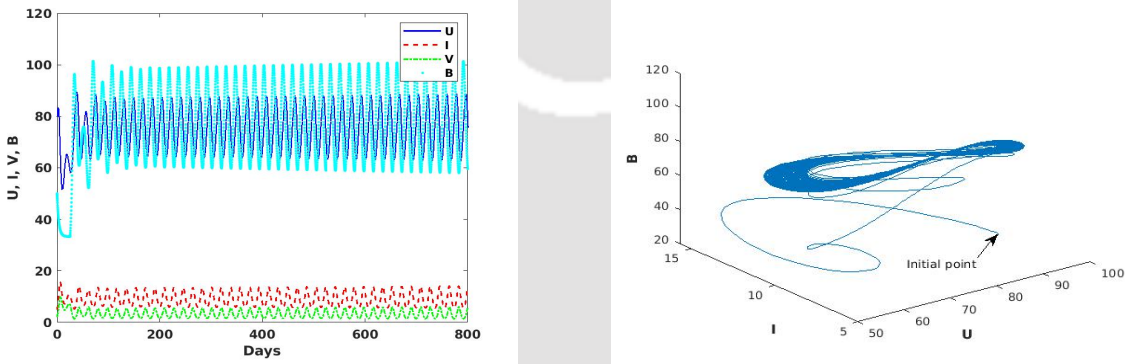

(a) (b)

Figure 3.6: The time histories and the phase portraits of trajectories shows the existence of a periodic oscillation around E^* for immune delay $\tau = 25 \in (\tau_1^{(1)}, \tau_2^{(1)})$.

$$\tau_2^{(1)} = 26.5270,\ \tau_1^{(2)} = 41.5524,\ \tau_2^{(2)} = 45.6242$$

with the value of $\tau_n^{(j)}$ for $j \geq 3$ being calculated similarly. Therefore we get $\tau_0 = \tau_1^{(0)} = 5.7944$ and $G'(\omega_0^2) = 1.7072 > 0$, which satisfies the existential condition of Hopf bifurcation in Theorem 3.3.6. We plot the density levels against time (Figures 3.3(a)–3.8(a)) and the phase portraits (Figures 3.3(b)–3.8(b)) of the trajectories of uninfected and infected hepatocytes as well as virion population for various time delays (τ). It is clearly noticed in Figure 3.3 that $E^*(76.2402, 9.2375, 3, 79.2967)$ is locally asymptotically stable when $\tau = 5 < \tau_0$. From the numerical simulation, it can be observed that E^* is locally asymptotically stable when $\tau \in [0, \tau_0)$, which is obtained theoretically in Theorem 3.3.6. Moreover, by Theorem 3.3.6, when τ is increased passed the critical value τ_0, a Hopf bifurcation occurs at $\tau = \tau_0$. The result for $\tau = 6 > \tau_0$ is shown in Figure 3.4, which implies that E^* becomes

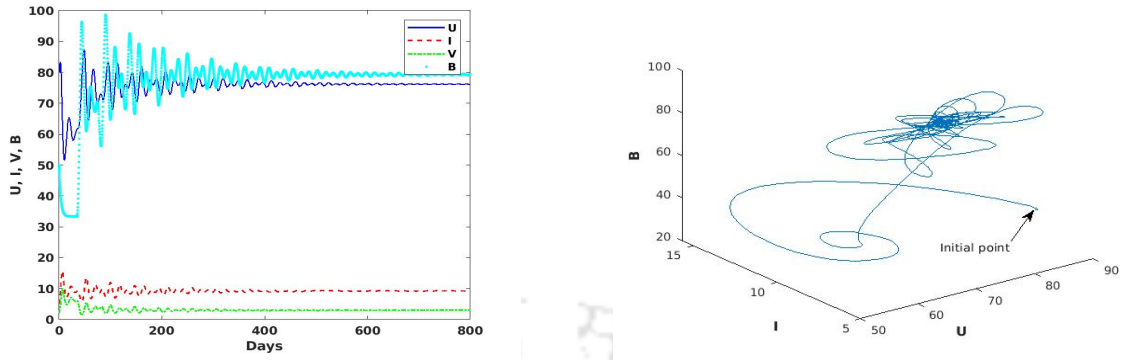

(a) (b)

Figure 3.7: The time histories and the phase portraits of trajectories shows the local asymptotic stability of E^* for immune delay $\tau = 35 \in (\tau_2^{(1)}, \tau_1^{(2)})$.

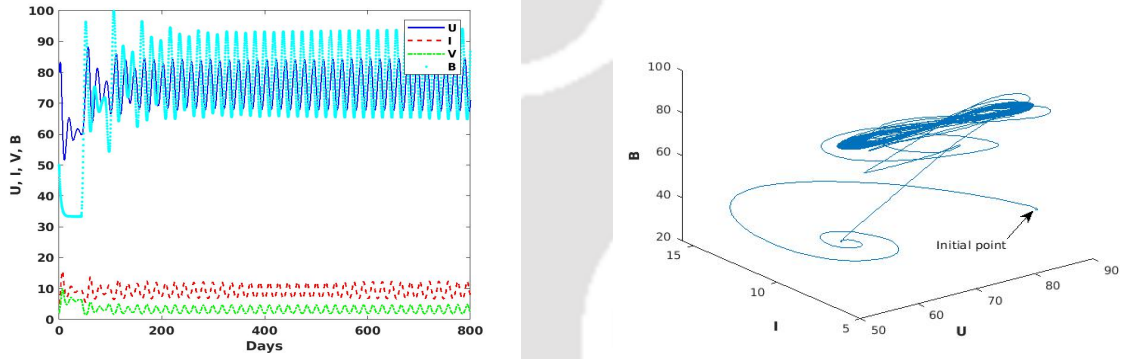

(a) (b)

Figure 3.8: The time histories and the phase portraits of trajectories shows the existence of a periodic bifurcation around E^* for immune delay $\tau = 43 \in (\tau_1^{(2)}, \tau_2^{(2)})$.

unstable and consequently a bifurcating periodic solution exists for $\tau \in (\tau_0, \tau_2^{(0)})$. Again, when τ crosses another critical value $\tau_2^{(0)}$, E^* regains local asymptotical stability which is presented for a particular value $\tau = 14$ in Figure 3.5. This shows that E^* is asymptotically stable again for $\tau \in (\tau_2^{(0)}, \tau_1^{(1)})$. For the case $\tau \in (\tau_1^{(1)}, \tau_2^{(1)})$, E^* losses stability and a periodic oscillation exists around the equilibrium E^* which is exhibited for $\tau = 25$ in Figure 3.6. If τ is increased and exceeds $\tau_2^{(1)}$, then the interior equilibrium E^* becomes stable again, which is illustrated with $\tau = 35 \in (\tau_2^{(1)}, \tau_1^{(2)})$ in Figure 3.7. Further, we simulate the system for a large value of τ, namely, $\tau = 43 \in (\tau_1^{(2)}, \tau_2^{(2)})$, which is demonstrated in Figure 3.8, showing that the stability switch occurs again with a periodic oscillation of the populations. In the same way, when the bifurcation parameter τ is increased and passes the critical bifurcation values τ_0, $\tau_2^{(0)}$, $\tau_1^{(1)}$, $\tau_2^{(1)}$, $\tau_1^{(2)}$, $\tau_2^{(2)}$ and so on, stability of

the interior equilibrium E^* of the system (3.1.1) changes from stable to unstable, Hopf bifurcation occurs at these critical values and then regains asymptotic stability from unstable behavior successively. From this numerical discussion, we can conclude that Hopf bifurcation and stability switches occur at the critical values of the bifurcation parameter, which are $\tau_1^{(j)}$ and $\tau_2^{(j)}$, $j = 0, 1, 2, \ldots$. Therefore, combining the numerical results obtained, one can finally conclude that the interior equilibrium $E^*(76.2402, 9.2375, 3, 79.2967)$ is locally asymptotically stable for $\tau \in [0, \tau_0) \bigcup \left[\bigcup_{j=0}^{\infty} \left(\tau_2^{(j)}, \tau_1^{(j+1)} \right) \right]$ with $\tau_2^{(j)} < \tau_1^{(j+1)}$, $j = 0, 1, 2, \ldots$.

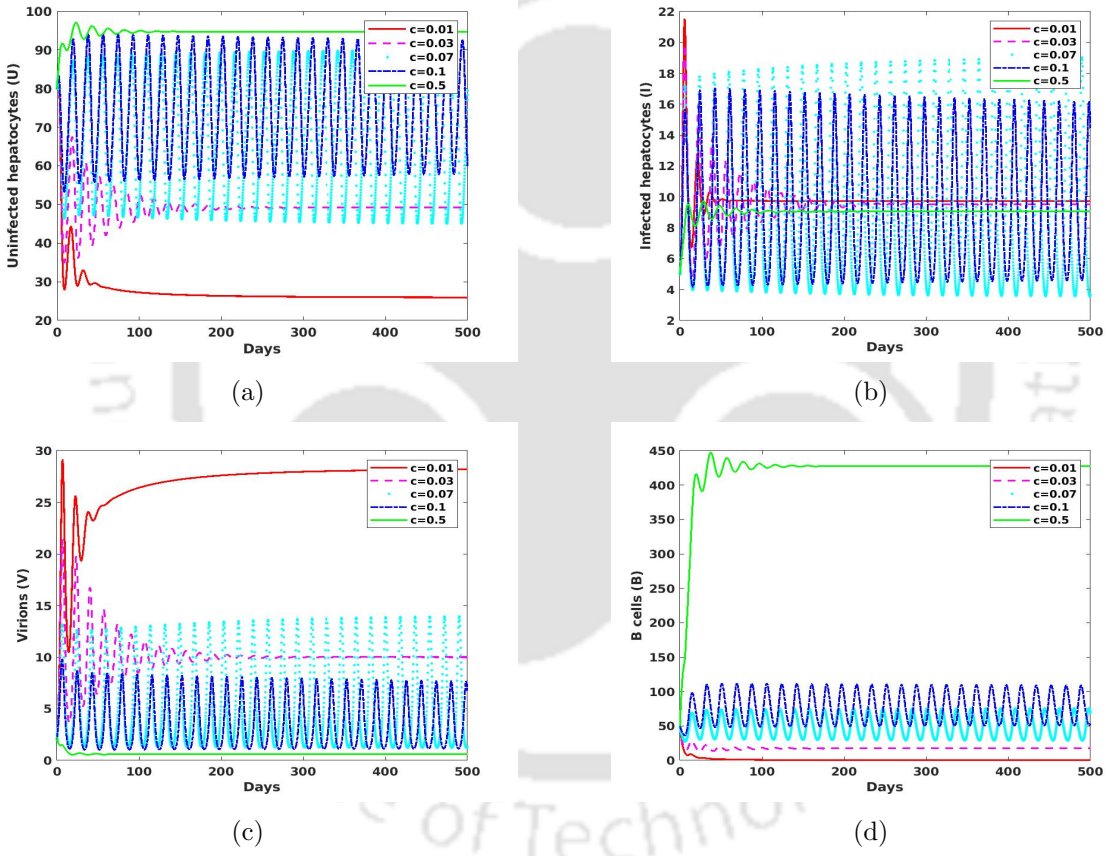

Figure 3.9: Effect of the development rate of B cells (c) on the dynamical behavior of the model system (3.1.1).

In the preceding discussion, we have shown that the time delay in generation of B cells has a significant influence on the dynamical behavior of the system. Moreover, as B cells are directly involved in the neutralization of the virions, so the viral infection can be affected depending on the development rate of B cells as well. We therefore investigate (in Figure 3.9), the effect of the development rate (c) of B cells on the dynamics of uninfected hepatocytes (Figure 3.9(a)), infected hepatocytes (Figure 3.9(b)) and viral load (Figure 3.9(c)) as well

as antibody response (Figure 3.9(d)). For this, the numerical simulation is performed for five different values of c, namely, $c = 0.01, 0.03, 0.07, 0.1, 0.5$ and the other parameters values are chosen from Table 3.1 with $\lambda = 10$, $\beta_2 = 0.01$ and $d_3 = 1$. It is observed from Figure 3.9 that when B cells are generated very slowly (in case of $c = 0.01$), the viral load as well as infected hepatocytes increase to a very high level, which results in a decrease of the uninfected hepatocytes to a very low level resulting in the antibody not responding anymore. Moreover, a slight increase in the development rate of B cells, raises the uninfected hepatocytes highly with a significant decrease in virions density. However, the changes in density of infected hepatocytes with the development rate of B cells is relatively very small. For a certain range of c (for example $c = 0.07, 0.1$), disturbance in the stability of the equilibrium and subsequent occurrence of bifurcating periodic orbits are noticed. Finally, one can observe from the expression of R_0 and R_H, that R_H is positively correlated with c, but c does not affect R_0. Therefore complete cure of infection for a patient is not possible by only magnifying the development rate of B cells. However, a high antigenic stimulation in the generation of B cells is beneficial for uninfected hepatocytes.

3.6 Conclusions

We investigated the effect of the humoral immune delay in a DDE model for HCV infection considering both virus-to-cell and cell-to-cell transmissions as well as the cure rate. The feasibility of the model has been justified by establishing the positivity and boundedness of the solution. We theoretically as well as numerically found that the two boundary equilibria are locally as well as globally asymptotically stable under the restrictions on R_0 and R_H. It is also obtained that the model system undergoes a Hopf bifurcation from the interior equilibrium when the bifurcation parameter crosses the critical values. The numerical results demonstrate the existence of stability switches and bifurcating periodic solutions due to increase in the immune delay. Further, the numerical findings showed that the development rate of B cells drives the system from stable to unstable and then from unstable to stable again. The findings suggested that a small increment in the development rate of B cells significantly increases the neutralization of the virions by the uninfected hepatocytes. Therefore, a high antigenic stimulation in the generation of B cells is beneficial for uninfected hepatocytes. However, complete cure from infection not possible by only magnifying the development rate of B cells.

Chapter 4

Reaction-Diffusion Model for HCV Dynamics Capturing Spatial Mobility of Virions and B Cells

The idea of diffusive motion of virus particle following Fickian diffusion process has been gaining greater evidence in the recent past [116]. The analysis of the diffusion models for various virological infection can be found in [12, 13, 70, 74, 118, 120, 124]. Further, Wang et al. [116] reported that the spatial domain for a biological system should be bounded and it is not realistic to assume this domain to be a square. Typically the diffusion modeling of the viral dynamics were studied with no-flux condition at the boundary in a general domain which is bounded and has smooth boundary [120]. Recent literature involves the study of the viral dynamics models with general type of infection transmission (incidence) function [105, 131].

In this chapter, we study the dynamics after the incorporation of the spatial mobility for virions and immune B cells, to the HCV model (2.1.1), with the consideration of general nonlinear incidence functions for virus-to-cell as well as cell-to-cell transmissions. We examine the properties of the solution to this PDE driven model. Next, we determine the existential conditions and the global stability of the possible non-negative equilibrium points for the model. The global stability of the equilibria is investigated by constructing suitable Lyapunov functionals. Further, the numerical illustrations of the theoretical findings are presented for the case of bilinear as well as Holling type-II incidence functions in a one-dimensional spatial domain.

4.1 Model Formulation

In the preceding chapters, the HCV models with or without delay were analyzed under the assumption of bilinear transmission function. The different types of incidence function, particularly the Holling type-II and Beddington-DeAngelis functional response were considered for the modeling of virus dynamics in [132] and [123], respectively. Further, it is observed that the spatial mobility of the virus and the immune cells were introduced in [11, 12, 74]. However, it has been noted in [120, 132] that the host cells do not exhibit diffusive behaviour. Therefore, motivated by the Fickian diffusion process driven motion of the virions as well as the immune B cells, we present the following reaction-diffusion model for HCV dynamics with general nonlinear incidence functions for both the modes of transmission accompanying non-cytolytic cure of infected hepatocytes,

$$\begin{aligned}
\frac{\partial U(x,t)}{\partial t} &= \lambda - \beta_1 h_1(U(x,t),V(x,t)) - \beta_2 h_2(U(x,t),I(x,t)) - d_1 U(x,t) + \alpha I(x,t),\\
\frac{\partial I(x,t)}{\partial t} &= \beta_1 h_1(U(x,t),V(x,t)) + \beta_2 h_2(U(x,t),I(x,t)) - d_2 I(x,t) - \alpha I(x,t),\\
\frac{\partial V(x,t)}{\partial t} &= d_V \Delta V(x,t) + kI(x,t) - d_3 V(x,t) - pV(x,t)B(x,t),\\
\frac{\partial B(x,t)}{\partial t} &= d_B \Delta B(x,t) + cV(x,t)B(x,t) - d_4 B(x,t).
\end{aligned} \tag{4.1.1}$$

Here $U(x,t)$, $I(x,t)$, $V(x,t)$ and $B(x,t)$ are the concentrations of uninfected hepatocytes, infected hepatocytes, virions and B cells at position x and at time t, respectively. The nonlinear incidence functions $h_1(U(x,t),V(x,t))$ and $h_2(U(x,t),I(x,t))$ represent the influence of infection transmission through the virus-to-cell and cell-to-cell mode, respectively. The parameters d_V and d_B denote the diffusion coefficients of virions and B cells, respectively, whereas Δ represents the Laplacian operator. The other parameters refer to the same meaning as in model (2.1.1).

Assuming a general bounded spatial domain $\Omega \subset \mathbb{R}^n$ with smooth boundary $\partial\Omega$, we take the initial conditions as follows

$$\begin{aligned}
&U(x,0) = U_0(x) > 0,\ I(x,0) = I_0(x) > 0,\\
&V(x,0) = V_0(x) > 0 \ \text{ and } \ B(x,0) = B_0(x) > 0, \ \ \forall\ x \in \overline{\Omega},
\end{aligned} \tag{4.1.2}$$

where $\overline{\Omega}$ denotes the closure of Ω. Further, suppose that $U_0(x)$, $I_0(x)$, $V_0(x)$ and $B_0(x)$ are Hölder continuous in $\overline{\Omega}$. In absence of any movement of the virions as well as the immune cells, across the boundary of the domain, we incorporate the homogeneous Neumann boundary conditions, given by

$$\frac{\partial V(x,t)}{\partial \nu} = 0 \ \text{ and } \ \frac{\partial B(x,t)}{\partial \nu} = 0, \ \ \forall\ (x,t) \in \partial\Omega \times (0,+\infty), \tag{4.1.3}$$

where $\frac{\partial}{\partial \nu}$ operates the outward normal derivative on the boundary $\partial\Omega$.

For notational convenience, we write $U,\ I,\ V$ and B to mean $U(x,t),\ I(x,t),\ V(x,t)$ and $B(x,t)$, respectively, and also write $U_0,\ I_0,\ V_0$ and B_0 to mean $U_0(x),\ I_0(x),\ V_0(x)$ and $B_0(x)$, respectively, throughout the discussion.

We suppose that the general nonlinear incidence functions $h_1(U,V)$ and $h_2(U,I)$ satisfy the following assumption:

Assumption 4.1.1. *The general nonlinear incidence functions $h_1(U,V)$ and $h_2(U,I)$ are continuously differentiable in the interior of $\mathbb{R}^2_+$ and satisfy the following conditions:*

(i) $h_1(U,V) > 0$ *and* $h_2(U,I) > 0,\ \forall\ U,\ I,\ V > 0.$

(ii) $h_1(U,0) = h_1(0,V) = 0$ *and* $h_2(U,0) = h_2(0,I) = 0,\ \forall\ U,\ I,\ V \geq 0.$

(iii) $\frac{\partial h_1(U,V)}{\partial U},\ \frac{\partial h_1(U,V)}{\partial V},\ \frac{\partial h_2(U,I)}{\partial U}$ *and* $\frac{\partial h_2(U,I)}{\partial I}$ *are continuous and non-negative,* $\forall\ U,\ I,\ V \geq 0.$

(iv) $\frac{\partial^2 h_1(U,V)}{\partial U^2},\ \frac{\partial^2 h_1(U,V)}{\partial V^2},\ \frac{\partial^2 h_2(U,I)}{\partial U^2}$ *and* $\frac{\partial^2 h_2(U,I)}{\partial I^2}$ *are non-positive,* $\forall\ U,\ I,\ V \geq 0.$

From the biological perspective, all three criteria in Assumption 4.1.1 are reasonable and realistic. The general nonlinear incidence functions $h_1(U,V)$ and $h_2(U,I)$ include several types of incidence function such as the bilinear incidence functions $h(x,y) = xy$, the standard incidence function $h(x,y) = \frac{xy}{x+y}$, the saturation or Holling type-II incidence function $h(x,y) = \frac{xy}{1+by}$, Beddington-DeAngelis type incidence function $h(x,y) = \frac{xy}{1+ax+by}$, Crowley-Martin type incidence function $h(x,y) = \frac{xy}{(1+ax)(1+by)}$, where $a, b \geq 0$. These all functional responses satisfy the conditions in Assumption 4.1.1.

4.2 Properties of Solutions and Equilibria

In this section, we first justify the feasibility of the presented model by proving the existence, uniqueness, positivity and boundedness of solution to the system (4.1.1). Then we examine the existence of equilibrium points for the system (4.1.1) under the condition on the basic reproduction number.

4.2.1 Properties of Solutions

Theorem 4.2.1. *The system (4.1.1) with the initial conditions* (4.1.2) *and boundary conditions* (4.1.3)*, admits a unique, non-negative and bounded solution for all $t \geq 0$, $x \in \overline{\Omega}$.*

Proof. In order to establish this theorem, we adopt the approach in [74, 118, 131, 132]. It is observed that the right hand side (ignoring diffusion term) of each equation of system (4.1.1) is locally Lipschitz in $C(\overline{\Omega}, \mathbb{R}^4)$ (space of continuous functions). Therefore, by [8, 108, 129], we conclude that the system (4.1.1) has a unique local solution for $t \in [0, t_m)$, $t_m > 0$.

Let us define

$$W = U + I \text{ and } Y = V + \frac{p}{c}B.$$

From first and second equation of (4.1.1), we can write

$$\frac{\partial W}{\partial t} = \lambda - d_1 U - d_2 I \leq \lambda - d_{12} W,$$

where $d_{12} = \min\{d_1, d_2\}$. Therefore

$$W \leq \max\left\{\frac{\lambda}{d_{12}}, \ \max_{x\in\overline{\Omega}}\{U_0 + I_0\}\right\} := M_1. \tag{4.2.1}$$

Further, from third and fourth equation of (4.1.1), we can write

$$\frac{\partial Y}{\partial t} - d_V \Delta V - \frac{p}{c} d_B \Delta B \leq k\gamma - d_3 V - \frac{d_4 p}{c} B,$$

where $\gamma = \max\left\{\frac{\lambda}{d_{12}}, \ \max_{x\in\overline{\Omega}}\{U_0 + I_0\}\right\}$. This implies

$$\frac{\partial Y}{\partial t} - d_Y \Delta Y \leq k\gamma - d_{34} Y,$$

where $d_Y = \max\{d_V, d_B\}$ and $d_{34} = \min\{d_3, d_4\}$. We have the boundary and initial conditions as

$$\frac{\partial Y}{\partial \nu} = 0, \ \ Y(x, 0) = V_0 + \frac{p}{c} B_0 > 0.$$

Let $\tilde{Y}(t)$ be a solution to the following ODE:

$$\frac{d\tilde{Y}(t)}{dt} = k\gamma - d_{34} Y(t), \ \ Y(0) = \max_{x\in\overline{\Omega}}\left\{V_0 + \frac{p}{c} B_0\right\}.$$

Hence, we get

$$\tilde{Y}(t) \leq \max\left\{\frac{k\gamma}{d_{34}}, \ \max_{x\in\overline{\Omega}}\left\{V_0 + \frac{p}{c} B_0\right\}\right\}, \ \forall\ t \in [0, t_m).$$

By the comparison principle [92], we have $Y \leq \tilde{Y}(t)$, $\forall\ \in \overline{\Omega} \times [0, t_m)$. Hence

$$Y \leq \max\left\{\frac{k\gamma}{d_{34}}, \ \max_{x\in\overline{\Omega}}\left\{V_0 + \frac{p}{c} B_0\right\}\right\} := M_2, \ \forall\ \in \overline{\Omega} \times [0, t_m). \tag{4.2.2}$$

Thus, (4.2.1) and (4.2.2) imply that U, I, V and B are bounded in $\overline{\Omega} \times [0, t_m)$. Using the theory of semi-linear parabolic systems [45], we conclude that $t_m = +\infty$.

Furthermore, it is noted that $(0,0,0,0)$ and (M_1, M_1, M_2, M_3) are a pair of sub and super solution for the system (4.1.1) - (4.1.3), where $M_3 = \dfrac{cM_2}{p}$. Hence, using the theory in [94], it follows that the system (4.1.1) - (4.1.3) admits a unique non-negative solution (U, I, V, B) satisfying $0 \leq U \leq M_1$, $0 \leq I \leq M_1$, $0 \leq V \leq M_2$ and $0 \leq B \leq M_3$, $\forall\ \in \overline{\Omega} \times (0, +\infty)$. □

4.2.2 Existence of Equilibria

The system (4.1.1) admits a unique infection-free equilibrium $\left(\dfrac{\lambda}{d_1}, 0, 0, 0\right)$. Therefore, using next generation method [44], we obtain the basic reproduction number for the model (4.1.1) in the absence of special dependence, given by

$$R_0 = \frac{1}{d_3(d_2+\alpha)}\left[\beta_1 k \frac{\partial h_1}{\partial V}\bigg|_{\left(\frac{\lambda}{d_1},0\right)} + \beta_2 d_3 \frac{\partial h_2}{\partial I}\bigg|_{\left(\frac{\lambda}{d_1},0\right)}\right]. \tag{4.2.3}$$

The system (4.1.1) admits three possible non-negative equilibria as follows:

1. The infection-free equilibrium $E_0 = (U_0, I_0, V_0, B_0) = \left(\frac{\lambda}{d_1}, 0, 0, 0\right)$.
2. The immune-free infected equilibrium $E_1 = (U_1, I_1, V_1, B_1)$ is given by the solution of the system

$$\begin{aligned} \lambda - \beta_1 h_1(U_1, V_1) - \beta_2 h_2(U_1, I_1) - d_1 U_1 + \alpha I_1 &= 0, \\ \beta_1 h_1(U_1, V_1) + \beta_2 h_2(U_1, I_1) - d_2 I_1 - \alpha I_1 &= 0, \\ k I_1 - d_3 V_1 &= 0, \\ B_1 &= 0. \end{aligned} \tag{4.2.4}$$

From the third equation of (4.2.4), we get $V_1 = \dfrac{kI_1}{d_3}$. Combining first and second equation of (4.2.4), we get $\lambda - d_1 U_1 - d_2 I_1 = 0$, which implies $U_1 = \dfrac{\lambda - d_2 I_1}{d_1}$ where $I_1 \in \left(0, \dfrac{\lambda}{d_2}\right]$. Therefore the second equation of (4.2.4) gives

$$\beta_1 h_1\left(\frac{\lambda - d_2 I_1}{d_1}, \frac{kI_1}{d_3}\right) + \beta_2 h_2\left(\frac{\lambda - d_2 I_1}{d_1}, I_1\right) - (d_2+\alpha) I_1 = 0. \tag{4.2.5}$$

We now show that the equation (4.2.5) has a solution $I_1 \in \left(0, \dfrac{\lambda}{d_2}\right]$. We define

$$H_1(I) = \beta_1 h_1\left(\frac{\lambda - d_2 I}{d_1}, \frac{kI}{d_3}\right) + \beta_2 h_2\left(\frac{\lambda - d_2 I}{d_1}, I\right) - (d_2+\alpha) I.$$

Observe that

(i) $H_1(0) = \beta_1 h_1\left(\frac{\lambda}{d_1}, 0\right) + \beta_2 h_2\left(\frac{\lambda}{d_1}, 0\right) = 0$, using Assumption 4.1.1$(ii)$.

(ii) $H_1\left(\frac{\lambda}{d_2}\right) = \beta_1 h_1\left(0, \frac{\lambda k}{d_2 d_3}\right) + \beta_2 h_2\left(0, \frac{\lambda}{d_2}\right) - (d_2+\alpha)\frac{\lambda}{d_2} = -(d_2+\alpha)\frac{\lambda}{d_2} < 0$, using Assumption 4.1.1$(ii)$.

(iii) $H_1'(0) = -\frac{\beta_1 d_2}{d_1}\frac{\partial h_1}{\partial U}\Big|_{\left(\frac{\lambda}{d_1},0\right)} + \frac{\beta_1 k}{d_3}\frac{\partial h_1}{\partial V}\Big|_{\left(\frac{\lambda}{d_1},0\right)} - \frac{\beta_2 d_2}{d_1}\frac{\partial h_2}{\partial U}\Big|_{\left(\frac{\lambda}{d_1},0\right)} + \beta_2\frac{\partial h_2}{\partial I}\Big|_{\left(\frac{\lambda}{d_1},0\right)} - (d_2+\alpha)$.

By Assumption 4.1.1(ii), it follows that $\frac{\partial h_1}{\partial U}\Big|_{\left(\frac{\lambda}{d_1},0\right)} = \frac{\partial h_2}{\partial U}\Big|_{\left(\frac{\lambda}{d_1},0\right)} = 0$.

Therefore, $H_1'(0) = (d_2+\alpha)(R_0 - 1) > 0$ if $R_0 > 1$. Further, since $H_1(0) = 0$ and $H_1\left(\frac{\lambda}{d_2}\right) < 0$, hence there exists an $I_1 \in \left(0, \frac{\lambda}{d_2}\right]$ satisfying (4.2.5). Thus, the immune-free infected equilibrium E_1 exists if $R_0 > 1$.

3. The immune-activation infected equilibrium $E^* = (U^*, I^*, V^*, B^*)$ is given by the solution of the system

$$\begin{aligned} \lambda - \beta_1 h_1(U^*, V^*) - \beta_2 h_2(U^*, I^*) - d_1 U^* + \alpha I^* &= 0, \\ \beta_1 h_1(U^*, V^*) + \beta_2 h_2(U^*, I^*) - d_2 I^* - \alpha I^* &= 0, \\ k I^* - d_3 V^* - p V^* B^* &= 0, \\ c V^* B^* - d_4 B^* &= 0. \end{aligned} \tag{4.2.6}$$

From the forth equation of (4.2.6), we get $V^* = \frac{d_4}{c}$. The third equation of (4.2.6) gives $B^* = \frac{d_3}{p}\left(\frac{ck}{d_3 d_4} I^* - 1\right)$.

We now define

$$R_1 = \frac{ck}{d_3 d_4} I_2. \tag{4.2.7}$$

Now, combining first and second equation of (4.2.6), we get $U^* = \frac{\lambda - d_2 I^*}{d_1}$ where $I^* \in \left(0, \frac{\lambda}{d_2}\right]$. Therefore the second equation of (4.2.6) gives

$$\beta_1 h_1\left(\frac{\lambda - d_2 I^*}{d_1}, \frac{d_4}{c}\right) + \beta_2 h_2\left(\frac{\lambda - d_2 I^*}{d_1}, I^*\right) - (d_2+\alpha) I^* = 0. \tag{4.2.8}$$

We define

$$H_2(I) = \beta_1 h_1\left(\frac{\lambda - d_2 I}{d_1}, \frac{d_4}{c}\right) + \beta_2 h_2\left(\frac{\lambda - d_2 I}{d_1}, I\right) - (d_2+\alpha) I.$$

Observe that

(i) $H_2(0) = \beta_1 h_1\left(\frac{\lambda}{d_1}, \frac{d_4}{c}\right) + \beta_2 h_2\left(\frac{\lambda}{d_1}, 0\right) = \beta_1 h_1\left(\frac{\lambda}{d_1}, \frac{d_4}{c}\right) > 0$, using Assumption 4.1.1$(i)$ & 4.1.1(ii).

(ii) $H_2\left(\frac{\lambda}{d_2}\right) = \beta_1 h_1\left(0, \frac{d_4}{c}\right) + \beta_2 h_2\left(0, \frac{\lambda}{d_2}\right) - (d_2+\alpha)\frac{\lambda}{d_2} = -(d_2+\alpha)\frac{\lambda}{d_2} < 0$, using Assumption 4.1.1$(ii)$.

Thus, $H_2(0) > 0$ and $H_2\left(\frac{\lambda}{d_2}\right) < 0$. Hence, there exists an $I^* \in \left(0, \frac{\lambda}{d_2}\right]$ satisfying (4.2.8). Therefore, the immune-activation infected equilibriumE^* exists if $R_1 > 1$.

For the next discussion, we further define an another threshold parameter expressed as

$$R_2 = \frac{ck}{d_3 d_4} I_1. \tag{4.2.9}$$

4.3 Global Behavior of the System

In order to prove the global stability of equilibria of the system (4.1.1), we use the LaSalle's invariance principle [40]. For our computational convenience, we define a function $\psi(z) = z - 1 - \ln(z)$, $z > 0$. In addition, we write $\frac{\partial h_1(E_0)}{\partial V}$ and $\frac{\partial h_2(E_0)}{\partial I}$ to mean $\left.\frac{\partial h_1}{\partial V}\right|_{\left(\frac{\lambda}{d_1},0\right)}$ and $\left.\frac{\partial h_2}{\partial I}\right|_{\left(\frac{\lambda}{d_1},0\right)}$ throughout the discussion. It can be easily verified that $\psi(z) \geq 0$, $\forall\ z > 0$ and $\psi(z) = 0$ if and only if $z = 1$. Further, for the global stability, we consider the following assumption.

Assumption 4.3.1. *The general nonlinear incidence functions $h_1(U,V)$ and $h_2(U,I)$ satisfy the following conditions:*

(i) $U_0 h_1(U,V) \leq UV\frac{\partial h_1(E_0)}{\partial V}$ *and* $U_0 h_2(U,V) \leq UI\frac{\partial h_2(E_0)}{\partial I}$.

(ii) $\left(\frac{U_i h_1(U,V)}{U h_1(U_i,V_i)} - \frac{V}{V_i}\right)\left(1 - \frac{U h_1(U_i,V_i)}{U_i h_1(U,V)}\right) \leq 0$ *and* $\left(\frac{U_i h_2(U,I)}{U h_2(U_i,I_i)} - \frac{I}{I_i}\right)\left(1 - \frac{U h_2(U_i,I_i)}{U_i h_2(U,I)}\right) \leq 0$, *where* $i = 1, 2$ *and* (U_2, I_2, V_2, B_2) *representing* (U^*, I^*, V^*, B^*).

One can easily verify that Assumption 4.3.1 holds for several types of incidence functions including the bilinear functional response $h(x,y) = xy$ as well as Holling type-II functional response $h(x,y) = \frac{xy}{1+y}$.

Theorem 4.3.2. *Suppose Assumption 4.3.1 holds. Then the infection-free equilibrium E_0 is globally asymptotically stable when $R_0 \leq 1$.*

Proof. We consider a Lyapunov functional $L_1(U, I, V, B)$ as

$$\begin{aligned} L_1(U,I,V,B) &= \int_\Omega \left\{ U_0 \psi\left(\frac{U}{U_0}\right) + I + \frac{\beta_1}{d_3}\frac{\partial h_1(E_0)}{\partial V} V + \frac{\beta_1 p}{c d_3}\frac{\partial h_1(E_0)}{\partial V} B \right. \\ &\quad \left. + \frac{\alpha}{2(d_1+d_2)U_0}\left[(U-U_0)+I\right]^2 \right\} dx. \end{aligned}$$

After calculation of the time derivative of $L_1(U, I, V, B)$ along the solution of (4.1.1), we get

$$\begin{aligned} \frac{dL_1}{dt} &= \int_\Omega \left\{ \left(1-\frac{U_0}{U}\right)\left[\lambda - \beta_1 h_1(U,V) - \beta_2 h_2(U,I) - d_1 U + \alpha I\right] \right. \\ &\quad + \left[\beta_1 h_1(U,V) + \beta_2 h_2(U,I) - d_2 I - \alpha I\right] + \frac{\beta_1}{d_3}\frac{\partial h_1(E_0)}{\partial V}\left[d_V \Delta V + kI - d_3 V - pVB\right] \\ &\quad \left. + \frac{\beta_1 p}{c d_3}\frac{\partial h_1(E_0)}{\partial V}\left[d_B \Delta B + cVB - d_4 B\right] + \frac{\alpha}{(d_1+d_2)U_0}\left[(U-U_0)+I\right]\left[\lambda - d_1 U - d_2 I\right] \right\} dx. \end{aligned}$$

We observe that

$$\alpha\left(1-\frac{U_0}{U}\right) I = -\alpha I \frac{(U-U_0)^2}{UU_0} + \frac{\alpha}{U_0}(U-U_0)\, I. \tag{4.3.1}$$

Therefore, using the relation $\lambda = d_1 U_0$ along with (4.3.1) and simplifying, we get

$$\begin{aligned} \frac{dL_1}{dt} &= \int_\Omega \left\{ -\left(d_1 U_0 + \alpha I + \frac{\alpha d_1 U}{d_1+d_2}\right)\frac{(U-U_0)^2}{UU_0} - \frac{\alpha d_2 I^2}{(d_1+d_2)U_0} - \frac{\beta_1 d_4 pB}{c d_3}\frac{\partial h_1(E_0)}{\partial V} \right. \\ &\quad + \frac{I}{d_3}\left[\beta_1 k \frac{\partial h_1(E_0)}{\partial V} + \beta_2 d_3 \frac{\partial h_2(E_0)}{\partial I}\right] + \frac{\beta_1}{U}\left[U_0 h_1(U,V) - UV\frac{\partial h_1(E_0)}{\partial V}\right] \\ &\quad \left. + \frac{\beta_2}{U}\left[U_0 h_2(U,V) - UI\frac{\partial h_2(E_0)}{\partial I}\right] - (d_2+\alpha) I \right\} dx \\ &\quad + \frac{\beta_1 d_V}{d_3}\frac{\partial h_2(E_0)}{\partial I}\int_\Omega \Delta V dx + \frac{\beta_1 p d_B}{c d_3}\frac{\partial h_2(E_0)}{\partial I}\int_\Omega \Delta B dx. \end{aligned}$$

Using the homogeneous Neumann boundary conditions and the divergence theorem [37], we have

$$\int_\Omega \Delta V dx = 0 \quad \text{and} \quad \int_\Omega \Delta B dx = 0.$$

Therefore, we have

$$\begin{aligned} \frac{dL_1}{dt} &= \int_\Omega \left\{ -\left(d_1 U_0 + \alpha I + \frac{\alpha d_1 U}{d_1+d_2}\right)\frac{(U-U_0)^2}{UU_0} - \frac{\alpha d_2 I^2}{(d_1+d_2)U_0} - \frac{\beta_1 d_4 pB}{c d_3}\frac{\partial h_1(E_0)}{\partial V} \right. \\ &\quad + (d_2+\alpha) I\,(R_0 - 1) + \frac{\beta_1}{U}\left[U_0 h_1(U,V) - UV\frac{\partial h_1(E_0)}{\partial V}\right] \\ &\quad \left. + \frac{\beta_2}{U}\left[U_0 h_2(U,V) - UI\frac{\partial h_2(E_0)}{\partial I}\right] \right\} dx. \end{aligned}$$

Hence, by Assumption 4.3.1(i), it follows that $\frac{dL_1}{dt} \leq 0$ when $R_0 \leq 1$. Let S_1 be the largest invariant set $\{(U, I, V, B) \mid \frac{dL_1}{dt} = 0\}$. We note that $\frac{dL_1}{dt} = 0$ if and only if $U = U_0$, $I = 0$, $V = 0$ and $B = 0$. Hence, $S_1 = \{E_0\}$. Therefore, using LaSalle's invariance principle, we conclude that E_0 is globally asymptotically stable when $R_0 \leq 1$. □

Theorem 4.3.3. *Suppose Assumption 4.3.1 holds. Then the immune-free infected equilibrium E_1 is globally asymptotically stable when $R_2 \leq 1 < R_0$ and $d_1U_1 - \alpha I_1 \geq 0$.*

Proof. We consider a Lyapunov functional $L_2(U, I, V, B)$ as

$$\begin{aligned} L_2(U, I, V, B) &= \int_\Omega \left\{ U_1 \psi\left(\frac{U}{U_1}\right) + I_1 \psi\left(\frac{I}{I_1}\right) + \frac{\beta_1 h_1(U_1, V_1) V_1}{kI_1} \psi\left(\frac{V}{V_1}\right) \right. \\ &\quad \left. + \frac{\beta_1 p h_1(U_1, V_1)}{ckI_1} B + \frac{\alpha}{2(d_1 + d_2)U_1} \left[(U - U_1) + (I - I_1)\right]^2 \right\} dx. \end{aligned}$$

After calculation of the time derivative of $L_2(U, I, V, B)$ along the solution of (4.1.1), we get

$$\begin{aligned} \frac{dL_2}{dt} &= \int_\Omega \left\{ \left(1 - \frac{U_1}{U}\right) \left[\lambda - \beta_1 h_1(U, V) - \beta_2 h_2(U, I) - d_1 U + \alpha I\right] \right. \\ &\quad + \left(1 - \frac{I_1}{I}\right) \left[\beta_1 h_1(U, V) + \beta_2 h_2(U, I) - d_2 I - \alpha I\right] \\ &\quad + \frac{\beta_1 h_1(U_1, V_1)}{kI_1} \left(1 - \frac{V_1}{V}\right) \left[d_V \Delta V + kI - d_3 V - pVB\right] \\ &\quad + \frac{\beta_1 p h_1(U_1, V_1)}{ckI_1} \left[d_B \Delta B + cVB - d_4 B\right] \\ &\quad \left. + \frac{\alpha}{(d_1 + d_2)U_1} \left[(U - U_1) + (I - I_1)\right] \left[\lambda - d_1 U - d_2 I\right] \right\} dx. \end{aligned}$$

Using (4.2.4), we get

$$\begin{aligned} \frac{dL_2}{dt} &= \int_\Omega \left\{ \left(1 - \frac{U_1}{U}\right) \left[\beta_1 h_1(U_1, V_1) + \beta_2 h_2(U_1, I_1) + d_1 U_1 - \alpha I_1 \right.\right. \\ &\qquad \left. - \beta_1 h_1(U, V) - \beta_2 h_2(U, I) - d_1 U + \alpha I\right] \\ &\quad + \left(1 - \frac{I_1}{I}\right) \left[\beta_1 h_1(U, V) + \beta_2 h_2(U, I) - \frac{\beta_1 h_1(U_1, V_1)}{I_1} I - \frac{\beta_2 h_2(U_1, I_1)}{I_1} I\right] \\ &\quad + \frac{\beta_1 h_1(U_1, V_1)}{kI_1} \left(1 - \frac{V_1}{V}\right) \left[d_V \Delta V + kI - \frac{kI_1}{V_1} V - pVB\right] \\ &\quad + \frac{\beta_1 p h_1(U_1, V_1)}{ckI_1} \left[d_B \Delta B + cVB - d_4 B\right] \\ &\quad \left. + \frac{\alpha}{(d_1 + d_2)U_1} \left[(U - U_1) + (I - I_1)\right] \left[-d_1(U - U_1) - d_2(I - I_1)\right] \right\} dx. \end{aligned}$$

We observe that

$$\alpha\left(1-\frac{U_1}{U}\right)(I-I_1) = -\alpha(I-I_1)\frac{(U-U_1)^2}{UU_1} + \frac{\alpha}{U_1}(U-U_1)(I-I_1).$$

Thus

$$\begin{aligned}
\frac{dL_2}{dt} &= \int_\Omega \Bigg\{ -\left[d_1U_1 - \alpha I_1 + \alpha I + \frac{\alpha d_1 U}{d_1+d_2}\right]\frac{(U-U_1)^2}{UU_1} - \frac{\alpha d_2}{(d_1+d_2)U_1}(I-I_1)^2 \\
&\quad - \beta_1 h_1(U_1,V_1)\Bigg[\psi\left(\frac{U_1}{U}\right) + \psi\left(\frac{IV_1}{I_1V}\right) + \psi\left(\frac{I_1h_1(U,V)}{Ih_1(U_1,V_1)}\right) \\
&\quad + \psi\left(\frac{UVh_1(U_1,V_1)}{U_1V_1h_1(U,V)}\right) - \left(\frac{U_1h_1(U,V)}{Uh_1(U_1,V_1)} - \frac{V}{V_1}\right)\left(1-\frac{Uh_1(U_1,V_1)}{U_1h_1(U,V)}\right)\Bigg] \\
&\quad - \beta_2 h_2(U_1,I_1)\Bigg[\psi\left(\frac{U_1}{U}\right) + \psi\left(\frac{I_1h_2(U,I)}{Ih_2(U_1,I_1)}\right) + \psi\left(\frac{UIh_2(U_1,I_1)}{U_1I_1h_2(U,I)}\right) \\
&\quad - \left(\frac{U_1h_2(U,I)}{Uh_2(U_1,I_1)} - \frac{I}{I_1}\right)\left(1-\frac{Uh_2(U_1,I_1)}{U_1h_2(U,I)}\right)\Bigg] + \frac{\beta_1 p h_1(U_1,V_1)B}{kI_1}\left(V_1 - \frac{d_4}{c}\right)\Bigg\}dx \\
&\quad + \frac{\beta_1 h_1(U_1,V_1)d_V}{kI_1}\int_\Omega\left(1-\frac{V_1}{V}\right)\Delta V dx + \frac{\beta_1 p h_1(U_1,V_1)d_B}{ckI_1}\int_\Omega \Delta B dx.
\end{aligned}$$

Using the homogeneous Neumann boundary conditions and the divergence theorem [37], we have

$$\int_\Omega \Delta V dx = 0, \quad \int_\Omega \Delta B dx = 0 \quad \text{and} \quad \int_\Omega \frac{\Delta V}{V}dx = \int_\Omega \frac{||\nabla V||^2}{V^2}dx.$$

Therefore, we have

$$\begin{aligned}
\frac{dL_2}{dt} &= \int_\Omega \Bigg\{ -\left[d_1U_1 - \alpha I_1 + \alpha I + \frac{\alpha d_1 U}{d_1+d_2}\right]\frac{(U-U_1)^2}{UU_1} - \frac{\alpha d_2}{(d_1+d_2)U_1}(I-I_1)^2 \\
&\quad - \beta_1 h_1(U_1,V_1)\Bigg[\psi\left(\frac{U_1}{U}\right) + \psi\left(\frac{IV_1}{I_1V}\right) + \psi\left(\frac{I_1h_1(U,V)}{Ih_1(U_1,V_1)}\right) \\
&\quad + \psi\left(\frac{UVh_1(U_1,V_1)}{U_1V_1h_1(U,V)}\right) - \left(\frac{U_1h_1(U,V)}{Uh_1(U_1,V_1)} - \frac{V}{V_1}\right)\left(1-\frac{Uh_1(U_1,V_1)}{U_1h_1(U,V)}\right)\Bigg] \\
&\quad - \beta_2 h_2(U_1,I_1)\Bigg[\psi\left(\frac{U_1}{U}\right) + \psi\left(\frac{I_1h_2(U,I)}{Ih_2(U_1,I_1)}\right) + \psi\left(\frac{UIh_2(U_1,I_1)}{U_1I_1h_2(U,I)}\right) \\
&\quad - \left(\frac{U_1h_2(U,I)}{Uh_2(U_1,I_1)} - \frac{I}{I_1}\right)\left(1-\frac{Uh_2(U_1,I_1)}{U_1h_2(U,I)}\right)\Bigg] \\
&\quad + \frac{\beta_1 d_4 p h_1(U_1,V_1)B}{ckI_1}\left(\frac{ck}{d_3d_4}I_1 - 1\right)\Bigg\}dx - \frac{\beta_1 h_1(U_1,V_1)V_1 d_V}{kI_1}\int_\Omega \frac{||\nabla V||^2}{V^2}dx.
\end{aligned}$$

Hence, by Assumption 4.3.1(ii), it follows that $\frac{dL_2}{dt} \leq 0$ when $R_2 \leq 1$ and $d_1U_1 - \alpha I_1 \geq 0$. Let S_2 be the largest invariant set $\{(U,I,V,B) \mid \frac{dL_2}{dt} = 0\}$. We note that $\frac{dL_2}{dt} = 0$ if and only if $U = U_1$, $I = I_1$, $V = V_1$ and $B = B_1$. Hence, $S_2 = \{E_1\}$. Again, E_1 exists when $R_0 > 1$. Therefore, using LaSalle's invariance principle, we conclude that E_1 is globally asymptotically stable when $R_2 \leq 1 < R_0$ and $d_1U_1 - \alpha I_1 \geq 0$. □

Theorem 4.3.4. *Suppose Assumption 4.3.1 holds. Then the immune-activation infected equilibrium E^* is locally asymptotically stable when $R_1 > 1$ and $d_1U^* - \alpha I^* \geq 0$.*

Proof. We consider a Lyapunov functional $L_3(U, I, V, B)$ as

$$\begin{aligned} L_3(U,I,V,B) &= \int_\Omega \left\{ U^*\psi\left(\frac{U}{U^*}\right) + I^*\psi\left(\frac{I}{I^*}\right) + \frac{\beta_1 h_1(U^*,V^*)V^*}{kI^*}\psi\left(\frac{V}{V^*}\right) \right. \\ &\quad \left. + \frac{\beta_1 p h_1(U^*,V^*)B^*}{ckI^*}\psi\left(\frac{B}{B^*}\right) + \frac{\alpha}{2(d_1+d_2)U^*}\left[(U-U^*)+(I-I^*)\right]^2 \right\} dx. \end{aligned}$$

After calculation of the time derivative of $L_3(U, I, V, B)$ along the solution of (4.1.1), we get

$$\begin{aligned} \frac{dL_3}{dt} &= \int_\Omega \left\{ \left(1-\frac{U^*}{U}\right)\left[\lambda - \beta_1 h_1(U,V) - \beta_2 h_2(U,I) - d_1U + \alpha I\right] \right. \\ &\quad + \left(1-\frac{I^*}{I}\right)\left[\beta_1 h_1(U,V) + \beta_2 h_2(U,I) - d_2 I - \alpha I\right] \\ &\quad + \frac{\beta_1 h_1(U^*,V^*)}{kI^*}\left(1-\frac{V^*}{V}\right)\left[d_V\Delta V + kI - d_3V - pVB\right] \\ &\quad + \frac{\beta_1 p h_1(U^*,V^*)}{ckI^*}\left(1-\frac{B^*}{B}\right)\left[d_B\Delta B + cVB - d_4B\right] \\ &\quad \left. + \frac{\alpha}{(d_1+d_2)U^*}\left[(U-U^*)+(I-I^*)\right]\left[\lambda - d_1U - d_2I\right] \right\} dx. \end{aligned}$$

Using (4.2.6), we get

$$\begin{aligned} \frac{dL_3}{dt} &= \int_\Omega \left\{ \left(1-\frac{U^*}{U}\right)\left[\beta_1 h_1(U^*,V^*) + \beta_2 h_2(U^*,I^*) + d_1U^* - \alpha I^* \right.\right. \\ &\qquad \left. - \beta_1 h_1(U,V) - \beta_2 h_2(U,I) - d_1U + \alpha I\right] \\ &\quad + \left(1-\frac{I^*}{I}\right)\left[\beta_1 h_1(U,V) + \beta_2 h_2(U,I) - \frac{\beta_1 h_1(U^*,V^*)}{I^*}I - \frac{\beta_2 h_2(U^*,I^*)}{I^*}I\right] \\ &\quad + \frac{\beta_1 h_1(U^*,V^*)}{kI^*}\left(1-\frac{V^*}{V}\right)\left[d_V\Delta V + kI - \frac{kI^*}{V^*}V + pB^*V - pVB\right] \\ &\quad + \frac{\beta_1 p h_1(U^*,V^*)}{ckI^*}\left(1-\frac{B^*}{B}\right)\left[d_B\Delta B + cVB - cV^*B\right] \\ &\quad \left. + \frac{\alpha}{(d_1+d_2)U^*}\left[(U-U^*)+(I-I^*)\right]\left[-d_1(U-U^*) - d_2(I-I^*)\right] \right\} dx. \end{aligned}$$

We observe that

$$\alpha\left(1-\frac{U^*}{U}\right)(I-I^*) = -\alpha(I-I^*)\frac{(U-U^*)^2}{UU^*} + \frac{\alpha}{U^*}(U-U^*)(I-I^*).$$

Thus

$$\begin{aligned}\frac{dL_3}{dt} &= \int_\Omega \Bigg\{ -\left[d_1U^* - \alpha I^* + \alpha I + \frac{\alpha d_1 U}{d_1+d_2}\right]\frac{(U-U^*)^2}{UU^*} - \frac{\alpha d_2}{(d_1+d_2)U^*}(I-I^*)^2 \\ &\quad - \beta_1 h_1(U^*,V^*)\Bigg[\psi\left(\frac{U^*}{U}\right) + \psi\left(\frac{IV^*}{I^*V}\right) + \psi\left(\frac{I^*h_1(U,V)}{Ih_1(U^*,V^*)}\right) \\ &\quad + \psi\left(\frac{UVh_1(U^*,V^*)}{U^*V^*h_1(U,V)}\right) - \left(\frac{U^*h_1(U,V)}{Uh_1(U^*,V^*)} - \frac{V}{V^*}\right)\left(1 - \frac{Uh_1(U^*,V^*)}{U^*h_1(U,V)}\right)\Bigg] \\ &\quad - \beta_2 h_2(U^*,I^*)\Bigg[\psi\left(\frac{U^*}{U}\right) + \psi\left(\frac{I^*h_2(U,I)}{Ih_2(U^*,I^*)}\right) + \psi\left(\frac{UIh_2(U^*,I^*)}{U^*I^*h_2(U,I)}\right) \\ &\quad - \left(\frac{U^*h_2(U,I)}{Uh_2(U^*,I^*)} - \frac{I}{I^*}\right)\left(1 - \frac{Uh_2(U^*,I^*)}{U^*h_2(U,I)}\right)\Bigg]\Bigg\}dx \\ &\quad + \frac{\beta_1 h_1(U^*,V^*)d_V}{kI^*}\int_\Omega\left(1-\frac{V^*}{V}\right)\Delta V dx + \frac{\beta_1 p h_1(U^*,V^*)d_B}{ckI^*}\int_\Omega\left(1-\frac{B^*}{B}\right)\Delta B dx.\end{aligned}$$

Using the homogeneous Neumann boundary conditions and the divergence theorem [37], we have

$$\begin{aligned}\int_\Omega \Delta V dx = 0, \quad \int_\Omega \frac{\Delta V}{V}dx = \int_\Omega \frac{||\nabla V||^2}{V^2}dx, \\ \int_\Omega \Delta B dx = 0, \quad \int_\Omega \frac{\Delta B}{B}dx = \int_\Omega \frac{||\nabla B||^2}{B^2}dx.\end{aligned}$$

Therefore, we have

$$\begin{aligned}\frac{dL_3}{dt} &= \int_\Omega \Bigg\{ -\left[d_1U^* - \alpha I^* + \alpha I + \frac{\alpha d_1 U}{d_1+d_2}\right]\frac{(U-U^*)^2}{UU^*} - \frac{\alpha d_2}{(d_1+d_2)U^*}(I-I^*)^2 \\ &\quad - \beta_1 h_1(U^*,V^*)\Bigg[\psi\left(\frac{U^*}{U}\right) + \psi\left(\frac{IV^*}{I^*V}\right) + \psi\left(\frac{I^*h_1(U,V)}{Ih_1(U^*,V^*)}\right) \\ &\quad + \psi\left(\frac{UVh_1(U^*,V^*)}{U^*V^*h_1(U,V)}\right) - \left(\frac{U^*h_1(U,V)}{Uh_1(U^*,V^*)} - \frac{V}{V^*}\right)\left(1 - \frac{Uh_1(U^*,V^*)}{U^*h_1(U,V)}\right)\Bigg] \\ &\quad - \beta_2 h_2(U^*,I^*)\Bigg[\psi\left(\frac{U^*}{U}\right) + \psi\left(\frac{I^*h_2(U,I)}{Ih_2(U^*,I^*)}\right) + \psi\left(\frac{UIh_2(U^*,I^*)}{U^*I^*h_2(U,I)}\right) \\ &\quad - \left(\frac{U^*h_2(U,I)}{Uh_2(U^*,I^*)} - \frac{I}{I^*}\right)\left(1 - \frac{Uh_2(U^*,I^*)}{U^*h_2(U,I)}\right)\Bigg]\Bigg\}dx \\ &\quad - \frac{\beta_1 h_1(U^*,V^*)V^*d_V}{kI^*}\int_\Omega \frac{||\nabla V||^2}{V^2}dx - \frac{\beta_1 p h_1(U^*,V^*)B^*d_V}{ckI^*}\int_\Omega \frac{||\nabla B||^2}{B^2}dx.\end{aligned}$$

Hence, by Assumption 4.3.1(ii), it follows that $\frac{dL_3}{dt} \leq 0$ when $d_1U^* - \alpha I^* \geq 0$. Let S_3 be the largest invariant set $\{(U,I,V,B) \mid \frac{dL_2}{dt} = 0\}$. We note that $\frac{dL_3}{dt} = 0$ if and only if $U = U^*$, $I = I^*$, $V = V^*$ and $B = B^*$. Hence, $S_3 = \{E^*\}$. Again, E^* exists when $R_1 > 1$. Therefore, using LaSalle's invariance principle, we conclude that E^* is globally asymptotically stable when $R_1 > 1$ and $d_1U^* - \alpha I^* \geq 0$. □

Remark 4.3.5. *The conditions for the global stability in Theorems 4.3.2–4.3.4 are only sufficient, but not necessary. Furthermore, the additional conditions required in Theorem 4.3.3 and Theorem 4.3.4 are* $d_1U_i - \alpha I_i \geq 0$, *which implies* $\lambda - \beta_1 U_i V_i - \beta_2 U_i I_i \geq 0$, *where* $i = 1, 2$ *and* (U_2, I_2, V_2, B_2) *representing* (U^*, I^*, V^*, B^*). *These additional conditions reflect that the infection rate does not exceed the recruitment rate of uninfected hepatocytes, which is reasonable from the biological perspective.*

Remark 4.3.6. *The condition* $R_2 \leq 1$, *which appears in Theorems 4.3.3 for the global stability of* E_2, *is equivalent to the condition* $V_1 \leq \dfrac{d_4}{c}$.

4.4 Numerical Illustrations

In this section, we present some numerical results in order to illustrate the analytical findings obtained in the preceding section. We carry out numerical simulations for the model (4.1.1), considering two types of incidence functions for both virus-to-cell and cell-to-cell infection and then compare the results. The incidence functions h_1 and h_2 are to be taken:

(a) Bilinear incidence function: $h_1(U, V) = UV$ and $h_2(U, I) = UI$,

(b) Holling type-II incidence function: $h_1(U, V) = \dfrac{UV}{1+V}$ and $h_2(U, I) = \dfrac{UI}{1+I}$.

Note that the values of R_0 determined for both cases (a) and (b) are identical and is given by

$$R_0 = \frac{\lambda(\beta_1 k + \beta_2 d_3)}{d_1 d_3 (d_2 + \alpha)}.$$

Further, the values of R_1 and R_2 are calculated for both the incidence functions using (4.2.7) and (4.2.9), respectively. The computations are performed for both these types of incidence functions with same parameter values, and same initial and boundary conditions. We use the set of parameter values as listed in Table 3.1 and the values of diffusion coefficients as $d_V = 0.25$ mm^2 day^{-1} and $d_B = 0.1$ mm^2 day^{-1} (these choices are for illustrative purpose). Also, we take the uniform grid sizes as $\Delta x = 0.1$ and $\Delta t = 0.1$. The initial levels of the model variables are chosen as,

$$U(x, 0) = 80,\ I(x, 0) = 10,\ V(x, 0) = 5 \ \text{ and } \ B(x, 0) = 100, \quad x \in [0, 50],$$

along with the homogeneous Neumann boundary conditions

$$\frac{\partial V}{\partial x} = 0 \ \text{ and } \ \frac{\partial B}{\partial x} = 0, \quad t > 0,\ x = 0, 50.$$

Note that here we consider a one-dimensional spatial domain, $\Omega = [0, 50]$. In order to study the various cases, we vary the values of λ and β_2 with all other parameter values retaining the same as in Table 3.1. The variation of the values of λ, β_2 and d_3 leads to the cases of $R_0 < 1$, $R_2 < 1 < R_0$ and $R_1 > 1$. These scenarios are illustrated in the following discussion:

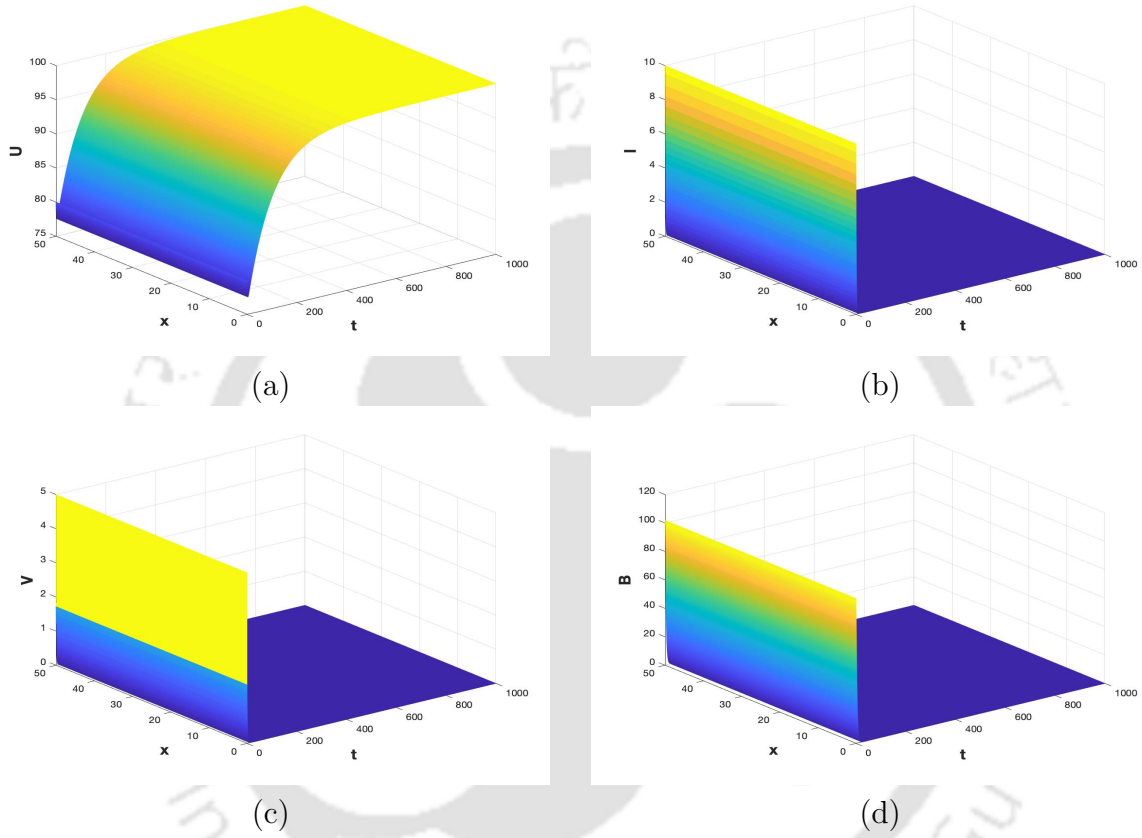

Figure 4.1: Dynamics of uninfected hepatocytes (U), infected hepatocytes (I), virions (V) and B cells (B) when $R_0 < 1$ for the case of bilinear transmission function.

Case I: $R_0 < 1$. For this case, we choose $\lambda = 1$, $\beta_2 = 0.001$ and $d_3 = 6$, resulting in $R_0 = 0.5775 < 1$, for both types of incidence functions. The resulting dynamics of the model variables are presented in Figure 4.1 (for bilinear incidence function) and Figure 4.2 (for Holling type-II incidence function). From Figure 4.1(a), we observe that the healthy hepatocytes initially decrease but then increase thereafter eventually stabilizing at the peak level of $U = 100$ (corresponding to E_0). Simultaneously, it is observed that the productively infected hepatocytes (Figure 4.1(b)), viruses (Figure 4.1(c)) and B cells (Figure 4.1(d)) gradually decrease with eventual convergence to zero level. This simulation signifies that infection-free equilibrium E_0 $(100, 0, 0, 0)$ is globally asymptotically stable, which supports the analytical result in Theorem 4.3.2. Similar scenario is observed from Figure 4.2 where

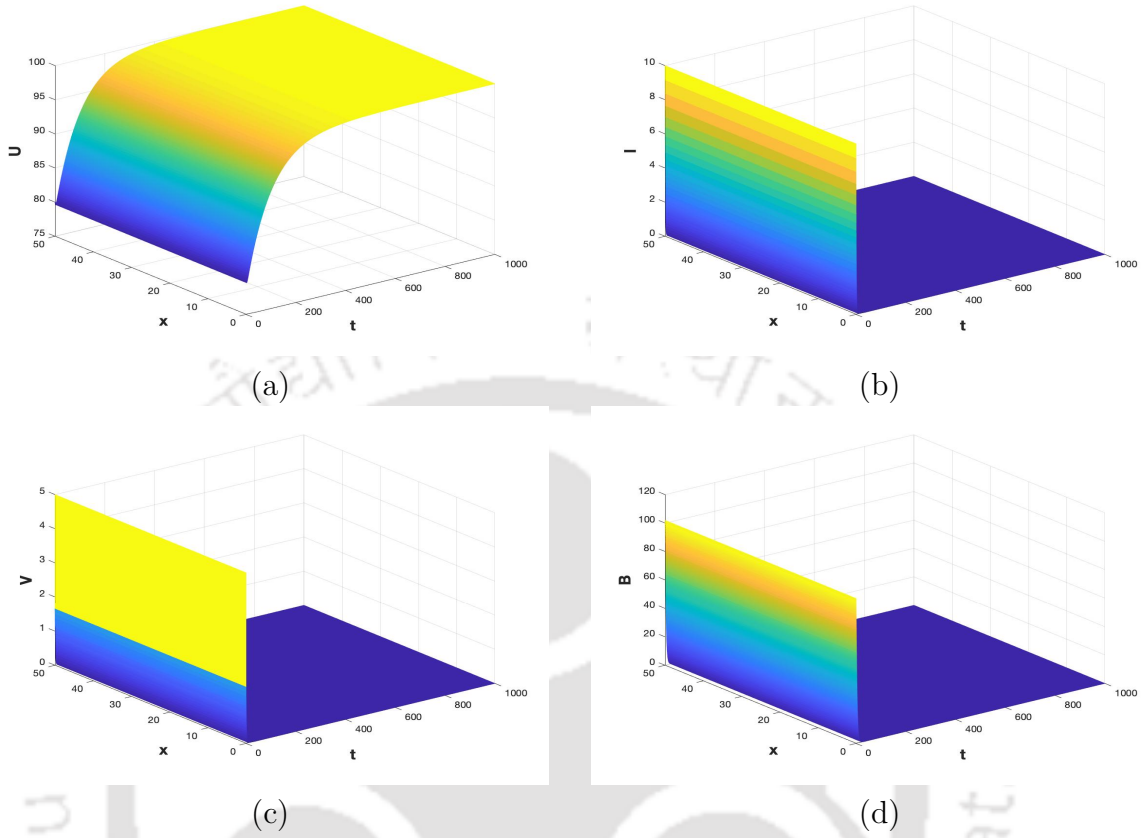

Figure 4.2: Dynamics of uninfected hepatocytes (U), infected hepatocytes (I), virions (V) and B cells (B) when $R_0 < 1$ for the case of Holling type-II transmission function.

Holling type-II incidence function is considered and in this case, the stable infection-free equilibrium is found to be the level $(100,\ 0,\ 0,\ 0)$ as was the case earlier. These results suggest that the infection and viruses die out after some time and consequently, the B cell response is not activated in case of $R_0 < 1$.

Case II: $R_2 < 1 < R_0$. In order to demonstrate this case, we take $\lambda = 1$, $\beta_2 = 0.01$ and $d_3 = 1$, which correspond to $R_0 = 3.8614 > 1$ (for both types of incidence functions). Further, these parameter values result in (a) $R_2 = 0.7163 < 1$ and $d_1U_1 - \alpha I_1 = 0.2516 > 0$ (condition for global stability of E_1 (Theorem 4.3.3)), for bilinear incidence function; and (b) $R_2 = 0.4546 < 1$ and $d_1U_1 - \alpha I_1 = 0.5249 > 0$, for Holling type-II incidence function. The scenario in case of bilinear incidence function is presented in Figure 4.3. From Figures 4.3(a), 4.3(b) and 4.3(c), it is seen that the healthy hepatocytes, productively infected hepatocytes and viruses exhibit oscillatory behavior before eventually stabilizing at the level of $U = 25.8974$, $I = 0.7410$ and $V = 2.1489$, respectively. Simultaneously, the B cell population stabilizes at zero level (Figure 4.3(d)). This simulation signifies that immune-free infected

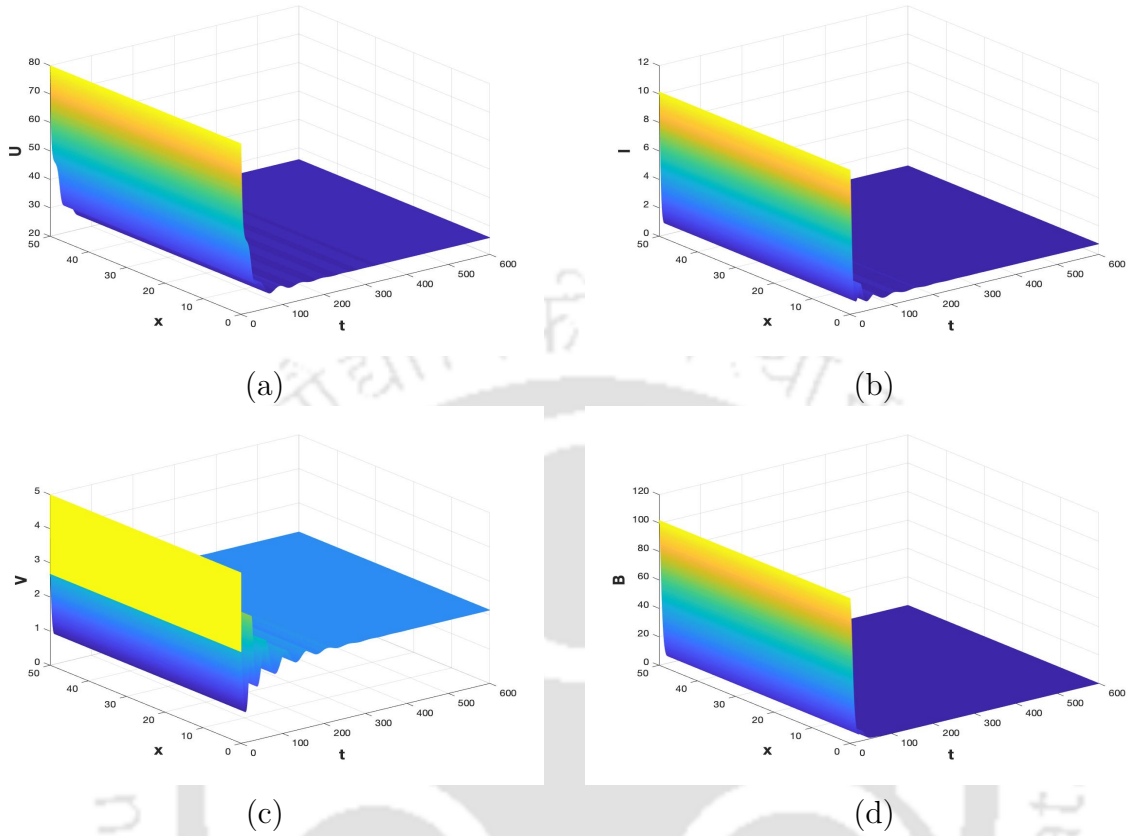

(a) (b)

(c) (d)

Figure 4.3: Dynamics of uninfected hepatocytes (U), infected hepatocytes (I), virions (V) and B cells (B) when $R_2 < 1 < R_0$ for the case of bilinear transmission function.

equilibrium E_1 (25.8974, 0.7410, 2.1489, 0) is globally asymptotically stable, which agrees with the analytical result in Theorem 4.3.3. Further, the simulations with these parameter values and Holling type-II incidence function is depicted in Figure 4.4, which shows that the model populations are getting rapidly stabilized without exhibiting oscillations and the stable immune-free infected equilibrium is observed at the level $(52.9665, 0.4703, 1.3640, 0)$. Thus when Holling type-II incidence function is considered, the healthy hepatocytes stabilize at much higher level, while the productively infected hepatocytes as well as viruses decline to a very low level.

Case III: $R_1 > 1$. Finally, in order to illustrate this case, we choose $\lambda = 10$, $\beta_2 = 0.01$ and $d_3 = 1$, resulting in $R_0 = 38.6139 > 1$ (for both types of incidence functions). This set of parameter values correspond to (a) $R_1 = 8.9297 > 1$ and $d_1U^* - \alpha I^* = 0.67 > 0$ (condition for global stability of E_2 (Theorem 4.3.4)), for bilinear incidence function; and (b) $R_1 = 5.9403 > 1$ and $d_1U_1 - \alpha I_1 = 3.7934 > 0$, for Holling type-II incidence function. In this case, the scenario for the bilinear incidence function is depicted in Figure 4.5. In this case, all four

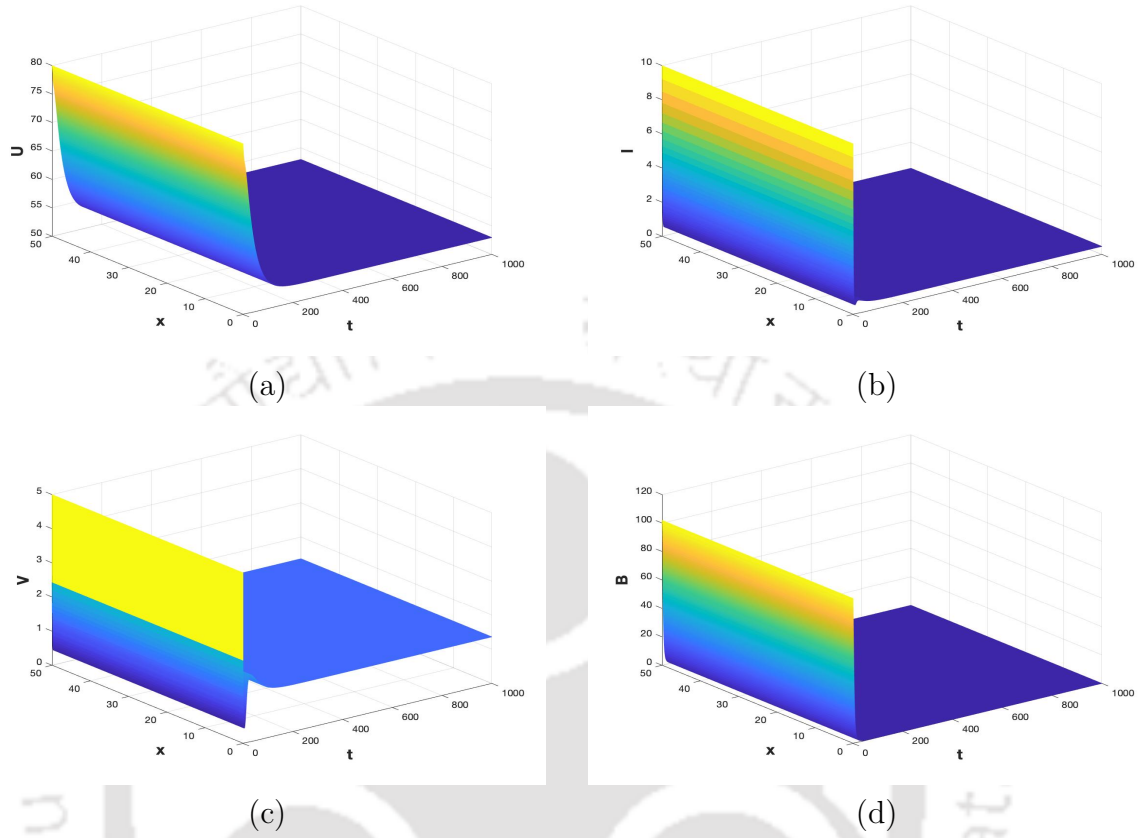

Figure 4.4: Dynamics of uninfected hepatocytes (U), infected hepatocytes (I), virions (V) and B cells (B) when $R_2 < 1 < R_0$ for the case of Holling type-II transmission function.

variables exhibit oscillatory behavior before eventually converging to the corresponding levels associated with the immune-activation infected equilibrium E^* (76.2402, 9.2376, 3, 79.2968). This simulation indicates that the immune-activation infected equilibrium E^* is globally asymptotically stable, which supports the analytical result in Theorem 4.3.4. Further, in this case, the results for Holling type-II incidence function is presented in Figure 4.6. It is observed that the healthy hepatocytes increase and eventually converge at a very high level of $U = 385.4897$ and productively infected hepatocytes reduce to the level of $I = 6.1451$. Hence the stable immune-activation infected equilibrium is observed at the level $(385.4897, 6.1451, 3, 49.4026)$. Thus when Holling type-II incidence function is considered, the healthy hepatocytes reach a very high level, while the productively infected hepatocytes decrease to relatively much lower level.

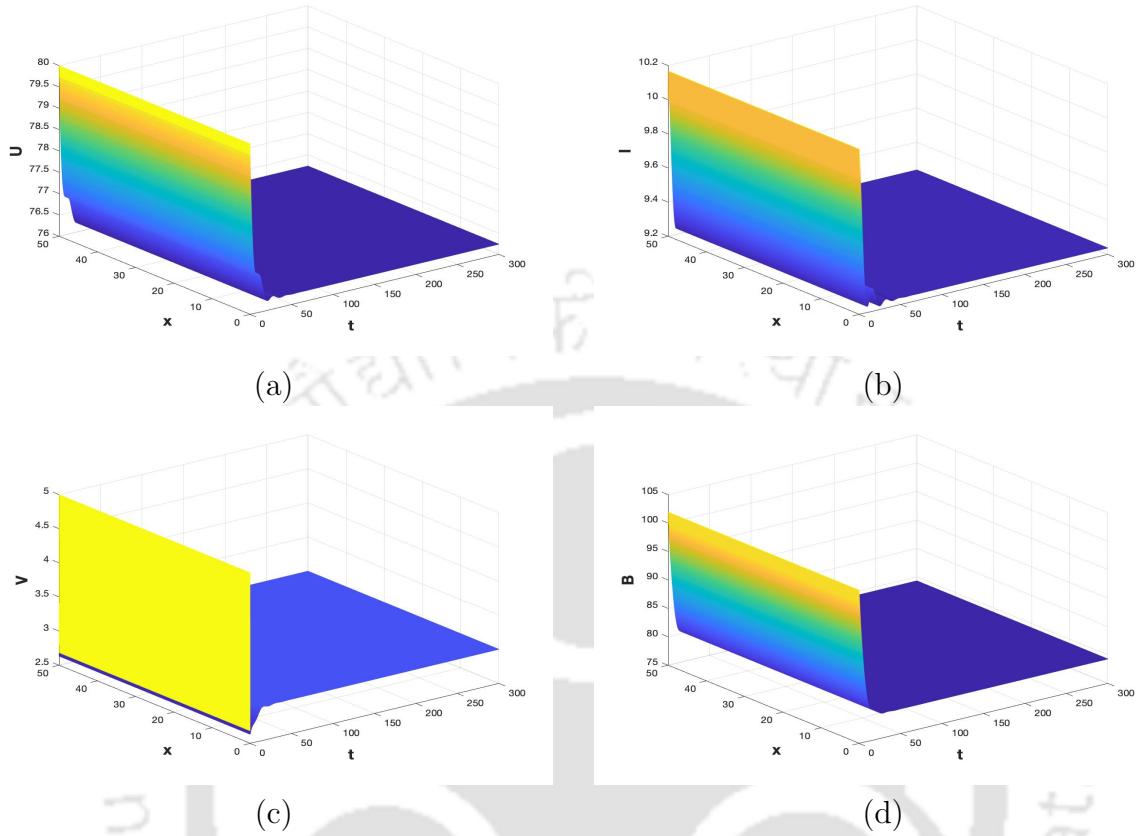

(a) (b)

(c) (d)

Figure 4.5: Dynamics of uninfected hepatocytes (U), infected hepatocytes (I), virions (V) and B cells (B) when $R_1 > 1$ for the case of bilinear transmission function.

4.5 Conclusions

A reaction-diffusion model for HCV dynamics capturing the diffusion of the viruses as well as the immune cells with general incidence functions for both virus-to-cell and cell-to-cell modes and incorporating the role of B cells has been studied. The positivity and boundedness of the solution prove the feasibility of the model. The conditions for the global asymptotic stability of the three equilibria are analytically examined by constructing suitable Lyapunov functionals. The globally asymptotic stability of the infection-free equilibrium is shown in case of $R_0 \leq 1$. The global asymptotic stability of the immune-free and immune-activation infected equilibrium can be found in case of $R_2 < 1 < R_0$ and $R_1 > 1$, respectively.

The numerical illustration for bilinear as well as Holling type-II incidence function in one-dimensional spatial domain, supports the theoretical results obtained. It is observed that the infection will persist or die out depending upon the case of $R_0 > 1$ or $R_0 \leq 1$, respectively. Furthermore, the findings suggest that the global behavior of the system is not dependent on the diffusive action of the viruses or the immune B cells. The numerical results

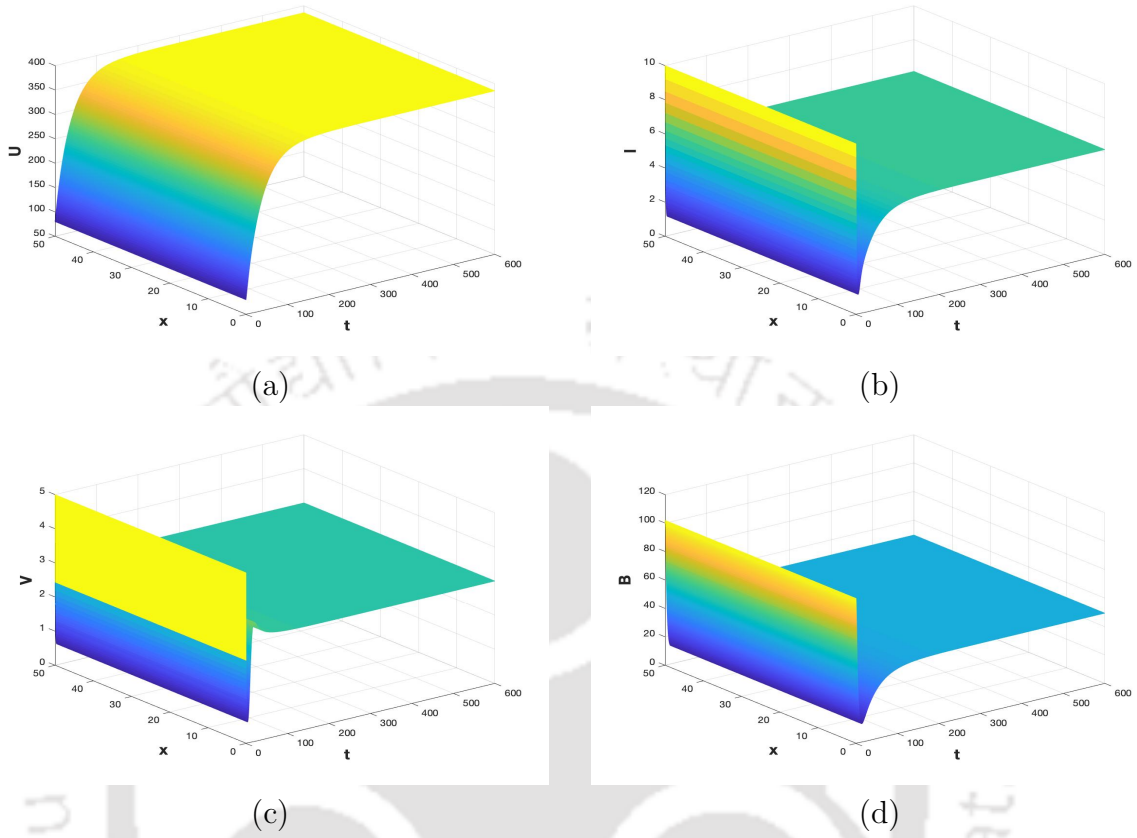

Figure 4.6: Dynamics of uninfected hepatocytes (U), infected hepatocytes (I), virions (V) and B cells (B) when $R_1 > 1$ for the case of Holling type-II transmission function.

also show that the system with Holling type-II incidence function stabilizes at the equilibria with higher level of healthy hepatocytes and lower level of infection, as compared to bilinear incidence function.

Chapter 5

Stochastic Modeling and Branching Process Approximation for Within-Host Dynamics of HCV Infection

Usage of the stochastic approach may provide better insights while analyzing random phenomena such as birth or death process of cells, activities of virus and response of the immune system. Further, there are cases where a stochastic model can better predict the uncertainty and variability of the dynamics and can also help in the estimation of likelihood of disease extinction in finite time [5, 6, 7]. In order to introduce randomness in modeling, approaches such as parameter perturbation [61, 86] and continuous-time Markov chain (CTMC) approximation [2, 3, 56, 113, 115, 139] are typically used.

In this chapter [1], we formulate and analyze stochastic models based on the possible state changes in the variables of the deterministic model (2.1.1) and also depending on the process for release of virions. We consider two different processes for the release of virions from the infected hepatocytes, namely, the budding process and the bursting process. The Itô SDE models for both budding and bursting processes with fixed as well as variable burst size are constructed using the property of linear transformation for multivariate normal distribution. Note that while most of the deterministic models for HCV infection [10, 22, 23, 24, 28, 64, 77, 81, 96, 126, 127] are discussed with the budding process, however, the bursting process is assumed in the deterministic model of HCV dynamics in [140, 141]. Further, we apply the theory of multitype continuous-time branching process approximation to obtain the probability of virus extinction from CTMC models. We also derive the forward

[1]The presentation in this chapter is based on the article: "Sonjoy Pan and Siddhartha P. Chakrabarty. Stochastic analysis of in-host HCV dynamics through budding and bursting process. *Commun. Nonlinear Sci. Numer. Simul.* 80 (2019): 104955".

Kolmogorov equations and the moment equations for the model variables to elicit an idea of their distribution patterns. A number of numerical illustrative computations for the stochastic models is carried out in order to obtain various dynamics of HCV infection, as well as for comparison of observation from the stochastic model and the deterministic model (2.1.1).

5.1 Stochastic Model Formulation

In this section, we derive the SDE models approximated by CTMC models using the deterministic model system given by (2.1.1). In order to formulate the system of SDEs, we use the properties of linear transformation for the multivariate normal distribution adopting the approach in [2, 3, 6, 139]. In order to construct the Itô SDE model, we identify the possible state changes along with their corresponding probabilities based on the deterministic model (2.1.1). The possible state changes refer to the effect on the population sizes of uninfected hepatocytes, infected hepatocytes, virions and immune cells. For notational convenience, let X_1, X_2, X_3 and X_4 be the four continuous random variables denoting the deterministic variables U, I, V and B, respectively. In the vector form, $\vec{X} = (X_1, X_2, X_3, X_4)^\top$, represents a continuous random vector whose each component X_i, $i = 1, 2, 3, 4$ can take the values from $[0, \infty)$. The incremental change in a small time interval of length Δt is given by $\Delta\vec{X} = \vec{X}(t + \Delta t) - \vec{X}(t)$, $t \in [0, \infty)$. Further, let N be the "burst size" that represents the number of new free virions produced during the entire life of an infected hepatocyte, which therefore results in $k = Nd_2$. From the biological perspective, we consider N to be a positive integer. Note that the basic reproduction number corresponding to the deterministic model (2.1.1) is represented as, $R_0 = \dfrac{\lambda(\beta_1 k + \beta_2 d_3)}{d_1 d_3 (d_2 + \alpha)}$. Another threshold parameter, namely, a type reproduction number corresponding to the infected hepatocytes, $\mathcal{T}_I$ [139], in this case is equal to R_0. Based on the release process of virions, the Itô SDE models for both budding and bursting cases are discussed in the following presentation:

5.1.1 SDE for Budding Process

In case of the budding process, the virions are produced and released continuously during the lifetime of infected hepatocytes. Therefore, in this case, the production rate of virions (k) is independent of the death rate of infected hepatocytes (d_2). The possible state changes in the continuous random vector $\vec{X} = (X_1, X_2, X_3, X_4)^\top$ during a small time interval Δt for the budding case with their corresponding probabilities are summarized in Table 5.1.

In order to formulate the SDEs, we compute the expectation vector (mean vector) and

i	State change $((\Delta\vec{X})_i)$	Probability (p_i)	Description
1	$(1,0,0,0)^\top$	$\lambda\Delta t$	Recruitment of an uninfected hepatocyte
2	$(-1,1,0,0)^\top$	$(\beta_1 X_3+\beta_2 X_2)X_1\Delta t$	Infection by a virion/an infected hepatocyte
3	$(-1,0,0,0)^\top$	$d_1X_1\Delta t$	Natural death of an uninfected hepatocyte
4	$(1,-1,0,0)^\top$	$\alpha X_2\Delta t$	Cure of an infected hepatocyte
5	$(0,0,-1,0)^\top$	$(d_3+pX_4)X_3\Delta t$	Natural death/clearance by B cells of a virion
6	$(0,0,0,1)^\top$	$cX_3X_4\Delta t$	Development of a B cell
7	$(0,0,0,-1)^\top$	$d_4X_4\Delta t$	Natural death of a B cell
8	$(0,-1,0,0)^\top$	$d_2X_2\Delta t$	Natural death of an infected hepatocyte
9	$(0,0,1,0)^\top$	$kX_2\Delta t$	Budding of a virion
10	$(0,0,0,0)^\top$	$1-\sum_{i=1}^{9} p_i$	No change

Table 5.1: Possible state change during a small time interval Δt, resulting from budding.

covariance matrix of $\Delta\vec{X}$. Accordingly, the expectation vector, based on the state changes with associated probabilities, is calculated as follows:

$$E(\Delta\vec{X})=\sum_{i=1}^{9} p_i(\Delta\vec{X})_i=\vec{f}(\vec{X})\Delta t,$$

where

$$\vec{f}(\vec{X})=\begin{pmatrix}\lambda-\beta_1X_1X_3-\beta_2X_1X_2-d_1X_1+\alpha X_2\\ \beta_1X_1X_3+\beta_2X_1X_2-d_2X_2-\alpha X_2\\ kX_2-d_3X_3-pX_3X_4\\ cX_3X_4-d_4X_4\end{pmatrix},$$

and is known as the drift vector. The entries of the expectation vector is the same as the right hand side of the deterministic model (2.1.1). However, the covariance matrix characterizes the distinction of the SDE model from the deterministic model. It measures the variability due to consideration of the randomness in the stochastic system. The covariance matrix of $\Delta\vec{X}$ is given by

$$E[(\Delta\vec{X})(\Delta\vec{X})^\top]-E(\Delta\vec{X})[E(\Delta\vec{X})]^\top.$$

Neglecting the $O(\Delta t)^2$ terms, the covariance matrix becomes (approximately)

$$E[(\Delta\vec{X})(\Delta\vec{X})^\top]=\sum_{i=1}^{9} p_i(\Delta\vec{X})_i(\Delta\vec{X})_i{}^\top=C\Delta t,$$

where

$$C=\begin{pmatrix}\lambda+d_1X_1+v_c & -v_c & 0 & 0\\ -v_1 & d_2X_2+v_c & 0 & 0\\ 0 & 0 & kX_2+d_3X_3+pX_3X_4 & 0\\ 0 & 0 & 0 & cX_3X_4+d_4X_4\end{pmatrix},$$

where $v_c = \beta_1 X_1 X_3 + \beta_2 X_1 X_2 + \alpha X_2$. A diffusion matrix H satisfying $C = HH^\top$ is given by

$$H = \begin{pmatrix} \sqrt{\lambda + d_1 X_1} & \sqrt{v_c} & 0 & 0 & 0 \\ 0 & -\sqrt{v_c} & \sqrt{d_2 X_2} & 0 & 0 \\ 0 & 0 & 0 & \sqrt{kX_2 + d_3 X_3 + pX_3 X_4} & 0 \\ 0 & 0 & 0 & 0 & \sqrt{cX_3 X_4 + d_4 X_4} \end{pmatrix}.$$

Note that the diffusion matrix H is not necessarily unique and an alternative diffusion matrix H_a can be determined from $V = H_a H_a^\top$, which can be accomplished using Cholesky decomposition. Such alternative diffusion matrix will lead to an equivalent SDE system. The solutions of these equivalent SDE systems have the same probability distribution and moreover, any sample-path solution of one system satisfies the other system [3]. Thus, the system of Itô SDEs for the budding case along with the initial conditions is as follows:

$$\begin{aligned} d\vec{X}(t) &= \vec{f}(\vec{X}(t))dt + H(\vec{X}(t))d\vec{W}(t), \\ \vec{X}(0) &= (X_1(0), X_2(0), X_3(0), X_4(0))^\top, \end{aligned}$$

where $\vec{W}(t) = (W_1(t), W_2(t), W_3(t), W_4(t), W_5(t))^\top$ with $W_i, i = 1, 2, \ldots, 5$ being five independent Wiener processes. Hence the SDE model in the budding case can be written in the following explicit form:

$$\begin{aligned} dX_1 &= (\lambda - \beta_1 X_1 X_3 - \beta_2 X_1 X_2 - d_1 X_1 + \alpha X_2)dt \\ &\quad + \sqrt{\lambda + d_1 X_1}dW_1 + \sqrt{\beta_1 X_1 X_3 + \beta_2 X_1 X_2 + \alpha X_2}dW_2, \\ dX_2 &= (\beta_1 X_1 X_3 + \beta_2 X_1 X_2 - d_2 X_2 - \alpha X_2)dt \\ &\quad - \sqrt{\beta_1 X_1 X_3 + \beta_2 X_1 X_2 + \alpha X_2}dW_2 + \sqrt{d_2 X_2}dW_3, \\ dX_3 &= (kX_2 - d_3 X_3 - pX_3 X_4)dt + \sqrt{kX_2 + d_3 X_3 + pX_3 X_4}dW_4, \\ dX_4 &= (cX_3 X_4 - d_4 X_4)dt + \sqrt{cX_3 X_4 + d_4 X_4}dW_5. \end{aligned} \tag{5.1.1}$$

5.1.2 SDE for Bursting Process

In case of the bursting process, the number of free virions remains unchanged until an infected hepatocyte dies and the death of this hepatocyte results in a release of N (burst size) virions. In this case, the production rate of virions (k) depends on the death rate of infected hepatocytes (d_2) and therefore k is replaced by the term Nd_2. The possible state changes in the continuous random vector $\vec{X} = (X_1, X_2, X_3, X_4)^\top$ during a small time interval Δt for the bursting case with their corresponding probabilities are summarized in Table 5.2. The state changes $(\Delta\vec{X})_i,\ i = 1, 2, ..., 7$ are same for both budding and bursting cases with the only difference between those two being in the state changes $(\Delta\vec{X})_i,\ i \geq 8$. Following

the procedure adopted as in case of budding, we determine the drift vector and a diffusion matrix for the bursting case also.

i	State change $((\Delta\vec{X})_i)$	Probability $(\tilde{p}_i)$	Description
1	$(1,0,0,0)^\top$	$\lambda\Delta t$	Recruitment of an uninfected hepatocyte
2	$(-1,1,0,0)^\top$	$(\beta_1 X_3 + \beta_2 X_2)X_1\Delta t$	Infection by a virion/an infected hepatocyte
3	$(-1,0,0,0)^\top$	$d_1 X_1 \Delta t$	Natural death of an uninfected hepatocyte
4	$(1,-1,0,0)^\top$	$\alpha X_2 \Delta t$	Cure of an infected hepatocyte
5	$(0,0,-1,0)^\top$	$(d_3 + pX_4)X_3\Delta t$	Natural death/clearance by B cells of a virion
6	$(0,0,0,1)^\top$	$cX_3X_4\Delta t$	Development of a B cell
7	$(0,0,0,-1)^\top$	$d_4 X_4 \Delta t$	Natural death of a B cell
8	$(0,-1,N,0)^\top$	$d_2 X_2 \Delta t$	Bursting and release of virions
9	$(0,0,0,0)^\top$	$1 - \sum_{i=1}^{8} \tilde{p}_i$	No change

Table 5.2: Possible state change during a small time interval Δt, resulting from bursting.

We obtain the expectation vector $E(\Delta\vec{X})$ to be the same as in the budding case and hence the drift vector given by $\vec{f}(\vec{X})$ is also same as in the budding case (except that k is replaced by Nd_2). However, the covariance matrix of $\Delta\vec{X}$ differs from the previous case, which for the bursting case is obtained (after neglecting the $O(\Delta t)^2$ terms) and is as follows:

$$E[(\Delta\vec{X})(\Delta\vec{X})^\top] - E(\Delta\vec{X})[E(\Delta\vec{X})]^\top \approx E[(\Delta\vec{X})(\Delta\vec{X})^\top] = \sum_{i=1}^{8} \tilde{p}_i (\Delta\vec{X})_i (\Delta\vec{X})_i{}^\top = \tilde{C}\Delta t,$$

where

$$\tilde{C} = \begin{pmatrix} \lambda + d_1X_1 + v_c & -v_c & 0 & 0 \\ -v_c & d_2X_2 + v_c & -Nd_2X_2 & 0 \\ 0 & -Nd_2X_2 & N^2d_2X_2 + d_3X_3 + pX_3X_4 & 0 \\ 0 & 0 & 0 & cX_3X_4 + d_4X_4 \end{pmatrix}.$$

A diffusion matrix $\tilde{H}$ satisfying $\tilde{C} = \tilde{H}\tilde{H}^\top$ is given by

$$\tilde{H} = \begin{pmatrix} \sqrt{\lambda + d_1X_1} & \sqrt{v_c} & 0 & 0 & 0 \\ 0 & -\sqrt{v_c} & \sqrt{d_2X_2} & 0 & 0 \\ 0 & 0 & -N\sqrt{d_2X_2} & \sqrt{d_3X_3 + pX_3X_4} & 0 \\ 0 & 0 & 0 & 0 & \sqrt{cX_3X_4 + d_4X_4} \end{pmatrix}.$$

Again, note that matrix $\tilde{H}$ is not necessarily unique. Therefore, the SDE model for the

bursting case is as follows:

$$\begin{aligned}
dX_1 &= (\lambda - \beta_1 X_1 X_3 - \beta_2 X_1 X_2 - d_1 X_1 + \alpha X_2)dt \\
&\quad + \sqrt{\lambda + d_1 X_1}d\tilde{W}_1 + \sqrt{\beta_1 X_1 X_3 + \beta_2 X_1 X_2 + \alpha X_2}d\tilde{W}_2, \\
dX_2 &= (\beta_1 X_1 X_3 + \beta_2 X_1 X_2 - d_2 X_2 - \alpha X_2)dt \\
&\quad - \sqrt{\beta_1 X_1 X_3 + \beta_2 X_1 X_2 + \alpha X_2}d\tilde{W}_2 + \sqrt{d_2 X_2}d\tilde{W}_3, \\
dX_3 &= (N d_2 X_2 - d_3 X_3 - p X_3 X_4)dt - N\sqrt{d_2 X_2}d\tilde{W}_3 + \sqrt{d_3 X_3 + p X_3 X_4}d\tilde{W}_4, \\
dX_4 &= (c X_3 X_4 - d_4 X_4)dt + \sqrt{c X_3 X_4 + d_4 X_4}d\tilde{W}_5,
\end{aligned} \tag{5.1.2}$$

with the initial state values being given by $X_i(0), i = 1, 2, 3, 4$ and $\tilde{W}_i,\ i = 1, 2, \ldots, 5$ being five independent Wiener processes.

5.2 CTMC Model Analysis

In this section, we make linear approximation of the nonlinear CTMC models near the infection-free equilibrium $E_0 = (\lambda/d_1, 0, 0, 0)$, using the theory and techniques of multitype continuous-time branching process [54, 113, 115]. In order to analyze the CTMC models, we derive the offspring probability generating functions (PGFs), expectation matrices and the probability of virus extinction [112]. We suppose $(X_2(0), X_3(0)) = (\delta_{1i}, \delta_{2i})$, $i = 1, 2$, where δ_{ji} denotes the Kronecker delta function. Then the offspring PGFs, $f_i : [0, 1] \times [0, 1] \to [0, 1],\ i = 1, 2$, corresponding to infected hepatocytes and virions, respectively, are defined as [54]

$$f_i(s_1, s_2) = \sum_{l_1=0}^{\infty}\sum_{l_2=0}^{\infty} P_i(l_1, l_2)s_1^{l_1}s_2^{l_2},\ s_i \in [0, 1],\ i = 1, 2,$$

where $P_i(l_1, l_2) = \text{Prob}\{Y_{1i} = l_1, Y_{2i} = l_2\}$ with Y_{ji} denoting that an individual of type i gives birth to Y_{ji} number of offspring of type j and $l_i \in \{0, 1, 2, \}, i = 1, 2$. The expectation matrix for PGFs is defined as $M = [m_{ji}]_{2\times 2}$, where m_{ji} represents the average number of offspring of type j from type i and is given by

$$m_{ji} = \left.\frac{\partial f_i(s_1, s_2)}{\partial s_j}\right|_{s_1=s_2=1},\ i, j = 1, 2.$$

We now suppose that $\vec{Y}(0) = (X_2(0), X_3(0)) = (m, n)$. Let (q_1, q_2) be the smallest fixed point of (f_1, f_2) such that $q_i \in (0, 1]$, *i.e.*, $f_i(q_1, q_2) = q_i,\ i = 1, 2$. Using Galton-Watson branching theory [41], it follows that the probability of virus extinction for the CTMC model is $q_1^m q_2^n$.

5.2.1 Branching Process Approximation in Case of Budding

The offspring PGF for X_2 in case of budding (corresponding to $i = 2, 4, 8, 9$ in Table 5.1) is given by

$$f_1(s_1, s_2) = \frac{d_1(d_2 + \alpha) + \lambda\beta_2 s_1^2 + d_1 k s_1 s_2}{d_1(d_2 + \alpha + k) + \lambda\beta_2}. \tag{5.2.1}$$

Similarly, the offspring PGF for X_3 in case of budding (corresponding to $i = 2, 5, 6$ in Table 5.1) is given by

$$f_2(s_1, s_2) = \frac{d_1 d_3 + \lambda\beta_1 s_1 s_2}{d_1 d_3 + \lambda\beta_1}. \tag{5.2.2}$$

Hence the expectation matrix for PGFs in case of budding is computed as

$$M_1 = \begin{pmatrix} \frac{2\lambda\beta_2 + d_1 k}{d_1(d_2+\alpha+k)+\lambda\beta_2} & \frac{\lambda\beta_1}{d_1 d_3 + \lambda\beta_1} \\ \frac{d_1 k}{d_1(d_2+\alpha+k)+\lambda\beta_2} & \frac{\lambda\beta_1}{d_1 d_3 + \lambda\beta_1} \end{pmatrix}. \tag{5.2.3}$$

Further, in order to find the probability of virus extinction in case of budding, we suppose that (q_1, q_2) be a fixed point of (f_1, f_2). Therefore, from the offspring PGFs, we have

$$\begin{aligned} \frac{d_1(d_2 + \alpha) + \lambda\beta_2 q_1^2 + d_1 k q_1 q_2}{d_1(d_2 + \alpha + k) + \lambda\beta_2} &= q_1, \\ \frac{d_1 d_3 + \lambda\beta_1 q_1 q_2}{d_1 d_3 + \lambda\beta_1} &= q_2, \end{aligned}$$

which gives

$$q_2 = \frac{d_1 d_3}{d_1 d_3 + (1 - q_1)\lambda\beta_1}, \tag{5.2.4}$$

with q_1 being expressed in terms of the following cubic equation

$$A_3 q_1^3 - A_2 q_1^2 + A_1 q_1 - A_0 = 0, \tag{5.2.5}$$

where

$$\begin{aligned} A_0 &= d_1(d_2 + \alpha)(d_1 d_3 + \lambda\beta_1), \\ A_1 &= (\lambda\beta_1 + d_1 d_3)(\lambda\beta_2 + d_1 d_2 + d_1\alpha + d_1 k) + (d_2 + \alpha)\lambda\beta_1 d_1 - k d_1^2 d_3, \\ A_2 &= 2\lambda^2\beta_1\beta_2 + \lambda\beta_2 d_1 d_3 + (d_2 + \alpha + k)\lambda\beta_1 d_1, \\ A_3 &= \lambda^2\beta_1\beta_2. \end{aligned}$$

This cubic equation can be solved by using the Cardan's method. However, one can easily check that the equations (5.2.4) and (5.2.5) have a solution $q_1 = 1 = q_2$. We now check whether there exists any solution in $(0, 1)$ satisfying the equations (5.2.4) and (5.2.5). Let

$h(q_1) = A_3q_1^3 - A_2q_1^2 + A_1q_1 - A_0$. By Descartes' rule of signs, it follows that $h(q_1)$ has at least one positive real root. Now, $h(0) = -A_0 < 0$ and $h(\infty) \to +\infty$. Further, $h'(1) = 3A_3 - 2A_2 + A_1 = d_1^2 d_3(d_2+\alpha)(1-R_0) < 0$ if $R_0 > 1$. This implies that $h(q_1)$ is monotonically decreasing in the neighborhood of $q_1 = 1$ if $R_0 > 1$. Since, $h(1) = A_3 - A_2 + A_1 - A_0 = 0$, therefore, $h(1-\epsilon) > 0$, where ϵ is a very small positive quantity. Hence, there exists a solution $q_1 \in (0,1)$ of equation (5.2.5) if $R_0 > 1$. Thus, there exist $q_i \in (0,1)$, $i = 1,2$ satisfying the equations (5.2.4) and (5.2.5) if $R_0 > 1$.

5.2.2 Branching Process Approximation in Case of Bursting

The offspring PGF for X_2 in case of bursting (corresponding to $i = 2,4,8$ in Table 5.2) is expressed as

$$\tilde{f}_1(s_1,s_2) = \frac{d_1\alpha + \lambda\beta_2 s_1^2 + d_1 d_2 s_2^N}{d_1(d_2+\alpha) + \lambda\beta_2}. \tag{5.2.6}$$

Similarly, the offspring PGF for X_3 in the case of bursting (corresponding to $i = 2,5,6$ in Table 5.2) is expressed as

$$\tilde{f}_2(s_1,s_2) = \frac{d_1 d_3 + \lambda\beta_1 s_1 s_2}{d_1 d_3 + \lambda\beta_1}. \tag{5.2.7}$$

Hence the expectation matrix for PGFs in case of bursting is computed as

$$M_2 = \begin{pmatrix} \frac{2\lambda\beta_2}{d_1(d_2+\alpha)+\lambda\beta_2} & \frac{\lambda\beta_1}{d_1 d_3+\lambda\beta_1} \\ \frac{N d_1 d_2}{d_1(d_2+\alpha)+\lambda\beta_2} & \frac{\lambda\beta_1}{d_1 d_3+\lambda\beta_1} \end{pmatrix}. \tag{5.2.8}$$

Further, in order to derive the probability of virus extinction in case of bursting, let $(\tilde{q}_1, \tilde{q}_2)$ be a fixed point of $(\tilde{f}_1, \tilde{f}_2)$. Therefore, from the offspring PGFs, we have

$$\begin{aligned} \frac{d_1\alpha + \lambda\beta_2\tilde{q}_1^2 + d_1 d_2 \tilde{q}_2^N}{d_1(d_2+\alpha) + \lambda\beta_2} &= \tilde{q}_1, \\ \frac{d_1 d_3 + \lambda\beta_1 \tilde{q}_1\tilde{q}_2}{d_1 d_3 + \lambda\beta_1} &= \tilde{q}_2. \end{aligned}$$

Due to computational difficulties using all the values of N, we consider an illustrative case of the burst number N being equal to 2, in which case $\tilde{q}_2$ is given by

$$\tilde{q}_2 = \frac{d_1 d_3}{d_1 d_3 + (1-\tilde{q}_1)\lambda\beta_1} \tag{5.2.9}$$

and $\tilde{q}_1$ being expressed in terms of the following quartic equation

$$B_4\tilde{q}_1^4 - B_3\tilde{q}_1^3 + B_2\tilde{q}_1^2 - B_1\tilde{q}_1 + B_0 = 0, \tag{5.2.10}$$

where

$$\begin{aligned}
B_0 &= (d_2+\alpha)d_1^3d_3^2 + \lambda\alpha\beta_1 d_1(2d_1d_3+\lambda\beta_1),\\
B_1 &= (d_1d_3+\lambda\beta_1)[(d_1d_3+\lambda\beta_1)(d_1d_2+d_1\alpha+\lambda\beta_2+2\lambda\alpha\beta_1d_1)]\\
B_2 &= \lambda\beta_2d_1d_3(d_1d_3+2\lambda\beta_1)+\lambda^2\beta_1^2(\alpha d_1+\lambda\beta_2)+2\lambda\beta_1(d_1d_3+\lambda\beta_1)\left[d_1(d_2+\alpha)+\lambda\beta_2\right],\\
B_3 &= (d_2+\alpha)\lambda^2\beta_1^2d_1+\lambda^2\beta_1\beta_2(2d_1d_3+3\lambda\beta_1),\\
B_4 &= \lambda^3\beta_1^2\beta_2.
\end{aligned}$$

This quartic equation can be solved using several techniques. However, one can easily check that the equations (5.2.9) and (5.2.10) have a solution $\tilde{q}_1 = 1 = \tilde{q}_2$. Using an argument similar to the one applied in case of budding, we obtain that there exist $\tilde{q}_i \in (0,1),\ i = 1,2$ satisfying the equations (5.2.9) and (5.2.10) if $R_0 > 1$.

The following theorem shows that the deterministic threshold parameter (R_0) and the stochastic threshold parameter related to the expectation matrix for PGFs are equivalent for both the budding and the bursting cases.

Theorem 5.2.1. *Let $\rho(M_i)$ denote the spectral radius of M_i, $i = 1$ (budding case), 2 (bursting case). Then $\rho(M_i) < (>)1$ if and only if $R_0 < (>)1$.*

Proof. Recall that all entries of $M_i > 0,\ i = 1,2$. Then, according to Jurry conditions [4], $\rho(M_i) < 1$ if and only if $\text{Trace}(M_i) < 1 + \det(M_i) < 2$.
Now,

$$\begin{aligned}
1-\det(M_i) &= \frac{\lambda^2\beta_1^2l_1 + d_1^2d_3^2l_2 + d_1d_3(d_2+\alpha)[d_1d_3(1+R_0)+\lambda\beta_1(1-R_0)]}{d_3(d_1d_3+\lambda\beta_1)[d_1(d_2+\alpha+k)+\lambda\beta_2]}\\
&> 0 \text{ if } R_0 < 1, \qquad (5.2.11)
\end{aligned}$$

where $l_1 = l_2 = k$ for $i = 1$ (budding case) and $l_1 = Nd_2,\ l_2 = 0$ for $i = 2$ (bursting case). Also,

$$\begin{aligned}
1-\text{Trace}(M_i)+\det(M_i) &= \frac{d_1^2d_3(d_2+\alpha)(1-R_0)}{(d_1d_3+\lambda\beta_1)[d_1(d_2+\alpha+k)+\lambda\beta_2]}\\
&> 0 \text{ iff } R_0 < 1,\ i = 1,2. \qquad (5.2.12)
\end{aligned}$$

Therefore it follows from relations (5.2.11) and (5.2.12) that $\text{Trace}(M_i) < 1 + \det(M_i) < 2$ iff $R_0 < 1$ and hence, $\rho(M_i) < 1$ iff $R_0 < 1,\ i = 1,2$.

Further, the characteristic equation for M_i is as follows

$$P(x) = x^2 - \text{Trace}(M_i)x + \det(M_i) = 0,\ i = 1,2.$$

By Descartes' rule of signs, $P(x)$ either has none or two positive real roots. Now, $P(0) = \det(M_i) > 0$ and $P(\infty) \to +\infty$. Also, $P(1) = 1 - \text{Trace}(M_i) + \det(M_i) < 0$ iff $R_0 > 1$. This implies that $P(x) = 0$ has a solution in $(1, +\infty)$ iff $R_0 > 1$. Hence, $\rho(M_i) > 1$ iff $R_0 > 1,\ i = 1, 2$. □

From the above discussion and using Galton-Watson branching theory [41] as stated earlier, the probability of virus extinction can be summarized as the following theorem for both budding and bursting cases:

Theorem 5.2.2. *Let $\vec{Y}(t) = (X_2(t), X_3(t))$ with $\vec{Y}(0) = (m, n)$. Then*

(i) $\lim_{t\to\infty} Prob\{\vec{Y}(t) = \vec{0}\} = 1$ *when $R_0 < 1$ i.e., the probability of virus extinction is one when $R_0 < 1$ (or equivalently, $\rho(M_i) < 1$).*

(ii) $\lim_{t\to\infty} Prob\{\vec{Y}(t) = \vec{0}\} = q_1^m q_2^n$ *(budding case) or $\tilde{q}_1^m \tilde{q}_2^n$ (bursting case) when $R_0 > 1$, i.e., the probability of virus extinction is $q_1^m q_2^n$ (budding case) or $\tilde{q}_1^m \tilde{q}_2^n$ (bursting case) when $R_0 > 1$ (or equivalently, $\rho(M_i) > 1$), where $q_1 \in (0, 1)$ and $\tilde{q}_1 \in (0, 1)$ are the smallest positive roots of (5.2.5) and (5.2.10), respectively, with q_2 and $\tilde{q}_2$ being defined in (5.2.4) and (5.2.9), respectively.*

Note that the corresponding deterministic model (2.1.1) admits only one infection-free equilibrium E_0, and hence the linearization is considered around E_0, only. However, in case of the existence of multiple infection-free equilibria, one has to identify those equilibria which are stable and ignore the unstable ones. Further, in case of the existence of multiple stable infection-free equilibria, multiple expectation matrices and multiple fixed points have to be determined. Accordingly, the associated probability that viruses become extinct and the system stabilizes to an infection-free state, can be obtained using the corresponding fixed point.

5.3 Variable Burst Size

In the previous sections, we discussed the stochastic model system with the fixed burst size, N. In this section, we consider the burst size as a random variable $N(t)$ that follows the following mean-reverting Ornstein-Uhlenbeck process [86]

$$dN(t) = \mu(N_e - N(t))dt + \sigma dW(t), \tag{5.3.1}$$

where μ, N_e and σ (all positive) denote the rate of reversion, long term mean value of the burst size and variability of the burst size, respectively. The solution of (5.3.1) along with

the mean and variance of the variable burst size is given by [115]

$$N(t) = N_e + (N(0) - N_e)e^{-\mu t} + \sigma e^{-\mu t}\int_0^t e^{\mu s} dW(s). \tag{5.3.2}$$

$$E[N(t)] = N_e + (N(0) - N_e)e^{-\mu t} \text{ and } V[N(t)] = \frac{\sigma^2(1 - e^{-2\mu t})}{2\mu}.$$

Thus the Itô SDE model for the bursting case with variable burst size N_t (meant by $N(t)$) is as follows:

$$\begin{aligned}
dX_1 &= (\lambda - \beta_1 X_1 X_3 - \beta_2 X_1 X_2 - d_1 X_1 + \alpha X_2)dt \\
&\quad + \sqrt{\lambda + d_1 X_1}d\tilde{W}_1 + \sqrt{\beta_1 X_1 X_3 + \beta_2 X_1 X_2 + \alpha X_2}d\tilde{W}_2, \\
dX_2 &= (\beta_1 X_1 X_3 + \beta_2 X_1 X_2 - d_2 X_2 - \alpha X_2)dt \\
&\quad - \sqrt{\beta_1 X_1 X_3 + \beta_2 X_1 X_2 + \alpha X_2}d\tilde{W}_2 + \sqrt{d_2 X_2}d\tilde{W}_3, \\
dX_3 &= (N_t d_2 X_2 - d_3 X_3 - p X_3 X_4)dt - N_t\sqrt{d_2 X_2}d\tilde{W}_3 + \sqrt{d_3 X_3 + p X_3 X_4}d\tilde{W}_4, \\
dX_4 &= (cX_3 X_4 - d_4 X_4)dt + \sqrt{cX_3 X_4 + d_4 X_4}d\tilde{W}_5, \\
dN_t &= \mu(N_e - N_t)dt + \sigma d\tilde{W}_6.
\end{aligned} \tag{5.3.3}$$

For the branching process approximation, we consider the burst size as a discrete random variable whose mean is equal to fixed burst size, N. Let P_i be the probability that the burst size is i, *i.e.*, $\sum_{i=0}^{\infty} P_i = 1$. Also, let $F(s) = \sum_{i=0}^{\infty} P_i s^i$ be the PGF for the burst size. Therefore, the mean of the burst size is $F'(1) = \sum_{i=0}^{\infty} iP_i = N$. Hence, the offspring PGF for X_2 (infected hepatocytes) with the variable burst size (bursting case) is given by

$$\tilde{f}_1(s_1, s_2) = \frac{d_1\alpha + \lambda\beta_2 s_1^2 + d_1 d_2 \sum_{i=0}^{\infty} P_i s_2^i}{d_1(d_2 + \alpha) + \lambda\beta_2} \tag{5.3.4}$$

and the offspring PGF for X_3 (virions) and the expectation matrix for the PGFs represented by $\tilde{f}_2(s_1, s_2)$ and M_2, respectively, are the same as for the fixed burst size given by (5.2.6) and (5.2.8), respectively. In this case, we obtain a different probability (from the case of fixed burst size) for the virus extinction given by the solution $(\tilde{q}_1, \tilde{q}_2) \in (0, 1) \times (0, 1)$ of the following coupled equations

$$\frac{d_1\alpha + \lambda\beta_2\tilde{q}_1^2 + d_1 d_2 \sum_{i=0}^{\infty} P_i \tilde{q}_2^i}{d_1(d_2 + \alpha) + \lambda\beta_2} = \tilde{q}_1, \tag{5.3.5}$$

$$\frac{d_1 d_3 + \lambda\beta_1\tilde{q}_1\tilde{q}_2}{d_1 d_3 + \lambda\beta_1} = \tilde{q}_2. \tag{5.3.6}$$

The relation (5.3.5) is dependent on the variable burst size, i. Assuming the variable burst size and following the same procedure as discussed for the fixed burst size in the previous section, one can obtain the values of $\tilde{q}_1$ and $\tilde{q}_2$ in case of variable burst size. Hence, applying Theorem 5.2.2, the probability of virus extinction can be calculated in this case.

5.4 Forward Kolmogorov and Moment Equations

In order to derive the forward Kolmogorov differential equations [3, 86, 114] corresponding to the system of SDEs (5.1.1) (or (5.1.2)), we use the drift vector $\vec{f}(t,\vec{X})$ and diffusion matrix H (or $\tilde{H}$). Then the probability density function (PDF) $P(t,\vec{X})$ (in case of budding) associated with the system (5.1.1) is given by the solution to the following PDE:

$$\begin{aligned}
\frac{\partial P(t,\vec{X})}{\partial t} &= \frac{1}{2}\sum_{i=1}^{4}\sum_{j=1}^{4}\frac{\partial^2}{\partial X_i \partial X_j}\left[P(t,\vec{X})\sum_{m=1}^{5}H_{im}H_{jm}\right] - \sum_{i=1}^{4}\frac{\partial[P(t,\vec{X})f_i(t,\vec{X})]}{\partial X_i} \\
&= \frac{1}{2}\frac{\partial^2}{\partial X_1^2}P(t,\vec{X})\left[\lambda + d_1X_1 + \beta_1X_1X_3 + \beta_2X_1X_2 + \alpha X_2\right] \\
&\quad + \frac{1}{2}\frac{\partial^2}{\partial X_2^2}P(t,\vec{X})\left[\beta_1X_1X_3 + \beta_2X_1X_2 + \alpha X_2 + d_2X_2\right] \\
&\quad + \frac{1}{2}\frac{\partial^2}{\partial X_3^2}P(t,\vec{X})\left[kX_2 + d_3X_3 + pX_3X_4\right] + \frac{1}{2}\frac{\partial^2}{\partial X_4^2}P(t,\vec{X})\left[cX_3X_4 + d_4X_4\right] \\
&\quad - \frac{\partial^2}{\partial X_1 X_2}P(t,\vec{X})\left[\beta_1X_1X_3 + \beta_2X_1X_2 + \alpha X_2\right] \\
&\quad - \frac{\partial}{\partial X_1}P(t,\vec{X})\left[\lambda - \beta_1X_1X_3 - \beta_2X_1X_2 - d_1X_1 + \alpha X_2\right] \\
&\quad - \frac{\partial}{\partial X_2}P(t,\vec{X})\left[\beta_1X_1X_3 + \beta_2X_1X_2 - d_2X_2 - \alpha X_2\right] \\
&\quad - \frac{\partial}{\partial X_3}P(t,\vec{X})\left[kX_2 - d_3X_3 - pX_3X_4\right] - \frac{\partial}{\partial X_4}P(t,\vec{X})\left[cX_3X_4 - d_4X_4\right],
\end{aligned}$$

where $\vec{f} = (f_1, f_2, f_3, f_4)^\top$, $H = [H_{ij}]_{4\times 5}$ and $\sum_{m=1}^{5} H_{im}H_{jm}$ is the $(i,j)^{th}$ entry of the covariance matrix V. Similarly, the forward Kolmogorov differential equations (in case of bursting)

corresponding to the system of SDEs (5.1.2) is given by the following PDE:

$$\begin{aligned}
\frac{\partial \tilde{P}(t,\vec{X})}{\partial t} &= \frac{1}{2}\sum_{i=1}^{4}\sum_{j=1}^{4}\frac{\partial^2}{\partial X_i \partial X_j}\left[\tilde{P}(t,\vec{X})\sum_{m=1}^{5}\tilde{H}_{im}\tilde{H}_{jm}\right] - \sum_{i=1}^{4}\frac{\partial[\tilde{P}(t,\vec{X})f_i(t,\vec{X})]}{\partial X_i} \\
&= \frac{1}{2}\frac{\partial^2}{\partial X_1^2}\tilde{P}(t,\vec{X})\left[\lambda + d_1X_1 + \beta_1X_1X_3 + \beta_2X_1X_2 + \alpha X_2\right] \\
&\quad + \frac{1}{2}\frac{\partial^2}{\partial X_2^2}\tilde{P}(t,\vec{X})\left[\beta_1X_1X_3 + \beta_2X_1X_2 + \alpha X_2 + d_2X_2\right] \\
&\quad + \frac{1}{2}\frac{\partial^2}{\partial X_3^2}\tilde{P}(t,\vec{X})\left[N^2d_2X_2 + d_3X_3 + pX_3X_4\right] + \frac{1}{2}\frac{\partial^2}{\partial X_4^2}\tilde{P}(t,\vec{X})\left[cX_3X_4 + d_4X_4\right] \\
&\quad - \frac{\partial^2}{\partial X_1X_2}\tilde{P}(t,\vec{X})\left[\beta_1X_1X_3 + \beta_2X_1X_2 + \alpha X_2\right] - \frac{\partial^2}{\partial X_2X_3}\tilde{P}(t,\vec{X})\left[Nd_2X_2\right] \\
&\quad - \frac{\partial}{\partial X_1}\tilde{P}(t,\vec{X})\left[\lambda - \beta_1X_1X_3 - \beta_2X_1X_2 - d_1X_1 + \alpha X_2\right] \\
&\quad - \frac{\partial}{\partial X_2}\tilde{P}(t,\vec{X})\left[\beta_1X_1X_3 + \beta_2X_1X_2 - d_2X_2 - \alpha X_2\right] \\
&\quad - \frac{\partial}{\partial X_3}\tilde{P}(t,\vec{X})\left[Nd_2X_2 - d_3X_3 - pX_3X_4\right] - \frac{\partial}{\partial X_4}\tilde{P}(t,\vec{X})\left[cX_3X_4 - d_4X_4\right],
\end{aligned}$$

where $\vec{f} = (f_1, f_2, f_3, f_4)^\top$, $\tilde{H} = [\tilde{H}_{ij}]_{4\times 5}$ and $\sum_{m=1}^{5}\tilde{H}_{im}\tilde{H}_{jm}$ is the $(i,j)^{th}$ entry of the covariance matrix $\tilde{V}$. Given the difficulty in obtaining a solution to the above Kolmogorov PDEs, we seek alternative approaches to obtain information about the PDF $P(t,\vec{X})$ (or $\tilde{P}(t,\vec{X})$). Accordingly, we use the multivariate Itô formula [3, 86, 114] to derive the SDEs for the random variables $X_iX_j,\ i,j = 1,2,3,4$. We have the system of Itô SDEs in case of budding being given by

$$d\vec{X}(t) = \vec{f}(\vec{X}(t))dt + H(\vec{X}(t))d\vec{W}(t).$$

Let $F(t,x)$ be a real valued function defined for $x = (x_1,x_2,x_3,x_4) \in \mathbb{R}^4$ and $t \in [0,\infty)$ such that the partial derivatives $\partial F/\partial t$, $\partial F/\partial x_i$, $\partial^2 F/\partial x_i\partial x_j$ $(i,j = 1,2,3,4)$ be continuous. Then by the multivariate Itô formula, we obtain

$$dF(t,\vec{X}(t)) = h(t,\vec{X}(t))dt + \vec{g}(t,\vec{X}(t))\cdot d\vec{W}(t),$$

where

$$\begin{aligned}
h(t,x) &= \frac{\partial F}{\partial t} + \sum_{i=1}^{4}\frac{\partial F}{\partial x_i}f_i + \frac{1}{2}\sum_{i=1}^{4}\sum_{j=1}^{4}\sum_{m=1}^{5}\frac{\partial^2 F}{\partial x_i\partial x_j}H_{im}H_{jm}, \\
\vec{g}(t,x)\cdot d\vec{W}(t) &= \sum_{m=1}^{5}\sum_{i=1}^{4}\frac{\partial F}{\partial x_i}H_{im}dW_m(t).
\end{aligned}$$

In order to determine the second order moment of X_1, we consider the function $F(t,x) = x_1^2$ which gives $\frac{\partial F}{\partial t} = 0$, $\frac{\partial F}{\partial x_1} = 2x_1$, $\frac{\partial^2 F}{\partial x_1^2} = 2$ with the remaining partial derivatives and mixed partial derivatives being equal to zero. Thus,

$$\begin{aligned} h(t,\vec{X}) &= 2X_1(\lambda - \beta_1 X_1 X_3 - \beta_2 X_1 X_2 - d_1 X_1 + \alpha X_2) \\ &\quad + (\lambda + \beta_1 X_1 X_3 + \beta_2 X_1 X_2 + d_1 X_1 + \alpha X_2), \\ \vec{g}(t,\vec{X}) \cdot d\vec{W} &= 2X_1\sqrt{\lambda + d_1 X_1}dW_1 + 2X_1\sqrt{\beta_1 X_1 X_3 + \beta_2 X_1 X_2 + \alpha X_2}dW_2. \end{aligned}$$

Hence,

$$\begin{aligned} dX_1^2 &= (\lambda + \alpha X_2)(2X_1 + 1)dt - (\beta_1 X_1 X_3 + \beta_2 X_1 X_2 + d_1 X_1)(2X_1 - 1)dt \\ &\quad + 2X_1\left(\sqrt{\lambda + d_1 X_1}dW_1 + \sqrt{\beta_1 X_1 X_3 + \beta_2 X_1 X_2 + \alpha X_2}dW_2\right). \end{aligned}$$

Similarly, we obtain the other second order SDEs associated with the system (5.1.1) as follows:

$$\begin{aligned} dX_2^2 &= (\beta_1 X_1 X_3 + \beta_2 X_1 X_2)(2X_2 + 1)dt - (d_2 + \alpha)(2X_2 - 1)X_2 dt \\ &\quad - 2X_2\sqrt{\beta_1 X_1 X_3 + \beta_2 X_1 X_2 + \alpha X_2}dW_2 - 2X_2\sqrt{d_2 X_2}dW_3, \\ dX_3^2 &= kX_2(2X_3 + 1)dt - (d_3 + pX_4)(2X_3 - 1)X_3 dt + 2X_3\sqrt{kX_2 + d_3 X_3 + pX_3 X_4}dW_4, \\ dX_4^2 &= cX_3 X_4(2X_4 + 1)dt - d_4 X_4(2X_4 - 1)dt + 2X_4\sqrt{cX_3 X_4 + d_4 X_4}dW_5, \\ dX_1 X_2 &= \lambda X_2 dt - (d_1 + d_2)X_1 X_2 dt + (\beta_1 X_1 X_3 + \beta_2 X_1 X_2)(X_1 - X_2 - 1)dt \\ &\quad - \alpha X_2(X_1 - X_2 + 1)dt + 2X_2\sqrt{\lambda + d_1 X_1}dW_1 \\ &\quad + (X_2 - X_1)\sqrt{\beta_1 X_1 X_3 + \beta_2 X_1 X_2 + \alpha X_2}dW_2 + X_1\sqrt{d_2 X_2}dW_3, \\ dX_1 X_3 &= X_3(\lambda - \beta_1 X_1 X_3 - \beta_2 X_1 X_2 - d_1 X_1 + \alpha X_2)dt + X_1(kX_2 - d_3 X_3 - pX_3 X_4)dt \\ &\quad + X_3\sqrt{\lambda + d_1 X_1}dW_1 + X_3\sqrt{\beta_1 X_1 X_3 + \beta_2 X_1 X_2 + \alpha X_2}dW_2 \\ &\quad + X_1\sqrt{kX_2 + d_3 X_3 + pX_3 X_4}dW_4, \\ dX_1 X_4 &= X_4(\lambda - \beta_1 X_1 X_3 - \beta_2 X_1 X_2 - d_1 X_1 + \alpha X_2)dt + X_1(cX_3 X_4 - d_4 X_4)dt \\ &\quad + X_4\sqrt{\lambda + d_1 X_1}dW_1 + X_4\sqrt{\beta_1 X_1 X_3 + \beta_2 X_1 X_2 + \alpha X_2}dW_2 \\ &\quad + X_1\sqrt{cX_3 X_4 + d_4 X_4}dW_5, \\ dX_2 X_3 &= X_3(\beta_1 X_1 X_3 + \beta_2 X_1 X_2 - d_2 X_2 - \alpha X_2)dt + X_2(kX_2 - d_3 X_3 - pX_3 X_4)dt \\ &\quad - X_3\sqrt{\beta_1 X_1 X_3 + \beta_2 X_1 X_2 + \alpha X_2}dW_2 + X_3\sqrt{d_2 X_2}dW_3 \\ &\quad + X_2\sqrt{kX_2 + d_3 X_3 + pX_3 X_4}dW_4, \end{aligned}$$

$$\begin{aligned} dX_2X_4 &= X_4(\beta_1X_1X_3+\beta_2X_1X_2-d_2X_2-\alpha X_2)dt+X_2(cX_3X_4-d_4X_4)dt \\ &\quad -X_4\sqrt{\beta_1X_1X_3+\beta_2X_1X_2+\alpha X_2}dW_2+X_4\sqrt{d_2X_2}dW_3 \\ &\quad +X_2\sqrt{cX_3X_4+d_4X_4}dW_5, \\ dX_3X_4 &= X_4(kX_2-d_3X_3-pX_3X_4)dt+X_3(cX_3X_4-d_4X_4)dt \\ &\quad +X_4\sqrt{kX_2+d_3X_3+pX_3X_4}dW_4+X_3\sqrt{cX_3X_4+d_4X_4}dW_5. \end{aligned}$$

The Itô stochastic integral equations is derived by integrating the above obtained SDEs. Then differentiating the expectations of these Itô integrals, we obtain the differential equations for first and second order moments, for the budding SDE model (5.1.1). The SDE for X_1 in the case of budding is given by

$$\begin{aligned} dX_1 &= (\lambda-\beta_1X_1X_3-\beta_2X_1X_2-d_1X_1+\alpha X_2)dt \\ &\quad +\sqrt{\lambda+d_1X_1}dW_1+\sqrt{\beta_1X_1X_3+\beta_2X_1X_2+\alpha X_2}dW_2. \end{aligned}$$

Taking the expectation after integrating on the interval $[0,t]$ results in

$$\begin{aligned} E[X_1(t)]-E[X_1(0)] &= E\left\{\int_0^t\left[\lambda-\beta_1X_1X_3-\beta_2X_1X_2-d_1X_1+\alpha X_2\right]dt\right\} \\ &\quad +E\left\{\int_0^t\sqrt{\lambda+d_1X_1}dW_1\right\} \\ &\quad +E\left\{\int_0^t\sqrt{\beta_1X_1X_3+\beta_2X_1X_2+\alpha X_2}dW_2\right\}. \end{aligned}$$

Using the properties of Itô stochastic integral, we observe that the expectation of an Itô integral is zero. Assume that the integral and the expectation can be interchanged results in

$$E[X_1(t)]-E[X_1(0)] = \int_0^t E\left[\lambda-\beta_1X_1X_3-\beta_2X_1X_2-d_1X_1+\alpha X_2\right]dt.$$

Now, differentiating the above with respect to t, we obtain,

$$\frac{dE[X_1]}{dt} = \lambda-\beta_1E[X_1X_3]-\beta_2E[X_1X_2]-d_1E[X_1]+\alpha E[X_2].$$

Similarly, we obtain the other differential equations for first and second order moments as follows

$$
\begin{aligned}
\frac{dE[X_2]}{dt} &= \beta_1 E[X_1X_3] + \beta_2 E[X_1X_2] - (d_2+\alpha)E[X_2],\\
\frac{dE[X_3]}{dt} &= kE[X_2] - d_3E[X_3] - pE[X_3X_4],\\
\frac{dE[X_4]}{dt} &= cE[X_3X_4] - d_4E[X_4],\\
\frac{dE[X_1^2]}{dt} &= \lambda + (2\lambda+d_1)E[X_1] + \alpha E[X_2] + (2\alpha+\beta_2)E[X_1X_2] + \beta_1 E[X_1X_3]\\
&\quad - 2d_1E[X_1^2] - 2\beta_1 E[X_1^2X_3] - 2\beta_2 E[X_1^2X_2],\\
\frac{dE[X_2^2]}{dt} &= \beta_1 E[X_1X_3] + \beta_2 E[X_1X_2] + (d_2+\alpha)\left(E[X_2] - 2E[X_2^2]\right)\\
&\quad + 2\beta_1 E[X_1X_2X_3] + 2\beta_2 E[X_1X_2^2],\\
\frac{dE[X_3^2]}{dt} &= kE[X_2] + d_3E[X_3] + 2kE[X_2X_3] + pE[X_3X_4] - 2d_3E[X_3^2] - 2pE[X_3^2X_4],\\
\frac{dE[X_4^2]}{dt} &= cE[X_3X_4] + d_4E[X_4] + 2cE[X_3X_4^2] - 2d_4E[X_4^2],\\
\frac{dE[X_1X_2]}{dt} &= (\lambda-\alpha)E[X_2] + \alpha E[X_2^2] - (d_1+d_2+\alpha-\beta_2)E[X_1X_2] - \beta_1 E[X_1X_3]\\
&\quad + \beta_1 E[X_1^2X_3] + \beta_2 E[X_1^2X_2] - \beta_2 E[X_1X_2^2] - \beta_1 E[X_1X_2X_3],\\
\frac{dE[X_1X_3]}{dt} &= \lambda E[X_3] + kE[X_1X_2] + \alpha E[X_2X_3] - (d_1+d_3)E[X_1X_3]\\
&\quad - \beta_1 E[X_1X_3^2] - \beta_2 E[X_1X_2X_3] - pE[X_1X_3X_4],\\
\frac{dE[X_1X_4]}{dt} &= \lambda E[X_4] - (d_1+d_4)E[X_1X_4] + \alpha E[X_2X_4]\\
&\quad - (\beta_1 - c)E[X_1X_3X_4] - \beta_2 E[X_1X_2X_4],\\
\frac{dE[X_2X_3]}{dt} &= \beta_1 E[X_1X_3^2] + \beta_2 E[X_1X_2X_3] - pE[X_2X_3X_4] + kE[X_2^2]\\
&\quad - (d_2+d_3+\alpha)E[X_2X_3],\\
\frac{dE[X_2X_4]}{dt} &= \beta_1 E[X_1X_3X_4] + \beta_2 E[X_1X_2X_4] + cE[X_2X_3X_4] - (d_2+d_4+\alpha)E[X_2X_4],\\
\frac{dE[X_3X_4]}{dt} &= kE[X_2X_4] - (d_3+d_4)E[X_3X_4] + cE[X_3^2X_4] - pE[X_3X_4^2].
\end{aligned}
$$

Adopting a similar procedure, one can obtain the moment differential equations for the case of bursting. The differential equations for first and second order moments in case of

bursting will be same as in the budding case except the following ones:

$$\begin{aligned}
\frac{dE[X_3]}{dt} &= Nd_2E[X_2] - d_3E[X_3] - pE[X_3X_4],\\
\frac{dE[X_3^2]}{dt} &= N^2d_2E[X_2] + d_3E[X_3] + 2Nd_2E[X_2X_3] + pE[X_3X_4]\\
&\quad - 2d_3E[X_3^2] - 2pE[X_3^2X_4],\\
\frac{dE[X_1X_3]}{dt} &= \lambda E[X_3] + Nd_2E[X_1X_2] + \alpha E[X_2X_3] - (d_1+d_3)E[X_1X_3]\\
&\quad - \beta_1E[X_1X_3^2] - \beta_2E[X_1X_2X_3] - pE[X_1X_3X_4],\\
\frac{dE[X_2X_3]}{dt} &= \beta_1E[X_1X_3^2] + \beta_2E[X_1X_2X_3] - pE[X_2X_3X_4] - Nd_2E[X_2] + Nd_2E[X_2^2]\\
&\quad - (d_2+d_3+\alpha)E[X_2X_3],\\
\frac{dE[X_3X_4]}{dt} &= Nd_2E[X_2X_4] - (d_3+d_4)E[X_3X_4] + cE[X_3^2X_4] - pE[X_3X_4^2].
\end{aligned}$$

It is observed that each moment differential equation involves the higher-order moments resulting in an infinite system of moment differential equations. Therefore, in order to avoid the computational difficulty, some assumptions for higher-order moments are necessary so that a finite system of differential equations can be obtained. These moment differential equations can be useful in estimating the expectations, variances, moments and distribution patterns of the model variables. In particular, if we consider the infection-free stage, *i.e.*, when $X_i = 0,\ i = 2, 3, 4$, the system of moment differential equations leads to the following single equation for both budding and bursting models

$$\frac{dE[X_1]}{dt} = \lambda - d_1E[X_1]. \tag{5.4.1}$$

Hence, the moment of X_1 is given by $E[X_1] = \left(X_1(0) - \frac{\lambda}{d_1}\right)e^{-d_1t} + \frac{\lambda}{d_1}$. Therefore, when $t \to \infty$, we have $E[X_1] = \frac{\lambda}{d_1}$.

5.5 Numerical Results and Discussions

In this section, we present several numerical simulations in order to illustrate the dynamics of the stochastic models and related results for both budding and bursting processes (with fixed as well as variable burst size). In order to perform the numerical simulations, we list three sets of parameter values, as given in Table 5.3 and accordingly, use these for various scenarios. In order to numerically solve the SDEs, we apply the Euler-Maruyama (EM) method [6], due to its computational tractability. We take the initial condition as $(X_1(0), X_2(0), X_3(0), X_4(0)) = (U(0), I(0), V(0), B(0)) = (200, 20, 10, 40)$ for each of the simulations of SDE models throughout the discussion. For the convergence of EM method,

Parameters	Values [References]			Units
	Set-I	Set-II	Set-III	
λ	10 [126, 127]	2 [102]	1 [126, 127]	cells day^{-1}
β_1	0.01 [126, 127]	0.01 [126, 127]	0.00065 [19]	virion^{-1} day^{-1}
β_2	0.00065 [19]	0.00065 [19]	0.00065 [19]	cell^{-1} day^{-1}
d_1	0.01 [22]	0.01 [22]	0.01 [22]	day^{-1}
d_2	0.1 [126, 127]	0.1 [126, 127]	1 [22]	day^{-1}
d_3	6 [22]	6 [22]	6 [22]	day^{-1}
d_4	0.3 [97]	0.3 [97]	0.3 [97]	day^{-1}
α	0.01 [29]	0.01 [29]	0.01 [29]	day^{-1}
p	1 [126, 127]	1 [126, 127]	1 [126, 127]	cell^{-1} day^{-1}
c	0.1 [97]	0.1 [97]	0.1 [97]	virion^{-1} day^{-1}
N	20 (Assumed)	2 (Assumed)	20 (Assumed)	virions cell^{-1}
$k = Nd_2$	2	0.2	20	virions cell^{-1} day^{-1}

Table 5.3: The list of parameter values for numerical simulations for the stochastic models.

the stepsize Δt should be sufficiently small [2, 138]. Accordingly, we take a small stepsize, $\Delta t = 0.01$. Each stochastic mean path of the SDE models is determined based on 5000 sample paths. A sufficiently large number of sample paths considered for simulation (obviously) provides a better stochastic mean path. Moreover, for the case of variable burst size, we consider $N_e = 20,\ \mu = 0.5,\ \sigma = 10$ and $N(0) = 20$.

We use Set-I of the parameter values from Table 5.3 to analyze the dynamics of the SDE models for budding (5.1.1), bursting with fixed burst size (5.1.2) and bursting with variable burst size (5.3.3) and compare the results with the solution of deterministic model (2.1.1). The basic reproduction number for the deterministic model corresponding to this set of parameter values is $R_0 = 36.2121 > 1$. Therefore, the deterministic model (2.1.1) has a stable infected equilibrium point. In Figs. 5.1, 5.2 and 5.3, a sample path, the stochastic mean (based on 5000 sample paths) and the stochastic mean plus or minus standard deviation for the uninfected hepatocytes (Figs. 5.1(a), 5.2(a) and 5.3(a)), infected hepatocytes (Figs. 5.1(b), 5.2(b) and 5.3(b)), virions (Figs. 5.1(c), 5.2(c) and 5.3(c)) and B cells (Figs. 5.1(d), 5.2(d) and 5.3(d)) corresponding to the budding, fixed bursting and variable bursting model, respectively, are presented. The sample path for each of the population variables in Figs. 5.1, 5.2 and 5.3 signify the stochastic fluctuations over time, but the mean path stabilizes ultimately at its respective stable level. The stochastic fluctuation in the sample path for the virion population is much higher than that for the other populations in each case. The high variability in the virion density can be observed from the difference between the paths of mean and mean plus or minus standard deviation. This demonstrates that when the number of virions increases, the B cells become more effective in neutralizing the virions and

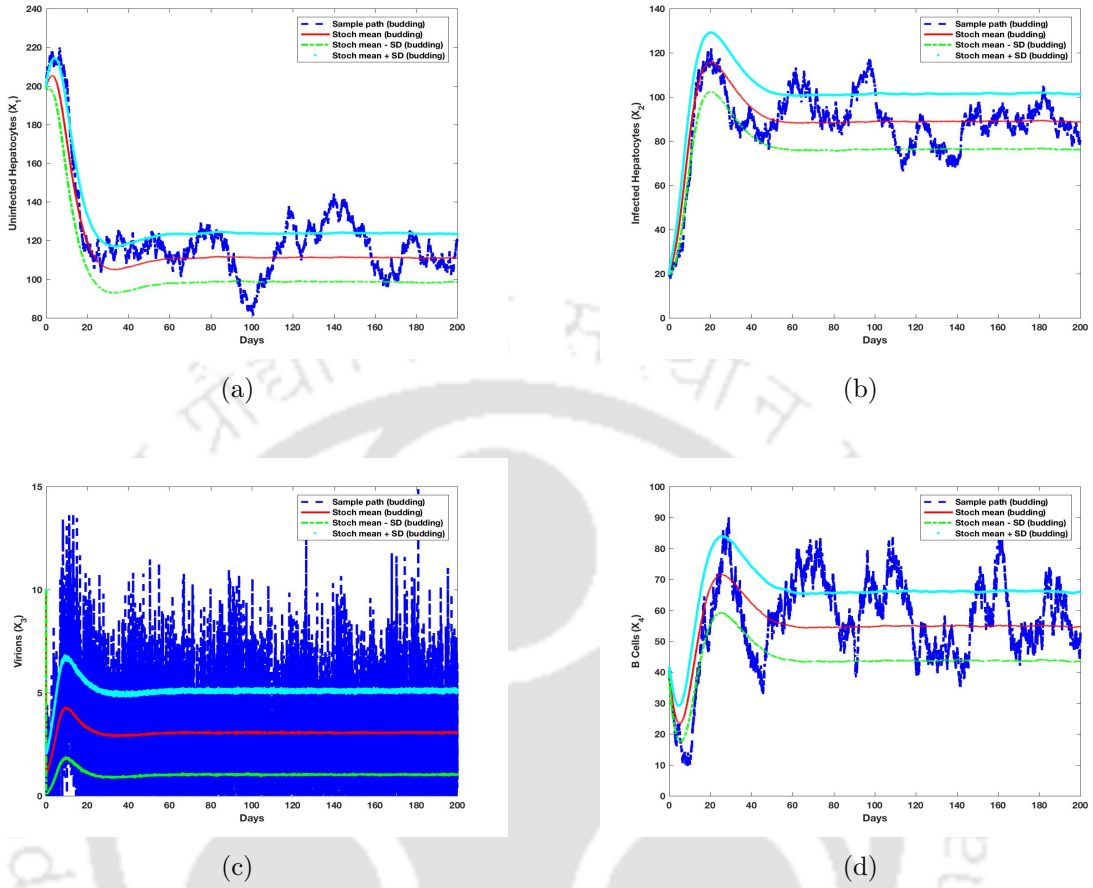

Figure 5.1: One sample path and mean of 5000 sample paths with plus or minus standard deviation of (*a*) uninfected hepatocytes, (*b*) infected hepatocytes, (*c*) virions and (*d*) B cells for the budding SDE model (5.1.1).

consequently, virions significantly decrease and so the activation of B cells gets slower. Then the virions increase gradually and the subsequent response of B cells increases again. Thus a high variation in the virions density is observed.

We now present the probability histogram plots in order to understand the probability distribution at $t = 150$ based on 5000 simulations for each of the population variables in case of budding as well as bursting with fixed and variable burst size separately. The time point of $t = 150$ was chosen for illustrative purpose, in order to show the probability distribution pattern at a stable state. As seen from Figs. 5.1, 5.2 and 5.3, the stochastic mean paths become stable beyond time $t = 50$, for all the cases. Another choice of $t > 50$, would result in similar distribution being observed. Figs. 5.4, 5.5 and 5.6 represent the probability histograms of the uninfected hepatocytes (Figs. 5.4(a), 5.5(a) and 5.6(a)), infected hepatocytes (Figs. 5.4(b), 5.5(b) and 5.6(b)), virions (Figs. 5.4(c), 5.5(c) and 5.6(c)) and B cells

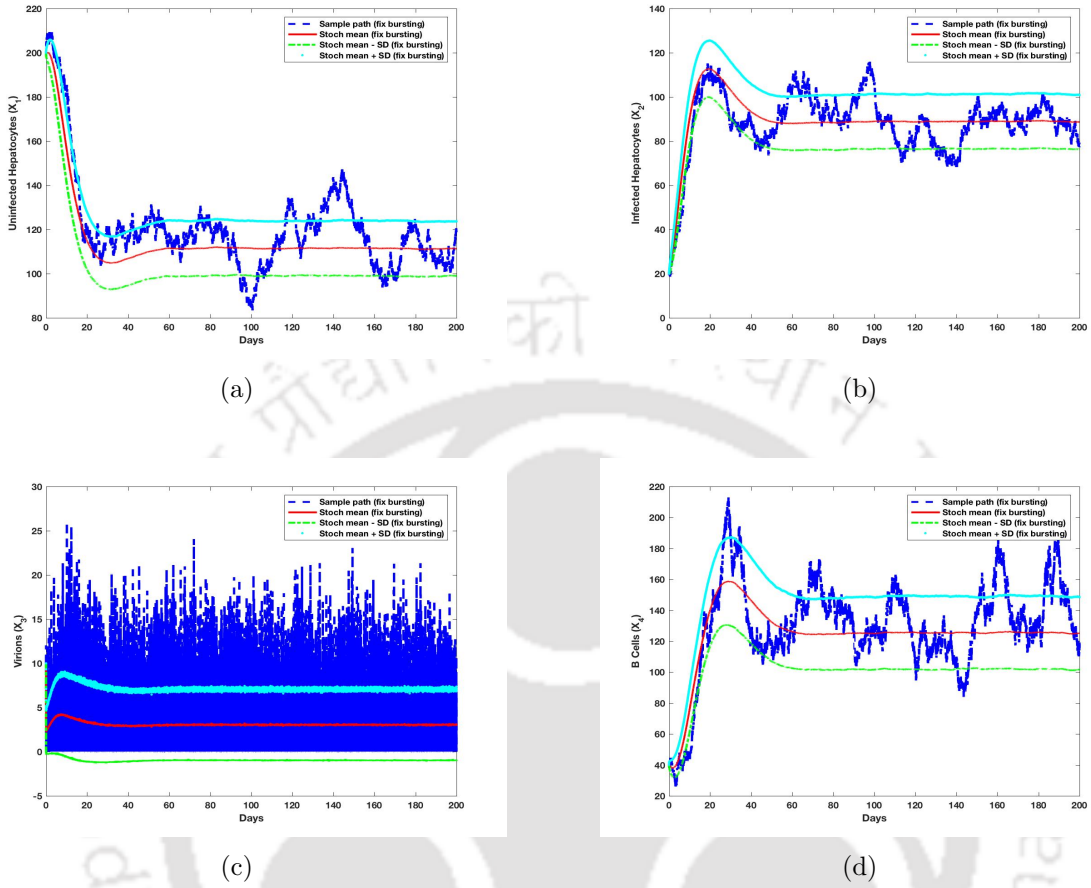

Figure 5.2: One sample path and mean of 5000 sample paths with plus or minus standard deviation of (a) uninfected hepatocytes, (b) infected hepatocytes, (c) virions and (d) B cells for the bursting SDE model with fixed burst size given by (5.1.2).

(Figs. 5.4(d), 5.5(d) and 5.6(d)) with the values taken from 5000 independent simulations at $t = 150$ for the budding, fixed bursting and variable bursting models, respectively. The mean ($\mu(X_i)$) and standard deviation ($\sigma(X_i)$) of each population at $t = 150$ based on 5000 independent simulations for the three cases are presented in Table 5.4. We plot the normally distributed curves with the mean and standard deviation (taken from Table 5.4) of the respective variables for the three cases and compare them with the probability histogram plots (Figs. 5.4, 5.5 and 5.6). It is observed that the probability distribution of the uninfected and infected hepatocytes are well fitted with the normal curves in all cases, whereas the distribution of the virion population does not fit with the normal curve. Moreover, the variability of the virion density is greater in case of bursting than budding and bursting process with variable burst size showing more variation than the fixed bursting model. In the budding case, the virions are produced continuously from the infected hepatocytes, but the number

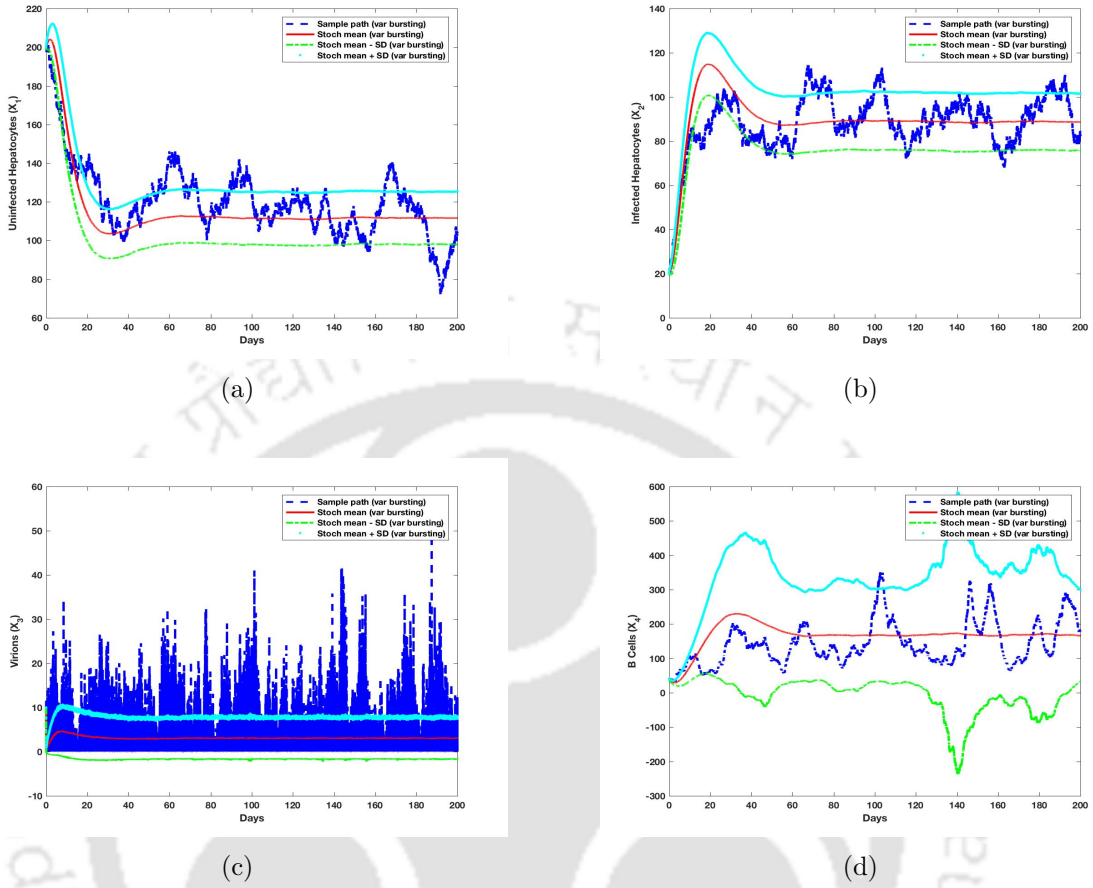

Figure 5.3: One sample path and mean of 5000 sample paths with plus or minus standard deviation of (a) uninfected hepatocytes, (b) infected hepatocytes, (c) virions and (d) B cells for the bursting SDE model with variable burst size given by (5.3.3).

of virions remains unchanged until the lysis of infected hepatocytes in case of bursting and the burst of an infected hepatocyte increases the virions density by N (or N_t, in case of variable burst size) resulting in greater stochastic variation for the virion population in this case. The mean and standard deviation values for B cell population are dependent on the virion release process and both values are elevated for the case of bursting and in case of variable burst size, these are much higher due to the variation in the production rate of the virions. A sample path, the stochastic mean path with plus or minus standard deviation (Fig. 5.7(a)) and probability histogram (Fig. 5.7(b)) with normal approximation curve (at $t = 150$ based on 5000 independent simulations) for the variable burst size are presented in Fig. 5.7. This is illustrative of the variability of burst size involved in the release rate of the virions.

In Fig. 5.8, we compare the mean solution of the SDE models (5.1.1), (5.1.2) and (5.3.3)

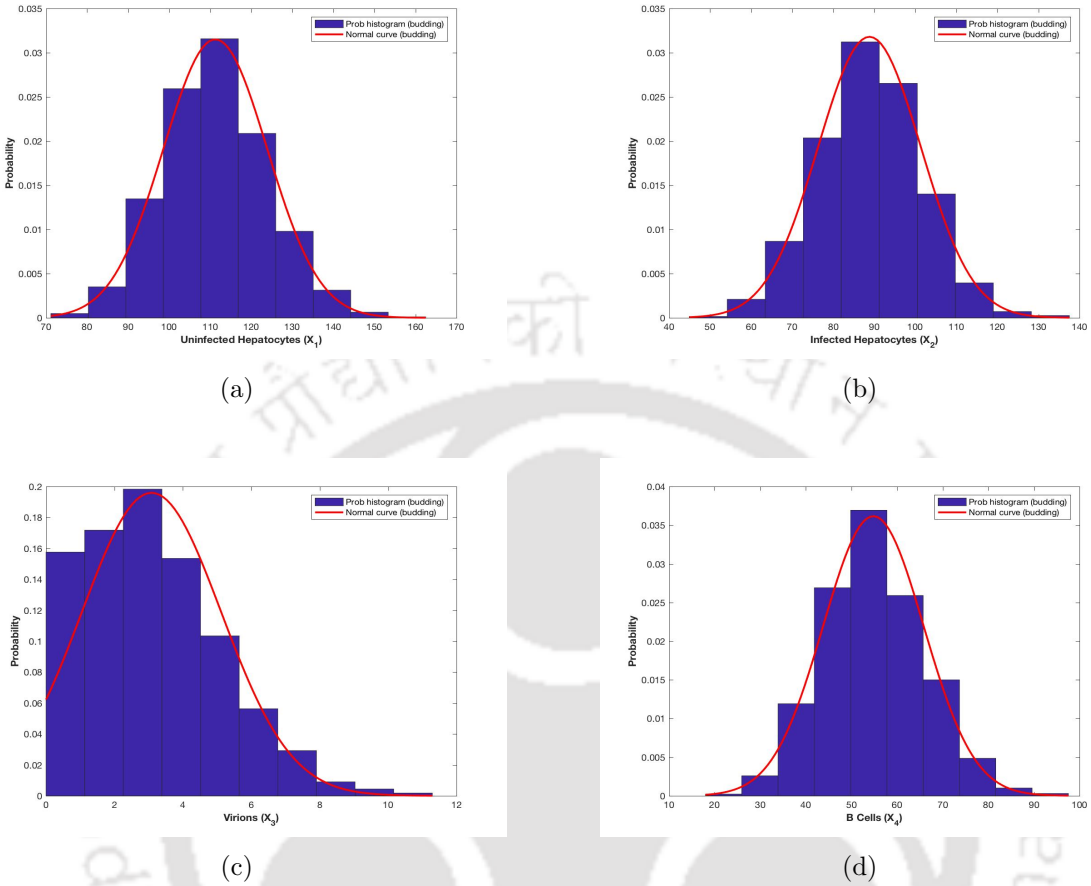

Figure 5.4: Probability histograms and approximate normal distributions of (a) uninfected hepatocytes, (b) infected hepatocytes, (c) virions and (d) B cells at $t = 150$ based on 5000 sample paths for the SDE budding model (5.1.1).

with the deterministic model (2.1.1). This simulation indicates that (111.3808,88.8619,3,53.2413) is the stable equilibrium point for the deterministic system. The mean paths of the uninfected hepatocytes (Fig. 5.8(a)) and infected hepatocytes (Fig. 5.8(b)) associated with the SDE models in all cases are very close to their respective deterministic paths. A high stochastic fluctuation in the stochastic mean path for virions is observed in Fig. 5.8(c). The measurement of variability in virion size can be obtained from the standard deviation of virions $(\sigma(X_3))$ which has already been calculated earlier. The difference between the deterministic value and stochastic mean value of B cells population (Fig. 5.8(d)) is very slight in case of budding, but it becomes significantly high in case of bursting and comparatively much higher when variable burst size is considered. In the bursting case, the number of virions increases suddenly after the death of an infected hepatocyte, resulting in a greater response of B cells. Thus, in the stochastic environment, the size of B cell population changes drastically due to

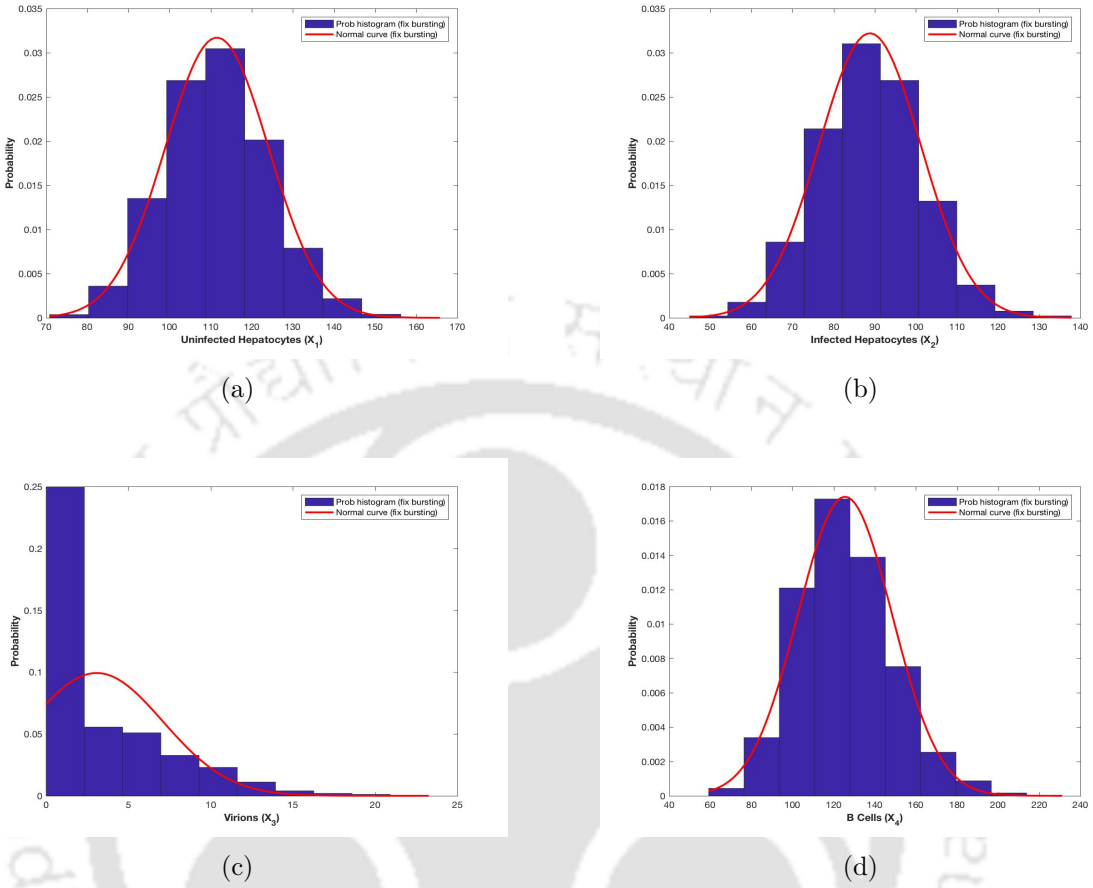

Figure 5.5: Probability histograms and approximate normal distributions of (a) uninfected hepatocytes, (b) infected hepatocytes, (c) virions and (d) B cells at $t = 150$ based on 5000 sample paths for the bursting SDE model with fixed burst size given by (5.1.2).

the fluctuation in virion population.

We now present a numerical comparison of the mean solutions to the SDE models obtained using the EM method, for various initial conditions and for various stepsizes. To demonstrate these cases, we consider the budding model (5.1.1) with the parameter values chosen from Set-I in Table 5.3 and compute the mean path for the four populations based on 5000 independent simulations using the EM method. To present the scenario of various initial conditions, we consider three different initial conditions as $ic_1 := (200, 20, 10, 40)$, $ic_2 := (100, 80, 30, 200)$ and $ic_3 := (300, 100, 50, 100)$ along with stepsize $\Delta t = 0.01$ and this result is depicted in Fig. 5.9, which shows that the variation in the initial condition for the SDE models ultimately leads to the same convergence level, except a variation in the paths and the time elapsed before reaching the steady states. However, the initial condition for the SDE models, does not effect on the resulting probabilistic means values. Further,

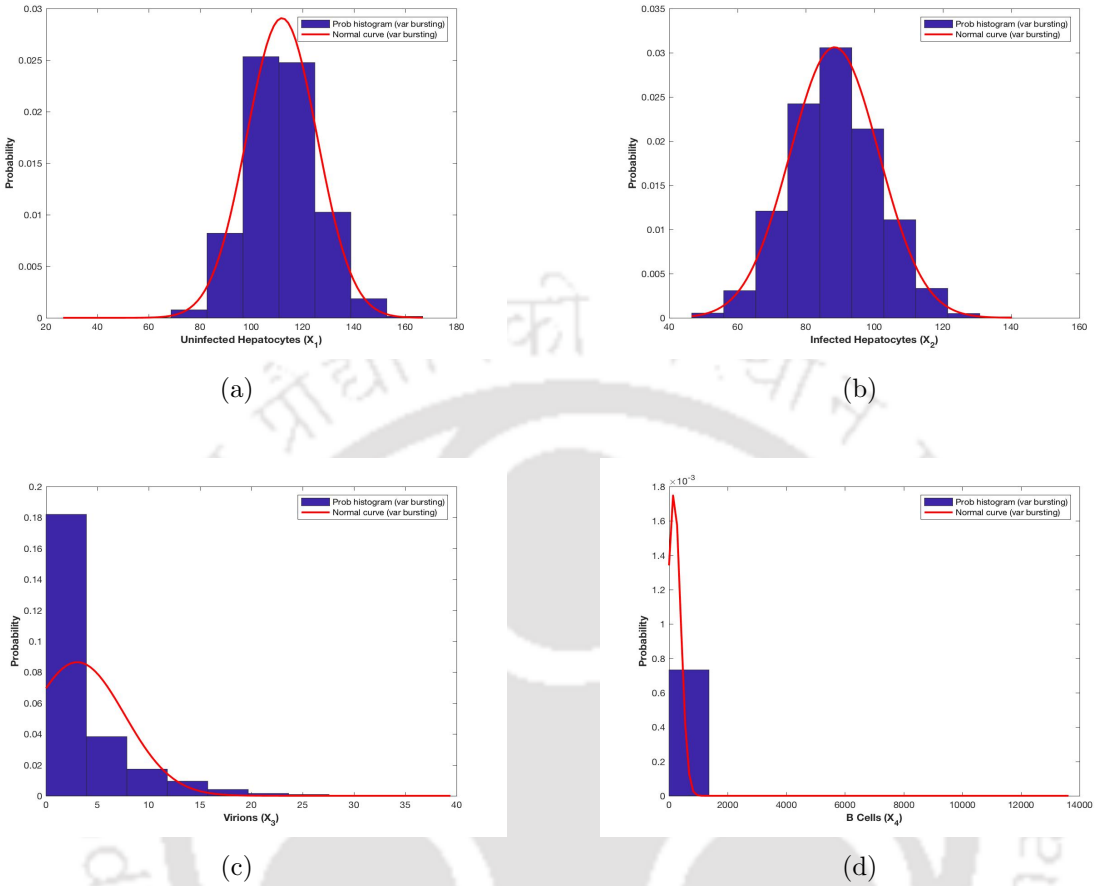

Figure 5.6: Probability histograms and approximate normal distributions of (a) uninfected hepatocytes, (b) infected hepatocytes, (c) virions and (d) B cells at $t = 150$ based on 5000 sample paths for the bursting SDE model with variable burst size given by (5.3.3).

in Fig. 5.10, we numerically investigate the stability of the mean solution obtained using the EM method by varying the stepsize Δt. For this simulation, we consider five different stepsizes $\Delta t = 0.005, 0.01, 0.02, 0.04, 0.1$. Means and standard deviations of the populations at $t = 150$, based on 5000 sample paths resulting from using the EM method with stepsizes $\Delta t = 0.005, 0.01, 0.02, 0.04, 0.1$ are listed in Table 5.5. From Fig. 5.10(a), it is observed that, for $\Delta t = 0.005, 0.01, 0.02$, the uninfected hepatocytes stabilize at the approximately same level, the value of which can be found from Table 5.5. A similar scenario is observed for the cases of infected hepatocytes (Fig. 5.10(b)), virions (Fig. 5.10(c)) and B cells (Fig. 5.10(d)) when $\Delta t = 0.005, 0.01, 0.02$. But in case of the large stepsize, that is, $\Delta t = 0.04, 0.1$, a different scenario is observed. In these cases, the uninfected hepatocytes, infected hepatocytes and virions stabilize at different levels from the earlier cases, with a great fluctuation in the mean path of the virions is observed when $\Delta t = 0.1$ (Fig. 5.10(c)).

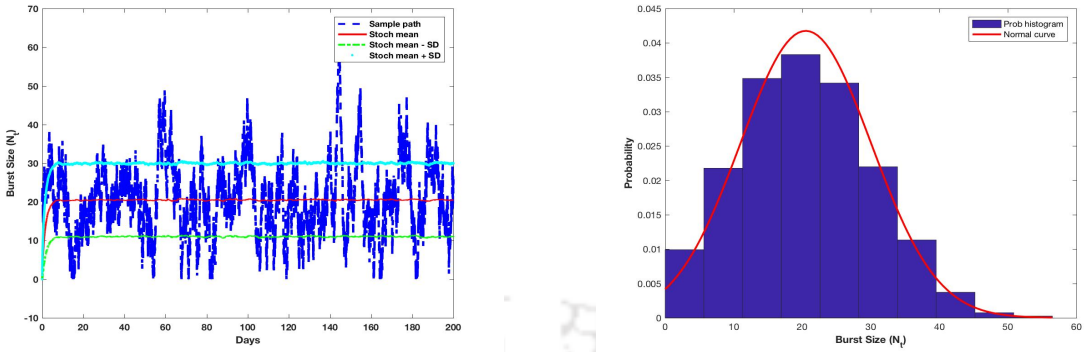

(a) (b)

Figure 5.7: (*a*) One sample path and mean path with plus or minus standard deviation and (*b*) probability histograms with approximate normal distribution at $t = 150$, based on 5000 sample paths of the variable burst size given by (5.3.1).

The B cell population is observed to undergo unrealistic growth after some time has elapsed (since the initial time), in both the cases of $\Delta t = 0.04, 0.1$. The values of the mean and standard deviation at $t = 150$ is tabulated in Table 5.5 which shows that these values for B cells in case of $\Delta t = 0.04, 0.1$ are very high. In fact at $t = 200$, this pattern persists with $\mu(X_4) = 5.7853 \times 10^8, 8.3838 \times 10^{58}$ for $\Delta t = 0.04, 0.1$, respectively. Therefore the solutions do not get stabilized in case of large stepsizes $\Delta t = 0.04, 0.1$. Thus this simulation indicates that the EM method gives a stable solution whenever the stepsize is chosen to be smaller than 0.2.

Further, we numerically estimate the probability of virus extinction for CTMC models in case of virus existence, *i.e.,* when $R_0 > 1$. In case of bursting, the fixed point $(\tilde{q}_1, \tilde{q}_2)$ given by (5.2.9) and (5.2.10) is obtained when $N = 2$, which is numerically illustrated in this discussion. Therefore, in order to maintain the consistency with the bursting model, we choose the production rate of virions, $k = Nd_2 = 0.2$ if $d_2 = 0.1$, for the bursting case. To discuss the virus extinction, we need such a set of parameter values so that $R_0 > 1$. Accordingly, we choose the parameter values from Set-II in Table 5.3, which corresponds to $R_0 = 1.7879$. In order to determine the probability of virus extinction in case of budding, the estimation for (q_1, q_2) calculated using (5.2.4) and (5.2.5) is $(0.5834, 0.8781)$. We assume that the initial infection is given by $(I(0), V(0)) = (20, 10)$. Therefore, the probability of virus extinction is 5.6908×10^{-6} (using Theorem 5.2.2). In case of bursting, the estimation for $(\tilde{q}_1, \tilde{q}_2)$ calculated from (5.2.9) and (5.2.10) is $(0.4469, 0.8443)$ and hence the probability of virus extinction in this case is 1.8565×10^{-8} (using Theorem 5.2.2). Thus, the chance of infection eradication is greater in case of budding than the bursting. The probability of virus

	Budding case	Bursting with fixed burst size	Bursting with variable burst size
$\mu(X_1)$	111.1833	111.7066	111.6539
$\sigma(X_1)$	12.5584	12.6329	13.6486
$\mu(X_2)$	88.7474	88.9109	88.7546
$\sigma(X_2)$	12.2260	12.3321	13.0253
$\mu(X_3)$	3.0512	3.0610	3.0939
$\sigma(X_3)$	2.0444	4.0167	4.7206
$\mu(X_4)$	54.9177	125.0189	163.6813
$\sigma(X_4)$	11.2525	23.1024	122.6164

Table 5.4: Means (μ) and standard deviations (σ) of four model populations (uninfected hepatocytes (X_1), infected hepatocytes (X_2), virions (X_3) and B cells (X_4)) calculated at $t = 150$ based on 5000 independent simulations for the cases of budding, bursting with fixed burst size and bursting with variable burst size.

	$\Delta t = 0.005$	$\Delta t = 0.01$	$\Delta t = 0.02$	$\Delta t = 0.04$	$\Delta t = 0.1$
$\mu(X_1)$	111.0923	111.1833	111.2198	105.7121	67.0908
$\sigma(X_1)$	12.4225	12.5584	12.5462	14.5256	10.6240
$\mu(X_2)$	88.6810	88.7474	88.6671	89.6547	93.2402
$\sigma(X_2)$	12.3730	12.2260	12.8003	14.1411	13.0082
$\mu(X_3)$	3.0228	3.0512	3.0572	3.6064	7.8339
$\sigma(X_3)$	1.8796	2.0444	2.4129	4.1211	9.8514
$\mu(X_4)$	54.1480	54.9177	58.1640	1.2916×10^7	5.6715×10^{44}
$\sigma(X_4)$	10.7908	11.2525	12.8253	7.9375×10^7	1.2041×10^{46}

Table 5.5: Means (μ) and standard deviations (σ) of four model populations (uninfected hepatocytes (X_1), infected hepatocytes (X_2), virions (X_3) and B cells (X_4)) calculated at $t = 150$ based on 5000 independent simulations, resulting from using EM method with stepsizes $\Delta t = 0.005, 0.01, 0.02, 0.04, 0.1$ (in budding case).

extinction for various range of initial infection in the budding (Fig. 5.11(a)) and bursting (Fig. 5.11(b)) cases are demonstrated in Fig. 5.11, which indicates that the probability of virus extinction decreases (in both cases) with an increase in the initial viral load or the initial level of infected hepatocytes. This figure also shows that the probability of virus extinction becomes very less at a comparatively faster rate in case of bursting than in case of budding, which agrees with our analytical results. Moreover, the probability of virus extinction approaches close to zero if the initial infection is significantly high and consequently there is a high chance of infection persistence irrespective of whether the process is budding or bursting, in case of high infection.

Finally, we choose the parameter values from Set-III in Table 5.3 to find out the numerical solution for the moment differential equations at the infection-free stage. This set of param-

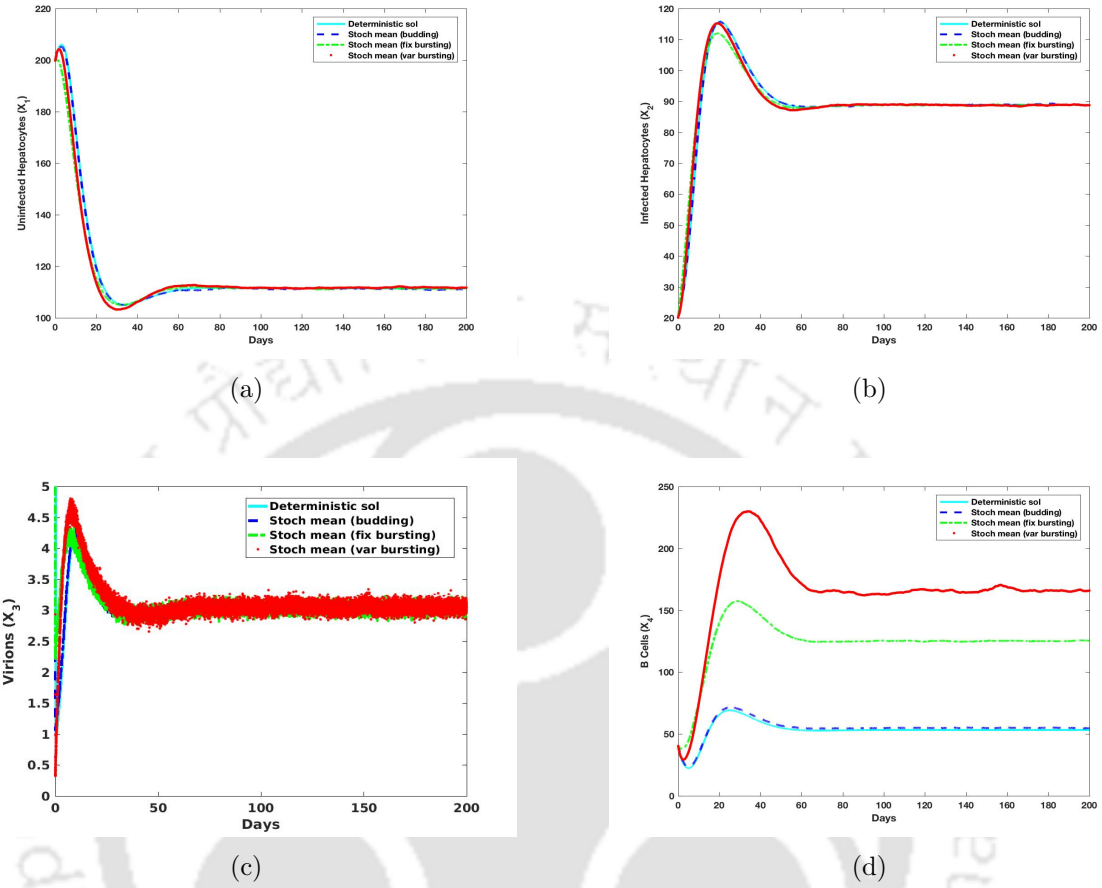

Figure 5.8: Comparison of the deterministic solution given by (2.1.1) for (a) uninfected hepatocytes, (b) infected hepatocytes, (c) virions and (d) B cells, with the stochastic mean of 5000 sample paths obtained from the SDE models in case of budding (5.1.1) and bursting with fixed (5.1.2) and variable (5.3.3) burst size.

eter values corresponds to $R_0 = 0.2789 < 1$. A comparison of the moment of uninfected hepatocytes obtained from the moment differential equation at infection-free stage (5.4.1) with the mean solutions obtained from the budding (5.1.1) and bursting models with fixed (5.1.2) and variable (5.3.3) burst size is presented in Fig. 5.12, which shows a good agreement of estimation for the solution obtained from the moment equations and SDE models.

5.6 Conclusions

The SDE and CTMC models for HCV dynamics based on the deterministic model (2.1.1) as well as depending on the viral release process (budding and bursting) have been developed and analyzed. The stochastic models considered the state changes of the uninfected hepatocytes, infected hepatocytes, virions and B cells, in a probabilistic manner, during HCV

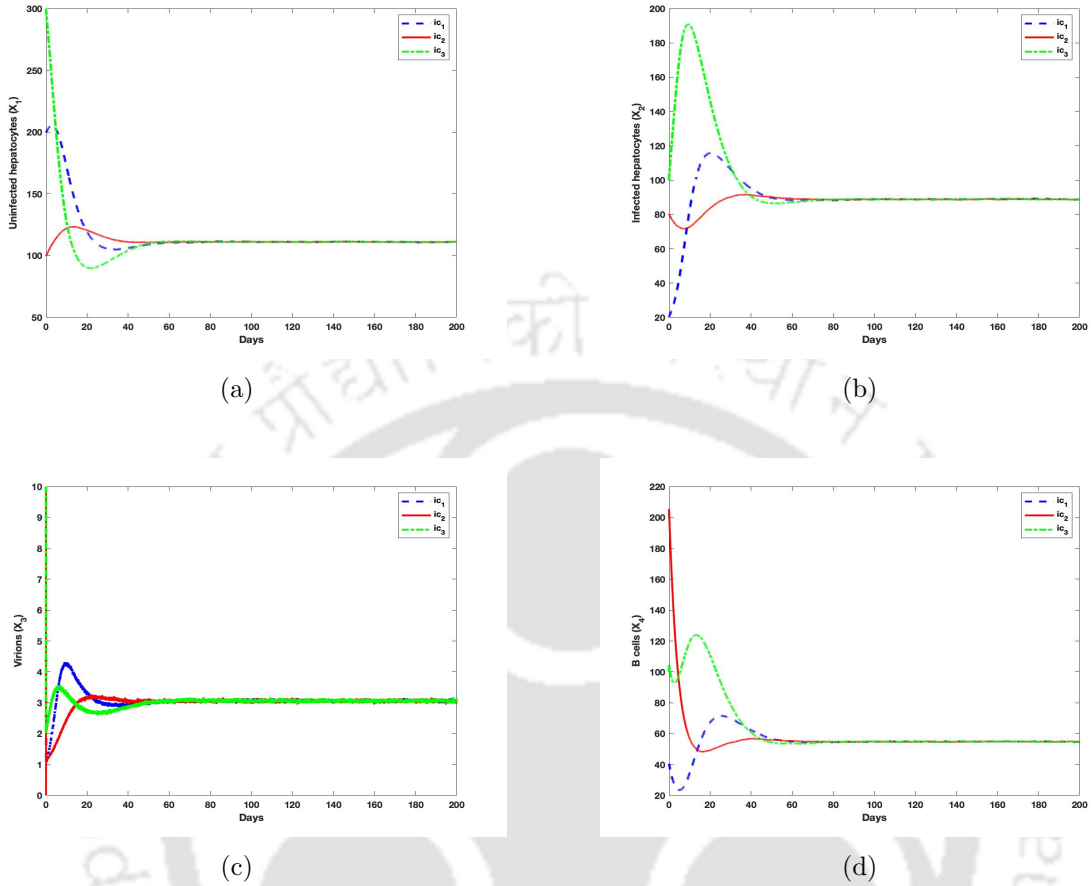

Figure 5.9: Mean path of 5000 sample paths for (a) uninfected hepatocytes, (b) infected hepatocytes, (c) virions and (d) B cells, resulting from using EM method with three different initial conditions $ic_1 := (200, 20, 10, 40)$, $ic_2 := (100, 80, 30, 200)$ and $ic_3 := (300, 100, 50, 100)$ in case of budding model (5.1.1).

infection. The results obtained from SDE models have shown that the sizes of the uninfected and infected hepatocytes based on 5000 simulations are normally distributed, whereas virions are randomly distributed. It is observed that the stochastic fluctuation in the virion density is relatively high in case of bursting. However, the stochastic means for these three variables are very close to their respective deterministic stable values in both budding and bursting cases, while for the B cell population, it is relatively even higher in case of bursting. The bursting model with variable burst size is observed to have significantly higher B cells response and relatively greater stochastic fluctuation in the virion population, with other populations being close to their deterministic stable trajectories. Further, it is observed that the B cells are highly responsive in case of bursting due to greater fluctuation of virions in this case. Thus the stochasticity disturbs the stability behavior of the virions and consequently the level of B cells is increased. The CTMC models estimated that the proba-

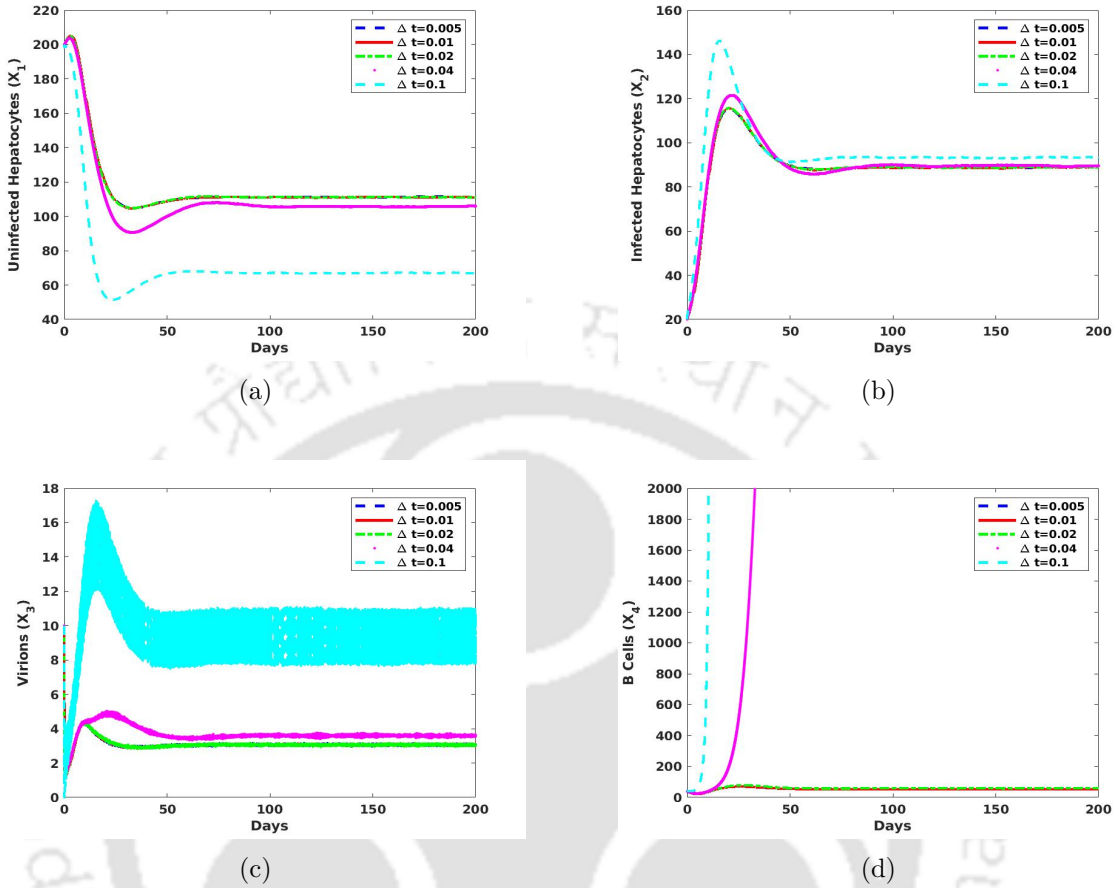

Figure 5.10: Mean path of 5000 sample paths for (a) uninfected hepatocytes, (b) infected hepatocytes, (c) virions and (d) B cells, resulting from using EM method with five different stepsizes $\Delta t = 0.005,\ 0.01,\ 0.02,\ 0.04,\ 0.1$ in case of budding model (5.1.1).

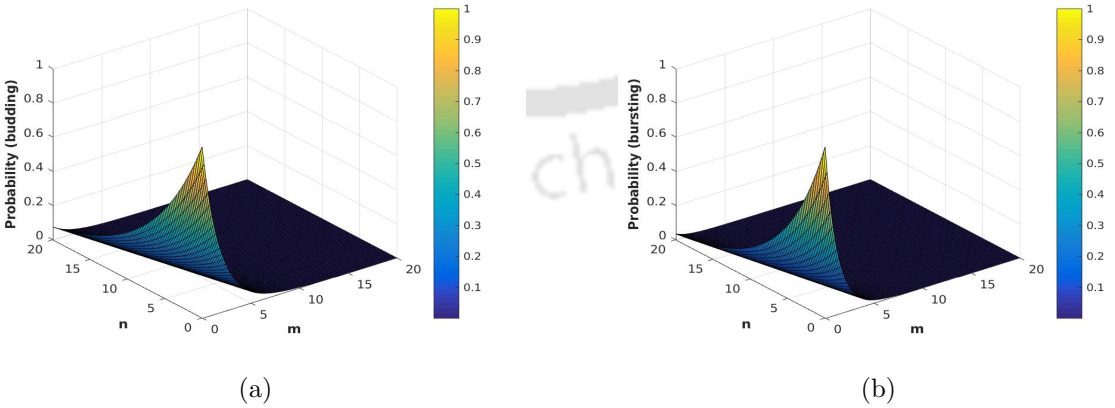

Figure 5.11: Probability of virus extinction for (a) the CTMC budding model and (b) the CTMC bursting model, with $I(0) = m$ and $V(0) = n$.

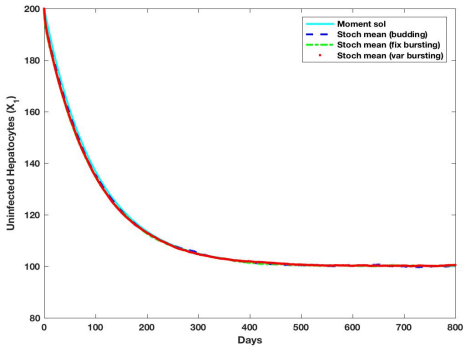

Figure 5.12: Comparison of the moment differential equation at infection-free stage (5.4.1) with the SDE models for budding (5.1.1) and bursting with fixed (5.1.2) and variable (5.3.3) burst size.

bility of virus extinction is approximately one when $R_0 < 1$ and is approximately $q_1^m q_2^n$ (for budding) or $\tilde{q}_1^m \tilde{q}_2^n$ (for bursting) when $R_0 > 1$ with (m, n) representing the initial infection $(I(0), V(0))$. The chance of virus extinction is not only dependent upon the condition on R_0, but is also dependent upon the initial amount of virions and infected hepatocytes. The chance of infection persistence is relatively less for the case of budding as compared to the case of bursting. Thus the stochastic models better predict whether the infection persists or dies out. These models also give the probability of virus extinction in case of $R_0 > 1$, which cannot be predicted by any deterministic model. Further, this study details the expectations, variances, moments and distribution patterns of the model variables. In contrast, no deterministic model can provide such prediction or insights into the dynamics. Finally, the numerical computation shows that the estimated mean of the uninfected hepatocytes using the moment differential equations is in agreement with the results obtained from the SDE models.

Chapter 6

Concluding Remarks and Future Directions

6.1 Concluding Remarks

In this thesis, we presented and analyzed some deterministic and stochastic models for HCV dynamics, incorporating various aspects such as virus-to-cell as well as cell-to-cell transmission and non-cytolytic cure rate, with the role of B cells in the activation of the humoral immunity. The deterministic models include the ODE model, the DDE model (which incorporates the time delay in the generation of B cells) and the PDE model (which captures the spatial mobility of virions and B cells along with the consideration of general transmission functions). The stochastic models considered refer to the SDE and the CTMC models for both budding and bursting processes. The key conclusions of this thesis are summarized as follows:

- **ODE Model (Chapter 2):** It is shown that all three equilibria, namely, E_0, E_1 and E^* are locally as well as globally asymptotically stable under certain conditions on R_0 and R_H. The infection is eradicated from the host if $R_0 \leq 1$ and persists if $R_0 > 1$. This study also suggests that the cell-to-cell transmission results in more rapid infectivity, as compared to virus-to-cell transmission. The cure rate is directly proportional to the uninfected hepatocytes and inversely proportional to the infected hepatocytes. In addition, B cells have a great influence on the neutralization of the virions.

- **DDE Model (Chapter 3):** The boundary equilibria, namely, E_0 and E_1 are locally as well as globally asymptotically stable under conditions on R_0 and R_H for any time delay. The occurrence of Hopf bifurcation and stability switches around the interior equilibrium, namely, E^* are observed when the bifurcation parameter crosses its critical

values. Further, the development rate of B cells drives the system from stable to unstable and vice versa for a fixed time delay. The numerical findings suggests that a high antigenic stimulation in the generation of B cells is beneficial for uninfected hepatocytes.

- **PDE Model (Chapter 4):** The diffusion of virions and immune B cells do not disturb the global stability of the equilibria for the system. Moreover, the dynamical behavior of the system remains unchanged but the transformation of the stable points occurred, under different types of transmission functions. The numerical findings also show that the system with Holling type-II incidence function stabilizes at the equilibria with higher level of uninfected hepatocytes and lower level of infection, as compared to bilinear incidence function.

- **SDE and CTMC Models (Chapter 5):** The stochastic changes of the uninfected and infected hepatocytes follow the normal distribution. The size of the B cell population changes drastically due to the random fluctuation in the virion population. It is also obtained that the chance of infection persistence is relatively less for the case of budding as compared to the bursting. These models give the probability of virus extinction in case of $R_0 > 1$, which cannot be predicted by any deterministic model. Further, this study details the expectations, variances, moments and distribution patterns of the model variables.

Important Note: It is noted that the considered models in this thesis can be applied to study the dynamics of other virus infections, which follows the specific aspects introduced in the modeling.

6.2 Future Directions

The possible future directions of this thesis work include:

- **Optimal Control Strategy:**
  The optimal treatment policy over a fixed time horizon can be determined. The aim of the objective functional is to reducing the amount of infected hepatocytes and viral load, as well as, minimizing the side effects of drugs, namely, IFN and ribavirin during the therapy. The model is described with the following objective functional:

$$J(\epsilon, \rho) = \int_0^{t_f} [A_1 I(t) + A_2 V(t) + B_1 \epsilon^2(t) + B_2 \rho^2(t)] dt.$$

An optimal control pair (ϵ^*, ρ^*) is to be determined such that

$$J(\epsilon^*, \rho^*) = \min\{J(\epsilon, \rho) \mid (\epsilon, \rho) \in \mathcal{N}\},$$

where $\mathcal{N} = \{(\epsilon, \rho) \mid \epsilon, \rho \text{ are measurable}, \ 0 \leq \epsilon \leq 1, \ 0 \leq \rho \leq 1, \ t \in [0, t_f]\}$ is the control set. t_f is the final time and the coefficients, $A_1, \ A_2, \ B_1, \ B_2$ are balancing cost coefficients for the respective variables. The square of the control variables is taken to consider the harm caused due to the side effects of the drugs.

- **Sampling Based Analysis:**
  A sampling based analysis of the model can be studied. The fact is that the patient based specific data is not widely available. Rather the parameter distribution for patient data are available. Therefore, Latin hypercube sampling method can be used to generate a large number of *in silico* parameter values for the model making use of clinically available data on the overall distribution of the parameters as well as the range of parameters. The sample parameter values will be generated from a multivariate normal distribution with a specified mean vector μ and covariance matric C given by,

$$\phi(x; \mu, C) = \frac{1}{(2\pi)^{n/2}|C|^{1/2}} \exp\left[-\frac{1}{2}(x-\mu)^\top C^{-1}(x-\mu)\right].$$

  The data generated will be used in analyzing the consistency of the model as well as the response rate of patients with clinically validated observations.

- **Multiscale Modeling and Analysis:**
  The dynamics of HCV infection under the therapeutic effect of DAAs can be analyzed through the multiscale modeling approach. This model captures various stages of HCV life cycle, including the intracellular HCV RNA replication process, as well as the dynamics of extracellular viral infection. This multiscale model considers the age-structured dynamics of replication or production of both positive and negative-stranded HCV RNA with the secretion of positive-stranded RNA as virions from infected cells as well as the degradation process of virions in order to analyze the kinetics of HCV infection resulting from administration of DAAs.

Bibliography

[1] D. Aisyah, L. Shallcross, A. Hully, A. O'brien, and A. Hayward. Assessing hepatitis C spontaneous clearance and understanding associated factors: A systematic review and meta-analysis. *Journal of Viral Hepatitis*, 25(6):680–698, 2018.

[2] E. Allen. *Modeling with Itô stochastic differential equations*, volume 22. Springer Science & Business Media, 2007.

[3] E. J. Allen, L. J. Allen, A. Arciniega, and P. E. Greenwood. Construction of equivalent stochastic differential equation models. *Stochastic Analysis and Applications*, 26(2):274–297, 2008.

[4] L. J. Allen. *Introduction to Mathematical Biology*. Pearson/Prentice Hall, 2007.

[5] L. J. Allen. An introduction to stochastic epidemic models. In *Mathematical Epidemiology*, pages 81–130. Springer, 2008.

[6] L. J. Allen. *An introduction to stochastic processes with applications to Biology*. Chapman and Hall/CRC, 2010.

[7] L. J. Allen and A. M. Burgin. Comparison of deterministic and stochastic SIS and SIR models. *Department of Mathematics and Statistics Technical Report Series*, pages 98–003, 1998.

[8] H. Amann. Dynamic theory of quasilinear parabolic systems. *Mathematische Zeitschrift*, 202(2):219–250, 1989.

[9] T. Asselah, N. Boyer, D. Saadoun, M. Martinot-Peignoux, and P. Marcellin. Direct-acting antivirals for the treatment of hepatitis C virus infection: Optimizing current IFN-free treatment and future perspectives. *Liver International*, 36:47–57, 2016.

[10] S. Banerjee, R. Keval, and S. Gakkhar. Modeling the dynamics of hepatitis C virus with combined antiviral drug therapy: Interferon and ribavirin. *Mathematical Biosciences*, 245(2):235–248, 2013.

[11] G. Bocharov, A. Meyerhans, N. Bessonov, S. Trofimchuk, and V. Volpert. Interplay between reaction and diffusion processes in governing the dynamics of virus infections. *Journal of Theoretical Biology*, 457:221–236, 2018.

[12] G. Bocharov, A. Meyerhans, N. Bessonov, S. Trofimchuk, and V. Volpert. Modelling the dynamics of virus infection and immune response in space and time. *International Journal of Parallel, Emergent and Distributed Systems*, 34(4):341–355, 2019.

[13] C. M. Brauner, D. Jolly, L. Lorenzi, and R. Thiebaut. Heterogeneous viral environment in a HIV spatial model. *arXiv preprint, arXiv:0905.2023*, 2009.

[14] S. B. Cashman, B. D. Marsden, and L. B. Dustin. The humoral immune response to HCV: Understanding is key to vaccine development. *Frontiers in Immunology*, 5:550, 2014.

[15] M. Castro, G. Lythe, C. Molina-París, and R. M. Ribeiro. Mathematics in modern immunology. *Interface Focus*, 6(2):20150093, 2016.

[16] S. P. Chakrabarty. Optimal efficacy of ribavirin in the treatment of hepatitis C. *Optimal Control Applications and Methods*, 30(6):594–600, 2009.

[17] S. P. Chakrabarty and H. R. Joshi. Optimally controlled treatment strategy using interferon and ribavirin for hepatitis C. *Journal of Biological Systems*, 17(01):97–110, 2009.

[18] S. P. Chakrabarty and J. M. Murray. Modelling hepatitis C virus infection and the development of hepatocellular carcinoma. *Journal of Theoretical Biology*, 305:24–29, 2012.

[19] S. S. Chen, C. Y. Cheng, and Y. Takeuchi. Stability analysis in delayed within-host viral dynamics with both viral and cellular infections. *Journal of Mathematical Analysis and Applications*, 442(2):642–672, 2016.

[20] Q. L. Choo, G. Kuo, A. J. Weiner, L. R. Overby, D. W. Bradley, and M. Houghton. Isolation of a cDNA clone derived from a blood-borne non-A, non-B viral hepatitis genome. *Science*, 244(4902):359–362, 1989.

[21] S. M. Ciupe, R. M. Ribeiro, P. W. Nelson, and A. S. Perelson. Modeling the mechanisms of acute hepatitis B virus infection. *Journal of Theoretical Biology*, 247(1):23–35, 2007.

[22] H. Dahari, A. Lo, R. M. Ribeiro, and A. S. Perelson. Modeling hepatitis C virus dynamics: Liver regeneration and critical drug efficacy. *Journal of Theoretical Biology*, 247(2):371–381, 2007.

[23] H. Dahari, M. Major, X. Zhang, K. Mihalik, C. M. Rice, A. S. Perelson, S. M. Feinstone, and A. U. Neumann. Mathematical modeling of primary hepatitis C infection: Noncytolytic clearance and early blockage of virion production. *Gastroenterology*, 128(4):1056–1066, 2005.

[24] H. Dahari, R. M. Ribeiro, and A. S. Perelson. Triphasic decline of hepatitis C virus RNA during antiviral therapy. *Hepatology*, 46(1):16–21, 2007.

[25] D. Das and M. Pandya. Recent advancement of direct-acting antiviral agents (DAAs) in hepatitis C therapy. *Mini Reviews in Medicinal Chemistry*, 18(7):584–596, 2018.

[26] S. DebRoy, B. M. Bolker, and M. Martcheva. Bistability and long-term cure in a within-host model of hepatitis C. *Journal of Biological Systems*, 19(04):533–550, 2011.

[27] A. Dev, V. Sundararajan, and W. Sievert. Ethnic and cultural determinants influence risk assessment for hepatitis C acquisition. *Journal of Gastroenterology and Hepatology*, 19(7):792–798, 2004.

[28] N. M. Dixit, J. E. Layden-Almer, T. J. Layden, and A. S. Perelson. Modelling how ribavirin improves interferon response rates in hepatitis C virus infection. *Nature*, 432(7019):922, 2004.

[29] B. Dubey, P. Dubey, and U. S. Dubey. Modeling the intracellular pathogen-immune interaction with cure rate. *Communications in Nonlinear Science and Numerical Simulation*, 38:72–90, 2016.

[30] L. B. Dustin, B. Bartolini, M. R. Capobianchi, and M. Pistello. Hepatitis C virus: life cycle in cells, infection and host response, and analysis of molecular markers influencing the outcome of infection and response to therapy. *Clinical Microbiology and Infection*, 22(10):826–832, 2016.

[31] A. Elaiw, A. Raezah, and A. Alofi. Effect of humoral immunity on HIV-1 dynamics with virus-to-target and infected-to-target infections. *AIP Advances*, 6(8):085204, 2016.

[32] L. Erbe, H. Freedman, and V. S. H. Rao. Three-species food-chain models with mutual interference and time delays. *Mathematical Biosciences*, 80(1):57–80, 1986.

[33] H. Freedman and V. S. H. Rao. The trade-off between mutual interference and time lags in predator-prey systems. *Bulletin of Mathematical Biology*, 45(6):991–1004, 1983.

[34] L. Golden-Mason and H. R. Rosen. Natural killer cells: Primary target for hepatitis C virus immune evasion strategies? *Liver Transplantation*, 12(3):363–372, 2006.

[35] S. A. Gourley, Y. Kuang, and J. D. Nagy. Dynamics of a delay differential equation model of hepatitis B virus infection. *Journal of Biological Dynamics*, 2(2):140–153, 2008.

[36] C. Gremion and A. Cerny. Hepatitis C virus and the immune system: A concise review. *Reviews in Medical Virology*, 15(4):235–268, 2005.

[37] J. Groeger. Divergence theorems and the supersphere. *Journal of Geometry and Physics*, 77:13–29, 2014.

[38] L. G. Guidotti, R. Rochford, J. Chung, M. Shapiro, R. Purcell, and F. V. Chisari. Viral clearance without destruction of infected cells during acute HBV infection. *Science*, 284(5415):825–829, 1999.

[39] J. K. Hale and H. Koçak. *Dynamics and bifurcations*, volume 3. Springer Science & Business Media, 2012.

[40] J. K. Hale and S. M. V. Lunel. *Introduction to functional differential equations*, volume 99. Springer Science & Business Media, 2013.

[41] T. E. Harris. *The theory of branching processes*. Springer Verlag, Berlin, 1963.

[42] K. Hattaf and N. Yousfi. A generalized virus dynamics model with cell-to-cell transmission and cure rate. *Advances in Difference Equations*, 2016(1):174, 2016.

[43] K. Hattaf, N. Yousfi, and A. Tridane. Mathematical analysis of a virus dynamics model with general incidence rate and cure rate. *Nonlinear Analysis: Real World Applications*, 13(4):1866–1872, 2012.

[44] J. M. Heffernan, R. J. Smith, and L. M. Wahl. Perspectives on the basic reproductive ratio. *Journal of the Royal Society Interface*, 2(4):281–293, 2005.

[45] D. Henry. *Geometric theory of semilinear parabolic equations*, volume 840. Springer, 1981.

[46] A. Herz, S. Bonhoeffer, R. M. Anderson, R. M. May, and M. A. Nowak. Viral dynamics in vivo: Limitations on estimates of intracellular delay and virus decay. *Proceedings of the National Academy of Sciences*, 93(14):7247–7251, 1996.

[47] M. Houghton. The long and winding road leading to the identification of the hepatitis C virus. *Journal of Hepatology*, 51(5):939–948, 2009.

[48] Q. Hu, Z. Hu, and F. Liao. Stability and Hopf bifurcation in a HIV-1 infection model with delays and logistic growth. *Mathematics and Computers in Simulation*, 128:26–41, 2016.

[49] G. Huang, W. Ma, and Y. Takeuchi. Global properties for virus dynamics model with Beddington-DeAngelis functional response. *Applied Mathematics Letters*, 22(11):1690–1693, 2009.

[50] E. Iio and Y. Tanaka. Hepatitis C virus infection. In *Human Pathobiochemistry*, pages 323–330. Springer, 2019.

[51] M. Imran, M. Hassan, M. Dur-E-Ahmad, and A. Khan. A comparison of a deterministic and stochastic model for hepatitis C with an isolation stage. *Journal of Biological Dynamics*, 7(1):276–301, 2013.

[52] C. Kang, H. Miao, X. Chen, J. Xu, and D. Huang. Global stability of a diffusive and delayed virus dynamics model with Crowley-Martin incidence function and CTL immune response. *Advances in Difference Equations*, 2017(1):324, 2017.

[53] H. K. Khalil. Nonlinear systems. *Upper Saddle River*, 2002.

[54] M. Kimmel and D. Axelrod. Branching processes in Biology, 2002.

[55] M. J. Koziel. Cellular immune responses against hepatitis C virus. *Clinical Infectious Diseases*, 41(Supplement_1):S25–S31, 2005.

[56] G. E. Lahodny and L. J. Allen. Probability of a disease outbreak in stochastic multi-patch epidemic models. *Bulletin of Mathematical Biology*, 75(7):1157–1180, 2013.

[57] X. Lai and X. Zou. Modeling cell-to-cell spread of HIV-1 with logistic target cell growth. *Journal of Mathematical Analysis and Applications*, 426(1):563–584, 2015.

[58] J. R. Larrubia, E. Moreno-Cubero, M. U. Lokhande, S. García-Garzón, A. Lázaro, J. Miquel, C. Perna, and E. Sanz-de Villalobos. Adaptive immune response during hepatitis C virus infection. *World Journal of Gastroenterology: WJG*, 20(13):3418, 2014.

[59] M. Lechmann and T. J. Liang. Vaccine development for hepatitis C. In *Seminars in Liver Disease*, volume 20, pages 211–226. Copyright© 2000 by Thieme Medical Publishers, Inc., 2000.

[60] S. R. Lewin, R. M. Ribeiro, T. Walters, G. K. Lau, S. Bowden, S. Locarnini, and A. S. Perelson. Analysis of hepatitis B viral load decline under potent therapy: Complex decay profiles observed. *Hepatology*, 34(5):1012–1020, 2001.

[61] D. Li, J. Cui, M. Liu, and S. Liu. The evolutionary dynamics of stochastic epidemic model with nonlinear incidence rate. *Bulletin of Mathematical Biology*, 77(9):1705–1743, 2015.

[62] D. Li and W. Ma. Asymptotic properties of a HIV-1 infection model with time delay. *Journal of Mathematical Analysis and Applications*, 335(1):683–691, 2007.

[63] F. Li and J. Wang. Analysis of an HIV infection model with logistic target-cell growth and cell-to-cell transmission. *Chaos, Solitons & Fractals*, 81:136–145, 2015.

[64] J. Li, K. Men, Y. Yang, and D. Li. Dynamical analysis on a chronic hepatitis C virus infection model with immune response. *Journal of Theoretical Biology*, 365:337–346, 2015.

[65] M. Y. Li and H. Shu. Impact of intracellular delays and target-cell dynamics on in vivo viral infections. *SIAM Journal on Applied Mathematics*, 70(7):2434–2448, 2010.

[66] M. Y. Li and H. Shu. Global dynamics of a mathematical model for HTLV-I infection of CD4+ T cells with delayed CTL response. *Nonlinear Analysis: Real World Applications*, 13(3):1080–1092, 2012.

[67] X. Li and J. Wei. On the zeros of a fourth degree exponential polynomial with applications to a neural network model with delays. *Chaos, Solitons & Fractals*, 26(2):519–526, 2005.

[68] H. Lodish, A. Berk, S. L. Zipursky, P. Matsudaira, D. Baltimore, and J. Darnell. Viruses: Structure, function, and uses. In *Molecular Cell Biology. 4th edition*. WH Freeman, 2000.

[69] J. Luo, W. Wang, H. Chen, and R. Fu. Bifurcations of a mathematical model for HIV dynamics. *Journal of Mathematical Analysis and Applications*, 434(1):837–857, 2016.

[70] K. Manna and S. P. Chakrabarty. Chronic hepatitis B infection and HBV DNA-containing capsids: Modeling and analysis. *Communications in Nonlinear Science and Numerical Simulation*, 22(1-3):383–395, 2015.

[71] K. Manna and S. P. Chakrabarty. Global stability and a non-standard finite difference scheme for a diffusion driven HBV model with capsids. *Journal of Difference Equations and Applications*, 21(10):918–933, 2015.

[72] J. E. Marsden and M. McCracken. *The Hopf bifurcation and its applications*, volume 19. Springer Science & Business Media, 2012.

[73] A. Meskaf, Y. Tabit, and K. Allali. Global analysis of a HCV model with CTL, antibody responses and therapy. *Applied Mathematical Sciences*, 9(81):3997–4008, 2015.

[74] H. Miao, X. Abdurahman, Z. Teng, and L. Zhang. Dynamical analysis of a delayed reaction-diffusion virus infection model with logistic growth and humoral immune impairment. *Chaos, Solitons & Fractals*, 110:280–291, 2018.

[75] H. Miao, Z. Teng, C. Kang, and A. Muhammadhaji. Stability analysis of a virus infection model with humoral immunity response and two time delays. *Mathematical Methods in the Applied Sciences*, 39(12):3434–3449, 2016.

[76] J. Micallef, J. Kaldor, and G. Dore. Spontaneous viral clearance following acute hepatitis C infection: a systematic review of longitudinal studies. *Journal of Viral Hepatitis*, 13(1):34–41, 2006.

[77] A. Mojaver and H. Kheiri. Dynamical analysis of a class of hepatitis C virus infection models with application of optimal control. *International Journal of Biomathematics*, 9(03):1650038, 2016.

[78] A. Murase, T. Sasaki, and T. Kajiwara. Stability analysis of pathogen-immune interaction dynamics. *Journal of Mathematical Biology*, 51(3):247–267, 2005.

[79] Y. Nakata. Global dynamics of a viral infection model with a latent period and Beddington-DeAngelis response. *Nonlinear Analysis: Theory, Methods & Applications*, 74(9):2929–2940, 2011.

[80] P. W. Nelson and A. S. Perelson. Mathematical analysis of delay differential equation models of HIV-1 infection. *Mathematical Biosciences*, 179(1):73–94, 2002.

[81] A. U. Neumann, N. P. Lam, H. Dahari, D. R. Gretch, T. E. Wiley, T. J. Layden, and A. S. Perelson. Hepatitis C viral dynamics in vivo and the antiviral efficacy of interferon-α therapy. *Science*, 282(5386):103–107, 1998.

[82] A. U. Neumann, S. Phillips, I. Levine, S. Ijaz, H. Dahari, R. Eren, S. Dagan, and N. V. Naoumov. Novel mechanism of antibodies to hepatitis B virus in blocking viral particle release from cells. *Hepatology*, 52(3):875–885, 2010.

[83] M. A. Nowak and C. R. Bangham. Population dynamics of immune responses to persistent viruses. *Science*, 272(5258):74–79, 1996.

[84] H. Nyquist. Regeneration theory. *Bell System Technical Journal*, 11(1):126–147, 1932.

[85] W. H. O. *Global hepatitis report 2017*. World Health Organization, 2017.

[86] B. Oksendal. *Stochastic differential equations: An introduction with applications*. Springer Science & Business Media, 2013.

[87] G. Pachpute and S. P. Chakrabarty. Analysis of hepatitis C viral dynamics using Latin hypercube sampling. *Communications in Nonlinear Science and Numerical Simulation*, 17(12):5125–5130, 2012.

[88] G. Pachpute and S. P. Chakrabarty. Dynamics of hepatitis C under optimal therapy and sampling based analysis. *Communications in Nonlinear Science and Numerical Simulation*, 18(8):2202–2212, 2013.

[89] K. A. Pawelek, S. Liu, F. Pahlevani, and L. Rong. A model of HIV-1 infection with two time delays: Mathematical analysis and comparison with patient data. *Mathematical Biosciences*, 235(1):98–109, 2012.

[90] A. S. Perelson, E. Herrmann, F. Micol, and S. Zeuzem. New kinetic models for the hepatitis C virus. *Hepatology*, 42(4):749–754, 2005.

[91] A. S. Perelson and R. M. Ribeiro. Introduction to modeling viral infections and immunity. *Immunological Reviews*, 285(1):5–8, 2018.

[92] M. H. Protter and H. F. Weinberger. *Maximum principles in differential equations*. Springer Science & Business Media, 2012.

[93] K. Razali, H. H. Thein, J. Bell, M. Cooper-Stanbury, K. Dolan, G. Dore, J. George, J. Kaldor, M. Karvelas, J. Li, et al. Modelling the hepatitis C virus epidemic in Australia. *Drug and Alcohol Dependence*, 91(2-3):228–235, 2007.

[94] R. Redlinger. Existence theorems for semilinear parabolic systems with functionals. *Nonlinear Analysis: Theory, Methods & Applications*, 8(6):667–682, 1984.

[95] B. Rehermann. Interaction between the hepatitis C virus and the immune system. In *Seminars in Liver Disease*, volume 20, pages 127–142. Copyright© 2000 by Thieme Medical Publishers, Inc., 2000.

[96] T. C. Reluga, H. Dahari, and A. S. Perelson. Analysis of hepatitis C virus infection models with hepatocyte homeostasis. *SIAM Journal on Applied Mathematics*, 69(4):999–1023, 2009.

[97] J. Reyes-Silveyra and A. R. Mikler. Modeling immune response and its effect on infectious disease outbreak dynamics. *Theoretical Biology and Medical Modelling*, 13(1):10, 2016.

[98] S. Riley. Large-scale spatial-transmission models of infectious disease. *Science*, 316(5829):1298–1301, 2007.

[99] B. Roe and W. W. Hall. Cellular and molecular interactions in coinfection with hepatitis C virus and human immunodeficiency virus. *Expert Reviews in Molecular Medicine*, 10, 2008.

[100] H. R. Rosen. Chronic hepatitis C infection. *New England Journal of Medicine*, 364(25):2429–2438, 2011.

[101] C. Selinger and M. G. Katze. Mathematical models of viral latency. *Current Opinion in Virology*, 3(4):402–407, 2013.

[102] X. Shi, X. Zhou, and X. Song. Dynamical behavior of a delay virus dynamics model with CTL immune response. *Nonlinear Analysis: Real World Applications*, 11(3):1795–1809, 2010.

[103] J. J. E. Slotine, W. Li, et al. *Applied nonlinear control*, volume 199. Prentice Hall Englewood Cliffs, NJ, 1991.

[104] E. Snoeck, P. Chanu, M. Lavielle, P. Jacqmin, E. Jonsson, K. Jorga, T. Goggin, J. Grippo, N. Jumbe, and N. Frey. A comprehensive hepatitis C viral kinetic model explaining cure. *Clinical Pharmacology & Therapeutics*, 87(6):706–713, 2010.

[105] H. Sun and J. Wang. Dynamics of a diffusive virus model with general incidence function, cell-to-cell transmission and time delay. *Computers & Mathematics with Applications*, 77(1):284–301, 2019.

[106] H. R. Thieme. *Mathematics in Population Biology*. Princeton University Press, 2003.

[107] J. M. Timpe, Z. Stamataki, A. Jennings, K. Hu, M. J. Farquhar, H. J. Harris, A. Schwarz, I. Desombere, G. L. Roels, P. Balfe, et al. Hepatitis C virus cell-cell transmission in hepatoma cells in the presence of neutralizing antibodies. *Hepatology*, 47(1):17–24, 2008.

[108] C. Travis and G. Webb. Existence and stability for partial functional differential equations. *Transactions of the American Mathematical Society*, 200:395–418, 1974.

[109] P. Van den Driessche and J. Watmough. Reproduction numbers and sub-threshold endemic equilibria for compartmental models of disease transmission. *Mathematical Biosciences*, 180(1-2):29–48, 2002.

[110] C. Vargas-De-León. On the global stability of SIS, SIR and SIRS epidemic models with standard incidence. *Chaos, Solitons & Fractals*, 44(12):1106–1110, 2011.

[111] C. Vargas-De-León. Stability analysis of a model for HBV infection with cure of infected cells and intracellular delay. *Applied Mathematics and Computation*, 219(1):389–398, 2012.

[112] S. W. Vidurupola. *Mathematical models for bacteriophage dynamics applicable to phage therapy*. PhD thesis, 2013.

[113] S. W. Vidurupola. Analysis of deterministic and stochastic mathematical models with resistant bacteria and bacteria debris for bacteriophage dynamics. *Applied Mathematics and Computation*, 316:215–228, 2018.

[114] S. W. Vidurupola and L. Allen. Basic stochastic models for viral infection within a host. *Mathematical Biosciences and Engineering: MBE*, 9(4):915–935, 2012.

[115] S. W. Vidurupola and L. J. Allen. Impact of variability in stochastic models of bacteriaphage dynamics applicable to phage therapy. *Stochastic Analysis and Applications*, 32(3):427–449, 2014.

[116] F. B. Wang, Y. Huang, and X. Zou. Global dynamics of a PDE in-host viral model. *Applicable Analysis*, 93(11):2312–2329, 2014.

[117] J. Wang, M. Guo, X. Liu, and Z. Zhao. Threshold dynamics of HIV-1 virus model with cell-to-cell transmission, cell-mediated immune responses and distributed delay. *Applied Mathematics and Computation*, 291:149–161, 2016.

[118] J. Wang, J. Yang, and T. Kuniya. Dynamics of a PDE viral infection model incorporating cell-to-cell transmission. *Journal of Mathematical Analysis and Applications*, 444(2):1542–1564, 2016.

[119] K. Wang, A. Fan, and A. Torres. Global properties of an improved hepatitis B virus model. *Nonlinear Analysis: Real World Applications*, 11(4):3131–3138, 2010.

[120] K. Wang and W. Wang. Propagation of HBV with spatial dependence. *Mathematical Biosciences*, 210(1):78–95, 2007.

[121] K. Wang, W. Wang, H. Pang, and X. Liu. Complex dynamic behavior in a viral model with delayed immune response. *Physica D: Nonlinear Phenomena*, 226(2):197–208, 2007.

[122] T. Wang, Z. Hu, and F. Liao. Stability and Hopf bifurcation for a virus infection model with delayed humoral immunity response. *Journal of Mathematical Analysis and Applications*, 411(1):63–74, 2014.

[123] W. Wang and W. Ma. A diffusive HIV infection model with nonlocal delayed transmission. *Applied Mathematics Letters*, 75:96–101, 2018.

[124] W. Wang and W. Ma. Hepatitis C virus infection is blocked by HMGB1: A new nonlocal and time-delayed reaction-diffusion model. *Applied Mathematics and Computation*, 320:633–653, 2018.

[125] Y. Wang, Y. Zhou, F. Brauer, and J. M. Heffernan. Viral dynamics model with CTL immune response incorporating antiretroviral therapy. *Journal of Mathematical Biology*, 67(4):901–934, 2013.

[126] D. Wodarz. Hepatitis C virus dynamics and pathology: The role of CTL and antibody responses. *Journal of General Virology*, 84(7):1743–1750, 2003.

[127] D. Wodarz. Mathematical models of immune effector responses to viral infections: Virus control versus the development of pathology. *Journal of Computational and Applied mathematics*, 184(1):301–319, 2005.

[128] D. Wu, Y. Su, and D. Sun. Stability properties and hopf bifurcation for a hepatitis B infection model with exposed state and humoral immunity-response delay. *Communications in Mathematical Biology and Neuroscience*, 2015:Article–ID, 2015.

[129] J. Wu. *Theory and applications of partial functional differential equations*, volume 119. Springer Science & Business Media, 2012.

[130] F. Xiao, I. Fofana, L. Heydmann, H. Barth, E. Soulier, F. Habersetzer, M. Doffoël, J. Bukh, A. H. Patel, M. B. Zeisel, et al. Hepatitis C virus cell-cell transmission and resistance to direct-acting antiviral agents. *PLoS Pathogens*, 10(5):e1004128, 2014.

[131] J. Xu, Y. Geng, and J. Hou. Global dynamics of a diffusive and delayed viral infection model with cellular infection and nonlinear infection rate. *Computers & Mathematics with Applications*, 73(4):640–652, 2017.

[132] R. Xu and Z. Ma. An HBV model with diffusion and time delay. *Journal of Theoretical Biology*, 257(3):499–509, 2009.

[133] X. Yang, L. Chen, and J. Chen. Permanence and positive periodic solution for the single-species nonautonomous delay diffusive models. *Computers & Mathematics with Applications*, 32(4):109–116, 1996.

[134] Y. Yang and Y. Xu. Global stability of a diffusive and delayed virus dynamics model with Beddington-DeAngelis incidence function and CTL immune response. *Computers & Mathematics with Applications*, 71(4):922–930, 2016.

[135] Y. Yang, J. Zhou, X. Ma, and T. Zhang. Nonstandard finite difference scheme for a diffusive within-host virus dynamics model with both virus-to-cell and cell-to-cell transmissions. *Computers & Mathematics with Applications*, 72(4):1013–1020, 2016.

[136] Y. Yang, L. Zou, and S. Ruan. Global dynamics of a delayed within-host viral infection model with both virus-to-cell and cell-to-cell transmissions. *Mathematical Biosciences*, 270:183–191, 2015.

[137] N. Yousfi, K. Hattaf, and M. Rachik. Analysis of a HCV model with CTL and antibody responses. *Applied Mathematical Sciences*, 3(57):2835–2845, 2009.

[138] C. Yuan and X. Mao. Stability in distribution of numerical solutions for stochastic differential equations. *Stochastic Analysis and Applications*, 22(5):1133–1150, 2004.

[139] Y. Yuan and L. J. Allen. Stochastic models for virus and immune system dynamics. *Mathematical Biosciences*, 234(2):84–94, 2011.

[140] F. Zhang, J. Li, C. Zheng, and L. Wang. Dynamics of an HBV/HCV infection model with intracellular delay and cell proliferation. *Communications in Nonlinear Science and Numerical Simulation*, 42:464–476, 2017.

[141] Y. Zhao and Z. Xu. Global dynamics for a delayed hepatitis C virus infection model. *Electronic Journal of Differential Equations*, 2014(132):1–18, 2014.

Biodata

Current Status

Senior Research Fellow, Department of Mathematics, Indian Institute of Technology Guwahati, Guwahati-781039, Assam, India.

Education

- **Master of Technology** (Operations Research, Department of Mathematics)
  National Institute of Technology Durgapur, Durgapur-713209, West Bengal, India.
- **Master of Science** (Mathematics)
  University of Gour Banga, Malda-732103, West Bengal, India.
- **Bachelor of Science** (Honours in Mathematics)
  Vidyasagar University, Midnapore-721102, West Bengal, India.

List of Published or Communicated Papers

Based on the work presented in this thesis, the following research articles have been published or communicated:

- Sonjoy Pan and Siddhartha P. Chakrabarty. Threshold dynamics of HCV model with cell-to-cell transmission and a non-cytolytic cure in the presence of humoral immunity. *Commun. Nonlinear Sci. Numer. Simul.* 61 (2018): 180-197.
- Sonjoy Pan and Siddhartha P. Chakrabarty. Hopf bifurcation and stability switches induced by humoral immune delay in hepatitis C. To appear in *Indian J. Pure Appl. Math.*
- Sonjoy Pan and Siddhartha P. Chakrabarty. Analysis of a reaction-diffusion HCV model with general cell-to-cell incidence function incorporating B cell activation and cure rate (Communicated).
- Sonjoy Pan and Siddhartha P. Chakrabarty. Stochastic analysis of in-host HCV dynamics through budding and bursting process. *Commun. Nonlinear Sci. Numer. Simul.* 80 (2019): 104955.